Technische Universität München
Fakultät für Elektrotechnik und Informationstechnik
Lehrstuhl für Informationstechnische Regelung

Shared Control for Human–Robot Team Interaction

Selma Musić

Vollständiger Abdruck der von der Fakultät für Elektrotechnik und Informationstechnik der Technischen Universität München zur Erlangung des akademischen Grades eines

Doktor-Ingenieurs (Dr.-Ing.)

genehmigten Dissertation.

Vorsitzende/-r: Prof. Gordon Cheng, Ph.D.

Prüfende/-r der Dissertation:

1. Prof. Dr.-Ing. Sandra Hirche

2. Prof. Dr. Oussama Khatib

Die Dissertation wurde am 01.03.2021 bei der Technischen Universität München eingereicht und durch die Fakultät für Elektrotechnik und Informationstechnik am 23.06.2021 angenommen.

You think because you understand "one"
you must also understand "two",
because one and one make two.
But you must also understand "and".

-Rumi

Preamble

The past six years have been challenging, but also very rewarding. Throughout this period the Chair of Information-oriented Control at the Technical University of Munich has been my home. I feel grateful to have had a sense of belonging and purpose. At the same time, I feel a sense of relief and empowerment for succeeding in what was my primary goal. I would not have been able to become the person I am today without the people who have enriched this journey.

First, I am deeply grateful to Sandra for giving me a chance to work at TUM, for her supervision, help, understanding and all the opportunities she has provided me. At ITR I had a friendly, highly competent and reliable support, be it with my research, project work, teaching duties or student supervision. Next to Sandra, this was all possible thanks to Stefan.

I am particularly proud and grateful that I worked as a visiting student researcher with Prof. Oussama Khatib at Stanford University. I thank Oussama and his team at Stanford Robotics Lab for the opportunity, support, valuable discussions and friendliness.

A big part of my thesis contribution and my research work at ITR was done during the *WEARHAP* project. I am especially grateful to my collaborators who taught me a lesson in constructive team work. I have admired their enthusiasm for science and positivity. Next to Sandra, I am thankful to Prof. Domenico Prattichizzo who introduced me to many fascinating possibilities of human-robot interaction with wearable haptics. To Gionata and Francesco for their support, appreciation and valuable feedback. I am also thankful to my colleagues at ITR who were a part of the *WEARHAP* project. In particular, to Dominik for his help at the very start of my PhD and the collaborative work on the cognitive control architecture and to Pablo for his help in experimental implementation and productive collaboration.

I am grateful to Prof. Martin Buss and Prof. Sami Haddadin for their valuable support, advice and giving me a sense of direction when needed.

I thank my students who have kept me inspired throughout these years: Martin Angerer, Ana Avdiaj, Elena Zhelondz, Christian Schmidt and Ricardo Chavez Rosas. I am thankful to my former and current colleagues: Faris and Precious for their friendliness and for making my work days more lighthearted.

I owe my deep gratitude and appreciation to Nadja for her support, empathy and kindness. To Ivana and my sister Esma for their help and encouragement. I'm grateful to my dear parents for prioritizing education, their unconditional support, belief in me and teaching me courage and perseverance.

Abstract

Rapid improvements of actuation and sensing capabilities of *collaborative robots (cobots)* have enabled *human-robot teams*. Robots are no longer only specialized and unsafe *tools*, but can have an active part in decision making as *partners* to humans. Fusing complementary capabilities of humans and robots is beneficial for many applications, e.g. extraterrestrial exploration, surgery, rehabilitation and collaborative manufacturing. Motivation for human-robot teams is that humans are excellent in reasoning and planning in unstructured environments, while robots are very good in performing tasks repetitively and precisely. The advancements of communication technologies enable interaction not only in a shared workspace, e.g. in *direct physical interaction*, but also in *remote interaction settings*. Consequences of these advancements are: (i) flexibility and dexterity of robots is further improving, enabling design of complex robot systems, such as multi robots, that are able to perform tasks comprising of multiple aspects and (ii) development of wearable haptic interfaces for remote interaction. Therefore, the interaction of humans with such robot systems, through novel interfaces and for complex tasks, is an emerging challenge.

One of the key research questions is how to combine human and robot decision making and task execution capabilities in order to exploit their complementary skills. An important control challenge is to resolve frequently *asymmetric interaction*, arising because robot(s) can have a relatively high number of controllable degrees of freedom compared to the human partner. Furthermore, human-robot teams typically need to achieve *multiple control objectives* in order to accomplish a task and *robust stability* needs to be guaranteed to facilitate safe interaction with the human and an a priori unknown environment. Finally, human and robot often need to *dynamically adjust* their roles in order to perform a task in an optimal way. In order to accomplish these challenges, a unified *shared-control approach* is still needed to enable human-robot teaming irrespective of the interaction setting, interface, complexity of the robot system and complexity of the task.

The main contribution of this thesis is a novel *shared-control framework* that enables: (i) asymmetric interaction, (ii) simultaneous execution of multiple control objectives and (iii) dynamic role adjustment in reaching a common control objective. The focus is on *haptic interaction* between the partners, either through *direct physical contacts* or *haptic devices*. The proposed control approach decouples the system dynamics into multiple subsystems, each having its own control objective. The formal guarantees which enable the achievement of multiple control objectives without conflicts are introduced. This enables partners to provide control inputs to different subsystems simultaneously and without interferences. With this control approach human-robot team interaction is established on spaces of reduced dimensionality taking into account the low number of human command and feedback signals imposed by interaction interfaces. The commands from the human are projected onto the spaces of subsystems' domain using a *command mapping* strategy and measured interacting forces are fed back to the haptic interface using a *feedback mapping* strategy. The role adjustment to achieve a common control objective is resolved by ensuring the total control input applied to the task is optimal according to *Nash equilibrium*. The proposed shared-control framework has been evaluated in simulation and realistic robot settings that include human-robot direct physical interaction and remote interaction of a human partner and multiple robots via wearable haptic devices. The suitability of wearable haptic devices in the remote interaction is evaluated in human user studies.

Contents

Notation

Function dependencies are omitted whenever they are clear from the context to improve readability.

Acronyms and Abbreviations

BF	binary feedback
CF	constant feedback
CLPS	closed-loop perfect state information pattern
DF	dynamic relative feedback
HRI	human-robot interaction
HRC	human-robot interaction
HRTI	human-robot team interaction
HITL	human-in-the-loop
HOTL	human-on-the-loop
I/O	input/output
IPC	intrinsically passive control
MIMO	multi-input multi-output
NE	Nash equilibrium
NF	no feedback
MF	measured feedback
pH	port-Hamiltonian
pHRI	physical human-robot interaction
SISO	single-input single-output

w.r.t.	with respect to

Mathematical Conventions

Sets and Distributions

$\mathcal{A} \cup \mathcal{B}$	union of manifolds $\mathcal{A}$ and $\mathcal{B}$
$\mathcal{M}, \mathcal{M}_i, \mathcal{M}_{b,i}, \mathcal{K}, \mathcal{K}_i, \mathcal{V}, \mathcal{V}_i$	manifolds
$\mathcal{M}^\perp$	kernel of $\mathcal{M}$
$\mathbb{N}$	set of natural numbers
$\mathbb{R}$	set of real numbers
SE(3)	special Euclidean group representing rigid body motions
SO(3)	special orthogonal group representing rotations
Spin(3)	group representing unit quaternions
$\tilde{\Delta}$	distribution related to the closed-loop system
Δ^c	controllability distribution
$\Delta^c_{b,i}$	controllability distribution of the i^{th} behavior
Δ^G	distribution of $\boldsymbol{G}$
$\Delta^G_{b,i}$	distribution of $\boldsymbol{G}_{b,i}$
Δ^K	kernel distribution
Ω	codistribution

Scalars, Vectors and Matrices

a	scalar (small letters)
$\boldsymbol{a}$	column vector (bold small letters)
$\boldsymbol{A}$	matrix (bold capital letters)
$\boldsymbol{A}^\dagger = \boldsymbol{A}^\top(\boldsymbol{A}\boldsymbol{A}^\top)^{-1} \in \mathbb{R}^{n\times n}$	Moore-Penrose pseudoinverse of matrix $\boldsymbol{A}$
$T_{\boldsymbol{\xi}_0}\mathcal{M}$	tangent space of $\mathcal{M}$ at point $\boldsymbol{\xi}_0$

$\boldsymbol{I}_n \in \mathbb{R}^{n\times n}$	identity matrix
$\mathbf{0}_n \in \mathbb{R}^{n\times n}, \mathbf{0}_{m\times n} \in \mathbb{R}^{m\times n}$	zero matrix
$\boldsymbol{S}(\cdot) \in \mathbb{R}^{3\times 3}$	skew-symmetric matrix

Differential operations

$\dot{x} = \frac{dx}{dt}$	first derivative w.r.t. time
$\frac{\partial f(\boldsymbol{x})}{\partial \boldsymbol{x}} = [\frac{\partial f(\boldsymbol{x})}{\partial x_1} ... \frac{\partial f(\boldsymbol{x})}{\partial x_n}]$	partial derivative
$ad^i_{\boldsymbol{f}}\boldsymbol{G} = [\boldsymbol{f},\, ad^{i-1}_{\boldsymbol{f}}\boldsymbol{G}]$	Lie product of $\boldsymbol{f}$ and $ad^{i-1}_{\boldsymbol{f}}\boldsymbol{G}$
$[\boldsymbol{f},\boldsymbol{g}](\boldsymbol{x}) = \frac{\partial \boldsymbol{g}}{\partial \boldsymbol{x}}\boldsymbol{f}(\boldsymbol{x}) - \frac{\partial \boldsymbol{f}}{\partial \boldsymbol{x}}\boldsymbol{g}(\boldsymbol{x})$	Lie product (or bracket) of $\boldsymbol{f}$ and $\boldsymbol{g}$
$\mathcal{L}_{\boldsymbol{g}}\boldsymbol{f}(\boldsymbol{x}) = \sum_{i=1}^{n} \frac{\partial \boldsymbol{f}}{\partial x_i}\boldsymbol{g}_i(\boldsymbol{x})$	Lie derivative of $\boldsymbol{f}$ along $\boldsymbol{g}$
$\mathcal{L}_{\boldsymbol{g}_1}\mathcal{L}_{\boldsymbol{g}_2}\boldsymbol{f}(\boldsymbol{x}) = \frac{\partial \mathcal{L}_{\boldsymbol{g}_2}\boldsymbol{f}}{\partial x}\boldsymbol{g}_1(\boldsymbol{x})$	repeated Lie derivative

Subscripts and Superscripts

$(\cdot)_a$	associated with robot autonomy
$(\cdot)_b$	associated with behaviors
$(\cdot)_c$	associated with cooperative behavior
$(\cdot)_h$	associated with human partner
$(\cdot)_r$	associated with relative behavior
$(\cdot)_x$	associated with Cartesian space
$(\cdot)^d$	associated with desired values
${}^t(\cdot)$	w.r.t. frame $\{t\}$

Variables

$\boldsymbol{c} \in \mathbb{R}^{n_\theta}$	generalized Coriolis and centripetal forces of the robot
$d \in \mathbb{R}$	displacement of the wearable device
$\boldsymbol{D} : \mathbb{R}^n \to \mathbb{R}^{n\times n}$	damping matrix

$d_c, d_r \in \mathbb{R}$	damping cooperative and relative translation parameters
$\boldsymbol{D}_c \in \mathbb{R}^{6\times6}$	desired cooperative damping matrix
$\boldsymbol{D}_r \in \mathbb{R}^{6\times6}$	desired relative damping matrix
$\boldsymbol{e}_{b,i} \in \mathbb{R}^{k_i}$	tracking error of the i^{th} behavior
$\boldsymbol{f} : \mathbb{R}^n \to \mathbb{R}^n$	system vector field
$\tilde{\boldsymbol{f}} : \mathbb{R}^n \to \mathbb{R}^n$	closed-loop system vector field
$\boldsymbol{f}_c \in \mathbb{R}^6$	cooperative force vector
$\boldsymbol{f}_i \in \mathbb{R}^3$	force vector of the i^{th} robot
$\boldsymbol{f}_r \in \mathbb{R}^6$	relative force vector
$g \in \mathbb{R}$	incremental cost
$g_T \in \mathbb{R}$	terminal cost
$\boldsymbol{g}_i : \mathbb{R}^n \to \mathbb{R}^n$	column i of system matrix $\boldsymbol{G}$
$\boldsymbol{G} : \mathbb{R}^n \to \mathbb{R}^{n\times m}$	system matrix field
$\tilde{\boldsymbol{G}} : \mathbb{R}^n \to \mathbb{R}^{n\times m}$	closed-loop system matrix field
$\boldsymbol{G}_b : \mathbb{R}^n \to \mathbb{R}^{n\times m}$	behavior system matrix field
$\boldsymbol{G}_h : \mathbb{R}^n \to \mathbb{R}^{n\times l}$	system matrix field mapping control input $\boldsymbol{u}_h$
$\boldsymbol{G}_a : \mathbb{R}^n \to \mathbb{R}^{n\times(m-l)}$	system matrix field mapping control input $\boldsymbol{u}_a$
$\boldsymbol{h} : \mathbb{R}^n \to \mathbb{R}^p$	system output function
$\boldsymbol{H} \in \mathrm{SE}(3)$	homogeneous matrix
$\mathcal{H} : \mathbb{R}^n \to \mathbb{R}$	Hamiltonian function
$J \in \mathbb{R}$	cost function
$\boldsymbol{J} : \mathbb{R}^n \to \mathbb{R}^{n\times n}$	structure matrix of a port-Hamiltonian system
$\boldsymbol{J}_b : \mathbb{R}^n \to \mathbb{R}^{n\times n}$	behavior Jacobian
$\boldsymbol{J}_{b,i} : \mathbb{R}^n \to \mathbb{R}^{n_i\times n}$	Jacobian of the i^{th} behavior
$\boldsymbol{J}_{b,r} : \mathbb{R}^{12} \to \mathbb{R}^{6\times12}$	relative Jacobian
$\boldsymbol{K}_{b,i} \in \mathbb{R}^{n\times k_i}$	kernel matrix of the i^{th} behavior
$\boldsymbol{k}_h, \boldsymbol{k}_a \in \mathbb{R}^n$	optimal feedforward terms

$k_r, k_c \in \mathbb{R}$	stiffness cooperative and relative translation gains
$\boldsymbol{K}_i \in \mathbb{R}^{k_i \times k_i}$	desired stiffness matrix of the i^{th} behavior
$\boldsymbol{K}_h, \boldsymbol{K}_a \in \mathbb{R}^{n \times n}$	control gains
$\boldsymbol{m}_i \in \mathbb{R}^3$	torque vector of the i^{th} robot in task space
$\boldsymbol{M} : \mathbb{R}^{n_\theta} \to \mathbb{R}^{n_\theta \times n_\theta}$	inertia matrix of the robot
$\boldsymbol{M}_{b,i} : \mathbb{R}^{k_i} \to \mathbb{R}^{k_i \times k_i}$	inertia matrix of the i^{th} behavior
$\boldsymbol{M}_c \in \mathbb{R}^{6 \times 6}$	desired cooperative inertia matrix
$\boldsymbol{M}_r \in \mathbb{R}^{6 \times 6}$	desired relative inertia matrix
$\hat{\boldsymbol{n}}_i \in \mathbb{R}^3$	vector of normal directions of the contact point i to a surface
$N \in \mathbb{N}$	number of robots in a robot team
$\boldsymbol{N} \in \mathbb{R}^{n \times n}$	null-space matrix
$\boldsymbol{p}_c \in \mathbb{R}^3$	cooperative position vector
$\boldsymbol{p}_{f,i} \in \mathbb{R}^3$	position vector of the i^{th} contact point of the human partner
$\boldsymbol{p}_h \in \mathbb{R}^3$	position vector of the human hand
$\boldsymbol{p}_i \in \mathbb{R}^3$	position vector of the i^{th} robot
$\tilde{\boldsymbol{p}}_i \in \mathbb{R}^6$	momentum of the i^{th} robot
$\boldsymbol{p}_{r,j} \in \mathbb{R}^3$	j^{th} relative position vector
$\boldsymbol{p}_{vo} \in \mathbb{R}^3$	position of the virtual object
$\boldsymbol{P}_{b,j} \in \mathbb{R}^{n \times n_j}$	inverse matrix of the j^{th} behavior Jacobian
$\boldsymbol{q}_c \in \text{Spin}(3)$	cooperative unit quaternion
$\boldsymbol{q}_h \in \text{Spin}(3)$	unit quaternion of the human hand orientation
$\boldsymbol{q}_i \in \text{Spin}(3)$	unit quaternion of the i^{th} robot
$\boldsymbol{q}_r \in \text{Spin}(3)$	relative unit quaternion
$\boldsymbol{q}_{vo} \in \text{Spin}(3)$	unit quaternion of the virtual object
$\boldsymbol{q}^\star \in \text{Spin}(3)$	quaternion conjugate
$\boldsymbol{r}_{h,vo} \in \mathbb{R}^3$	distance between the frame $\{h\}$ and the virtual object

$\boldsymbol{r}_i \in \mathbb{R}^3$	distance between the frames $\{c_i\}$ and $\{c\}$ in $\{\mathrm{w}\}$
$\boldsymbol{r}_{vo} \in \mathbb{R}^3$	distance between the fingertips
$\boldsymbol{R}_c \in \mathrm{SO}(3)$	rotation matrix of the frame $\{c\}$ w.r.t. the world frame
$\boldsymbol{R}_h \in \mathrm{SO}(3)$	rotation matrix of the human hand
$\boldsymbol{R}_i \in \mathrm{SO}(3)$	rotation matrix of the i^{th} robot
$S \in \mathbb{R}$	storage function
$\boldsymbol{t}_i \in \mathbb{R}^n$	twist vector of the i^{th} robot
$T \in \mathbb{R}^+$	time horizon
$\boldsymbol{u} \in \mathbb{R}^m$	control input
$\boldsymbol{u}_h \in \mathbb{R}^l$	control input (human partner)
$\boldsymbol{u}_a \in \mathbb{R}^{m-l}$	control input (robot partner)
$\boldsymbol{v}_{b,i} \in \mathbb{R}^{n_i}$	differential of the i^{th} behavior
$\boldsymbol{v}_h \in \mathbb{R}^6$	velocity vector of the human hand
$\boldsymbol{v}_i \in \mathbb{R}^6$	velocity vector of the i^{th} robot
$\boldsymbol{v}_r \in \mathbb{R}^6$	relative velocity vector
$\boldsymbol{v}_{vo} \in \mathbb{R}^{n_j}$	velocity vector of the virtual object
$V \in \mathbb{R}$	Lyapunov function
$V_K \in \mathbb{R}$	potential function of the desired stiffness behavior
$\boldsymbol{w}_i \in \mathbb{R}^6$	control wrench vector of the i^{th} robot
$\boldsymbol{w}_{g,i} \in \mathbb{R}^6$	gravitational forces of the i^{th} robot in Cartesian space
$\boldsymbol{w}_{K,i} \in \mathbb{R}^k_i$	desired stiffness wrench of the i^{th} behavior
$\boldsymbol{w}_{K,c} : \mathbb{R}^6 \to \mathbb{R}^6$	desired cooperative stiffness vector
$\boldsymbol{w}_{K,r} : \mathbb{R}^6 \to \mathbb{R}^6$	desired relative stiffness vector
$\boldsymbol{w}_{m,c} \in \mathbb{R}^6$	measured cooperative wrench vector
$\boldsymbol{w}_{m,i} \in \mathbb{R}^6$	measured wrench vector of the i^{th} robot
$\boldsymbol{w}_{m,r} \in \mathbb{R}^6$	measured relative wrench vector
$\boldsymbol{x} \in \mathrm{SE}(3)$	robot pose in task space

$\boldsymbol{x}_{b,i} \in \mathbb{R}^{k_i}$	abstract coordinates of the i^{th} behavior
$\boldsymbol{x}_c \in \text{SE}(3)$	cooperative pose vector
$\boldsymbol{x}_h \in \text{SE}(3)$	pose of the human hand
$\boldsymbol{x}_r \in \text{SE}(3)$	relative pose vector
$\boldsymbol{x}_{vo} \in \text{SE}(3)$	pose of the virtual object
$\boldsymbol{y} \in \mathbb{R}^p$	system output
$\boldsymbol{Z}_h, \boldsymbol{Z}_a \in \mathbb{R}^{n \times n}$	optimal control gains
$\alpha \in \mathbb{R}$	roll angle of the wearable device
$\boldsymbol{\alpha} : \mathbb{R}^{n_\theta} \to \mathbb{R}^{n_\theta}$	smooth vector field in static control law
$\beta \in \mathbb{R}$	pitch angle of the wearable device
$\boldsymbol{\gamma} \in \mathbb{R}^m$	permissible strategy
Γ_i	class of permissible strategies
$\boldsymbol{\Gamma} : \mathbb{R}^{n_\theta} \to \mathbb{R}^{n_\theta \times n_\theta}$	matrix in static control law
$\delta_c, \delta_r \in \mathbb{R}$	damping cooperative and relative rotation parameters
$\boldsymbol{\theta} \in \mathbb{R}^{n_\theta}$	generalized robot coordinates
$\kappa_c, \kappa_r \in \mathbb{R}$	stiffness cooperative and relative rotation parameters
$\boldsymbol{\xi} \in \mathbb{R}^n$	system state
$\boldsymbol{\xi}_b \in \mathbb{R}^n$	concatenated behavior state
$\boldsymbol{\xi}_{b,i} \in \mathbb{R}^{k_i}$	i^{th} behavior state
$\boldsymbol{\xi}_e \in \mathbb{R}^n$	system error state
$\boldsymbol{\phi}_i : \mathbb{R}^n \to \mathbb{R}^{k_i}$	behavior projection mapping
$\boldsymbol{\tau} \in \mathbb{R}^{n_\theta}$	robot input torque
$\boldsymbol{\tau}_c \in \mathbb{R}^{n_\theta}$	robot input control torque
$\boldsymbol{\tau}_e \in \mathbb{R}^{n_\theta}$	external input torque
$\boldsymbol{\tau}_g : \mathbb{R}^{n_\theta} \to \mathbb{R}^{n_\theta}$	generalized gravitational forces
$\boldsymbol{\omega}_i \in \mathbb{R}^3$	angular velocity vector of the i^{th} robot

1

Introduction

Robots are still predominantly used as: (i) specialized and preprogrammed tools capable of performing a limited set of tasks in a closed-off environment or (ii) teleoperators in hazardous or inaccessible environments which are remotely and almost fully controlled by human operators. However, the development of collaborative robots allowed humans and robots to share their workspace. Therefore, robots are no longer only tools to humans but are capable of being their collaborative partners and assistants. The benefit of human-robot collaboration lies in the complementary capabilities of humans and robots; humans are excellent in reasoning, (re-)planning and adapting in unstructured environments, while robots are very good in performing tasks repetitively and precisely. This makes the collaboration between humans and robots highly relevant in many application domains ranging from *industrial*, e.g. collaborative manufacturing and construction, *service*, e.g. cooperative object transportation, retrieval and storage in warehouses, as well as care for the elderly, to *medical*, e.g. telesurgery and rehabilitation. Figure 1.1 depicts some of these application examples.

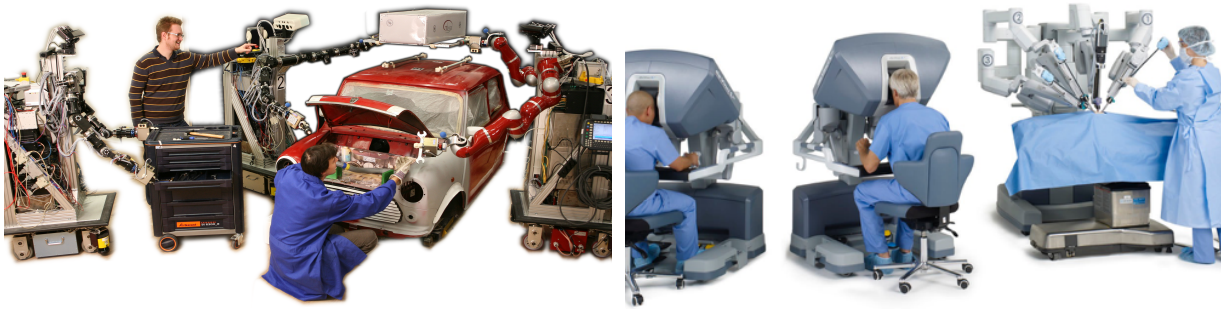

(a) Cooperative manipulation [Hir14]

(b) Remote surgery [dav13]

Figure 1.1: Application examples of human-robot interaction.

In order to establish a successful human-robot interaction, it is important to guarantee human *safety*, reduce human *workload* and at the same time effectively complement human cognitive capabilities with robot autonomy in order to maximize task *performance* and *intuitiveness* of the collaboration. A suitable way to achieve these requirements is with *shared control*, where commands and actions from the human operator and the robot autonomous functions are combined to achieve a task. Shared control is still a largely open research topic and one of its key research questions is how to combine human and robot decision-making

and task-execution capabilities in order to meet the aforementioned requirements.

The main challenges of human-robot interaction are listed and clarified in Section 1.1. The review of the existing literature on human-robot interaction, relevant to the development of shared-control strategies, is provided in Section 1.2. The overview of the thesis content is provided in Section 1.3. Discussion is provided in Section 1.4.

1.1 Challenges

The focus of this thesis is on *haptic shared-control approaches for continuous human-robot team interaction*. The concepts of *human-robot teams* and *continuous interaction* are defined below.

Definition 1.1.1. *Human-robot teams are teams of human(s) and robot(s) that jointly perform a task.*

Definition 1.1.2. *Continuous human-robot interaction is an interaction in which human and robot provide control inputs at all times during the task execution.*

Haptic information exchange between the human and the robot is suitable for continuous interaction and is essential in tasks where the robot physically interacts with human(s) and an unknown environment [HB12]. In this work *haptic interaction* is primarily achieved by communicating *motion and force* signals to the human. Haptic interaction can be in the form of a *direct physical interaction (pHRI)* [MLK+12] or *haptic device interaction*, e.g. in teleoperation or virtual environment settings [PK06].

Since there are many ways in which the human and the robot system may interact, it is necessary to define different interaction paradigms which do not depend on the type of the interaction setting (remote or direct physical interaction) nor on the robot system structure (its complexity and heterogeneity). Providing this classification formally and from a control-theoretical perspective can facilitate the shared-control design.

Challenge 1. *Classify interaction paradigms of continuous, haptic human-robot interaction from a control-theoretical perspective.*

Typically, multiple control objectives need to be defined for human-robot interaction in order to accomplish a task. Due to the robot system complexity (high number of degrees of freedom), task complexity (multiple simultaneous and sequential subtasks) and cognitive limitations of the human, the human partner may not be able to control all the aspects of the task toward accomplishing the control objectives. In consequence, the human can only take over a limited number of task variables to control, while the remainder is taken over by the autonomous robot functions. An additional challenge is coupling between the partners in continuous interaction, especially in the case of physical coupling. More specifically, control inputs provided by the robot autonomous functions may serve as disturbance inputs to the task variables controlled by the human partner and vice versa. Therefore, it is desirable to decouple the task variables controlled by the human partner from those controlled by the autonomous robot functions to avoid undesirable interference.

Challenge 2. *How can the human and the robot system complement each other to achieve multiple control objectives simultaneously and without interference?*

While shared-control approaches promise a flexible adjustment of the workload for the human depending on the level of robot autonomy, it is still unclear how to appropriately include human in the control loop with the robot partner. More specifically, it is necessary to understand which *command and feedback channels* are the most appropriate for certain task classes. Formally, the challenge is to find the most appropriate way in which the human partner can send commands to the robot partner and receive feedback about the relevant states from the robot partner.

Challenge 3. *How to select command and feedback channels between the human and the robot based on the task?*

Evidently, control sharing and the choice of command and feedback channels in human-robot interaction is highly dependable on the *interface* through which the human and the robot system establish the interaction. Choosing an appropriate haptic interface that increases the flexibility of shared control is still an open challenge and represents an important step toward its applicability in real-life settings.

Challenge 4. *What type of interfaces are the most suitable for shared control in continuous human-robot interaction?*

Shared control is also necessary when the human and the robot partner control the same task variables cooperatively. This type of interaction calls for sophisticated, fine-tuned control approach that is capable of: (i) monitoring human behavioral aspects online and (ii) modifying the robot participation in decision making w.r.t. the human behavior. While many existing shared-control approaches focus on achieving task efficiency and may consider models of human physical behavior, they do not consider how humans make decisions in shared tasks.

Challenge 5. *How to model human decision-making behavior for haptic shared-control in continuous human-robot collaboration?*

With an appropriate model of human decision-making behavior, the shared controller needs to enable effective and intuitive *role adjustment* between the partners. In this way, the control approach should ensure intuitive interaction to the human and task efficiency.

Challenge 6. *How can the robot partner be included in the decision-making process without inducing negative impact on the human behavior or conflicts in the cooperation?*

This thesis proposes a shared-control framework that resolves presented challenges.

1.2 Human-Robot Team Interaction

In this thesis an interaction between a human and a robot system is considered. A typical block architecture for human-robot interaction is depicted in Figure 1.2. It is inspired by the block architecture for human-machine interaction by Sheridan [She11] and extended to include shared control and robot system components.

The robot system can be a robot, e.g. a manipulator, or a robot team, e.g. cooperative robot manipulators. With Definitions 1.2.1-1.2.2 novel concepts, considered in this work, are introduced.

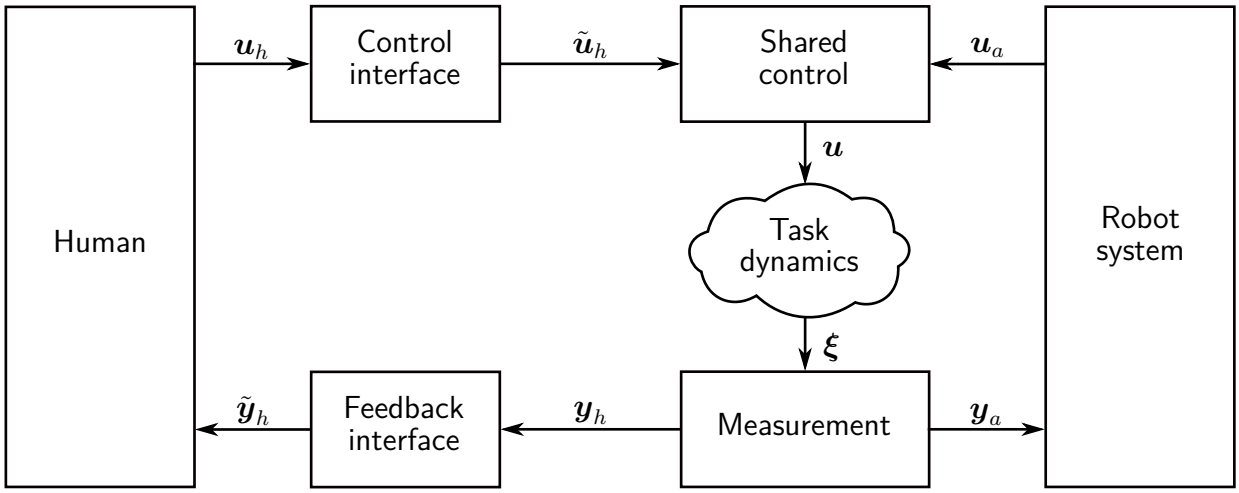

Figure 1.2: General control architecture for human-robot team interaction inspired by [She11]. The human partner provides the reference input, $\boldsymbol{u}_h$, to the control interface. The reference control input, transformed to an appropriate reference input to the shared control is $\tilde{\boldsymbol{u}}_h$. The robot system provides the reference input $\boldsymbol{u}_a$. Control inputs are $\boldsymbol{u}$ and states of the task dynamics $\boldsymbol{\xi}$. Measurements $\boldsymbol{y}_a$ and $\boldsymbol{y}_h$ are sent to the robot and the human partners, respectively. The feedback interface transforms $\boldsymbol{y}_h$ to a signal $\tilde{\boldsymbol{y}}_h$, appropriate as the feedback to the human partner.

Definition 1.2.1. *Robot teams are multi-robot cooperative systems that work together to achieve a common control objective.*

Robot teams can be a set of mobile manipulators, wheeled robots or UAVs. In the literature there is further the distinction between robot *swarms*, i.e. multi-robot systems with a relatively large number of "simple" and homogeneous robots, and heterogeneous multi-robot systems with more complex individual robots. Under the term of robot team both types are subsumed in this work. Below, human-robot team interaction is formally defined.

Definition 1.2.2. *Human-robot team interaction (HRTI) is an interaction between a human and a robot team.*

Figure 1.3 depicts two interaction types, included in the human-robot interaction taxonomy in [YD04], that are considered in this thesis: (i) interaction between a single human and a single robot and (ii) interaction between a single human and a robot team.

Figure 1.3: Human-robot interaction (HRI) and human-robot team interaction (HRTI). Robots in the robot team interact between each other.

Human-robot interaction depends on: (i) the human role in the interaction, (ii) the levels of robot autonomy, (iii) the type of the robot system, (iv) the interface through which the interaction is established, (v) the shared-control strategy, and (vi) the type of the task. State of the art for human-robot interaction, with the focus on human-robot teams, is reviewed through these six factors in this section.

1.2.1 Human Role

Literature distinguishes between an *active* and a *supervisory* human role [CB14]. The active role brings human *in* the control loop with the robot where the interaction is *continuous*. In this context, the human partner continuously provides desired reference input (Figure 1.4a). The supervisory role (Figure 1.4b) brings human *on* the loop where the interaction with the robot is typically symbolic (in the form of high-level instructions) and only when necessary. The human supervisor is aware of the overall goal and is capable of modifying it by re-planning. Additionally, the supervisor can intervene by providing reference inputs if needed. There are also approaches in which the human performs both roles. For example, in [FSR+12] the human is in the supervisory role to select the mode of interaction with the team of UAVs (to interact with the robot team as a single entity or to interact with the individual robots in the team) and in the active role by providing control input to the selected controller. Similarily, in [HCF15] the human switches manually between two controllers: the control of the robot team position and the control of the robot team velocity, and provides the input commands to the chosen controller. In [YD04], five human roles are identified: *supervisor, operator, teammate, mechanic/programmer*, and *bystander*. The roles of operator and teammate fall under the introduced concept of the active role, suitable for human-robot teams. The operator role is suitable in teleoperation scenarios, while the teammate role is suitable for joint task execution. In this thesis, teleoperation and direct pHRI are considered with human in the active role, when he/she is referred to as the operator or the partner, respectively.

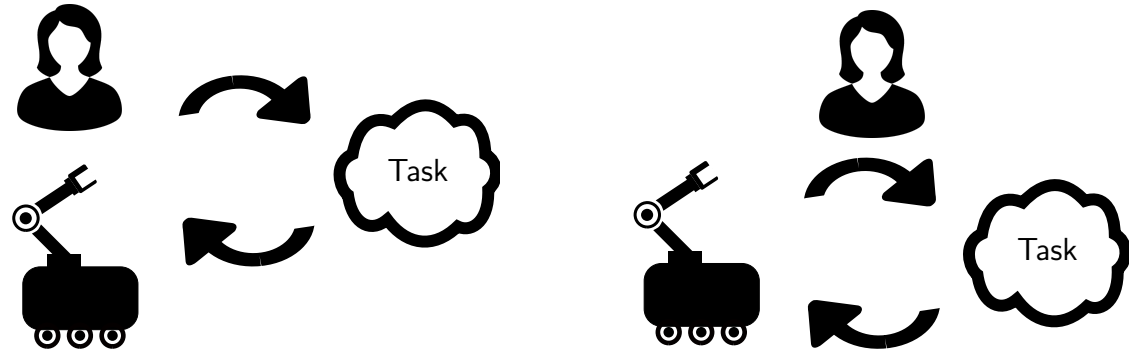

(a) Active role. (b) Supervisory role.

Figure 1.4: Human roles for shared control in human-robot interaction.

1.2.2 Levels of Autonomy

Before introducing the concept of the *levels of autonomy*, the concept of a *semi-autonomous system* needs to be defined.

Definition 1.2.3 ([Zil15]). *A semi-autonomous system can operate autonomously, but cannot complete the entire task without human intervention.*

Shared control primarily depends on the degree to which the semi-autonomous system (a robot in this thesis) can perform functions autonomously [SV78]. *Levels of autonomy (LoAs)* have first been introduced in the field of human-machine interaction (HMI) in the form of ten discretized levels, see Table 1.1 [SV78], but are applicable to human-robot interaction as well. In [PSW00] the authors extend this concept with four general stages of task execution: *information acquisition*, *information analysis*, *decision and action selection*, and *action implementation*. The authors suggest high level of autonomy for information acquisition and information analysis, but not for decision making as it may cause human skill degradation, complacency, and poor situational awareness. Therefore, the human partner should be included in the decision-making process and, depending on the skills and the task, in the action implementation stage as well. However, the formal analysis of the levels of autonomy from the control-theoretical perspective, that would serve as a set of guidelines on how to design shared controllers, is still missing.

	LoA	Characteristics
	1	The human executes all actions.
shared	2	The computer offers complete set of action alternatives.
	3	The computer offers a selection of action alternatives.
	4	The computer suggests one alternative.
	5	The computer executes an action autonomously if the human approves.
	6	The computer allows the human a restricted time to veto before automatic execution.
	7	The computer executes an action and informs the human.
	8	The computer executes an action and informs the human if asked.
	9	The computer executes an action and informs the human if it decides to.
	10	The computer executes all actions autonomously.

Table 1.1: Ten levels of autonomy by Sheridan [SV78].

Switching between discrete levels of autonomy during the task execution can increase flexibility and diversity of the interaction. The challenge is to perform the switching in the most efficient and intuitive way. The approach in which the human switches autonomy levels manually is termed as *human-initiative*, *adjustable* or *adaptable* interaction, see e.g. [CSB+16]. Experimental results show that in this mode humans do not use robot autonomy effectively and still perceive robots as tools, which results in the increase of mental workload [BY04]. If the levels of autonomy are selected by the system, the approach is termed as *adaptive* interaction [She11]. It is shown that this approach impairs transparency to the human, decreases human situational awareness and understanding of the system autonomy [MFG+05]. A compromise can be achieved with *mixed-initiative (MI)* interaction [OWLM14]. For the supervisory role it may be, for example, in the form of assistance to the human in a decision process [BY04]. For the active role it is in the form of robot assistance on the physical level of control inputs. Experimental results show that the mixed-initiative approach outperforms adaptable and adaptive approaches [HG09]. However, its effectiveness is highly dependable on the algorithms for the autonomous task execution and understanding of human behavior.

Succesful interaction and the appropriate choice of the level of autonomy depend on the *trust* in autonomy. Trust is the attitude that a (semi-)autonomous partner will help achieve goals in a situation characterized by uncertainty [LS04]. Analoguously, *overtrust* and *undertrust* in autonomy can cause overreliance (misuse) and underutilization (disuse), respectively [PR97]. Ultimately, the goal of levels of autonomy is to reduce the *human workload*, i.e. the extent to which a task places demands on the human's cognitive resources [SS79]. This is especially relevant in the case of complex robot systems such as robot teams [GMA+07]. However, with the increase of robot autonomy, *situational awareness (SA)* of the human degrades, reducing human apprehension of the robot states [End95]. It has been shown that if the robot is involved in decision making, the situational awareness is negatively affected [PBCM07]. Therefore, the higher the support from the autonomy, the greater the risk from complacency, impaired situational awareness and skill degradation. True danger from these effects can occur when the automation fails and the human does not react, has a delayed response or does not have the skill to react properly [OWLM14]. Therefore, transparency is essential for satisfactory situational awareness and can be improved by a suitable interface [CB14].

1.2.3 Interfaces

The user interface serves as the bridge between the human and the robot to transfer command and feedback information. According to [CB14] the interface needs to ensure the human understands intentions and behaviors of the robot, as well as the state of the environment. Furthermore, it needs to appropriately allocate human attention to important events and ensure the decision authority of the human. In order to increase transparency of the system to the human operator/partner, the interface should make the following system characteristics and their history visible: (i) *purpose* (degree to which the automation is used w.r.t. the designer intent), (ii) *process* (suitability of the autonomy level for a given situation) and (iii) *performance* (reliability, predictability and capability) [CB14].

Command interfaces: In the supervisory role, the human typically interacts with the robot via graphical user interface (GUI), e.g. touch screen [BFB+05] or voice [JBBJ10]. The action of the human supervisor is mapped into high-level commands, e.g. setting goals, assigning levels of autonomy, or interfering in the case of events. In the active role, the human provides continuous commands, e.g. motion and/or force commands. These types of commands are typically conveyed through a motion measuring device, e.g. touch screen [HCF15], vision-based system [SMH15, AMLL+15], or haptic device [DS05, MSB+17]. However, commands can be provided through other interfaces such as brain-computer interfaces (BCIs) [TLT+10], electromyographic signals (EMG) [CZMC08], or direct contacts with the robot [LCG+19]. The control input of the human operator is either direct or employed through mappings, e.g. task-based [SMG+17] and synergy-based [GSMP13] or through gestures [GFS+14, WAV+13]. However, for teleoperation a number of new command interfaces are available, e.g. hand motion tracking [SMH15], gesture recognition [GFS+14] and touch-screen devices [VZ13]. These interfaces are intuitive for use but do not provide reactive force-feedback to the user which can compromise passivity/stability guarantees of the closed-loop system and, in consequence, safety of the interaction. Therefore, this challenge needs to be resolved with passivity-based controllers that consider non-passive human behavior.

Feedback interfaces: In the supervisory role, the human typically receives visual feed-

back, e.g. directly or via video [GQC05]. In [CCDd11] authors distinguish between GUI interfaces for visual representation, warning systems (visual, auditory and haptic) and suggestion systems which indicate where the attention should be allocated. In [BFB+05] the authors show that if the levels of autonomy are changing during the task execution, the interface should provide *dynamic feedback*. In the active role, the feedback is typically visual as well. However, it has been shown that haptic feedback is essential for tasks including interaction with the environment [SFC+13]. Wearable haptic devices represent promising interfaces because the workspace of the human is not limited by the workspace of the haptic devices, thanks to their wearability and portability [PMC+15] which increases flexibility of interaction [PSS+17]. Apart from the interactive forces, haptic feedback channel may provide additional information about internal robot states, e.g. distance to an obstacle [RTE+10, SFC+13, NWL+13] and shape of robot swarm formation [AMCG15]. Analoguously to the supervisory role, the feedback of continuously changing states should be provided to the human in dynamic form in the active role as well [DCG09]. Developing control strategies that are suitable for wearable haptic interfaces is still an open challenge.

1.2.4 Shared Control

The focus of this thesis is on continuous human-robot interaction with the human partner in the active role. Therefore, special focus is put on shared-control approaches in this context. The consideration of specific control approaches would not be complete without reviewing approaches for human modeling as well.

Definition 1.2.4. *Shared control is a general term for all the control approaches that enable humans and semi-autonomous systems to share responsibilities over the task execution.*

According to Definitions 1.2.3-1.2.4, shared control can be any approach on the spectrum between *direct/manual* (the human executes all actions) and *autonomous* control (the system executes all actions), as depicted in Figure 1.5.

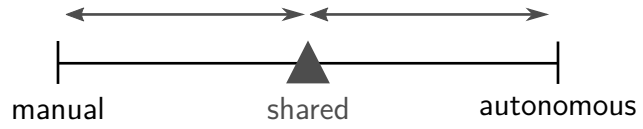

Figure 1.5: Shared-control spectrum from manual to autonomous control.

Control Approaches

The shared-control approaches are reviewed in the context of posed challenges in Section 1.1. In particular, Challenge 2 and Challenge 6 are in the focus in this section.

Task abstraction: In the context of Challenge 2 (achieving intuitive interaction with highly redundant systems and/or for complex tasks), various *task abstraction* shared-control approaches have been employed. Below the concept of a *task abstraction* is defined.

Definition 1.2.5. *Task abstraction is the creation of abstract states using the properties of the original system states.*

Definition 1.2.5 implies that task abstraction generates task-based states starting from the configuration space and corresponding states of the human-robot system. Task abstraction approaches have been particularly beneficial when the robot differs kinematically from the human operator. For example, in [KTC97] a *hidden robot concept* is proposed in which the human operator performs a task in a virtual environment which is translated into commands for the robot performing an actual task. *Virtual fixtures* are used for general haptic interaction scenarios and provide either *assistive* control along task directions or *resistive* control perpendicular to the task directions [AEK05].

In some works on human-multi-robot interaction, controlling specific behaviors of the multi-robot system, instead of controlling individual robot behaviors simultaneously, is termed as *control by policy* [CGON05]. This corresponds to the introduced concept of task abstraction. In this context, the human partner typically provides desired input to *global behaviors*, e.g. guides collective motion of the robot team, while the robots within the team autonomously maintain desired *local behaviors*. For example, in [DS05] *locked* and *shape behaviors* are introduced for multiple robots to describe their team motion and their formation shape, respectively. Therefore, task abstraction for robot teams is an abstraction from the individual to the collective behavior. In [BKG14] the human operator interacts with a robot team on higher levels of abstraction, termed in this work as *attractors*. They represent states of the collective team dynamics, or states of the subset of the team dynamics. They correspond to the introduced concept of global and local behaviors. The authors of [BKG14] additionally impose the stability requirement on the attractors. This is an important requirement for the shared-control design since it implies that the human control input does not need to stabilize the system. Furthermore, control design on the level of task abstractions/attractors reduced dimensionality of the system and, consequently, of the controller [KWC+16]. Reduced dimensionality additionally enables easier interfacing between the human and the complex robot system [BBE+07].

Control arbitration: In the context of Challenge 6 (including the robot partner in the decision-making process), shared control in interactive tasks is often defined through *arbitration* or *blending* of direct control inputs of the human and the robot autonomy, which is in general formulated as

$$\boldsymbol{u} = \boldsymbol{K}_h \boldsymbol{u}_h + \boldsymbol{K}_a \boldsymbol{u}_a, \tag{1.1}$$

where $\boldsymbol{K}_h$ and $\boldsymbol{K}_a$ are appropriate control gains. Typically, blending of control inputs is achieved with: (i) constant control gains, (ii) variable control gains, set using a human-oriented approach and (iii) optimal control approach.

Linear blending with constant control gains, see e.g. [YSD03], is simple but the resulting control may generate unwanted behaviors. For example, linear blending of control inputs that seeks to avoid an obstacle may result in the control input that drives the robot directly into the obstacle. To overcome this issue the robot can *predict human intent* [DS13, TGS11] that results in a human-oriented interaction, at the consequence of task efficiency. In this case the control gains are constant, while the robot control input is the predicted human intent $\boldsymbol{u}_a = \hat{\boldsymbol{u}}_h$. Furthermore, the constraint $\boldsymbol{K}_a = \boldsymbol{I} - \boldsymbol{K}_h$ is typically imposed on the robot control gain.

In order to increase flexibility of the control design, the control gains $\boldsymbol{K}_h$ and $\boldsymbol{K}_a$ can be variable and computed according to a suitable human-centric rule. This enables scaling of the human and the robot control inputs dynamically during task execution. For example, control parameters are computed with a *drift-diffusion decision-making model* in [CSP17].

This enables modeling of *reliance* of the human partner on the robot autonomy. The reliance is measured by *trust* of the human in the autonomy (preference for robot control) and by *self-confidence* of the human in his/her manual control. A human-centric function of *trust* is used to compute control gains in a teleoperation scheme in [SMS+16]. In this case human and robot control inputs are scaled with a function of human-to-robot trust, while the feedback to the human operator is scaled with a robot-to-human trust. However, these approaches do not capture the goal-oriented behavior of the human.

Optimal control is suitable for goal-oriented shared-control design [RBCC15]. Risk-sensitive optimal control and model predictive control (MPC) approaches have been variants applied to direct physical human-robot interaction [MLH15] and remote interaction [CDE13], respectively. The decision making of the human partner can be modeled with optimal control [JF18]. Combining the optimal behavior of the robot partner with the optimal control model of the human partner is possible within the *game-theoretical framework*. This has already been evaluated in human-robot interaction for reaching tasks [LOZ+18]. However, a deeper understanding of the human behavior in haptic interactive tasks, as well as the evaluation of suitability of the game-theoretical framework for shared-control design, are needed.

This literature review serves as a brief overview, since more details on the existing shared-control approaches can be found in Chapters 2- 6.

Human Behavior Modeling

An appropriate human model can predict under which conditions the human exhibits good or bad performance and may be beneficial in the design of shared-control strategies. Generic human behavior models over all levels of abstractions - from reasoning and planning to motion - are very difficult to establish if not infeasible. Therefore, modeling focuses on particular aspects of human behavior - typically distinguishing between: (i) *intention prediction*, (ii) *cognitive decision-making models* and (iii) *low-level physical interaction models*. The modeling type is closely related to the human role and the level of abstraction in the interaction.

In the supervisory role cognitive decision-making models play an important role. For example, human behavior is modeled with *artificial neural-networks* [PST+15], *Markov models* [SLP+15] and *accumulator models* [JL06,SCN+12,PST+15], among many others. Another way of representing human behavior in this role is through its constraints, namely *human workload* and *situational awareness* [CB14].

In the active role human motor sbehavior models play an important role. Therefore, impedance models of human arm/hand behavior in haptic interactions are common [HB12]. In that sense, human behavior is often assumed to be passive, especially in teleoperation scenarios, see e.g. [Sir05]. However, as there are different interaction modes and interfaces, humans cannot be considered passive in all the cases, particularly when the interface does not provide haptic feedback and passivity-short control design should be considered [HCF15]. High-level decision-making and low-level motor control components of human behavior can be unified with an optimal feedback control approach [TJ02a].

For a better overview, the reviewed literature is sorted in Table 1.2 with respect to the main concepts relevant to human-robot interaction.

Topic	References
Interaction paradigms	[SV78] [PSW00] [BY04] [OWLM14] [LTT+01] [RND02] [DY05] [JBR14] [CL12] [WNL+13] [STP06] [WTFR04] [FTG+09]
Supervisory role	[PST+15] [JL06] [CBH11] [RND02] [CHWT12] [MD07]
Active role	[CB14] [DS05] [HCF15] [SMH15] [SFC+13] [RTE+10] [Sir05] [Liu15] [FSR+12] [CSP17] [SMS+16] [MS11] [LFS+13] [LKL15] [Lee08] [LH10] [FRS+11]
Interfaces	[BFB+05] [AMLL+15] [DdlCE13] [GQC05] [SFC+13] [NWL+13] [AMCG15] [DCG09] [CBH11] [GPC05] [STP06] [SKE15] [NSR+08] [BAH+13]
Adjustable control	[CSB+16] [MFG+05] [HCF15] [FSR+12]
Adaptive control	[MFG+05] [GMA+07] [PBCM07]
Mixed-initiative control	[BY04] [HG09] [BFB+05] [DS13] [CSP17] [SMS+16] [MBF03] [BJG14] [GWHP16] [CDE13] [WL07] [RHH+04] [LTC+15] [Tra15] [LK07] [BSS04]
Human modeling	[LS04] [OWLM14] [BFB+05] [HCF15] [GQC05] [CCDd11] [PST+15] [SLP+15] [JL06] [SCN+12] [GMA+07] [End95] [Sir05] [CBH11] [CHWT12] [CSL08] [SOJ+11] [JF18] [AP01] [EBS+07] [TJ02a]
Shared control	[KTC97] [AEK05] [YSD03] [DS13] [TGS11] [CSP17] [SMS+16] [MLH15] [RBCC15] [LOZ+18]

Table 1.2: A literature overview for human-robot interaction.

1.3 Outline

This section introduces contents of the thesis by chapters. At the beginning of each chapter the relevant related work and the open problems are provided. Conclusion and potential future directions are provided in Chapter 7, while additional materials are provided in Appendices 8-10.

Chapter 2: Interaction Paradigms for Human-Robot Teams

This chapter addresses Challenge 1. Taxonomy and classification of interaction paradigms for control sharing in continuous, haptic human-robot interaction are proposed. They are formalized using a control-theoretical concept of *controllability*. In that sense, the classification enables a unified consideration of: (i) extreme haptic human-robot interaction modes - teleoperation (remote) and physical interaction (direct), (ii) varying levels of autonomy from manual to fully autonomous and (iii) robotic systems of varying complexity - from single robots to robot teams. In order to be able to consider interaction on a *higher level of abstraction* concepts of *behavior*, *subtask*, and *task* are formally introduced. Finally, this chapter conceptually introduces the developed shared-control framework, named *subtask-based architecture*. The results presented in this chapter have been partially published in [MH16], [MH17] and [MH18].

Chapter 3: Complementary Shared Control

This chapter addresses Challenge 2. Simultaneous execution of multiple control objectives is achieved with a novel *subtask-based control*. The proposed controller relies on defining decoupled dynamic subsystems and nominal, passive controllers that are implemented on the level of behaviors. The approach is passive and, therefore, suitable for various interaction forms (human-robot, robot-robot, robot-environment). The results presented in this chapter have been partially published in [MH18] and a journal publication is in preparation [MKH21].

Chapter 4: Human-Centric Shared Control for Cooperative Manipulation

This chapter addresses Challenges 2-4. The control approach, proposed in Chapter 3, is tested on a teleoperation scenario of a team of robot manipulators performing a cooperative manipulation task. An Euler-Lagrangian modeling approach is used.

In order to reduce the design space wearable interface solutions are considered. In consequence, the human is able to move freely in the teleoperation scenario. Proposed command mappings enable the human to control the robot team on spaces of reduced dimensionality, instead of controlling individual degrees of freedom of the robots, and feedback mappings provide relevant force information. The suitability of wearable haptic devices in teleoperation of a dual-manipulator system, cooperatively manipulating an object, is evaluated in a user study. The results presented in this chapter have been partially published in [MSB+17], [MSgD+19] and [MPH19].

Chapter 5: Port-Hamiltonian Cooperative Manipulation

This chapter addresses Challenge 2 using the port-Hamiltonian modeling and passivity-based control approaches. Additionally, safety of the human partner in a shared workspace is explicitly ensured with energy transfer control. Teleoperation of a team of robot manipulators for a cooperative manipulation task is considered, similar to the setting proposed in Chapter 4. The results presented in this chapter have been partially published in [AMH17].

Chapter 6: Overlapping Shared Control

This chapter addresses Challenges 5-6. Role adjustment of the human and the robot partners in haptic interaction is modeled within the game-theoretical framework. The human behavior is, therefore, modeled with a cost function (Challenge 5). The optimal control of the human partner and the autonomy partner are computed to obtain Nash equilibrium (Challenge 6). The results presented in this chapter have been partially published in [MH20].

1.4 Discussion

The goal of this thesis is to develop a shared-control framework for continuous haptic human-robot interaction. Furthermore, two modes of interaction are considered: human-robot interaction (single-human-single-robot) and human-robot team interaction (single-human-robot-team). The human partner is in the active role by continuously providing control inputs during the task execution.

The existing literature provides many individual studies on suitable interaction paradigms, control approaches, interfaces and models for human-robot interaction. However, a systematic control-theoretical understanding of the human-robot closed-loop system requirements, limitations and performance is still missing. A formal analysis of human-robot interaction from the control-theoretical perspective may provide guidelines on the appropriate shared-control approach.

In this thesis, different human-robot interaction paradigms, that do not depend on the complexity of the robot system, complexity of the task, or the interface between the human and the robot partners, are proposed. From the identified paradigms a set of formal guidelines on shared-control design are identified. This enables the development of a unified shared-control framework.

2

Interaction Paradigms for Human-Robot Teams

Depending on the responsibilities the human and the robot partners have in the execution of the task, it is reasonable to define *interaction paradigms* for human-robot teams. The specific aspects of the task can be assigned either to the human partner, the robot partner or both. In this thesis human-robot interaction is considered on *higher levels of abstraction*. In consequence, shared controllers of lower dimensionality, compared to the actual dimensionality of the interacting system, are developed. For that purpose the concepts of *behaviors*, *subtasks* and *tasks* are formally defined. The interaction paradigms are classified w.r.t. the *controllability property* of the interactive system.

Related Work and Open Problems

A comprehensive human-robot interaction taxonomy is introduced in [YD04], where it is classified w.r.t. multiple criteria, e.g. level of shared interaction among team members, interaction roles (supervisor, operator, teammate, programmer, bystander), type of human-robot physical proximity (avoiding, passing, following, approaching, touching), and autonomy level/amount of intervention (a continuum ranging from teleoperation to full autonomy). Varying levels of autonomy for human-robot interaction ranging from teleoperation (manual control) to full autonomy are proposed in [LTT+01] and [BY04]. However, a formal analysis of the levels of autonomy and the interaction paradigms, that can serve as control-design guidelines, is not provided. Furthermore, these taxonomies are focused on teleoperation scenarios, but do not consider direct physical human-robot interaction.

In [JCB12] a taxonomy of interactive behaviors between two agents, focused on physical interaction, is provided. The authors distinguish between *divisible* and *interactive tasks*. In divisible tasks, an agent can accomplish its subtasks without knowing anything about the actions of the other agent. The interactive tasks are further divided into *cooperative*, *collaborative* and *competitive*. According to the proposed taxonomy, cooperative tasks can be *assistive* (master-slave) and *educative* (teacher-student). However, the proposed taxonomy is suitable only for two-agent (single-human-single-robot) interactions and is not generalizable to interactions between a human partner and a multi-robot system.

The concept of *task abstraction*, see Definition 1.2.5, has been introduced in robotics to reduce the dimensionality of the problem, enable development of high-level controllers and achieve a complex task by executing a combination of simpler aspects of the task. For

example, in [MK97] a set of manipulation task primitives for single manipulators is introduced. Their combination enable execution of different manipulation tasks. Similarly, task abstraction is employed on more complex robot systems (e.g. humanoids) by combining *behavior primitives* [SK05]. Task abstraction concept is also applied to multi-robot systems by defining its global and local behaviors. For example, in [BK04] *locked* and *shape behaviors* are introduced for multiple robots to describe their team motion and their formation shape, respectively. In [AAC08] similar task abstraction is used to control multi-robot system using *null-space based behavioral control*. Abstracting a control problem in this way increases the intuitiveness of human-robot interaction [BBE+07]. A solution to an open problem of defining a task abstraction approach that does not depend on the complexity of the robot system, but still allows the use of classical modeling and control approaches, is still an open problem.

However, classification of interaction paradigms for human-robot teams that is independent of the complexity of the robot system (single robot or multiple robots), type of interaction (teleoperation or direct physical), and that serves as a set of control design guidelines, is needed. Additionally, a task abstraction approach that reduces the dimensionality of the interactive system, increases intuitiveness of the interaction, but still allows the use of classical modeling and control approaches, needs to be developed.

In this chapter human-robot interaction paradigms are defined and formally classified. In order to make a distinction between interaction paradigms, the suitable tool for classification is the system property of *controllability*. The problem statement is provided in Section 2.1. The concepts of a *behavior* and a *subtask*, to abstract various aspects of the task are proposed in Section 2.2. The interaction paradigms are classified based on the way the subtasks are distributed among the human and the robot into: *direct*, *complementary* and *overlapping*. Their classification is formally proposed in Section 2.3. The concept of the *subtask-based* shared-control architecture that can be used for all the proposed interaction paradigms, followed by the control-design guidelines, is proposed in Section 2.4. The discussion is provided in Section 2.5.

2.1 Problem Statement

Let us consider a robot system in its configuration space as a general *multi-input multi-output (MIMO)* nonlinear, affine dynamic system

$$\begin{aligned} \dot{\boldsymbol{\xi}} &= \boldsymbol{f}(\boldsymbol{\xi}) + \boldsymbol{G}(\boldsymbol{\xi})\boldsymbol{u} \\ \boldsymbol{y} &= \boldsymbol{h}(\boldsymbol{\xi}), \end{aligned} \tag{2.1}$$

where $\boldsymbol{\xi} \in \mathcal{M}$ is the state vector defined on an n-dimensional, smooth manifold $\mathcal{M}$, $\boldsymbol{u} \in \mathcal{K}$ is the control input vector defined on an m-dimensional, smooth manifold $\mathcal{K}$ and $\boldsymbol{y} \in \mathcal{V}$ is the output vector defined on a p-dimensional, smooth manifold $\mathcal{V}$. The matrix $\boldsymbol{G} = [\boldsymbol{g}_1, ..., \boldsymbol{g}_m]$ consists of m column vectors. The tangent space of the manifold $\mathcal{M}$ at state $\boldsymbol{\xi}_0$ is denoted as $T_{\boldsymbol{\xi}_0}\mathcal{M}$.

If multiple robots are considered, the dynamics of each robot $i \in \mathbb{N}$, where $i = 1, ..., N$, is

$$\begin{aligned} \dot{\boldsymbol{\xi}}_i &= \boldsymbol{f}_i(\boldsymbol{\xi}_i) + \boldsymbol{G}_i(\boldsymbol{\xi}_i)\boldsymbol{u}_i \\ \boldsymbol{y}_i &= \boldsymbol{h}_i(\boldsymbol{\xi}_i), \end{aligned} \tag{2.2}$$

where $\boldsymbol{\xi}_i \in \mathcal{M}_i$ is the n_i-dimensional state vector, $\boldsymbol{u}_i \in \mathcal{K}_i$ is the m_i-dimensional control input vector and $\boldsymbol{y}_i \in \mathcal{V}_i$ is the p_i-dimensional output vector. The dynamic system of N robots is then obtained by concatenating N equations given with (2.2), where $\boldsymbol{\xi} = [\boldsymbol{\xi}_1^\top \dots \boldsymbol{\xi}_i^\top \dots \boldsymbol{\xi}_N^\top]^\top$ is the concatenated state, $\boldsymbol{u} = [\boldsymbol{u}_1^\top \dots \boldsymbol{u}_i^\top \dots \boldsymbol{u}_N^\top]^\top$ is the concatenated control input and $\boldsymbol{y} = [\boldsymbol{y}_1^\top \dots \boldsymbol{y}_i^\top \dots \boldsymbol{y}_N^\top]^\top$ is the concatenated output vector.

Remark 1. *The dynamic system representation of a robot system in (2.1) generalizes common modeling approaches of robot dynamics:*

- Kinematic (single integrator)
$$\dot{\boldsymbol{\xi}} = \boldsymbol{u}, \tag{2.3}$$
where $\boldsymbol{\xi} = \boldsymbol{x} \in \mathbb{R}^n$ is the position of the robot in Cartesian space. This is the simplest representation, typically used to model swarm agents.

- Point mass (double integrator)
$$\ddot{\boldsymbol{x}} = \boldsymbol{M}^{-1}\boldsymbol{u}, \tag{2.4}$$
where $\ddot{\boldsymbol{x}} \in \mathbb{R}^n$ is the position of the robot system in Cartesian space and $\boldsymbol{M} \in \mathbb{R}^{m\times n}$ is its mass matrix. By defining $\boldsymbol{\xi} = [\boldsymbol{x}^\top \dot{\boldsymbol{x}}^\top]^\top \in \mathbb{R}^{2n}$ as the state, the dynamics (2.4) in the form (2.1) is
$$\dot{\boldsymbol{\xi}} = \underbrace{\begin{bmatrix} \boldsymbol{0} & \boldsymbol{I} \\ \boldsymbol{0} & \boldsymbol{0} \end{bmatrix}}_{\boldsymbol{f}(\boldsymbol{\xi})} \boldsymbol{\xi} + \underbrace{\begin{bmatrix} \boldsymbol{0} \\ \boldsymbol{M}^{-1} \end{bmatrix}}_{\boldsymbol{G}(\boldsymbol{\xi})} \boldsymbol{u}. \tag{2.5}$$

- Euler-Lagrange
$$\boldsymbol{M}(\boldsymbol{\theta})\ddot{\boldsymbol{\theta}} + \boldsymbol{c}(\boldsymbol{\theta}, \dot{\boldsymbol{\theta}}) + \boldsymbol{\tau}_g(\boldsymbol{\theta}) = \boldsymbol{\tau}, \tag{2.6}$$
where $\boldsymbol{\theta} \in \mathbb{R}^n$ is the vector of generalized coordinates, $\boldsymbol{M}(\boldsymbol{\theta}) \in \mathbb{R}^{n\times n}$ is the inertia matrix, $\boldsymbol{c}(\boldsymbol{\theta}, \dot{\boldsymbol{\theta}}) \in \mathbb{R}^n$ the vector of Coriolis and centrifugal forces, $\boldsymbol{\tau}_g(\boldsymbol{\theta}) \in \mathbb{R}^n$ the vector of gravitational forces, and $\boldsymbol{\tau} \in \mathbb{R}^n$ is the vector of control torques. By defining $\boldsymbol{\xi} = [\boldsymbol{\theta}^\top \dot{\boldsymbol{\theta}}^\top]^\top \in \mathbb{R}^{2n}$ as the state, the dynamics (2.4) in the form (2.1) is
$$\dot{\boldsymbol{\xi}} = \underbrace{\begin{bmatrix} \dot{\boldsymbol{\theta}} \\ -\boldsymbol{M}^{-1}(\boldsymbol{\theta})(\boldsymbol{c}(\boldsymbol{\theta}, \dot{\boldsymbol{\theta}}) + \boldsymbol{\tau}_g(\boldsymbol{\theta})) \end{bmatrix}}_{\boldsymbol{f}(\boldsymbol{\xi})} + \underbrace{\begin{bmatrix} \boldsymbol{0} \\ \boldsymbol{M}^{-1}(\boldsymbol{\theta}) \end{bmatrix}}_{\boldsymbol{G}(\boldsymbol{\xi})} \boldsymbol{\tau}. \tag{2.7}$$

- port-Hamiltonian
$$\begin{aligned} \dot{\boldsymbol{\xi}} &= \underbrace{[\boldsymbol{J}(\boldsymbol{\xi}) - \boldsymbol{D}(\boldsymbol{\xi})]\frac{\partial \mathcal{H}}{\partial \boldsymbol{\xi}}(\boldsymbol{\xi})}_{\boldsymbol{f}(\boldsymbol{\xi})} + \boldsymbol{G}(\boldsymbol{\xi})\boldsymbol{u} \\ \boldsymbol{y} &= \underbrace{\boldsymbol{G}^\top(\boldsymbol{\xi})\frac{\partial \mathcal{H}}{\partial \boldsymbol{\xi}}(\boldsymbol{\xi})}_{\boldsymbol{h}(\boldsymbol{\xi})}, \end{aligned} \tag{2.8}$$
where $\boldsymbol{\xi} \in \mathcal{M}$ is an n-dimensional vector of configuration variables, $\boldsymbol{J}(\boldsymbol{\xi}) \in \mathbb{R}^{n\times n}$ is a skew-symmetric structure matrix and $\boldsymbol{D}(\boldsymbol{\xi}) \in \mathbb{R}^{n\times n}$ is a damping/friction matrix, while $\mathcal{H} \in \mathbb{R}$ is a Hamiltonian function.

Let the control input $\boldsymbol{u}$ be defined as a stacked vector of the input commands provided by the two control sources - *the human and the autonomous robot controllers*

$$\boldsymbol{u} = [\underbrace{u_{h,1}, ..., u_{h,l}}_{\boldsymbol{u}_h}, \underbrace{u_{a,(l+1)}, ..., u_{a,m}}_{\boldsymbol{u}_a}]^\top, \tag{2.9}$$

where subscripts h and a indicate the human and the robot control inputs, respectively. Analogously, let us represent the matrix $\boldsymbol{G}$ as

$$\boldsymbol{G} = [\boldsymbol{G}_h \; \boldsymbol{G}_a] = [\underbrace{\boldsymbol{g}_1 \cdots \boldsymbol{g}_l}_{\boldsymbol{G}_h} \; \underbrace{\boldsymbol{g}_{l+1} \cdots \boldsymbol{g}_m}_{\boldsymbol{G}_a}],$$

so that $\boldsymbol{G}_h$ maps $\boldsymbol{u_h}$ and $\boldsymbol{G}_a$ maps $\boldsymbol{u}_a$. The challenges to be resolved in this chapter are summarized with Problems 1-2.

Problem 1. *Define higher level of abstraction in human-robot team task execution from a control-theoretical perspective.*

Problem 2. *Define interaction paradigms depending on the solution to Problem 1 and using the controllability property of the human-robot interactive system.*

2.2 Behaviors and Subtasks

In this section the concept of task abstraction is developed with the formal introduction of the concepts of *behavior*, *subtask* and *task*. Behaviors enable modeling and control of the human-robot system on a lower-dimensional space, which is defined w.r.t. the task. Therefore, it is more intuitive, less complex, but still allows the use of standard modeling and control approaches. The formal definition of *behaviors* is given below.

Definition 2.2.1. *Behavior* i *is an abstract state $\boldsymbol{\xi}_{b,i} \in \mathcal{M}_{b,i}$. It is a smooth submersion projection mapping from the state manifold $\mathcal{M}$ onto an $n_{b,i}$-dimensional manifold $\mathcal{M}_{b,i}$*

$$\boldsymbol{\phi}_i : \mathcal{M} \to \mathcal{M}_{b,i}, \quad \boldsymbol{\xi}_{b,i} = \boldsymbol{\phi}_i(\boldsymbol{\xi}). \tag{2.10}$$

The vector $\dot{\boldsymbol{\xi}}_{b,i}$ is the tangent map of $\boldsymbol{\xi}_{b,i}$

$$T\boldsymbol{\phi}_i : T\mathcal{M} \to T\mathcal{M}_{b,i}. \tag{2.11}$$

Remark 2. *According to Definition 2.2.1, behaviors are projections of robot states so that $dim(\mathcal{M}_{b,i}) \leq dim(\mathcal{M})$. Therefore, they impose* equality constraints *onto the system (2.1) and can, consequently, define system outputs*

$$\boldsymbol{y} = \begin{bmatrix} \boldsymbol{x}_{b,1} \\ \vdots \\ \boldsymbol{x}_{b,k} \end{bmatrix} = \underbrace{\begin{bmatrix} \boldsymbol{\phi_1}(\boldsymbol{\xi}) \\ \vdots \\ \boldsymbol{\phi_k}(\boldsymbol{\xi}) \end{bmatrix}}_{\boldsymbol{\phi}(\boldsymbol{\xi})}, \tag{2.12}$$

where $\boldsymbol{x}_{b,i} \in \mathcal{M}_{b,i}, i = 1, ..., k$ are abstract, behavior coordinates.

The consequence of the Remark 2 is that the appropriate design of input-output controllers leads to the achievement of subtasks, i.e. control goals associated with the system outputs/behaviors.

A concept of a *behavior Jacobian*, associated with the differential map of the behavior (2.11), is introduced with Definition 2.2.2.

Definition 2.2.2. *The behavior Jacobian is a full-rank matrix*

$$\boldsymbol{J}_b(\boldsymbol{\xi}) = \begin{bmatrix} \boldsymbol{J}_{b,1}(\boldsymbol{\xi}) \\ \vdots \\ \boldsymbol{J}_{b,k}(\boldsymbol{\xi}) \end{bmatrix} = \begin{bmatrix} \dfrac{\partial \boldsymbol{\phi_1}(\boldsymbol{\xi})}{\partial \boldsymbol{\xi}} \\ \vdots \\ \dfrac{\partial \boldsymbol{\phi_k}(\boldsymbol{\xi})}{\partial \boldsymbol{\xi}} \end{bmatrix}, \tag{2.13}$$

where $\boldsymbol{J}_{b,i}, \forall i = 1, .., k$, *is the* i^{th} *behavior Jacobian.*

Note that the defined behaviors can be *artificial*, imposed by the task requirements, or *natural*, imposed by the system limits or the environment. Furthermore, they are suitable for single robots as well as multi-robot systems, or other complex robot structures, e.g. humanoids.

Example 2.2.1. (Team behavior). *Consider the poses of* N *robots* $\boldsymbol{x}_i \in \mathbb{R}^2$, $i = 1, ..., N$, *modeled with (2.3). Then the concatenated state of the multi-robot system is* $\boldsymbol{\xi} = [\boldsymbol{x}_1^\top ... \boldsymbol{x}_N^\top]^\top$. *The center point of such a robot system*

$$\boldsymbol{\xi}_b = \boldsymbol{x}_b = \frac{1}{N} \sum_{i=1}^{N} \boldsymbol{x}_i \in \mathbb{R}^2, \tag{2.14}$$

is a behavior*, since (2.14) is a submersion projection mapping. This is in literature termed as* global *or* collective *behavior of the multi-robot/swarm system [AAC09].*

Remark 3. *The introduced concept of* behaviors *generalizes to the projection from the configuration space to the* task space *in Cartesian coordinates of robot manipulators. In that sense, forward kinematics*

$$\boldsymbol{x} = \boldsymbol{\phi}_{FK}(\boldsymbol{\theta}),$$

represents a behavior in Cartesian space, that is determined by the manipulator kinematic structure, i.e. the imposed behavior is natural.

Now it is possible to formally define the concepts of a *subtask* and a *task*. An example of a task and its required subtasks follows these definitions.

Definition 2.2.3. *A subtask* i *is a behavior* $\boldsymbol{\xi}_{b,i}$ *and its associated control objective* $\boldsymbol{\xi}_{b,i}^d$.

Definition 2.2.4. *A task is a collection of subtasks, i.e. a concatenated vector of all the required behaviors* $\boldsymbol{\xi}_b = [\boldsymbol{\xi}_{b,1}^\top ... \boldsymbol{\xi}_{b,i}^\top ... \boldsymbol{\xi}_{b,k}^\top]^\top$ *and a concatenated vector of all the associated control objectives* $\boldsymbol{\xi}_b^d = [\boldsymbol{\xi}_{b,1}^{d\top} ... \boldsymbol{\xi}_{b,i}^{d\top} ... \boldsymbol{\xi}_{b,k}^{d\top}]^\top$.

Example 2.2.2. (Formation control.) *In order to manipulate a common object in* $\mathbb{R}^2$ *from an initial to a final configuration, a team of* N *robot manipulators needs to collectively move to a desired location (see Example 2.2.1), while maintaining a fixed formation. Therefore, we can define two subtask functions: (i)* collective motion $\boldsymbol{f}_{s,1}(\cdot)$ *and (ii)* formation control $\boldsymbol{f}_{s,2}(\cdot)$

$$\begin{aligned}\boldsymbol{f}_{s,1}(\boldsymbol{\xi}_{b,1}, \boldsymbol{\xi}^d_{b,1}) &= \boldsymbol{\xi}_{b,1} - \boldsymbol{\xi}^d_{b,1} = \frac{1}{N}\sum_{i=1}^{N} \boldsymbol{x}_i - \boldsymbol{x}^d_{b,1},\\ \boldsymbol{f}_{s,2}(\boldsymbol{\xi}_{b,2}, \boldsymbol{\xi}^d_{b,2}) &= \boldsymbol{\xi}_{b,2} - \boldsymbol{\xi}^d_{b,2} = \begin{bmatrix} (\boldsymbol{x}_2 - \boldsymbol{x}_1) - \boldsymbol{d}_{12} \\ \vdots \\ (\boldsymbol{x}_N - \boldsymbol{x}_{N-1}) - \boldsymbol{d}_{(N-1)N} \end{bmatrix},\end{aligned} \tag{2.15}$$

where $\boldsymbol{x}_i \in \mathbb{R}^2$ *is the position of the* i^{th} *robot in the plane,* $\boldsymbol{x}^d_{b,1} \in \mathbb{R}^2$ *is the desired position of the robot team entity, and* $\boldsymbol{d}_{(i-1)i} \in \mathbb{R}^2$ *is the desired relative position bettwen robots* $i-1$ *and* i*. In a similar scenario, the human directly controls the mean position of the robot team,* $\boldsymbol{x}_{b,1} \in \mathbb{R}^2$ *and formation control is performed autonomously in [SMH15, SKE15]. Figure 2.1 depicts an example of such a task for three robots.*

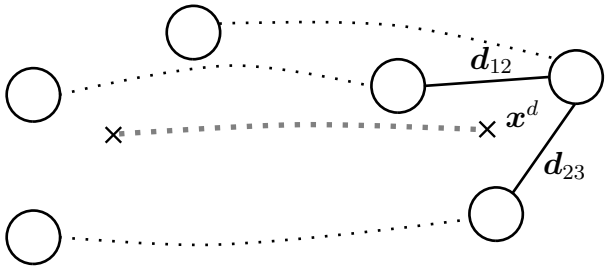

Figure 2.1: Example of formation control.

Equality constraint (2.10) can be used as a nonlinear, local change of coordinates, that can be applied to the dynamic system (2.1). Since (2.10) is task-based, such transformation *abstracts* the system into subsystems characterized by the imposed constraint, i.e. behavior. Therefore, this provides the solution to Problem 1. The following proposition gives the required conditions that need to be satisfied in order to be able to transform the system to new coordinates and its proof is given in Appendix 8.

Proposition 2.2.1. *Suppose* $\sum_{i=1}^{k} k_i = n$*. Furthermore, suppose the abstractions*

$$\boldsymbol{\phi}(\boldsymbol{\xi}) = [\boldsymbol{\phi}_1^\top(\boldsymbol{\xi}) \ldots \boldsymbol{\phi}_i^\top(\boldsymbol{\xi}) \ldots \boldsymbol{\phi}_k^\top(\boldsymbol{\xi})]^\top,$$

are smooth functions defined on a subset $\mathcal{M}_s \subset \mathcal{M}$ *and that the behavior Jacobian* $\boldsymbol{J}_b(\boldsymbol{\xi})$*, defined in (2.13), is nonsingular at point* $\boldsymbol{\xi} = \boldsymbol{\xi}_0 \in \mathcal{M}_s$*. Then,* $\boldsymbol{\phi}(\boldsymbol{\xi})$ *is a local diffeomorphism and (2.1) can be transformed into*

$$\begin{aligned}\dot{\boldsymbol{\xi}}_b &= \boldsymbol{f}_b(\boldsymbol{\xi}_b) + \boldsymbol{G}_b(\boldsymbol{\xi}_b)\boldsymbol{u}\\ \boldsymbol{y}_b &= \boldsymbol{h}_b(\boldsymbol{\xi}_b),\end{aligned} \tag{2.16}$$

where

$$\begin{aligned}\boldsymbol{f}_b(\boldsymbol{\xi}_b) &= [\boldsymbol{J}_b(\boldsymbol{\xi})\boldsymbol{f}(\boldsymbol{\xi})]_{\boldsymbol{\xi}=\boldsymbol{\phi}^{-1}(\boldsymbol{\xi}_b)}\\ \boldsymbol{G}_b(\boldsymbol{\xi}_b) &= [\boldsymbol{J}_b(\boldsymbol{\xi})\boldsymbol{G}(\boldsymbol{\xi})]_{\boldsymbol{\xi}=\boldsymbol{\phi}^{-1}(\boldsymbol{\xi}_b)}\\ \boldsymbol{h}_b(\boldsymbol{\xi}_b) &= [\boldsymbol{h}(\boldsymbol{\xi})]_{\boldsymbol{\xi}=\boldsymbol{\phi}^{-1}(\boldsymbol{\xi}_b)}.\end{aligned}$$

The consequence of Proposition 2.2.1 is that the system (2.1) is transformed into k *behavior subsystems* that preserve the initial model structure and can be controlled using classical control approaches, while having a task-based interpretation

$$\begin{aligned}
\dot{\boldsymbol{\xi}}_{b,1} &= \boldsymbol{f}_{b,1}(\boldsymbol{\xi}_b) + \boldsymbol{G}_{b,1}(\boldsymbol{\xi}_b)\boldsymbol{u} \\
&\vdots \\
\dot{\boldsymbol{\xi}}_{b,k} &= \boldsymbol{f}_{b,k}(\boldsymbol{\xi}_b) + \boldsymbol{G}_{b,k}(\boldsymbol{\xi}_b)\boldsymbol{u} \\
\boldsymbol{y}_{b,1} &= \boldsymbol{h}_{b,1}(\boldsymbol{\xi}_b) \\
&\vdots \\
\boldsymbol{y}_{b,k} &= \boldsymbol{h}_{b,k}(\boldsymbol{\xi}_b).
\end{aligned} \tag{2.17}$$

Figure 2.2 depicts how responsibilities over task execution can be assigned to the human and the robot partners based on the introduced concepts of task, subtasks, and behaviors. Tasks are achieved by a suitable combination of predefined *behaviors*, retrieved from a *library of behaviors*. The subtasks are prioritized according to the current state of the environment, decoupled to avoid interference if necessary, and preferably allocated dynamically to the human and/or the robot autonomous controllers.

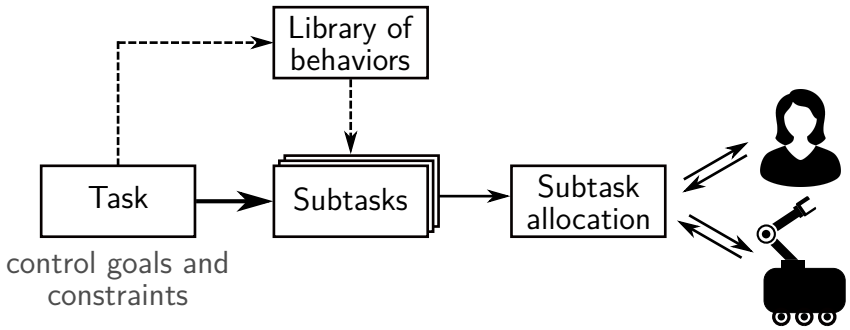

Figure 2.2: Task is formulated as a set of control goals and constraints (artificial and natural). Behaviors required to achieve a task are selected from the library of behaviors. Assigning specific control objectives to the behaviors generates a set of subtasks that can be allocated to the human and/or the robot partner.

Let us for further convenience define sets of behaviors controlled by the human and the robot partners, so that $\mathcal{M}_{bh}$ is a union of all the behaviors controlled by the human

$$\mathcal{M}_{bh} = \mathcal{M}_{b,1} \cup ... \cup \mathcal{M}_{b,d}$$

and let $\mathcal{M}_{ba}$ be a union of all the behaviors controlled by the robot

$$\mathcal{M}_{ba} = \mathcal{M}_{b,1} \cup ... \cup \mathcal{M}_{b,p}.$$

Based on how the behaviors are allocated to the partners, three interaction paradigms are proposed in the following section.

(a) Manual control. (b) Autonomous control.

Figure 2.3: Direct interaction paradigm.

2.3 Interaction Paradigms

In this section the classification of interaction paradigms for continuous, haptic human-robot interaction is provided with novel taxonomy. The interaction paradigms depend on the way the subtasks are allocated to the human and the robot partners. They are classified according to the controllability properties of the behavior dynamics subsystems (2.17) and are classified into: (i) *direct*, (ii) *complementary* and (iii) *overlapping* interaction paradigms. For that purpose the controllability property of the system (2.17) is analyzed locally using *controllability distribution* formulated in Definition 2.3.1. The following sections formally introduce the three interaction paradigms.

Definition 2.3.1 ([NVdS90])**.** *Controllability of the system (2.1) is in the following form*

$$\Delta^c(\boldsymbol{\xi}) = [\boldsymbol{G}(\boldsymbol{\xi}),\ ad_{\boldsymbol{f}}\boldsymbol{G}(\boldsymbol{\xi}), ..., ad_{\boldsymbol{f}}^{n-1}\boldsymbol{G}(\boldsymbol{\xi})], \tag{2.18}$$

where $ad_{\boldsymbol{f}}^0\boldsymbol{G} = \boldsymbol{G}$ *and* $ad_{\boldsymbol{f}}^i\boldsymbol{G} = [\boldsymbol{f},\ ad_{\boldsymbol{f}}^{i-1}\boldsymbol{G}]$ *is the* Lie product *of* $\boldsymbol{f}$ *and* $ad_{\boldsymbol{f}}^{i-1}\boldsymbol{G}$ *for* $i = 1, ..., n$ *[Isi13]. Controllability of the individual behavior subsystems in (2.17) is analogously*

$$\Delta_{b,i}^c(\boldsymbol{\xi}_b) = [\boldsymbol{G}_{b,i}(\boldsymbol{\xi}_b),\ ad_{\boldsymbol{f}_{b,i}}\boldsymbol{G}_{b,i}(\boldsymbol{\xi}_b), ..., ad_{\boldsymbol{f}_{b,i}}^{n-1}\boldsymbol{G}_{b,i}(\boldsymbol{\xi})], \quad i = 1, ..., k. \tag{2.19}$$

2.3.1 Direct Interaction Paradigm

First, a *direct interaction paradigm* is defined. It includes *manual* and *autonomous* control - two ends of the shared-control spectrum in Figure 1.5. It is formally defined below.

Definition 2.3.2. *Interaction paradigm is* direct *if the behavior subsystems in (2.17)* $\forall i = 1, ..., k$*, are locally controllable either with the control inputs* $\boldsymbol{u}_h$ *(manual interaction paradigm) or* $\boldsymbol{u}_a$ *(autonomous interaction paradigm).*

According to Definition 2.3.2, $\mathcal{M}_{bh} = \mathcal{M}_{b,1} \cup ... \cup \mathcal{M}_{b,k}$ and $\mathcal{M}_{ba} = \emptyset$ for the manual direct interaction paradigm and $\mathcal{M}_{ba} = \mathcal{M}_{b,1} \cup ... \cup \mathcal{M}_{b,k}$ and $\mathcal{M}_{bh} = \emptyset$ for the manual interaction paradigm, as depicted in Figure 2.3.

Example 2.3.1. (Direct interaction paradigm.) *Examples of the direct interaction paradigm in robotics can be direct physical human-robot interaction or bilateral teleoperation of the robot system with no level of autonomy. The human operator provides control input to all the available degrees of freedom either by applying forces directly on the robot, or by guiding the robot through the haptic teleoperation interface, respectively.*

In the remainder, formal conditions under which direct interaction paradigm is achieved, are identified. In the remainder of this section, focus is put on the manual direct interaction paradigm. Analogous conclusions are valid for the autonomous interaction paradigm. Let us represent matrix $\boldsymbol{G}_{b,i}$ in (2.17) as $\boldsymbol{G}_{b,i} = [\boldsymbol{G}_{bh,i}\, \boldsymbol{G}_{ba,i}]$, $\forall i = 1, ..., k$, where $\boldsymbol{G}_{bh,i}$ maps $\boldsymbol{u}_h$ on $T\mathcal{M}_{b,i}$ and where $\boldsymbol{G}_{ba,i}$ maps $\boldsymbol{u}_a$ on $T\mathcal{M}_{b,i}$. The distributions spanned by the vector fields in $\boldsymbol{G}_{b,i}$, $\boldsymbol{G}_{bh,i}$ and $\boldsymbol{G}_{ba,i}$, $\forall i = 1, ..., k$ are

$$\begin{aligned}
\Delta^G_{b,i}(\boldsymbol{\xi}_b) &= \text{span}\{\boldsymbol{g}_{b,1}, ..., \boldsymbol{g}_{b,m}\}, \quad \forall \boldsymbol{\xi}_b \in \mathcal{M}_{b,i} \\
\Delta^G_{bh,i}(\boldsymbol{\xi}_b) &= \text{span}\{\boldsymbol{g}_{bh,1}, ..., \boldsymbol{g}_{bh,l}\}, \quad \forall \boldsymbol{\xi}_b \in \mathcal{M}_{b,i} \\
\Delta^G_{ba,i}(\boldsymbol{\xi}_b) &= \text{span}\{\boldsymbol{g}_{ba,l+1}, ..., \boldsymbol{g}_{ba,m}\}, \quad \forall \boldsymbol{\xi}_b \in \mathcal{M}_{b,i}
\end{aligned} \tag{2.20}$$

and the corresponding controllability distributions, analogously to (2.18), are

$$\begin{aligned}
\Delta^c_{bh,i}(\boldsymbol{\xi}_b) &= [\boldsymbol{G}_{bh,i}(\boldsymbol{\xi}_b),\ \text{ad}_{\boldsymbol{f}_{b,i}}\boldsymbol{G}_{bh,i}(\boldsymbol{\xi}_b), ..., \text{ad}^{n-1}_{\boldsymbol{f}_{b,i}}\boldsymbol{G}_{bh,i}(\boldsymbol{\xi})], \\
\Delta^c_{ba,i}(\boldsymbol{\xi}_b) &= [\boldsymbol{G}_{ba,i}(\boldsymbol{\xi}_b),\ \text{ad}_{\boldsymbol{f}_{b,i}}\boldsymbol{G}_{ba,i}(\boldsymbol{\xi}_b), ..., \text{ad}^{n-1}_{\boldsymbol{f}_{b,i}}\boldsymbol{G}_{ba,i}(\boldsymbol{\xi}_b)].
\end{aligned} \tag{2.21}$$

In order to ensure controllability of the behavior system (2.17) with $\boldsymbol{u}_h$ and according to Definition 2.3.2, the distributions $\Delta^G_{bh,i}$ need to satisfy *involutivity* property, which is stated in Assumption 2.3.1.

Remark 4. *In order to guarantee manual direct interaction paradigm, $\boldsymbol{u}_a$ should not have an effect on the behavior subsystems in (2.17), i.e. the subsystems should be uncontrollable to $\boldsymbol{u}_a$. This can be achieved if: (i) the system has no autonomy, $\boldsymbol{u}_a = \boldsymbol{0}$, as in Example 2.3.1 or (ii) $\boldsymbol{u}_a$ is treated as a* disturbance *and an appropriate* disturbance decoupling controller *is developed to mitigate its effect [Isi13]. The same holds for the role of $\boldsymbol{u}_h$ in autonomous direct interaction paradigm.*

Assumption 2.3.1. *The distributions $\Delta^G_{b,i}, i = 1, ..., k$ is* involutive*, i.e. the Lie product of any $g_{b,ii}$ and $g_{b,ij}$ is contained in the distribution $\Delta^G_{b,i}$*

$$g_{b,ii} \in \Delta^G_{b,i},\ g_{b,ij} \in \Delta^G_{b,i}\ \Rightarrow [g_{b,ii},\ g_{b,ij}] \in \Delta^G_{b,i}, \tag{2.22}$$

where $[g_{b,ii},\ g_{b,ij}] = \dfrac{\partial g_{b,ij}}{\partial \boldsymbol{x}} g_{b,ii} - \dfrac{\partial g_{b,ii}}{\partial \boldsymbol{x}} g_{b,ij}$ is the Lie product of $g_{b,ii}$ and $g_{b,ij}$.

Assumption 2.3.2. *The distributions $\Delta^G_{ba,i}, i = 1, ..., k$ are empty sets.*

Assumption 2.3.1 implies that the distribution $\Delta^G_{b,i}$ is in the tangent space of $\mathcal{M}_{b,i}$, $T\mathcal{M}_{b,i}$, and leads to an integrable system, while Assumption 2.3.2 implies that an appropriate disturbance decoupling control has been applied or that the robot system has no autonomy.

Now it is possible to formally propose conditions under which an interaction is direct manual w.r.t. its accessibility/controllability property.

Proposition 2.3.1. *If Assumption 2.3.1 is satisfied and if*

$$\begin{aligned}
\sum_{i=1}^{k} dim\{\Delta^c_{bh,i}\} &= n \\
\sum_{i=1}^{k} dim\{\Delta^c_{ba,i}\} &= 0,
\end{aligned} \tag{2.23}$$

then the behavior subsystems in (2.17) are accessible *from* $\boldsymbol{\xi}_b$ *by the control input* $\boldsymbol{u}_h$ *and* inaccessible *by the control input* $\boldsymbol{u}_a$.

The controllability is a stronger property that does not always hold for nonlinear affine systems, see the remark below.

Remark 5. *If the drift of (2.17) is compensated, i.e.* $\boldsymbol{f}_{b,i} = \boldsymbol{0}, i = 1, ..., k$, *then the behavior subsystems in (2.17) are* controllable *from* $\boldsymbol{\xi}_b$ *by the control input* $\boldsymbol{u}_h$ *and* uncontrollable *by the control input* $\boldsymbol{u}_a$.

For the general proof of accessibility and controllability of nonlinear affine systems, the reader is refered to [NVdS90].

2.3.2 Complementary Interaction Paradigm

A complementary interaction paradigm enables the human and the robot partners to control different aspects of the task, i.e. different subtasks. The formal definition of the complementary interaction paradigm is given below.

Definition 2.3.3. *Interaction paradigm is* complementary *if a set of* d *behavior subsystems in (2.17) are controllable with the control input* $\boldsymbol{u}_h$ *and the remaining* $k - d$ *behavior subsystems are controllable with the control input* $\boldsymbol{u}_a$.

According to Definition 2.3.3, $\mathcal{M}_{bh} = \mathcal{M}_{b,1} \cup ... \cup \mathcal{M}_{b,d}$ and $\mathcal{M}_{ba} = \mathcal{M}_{b,d+1} \cup ... \cup \mathcal{M}_{b,k}$, as depicted illustratively in Figure 2.4.

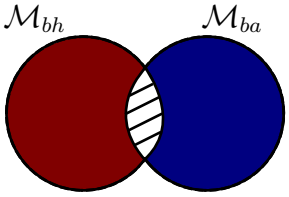

Figure 2.4: Complementary interaction paradigm.

Let us introduce a concatenated input matrix $\boldsymbol{G}_b$ in (2.17), structured as

$$\boldsymbol{G}_b = \begin{bmatrix} \boldsymbol{G}_{b,1} \\ \vdots \\ \boldsymbol{G}_{b,k} \end{bmatrix} = \begin{bmatrix} \boldsymbol{G}_{bh,1} & \boldsymbol{G}_{ba,1} \\ \vdots & \vdots \\ \boldsymbol{G}_{bh,k} & \boldsymbol{G}_{ba,k} \end{bmatrix}, \tag{2.24}$$

where $\boldsymbol{G}_{bh,i} = [\boldsymbol{g}_{bh,i1}, ..., \boldsymbol{g}_{h,il}]$ and $\boldsymbol{G}_{ba,i} = [\boldsymbol{g}_{ba,i(l+1)}, ..., \boldsymbol{g}_{a,im}]$. Let us assume, without loss of generality, after possibly a change of coordinates, that the first d behavior subsystems in (2.17) are controllable by $\boldsymbol{u}_h$ and the remaining $k - d$ subsystems are controllable by $\boldsymbol{u}_a$.

Remark 6. *In order to ensure the control inputs* $\boldsymbol{u}_h$ *affect first* d *subsystems in (2.17) and* $\boldsymbol{u}_a$ *affect the remaining* $k-d$ *subsystems, the matrices* $\boldsymbol{G}_{ba,1}, ..., \boldsymbol{G}_{ba,d}$ *as well as the matrices* $\boldsymbol{G}_{bh,d+1}, ..., \boldsymbol{G}_{bh,k}$ *need to be zero. In this way,* $\boldsymbol{u}_a$ *has no effect on the first* d *subsystems and* $\boldsymbol{u}_h$ *has no effect on the remaining* $k - d$ *subsystems.*

In the remainder the conditions under which an interaction is complementary w.r.t. its controllability property, are proposed. For that purpose, let us denote the tanget manifolds accessible to $\boldsymbol{u}_h$ and $\boldsymbol{u}_a$ respectively as

$$T\mathcal{M}_{bh} = T\mathcal{M}_{b,1} \cup ... \cup T\mathcal{M}_{b,d}$$
$$T\mathcal{M}_{ba} = T\mathcal{M}_{b,d+1} \cup ... \cup T\mathcal{M}_{b,k},$$

and impose Assumption 2.3.3.

Assumption 2.3.3. *The distributions in $T\mathcal{M}_{b,i}, i = 1, .., d$ are invariant under their corresponding vector fields $\boldsymbol{f}_{b,i}$, $\boldsymbol{g}_{bh,i1}, ..., \boldsymbol{g}_{bh,il}$, $i = 1, ..., d$, i.e. for any $\boldsymbol{\xi}_{b,i} \in \mathcal{M}_{b,i}, i = 1, .., d$*

$$\dot{\boldsymbol{\xi}}_{b,i} \in T\mathcal{M}_{b,i} \Rightarrow [\boldsymbol{f}_{b,i}, \dot{\boldsymbol{\xi}}_{b,i}] \in T\mathcal{M}_{b,i},$$
$$\dot{\boldsymbol{\xi}}_{b,i} \in T\mathcal{M}_{b,i} \Rightarrow [\boldsymbol{g}_{bh,ij}, \dot{\boldsymbol{\xi}}_{b,i}] \in T\mathcal{M}_{b,i}, \quad i = 1, ..., d, j = 1, ..., l$$

and the distributions in $T\mathcal{M}_{b,i}, i = d+1, .., k$ are invariant under their corresponding vector fields $\boldsymbol{f}_{b,i}$, $\boldsymbol{g}_{ba,i1}, ..., \boldsymbol{g}_{ba,il}$, $i = d+1, ..., k$, i.e. for any $\boldsymbol{\xi}_{b,i} \in \mathcal{M}_{b,i}, i = d+1, .., k$

$$\dot{\boldsymbol{\xi}}_{b,i} \in T\mathcal{M}_{b,i} \Rightarrow [\boldsymbol{f}_{b,i}, \dot{\boldsymbol{\xi}}_{b,i}] \in T\mathcal{M}_{b,i},$$
$$\dot{\boldsymbol{\xi}}_{b,i} \in T\mathcal{M}_{b,i} \Rightarrow [\boldsymbol{g}_{ba,ij}, \dot{\boldsymbol{\xi}}_{b,i}] \in T\mathcal{M}_{b,i}, \quad i = d+1, ..., k, j = l+1, ..., m.$$

The relevance of Assumption 2.3.3 is clear from the following Lemma, important in order to formally propose conditions under which an interaction is complementary using the system controllability property.

Lemma 1. *Let $T\mathcal{M}_{b,i}$ be nonsingular distributions and let Assumption 2.3.3 hold. Then, it is possible to find a neighborhood $\mathcal{U}_{b,i}$ of each state $\boldsymbol{\xi}_{b,i} \in \mathcal{M}_{b,i}$ and transformations $\boldsymbol{\xi}_{bh} = \boldsymbol{\phi}_{bh}(\boldsymbol{\xi}_b)$ and $\boldsymbol{\xi}_{ba} = \boldsymbol{\phi}_{ba}(\boldsymbol{\xi}_b)$, defined on $\mathcal{U}_{b,i}$, such that they are smooth submersion projection mappings and such that the system (2.17) is locally transformed to*

$$\begin{aligned} \dot{\boldsymbol{\xi}}_{bh} &= \boldsymbol{f}_{bh}(\boldsymbol{\xi}_{bh}, \boldsymbol{\xi}_{ba}) + \boldsymbol{G}_{bh}(\boldsymbol{\xi}_{bh}, \boldsymbol{\xi}_{ba})\boldsymbol{u}_h \\ \dot{\boldsymbol{\xi}}_{ba} &= \boldsymbol{f}_{ba}(\boldsymbol{\xi}_{bh}, \boldsymbol{\xi}_{ba}) + \boldsymbol{G}_{ba}(\boldsymbol{\xi}_{bh}, \boldsymbol{\xi}_{ba})\boldsymbol{u}_a, \end{aligned} \tag{2.25}$$

where $\boldsymbol{\xi}_{bh} \in \mathcal{M}_{bh}$ is a d-dimensional state and $\boldsymbol{\xi}_{ba} \in \mathcal{M}_{ba}$ is a $(k-d)$-dimensional state in the new coordinates. Furthermore, $\boldsymbol{\xi}_{bh}$ is constructed so that the last $k-d$ elements of its Jacobian, $\boldsymbol{J}_{bh} = \partial\boldsymbol{\phi}_{bh}/\partial\boldsymbol{\xi}_b$, span the orthogonal subspace of $T\mathcal{M}_{ba}$, $T\mathcal{M}_{ba}^{\perp}$, while $\boldsymbol{\xi}_{ba}$ is constructed so that the first d elements of its Jacobian, $\boldsymbol{J}_{ba} = \partial\boldsymbol{\phi}_{ba}/\partial\boldsymbol{\xi}_b$, span the orthogonal subspace of $T\mathcal{M}_{bh}$, $T\mathcal{M}_{bh}^{\perp}$.

Remark 7. *According to Lemma 1 additional coordinate transformations, $\boldsymbol{\phi}_{bh}(\cdot)$ and $\boldsymbol{\phi}_{ba}(\cdot)$, are needed in order to represent (2.17) in the form as given with (2.25). Representation (2.25) separates the behavior dynamics (2.17) into two subsystems, one controlled by $\boldsymbol{u}_h$ and another controlled by $\boldsymbol{u}_a$, which is important in establishing complementary interaction paradigm according to Definition 2.3.3.*

Example 2.3.2. (Behavior prioritization.) Redundancy resolution *of robot manipulators [HK87] and* null-space behavioral control *for multi-robot systems [AAC08] can be regarded as examples of transforming the system dynamics more than once. For example, let us consider two behaviors and their corresponding behavior Jacobians*

$$\boldsymbol{\phi}_b = \begin{bmatrix} \boldsymbol{\phi}_{b,1} \\ \boldsymbol{\phi}_{b,2} \end{bmatrix} \quad \boldsymbol{J}_b = \begin{bmatrix} \boldsymbol{J}_{b,1} \\ \boldsymbol{J}_{b,2} \end{bmatrix}. \tag{2.26}$$

According to the redundancy resolution algorithm, a lower-priority behavior, e.g. $\boldsymbol{\phi}_{b,2}$ needs to be projected into the null-space of the higher-priority behavior, $\boldsymbol{\phi}_{b,1}$. In order to achieve that, the behavior dynamics needs to be further projected with

$$\boldsymbol{J}_{b,11} = \boldsymbol{I}, \quad \boldsymbol{J}_{b,22} = \boldsymbol{N}_{b,1}, \tag{2.27}$$

where $\boldsymbol{N}_{b,1}$ is a null-space of $\boldsymbol{J}_{b,1}$. Here, $\boldsymbol{J}_{b,1}$ can correspond to $\boldsymbol{J}_{bh}$ and consequently $\boldsymbol{J}_{b,2}$ corresponds to $\boldsymbol{J}_{ba}$. The resulting Jacobian matrix applied to the original system (2.1) is

$$\tilde{\boldsymbol{J}}_b = \begin{bmatrix} \boldsymbol{J}_{b,1} \\ \boldsymbol{J}_{b,2}\boldsymbol{N}_{b,1} \end{bmatrix}. \tag{2.28}$$

For application of redundancy resolution in teleoperation scenarios the reader is referred to [BK18] (single robot system) and [LKL15] (multi-robot system).

In order to formally propose conditions under which an interaction is complementary w.r.t. its controllability property, let us denote the controllability distributions, analogous to (2.21), with Δ^c_{bh} and Δ^c_{ba}. The proposition for complementary interaction paradigm directly follows.

Proposition 2.3.2. *If the following equalities hold*

$$\begin{aligned} dim\{\Delta^c_{bh}\} &= \sum_{i=1}^{d} k_i \\ dim\{\Delta^c_{ba}\} &= \sum_{i=d+1}^{k} k_i, \end{aligned} \tag{2.29}$$

then the first d behavior subsystems in (2.25) are accessible *from $\boldsymbol{\xi}_{bh}$ by the control input $\boldsymbol{u}_h$ and last $k-d$ behavior subsystems in (2.25) are* accessible *from $\boldsymbol{\xi}_{ba}$ by the control input $\boldsymbol{u}_a$.*

Remark 8. *If the drift of (2.25) is compensated, i.e. $\boldsymbol{f}_{b,h} = \boldsymbol{0}, i = 1, ..., d$ and $\boldsymbol{f}_{b,a} = \boldsymbol{0}, i = d+1, ..., k$, then the firsts d behavior subsystems in (2.25) are* controllable *from $\boldsymbol{\xi}_b$ by the control input $\boldsymbol{u}_h$ and the last $k-d$ behavior subsystems in (2.25) are* controllable *by the control input $\boldsymbol{u}_a$.*

Application example of the complementary interaction paradigm can be found in Chapter 3, Section 3.3, Chapter 4 and Chapter 5.

2.3.3 Overlapping Interaction Paradigm

The overlapping interaction paradigm considers a coupled system in which the human control inputs $\boldsymbol{u}_h$ and the robot control inputs $\boldsymbol{u}_a$ jointly steer the states of the system as depicted in Figure 2.5. Formally, the overlapping interaction paradigm is defined below.

Definition 2.3.4. *Interaction paradigm is* overlapping *if a set of d behavior subsystems, where d can be any integer from the set $\{1, ..., k\}$, is controllable with the control inputs $\boldsymbol{u}_h$ and $\boldsymbol{u}_a$.*

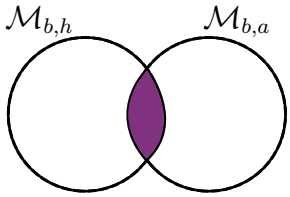

Figure 2.5: Overlapping interaction paradigm.

According to Definition 2.3.4, $\mathcal{M}_{b,h} = \mathcal{M}_{b,a} = \mathcal{M}_{b,1} \cup ... \cup \mathcal{M}_{b,d}$. Here, a combination of complementary and overlapping interaction paradigms is not considered explicitly for the sake of clarity. Furthermore, for the sake of simplicity and without loss of generality, let us simplify the discussion to only one behavior, i.e. $d = i$.

Remark 9. *In order to ensure the control inputs $\boldsymbol{u}_h$ and $\boldsymbol{u}_a$ affect i^{th} behavior subsystem jointly, the matrices $\boldsymbol{G}_{bh,i}$ and $\boldsymbol{G}_{ba,i}$ should be non-zero.*

In this thesis, two overlapping forms of interaction are identified: *cooperative* and *competitive*. The cooperative overlapping interaction paradigm is characterized by the action of the human and the robot control inputs along the same directions, which renders this type of interaction *assistive*. The competitive overlapping interaction paradigm is characterized by the opposing actions of the human and the robot control inputs, which renders this type of interaction *resistive*. The following definitions formalize these two concepts.

Definition 2.3.5. *Interaction paradigm is* cooperative overlapping *on $T\mathcal{M}_{b,i}$ if the Jacobian matrix of $\boldsymbol{G}_{b,i}$, $\dfrac{\partial \boldsymbol{G}_{b,i}}{\partial \boldsymbol{\xi}_b}(\boldsymbol{\xi}_b)$, has all non-negative off-diagonal elements.*

Definition 2.3.6. *Interaction paradigm is* competitive overlapping *on $T\mathcal{M}_{b,i}$ if the negative Jacobian matrix of $\boldsymbol{G}_{b,i}$, $-\dfrac{\partial \boldsymbol{G}_{b,i}}{\partial \boldsymbol{\xi}_b}(\boldsymbol{\xi}_b)$, has non-negative off-diagonal elements.*

The proposition with the condition under which an interaction is overlapping w.r.t. its controllability property, is given below.

Proposition 2.3.3. *If $T\mathcal{M}_{b,i}$ is an invariant and involutive distribution and if*

$$\begin{aligned} dim\{\Delta^c_{bh,i}\} &= k_i, \\ dim\{\Delta^c_{ba,i}\} &= k_i, \end{aligned} \tag{2.30}$$

then the behavior subsystem i in (2.17) is controllable by the control inputs $\boldsymbol{u}_h$ and $\boldsymbol{u}_a$.

Remark 10. *If the drift of the i^{th} subsystem in (2.17) is compensated, i.e. $\boldsymbol{f}_{b,i} = \boldsymbol{0}$, then it is* controllable *from $\boldsymbol{\xi}_b$ by the control inputs $\boldsymbol{u}_h$ and $\boldsymbol{u}_a$.*

Application example of the overlapping interaction paradigm can be found in Chapter 6, Section 6.3. A summary of the properties of the proposed interaction paradigms is given in Table 2.1 and Figure 2.6 gives their overview.

Interaction paradigms	Human responsibilities	Robot responsibilities	Examples
Manual direct	$T\mathcal{M}_{bh} = T\mathcal{M}$	$\emptyset$	Teleoperation
Autonomous direct	$\emptyset$	$T\mathcal{M}_{ba} = T\mathcal{M}$	Full autonomy
Complementary	$T\mathcal{M}_{bh} \subset T\mathcal{M}$	$T\mathcal{M}_{ba} = T\mathcal{M} \setminus T\mathcal{M}_{bh}$	Semi-autonomy
Cooperative overlapping	$T\mathcal{M}_{bh}$	$T\mathcal{M}_{ba}$, $T\mathcal{M}_{bh} \cap T\mathcal{M}_{ba} \neq \emptyset$	Assistance
Competitive overlapping	$T\mathcal{M}_{bh}$	$T\mathcal{M}_{ba}$, $T\mathcal{M}_{bh} \cap T\mathcal{M}_{ba} \neq \emptyset$	Resistance

Table 2.1: Properties of the interaction paradigms.

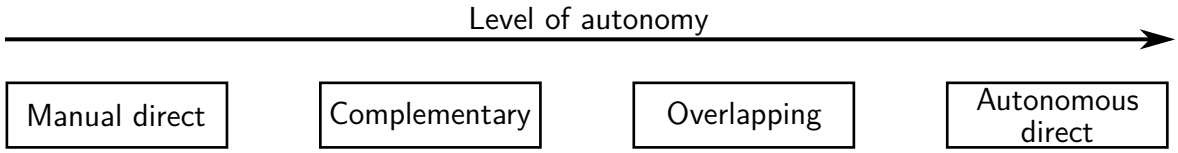

Figure 2.6: Overview of the interaction paradigms with respect to the level of autonomy.

2.4 Control Design Guidelines

The proposed interaction paradigms can be achieved through the design of appropriate control strategies. The control strategy depends on the degree to which the robot team can perform functions autonomously. In this section, the overall control architecture and a concept of *subtask-based control*, suitable for all interaction paradigms, are proposed.

2.4.1 Control Architecture

The envisioned overall control architecture is inspired by [Mur07], where a hierarchical approach is developed for robot teams. In this work it is suitably extended to human-robot team interaction and its application to human-robot interaction is straightforward by considering only one robot. It comprises of six layers: *task*, *planning*, *subtask*, *action*, *robot system* and *interaction* layer, as illustrated in Figure 2.7. The functionalities of the layers are described with particular focus on the task and the subtask layers.

The task goal is stored within the task layer. Often it is represented as a performance function to be optimized [Mur07]

$$J = \int_0^T g(\boldsymbol{\xi}_b, \boldsymbol{u}_h, \boldsymbol{u}_a)\mathrm{d}t + g_T(\boldsymbol{\xi}_b(T)), \tag{2.31}$$

where g and g_T are incremental and terminal costs, respectively. T is the time horizon in which the task should be accomplished. The control input to the individual parts of the robot system is determined through computations in the planning, subtask, and action layers. High-level planning in terms of the suitable combination of behaviors is performed within the planning layer. The subtask-based control architecture is located on the subtask layer. The action layer is concerned with the local low-level control actions.

Global and local behaviors: In this work *global* behaviors require information exchange between the human and the robot partner(s) and/or between the robot partner(s) within the robot team. *Local* behaviors require only the local information of an individual robot.

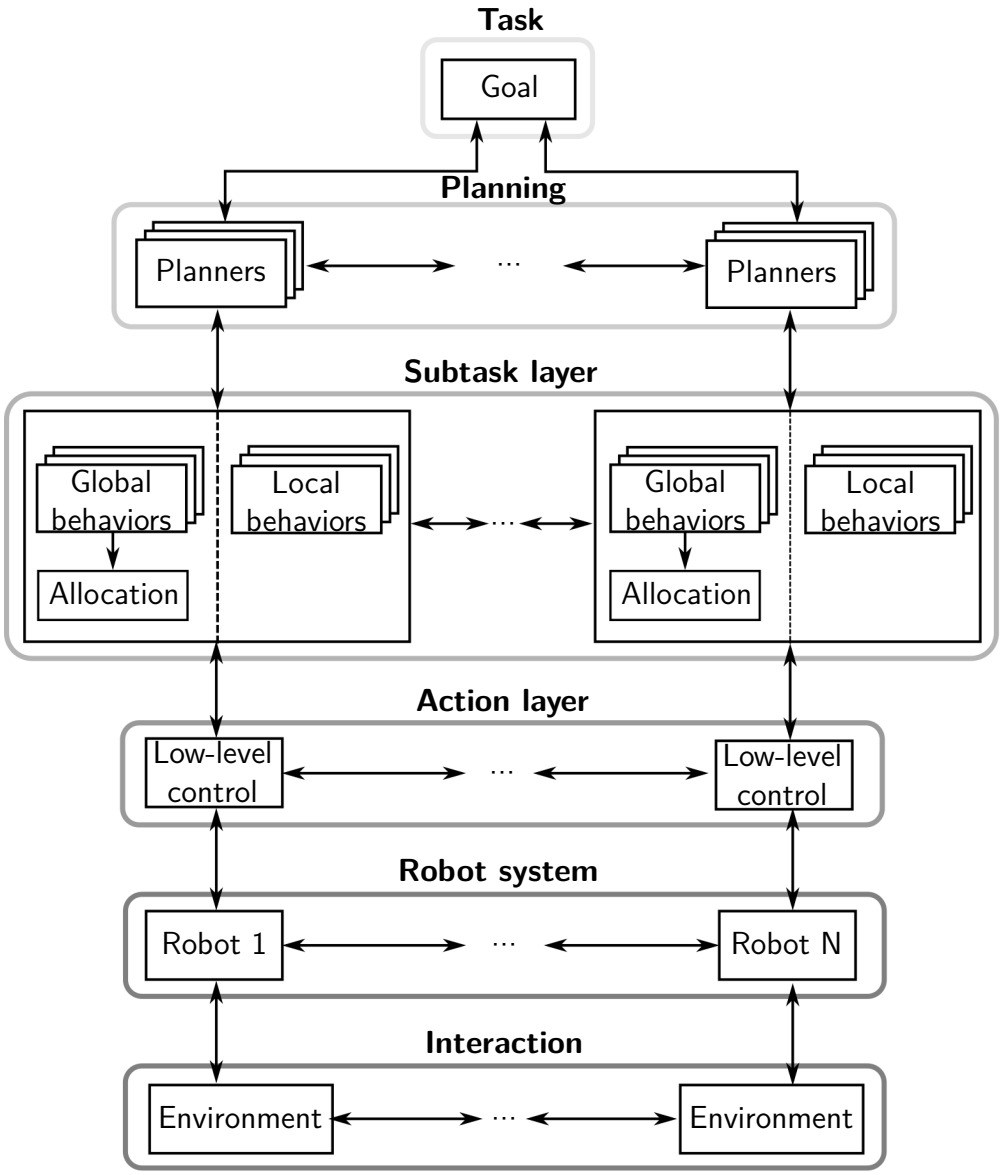

Figure 2.7: Hierarchical control architecture for robot systems. The task goal is determined and monitored in the *task layer*. Based on the goal, a set of global and local behaviors are activated in the *subtask layer* through the *planning layer*, which selects the behaviors from the *library of behaviors*. The outputs of this layer are control inputs to the low-level controllers of the robots in the *action layer*.

Typical global and local behaviors in robot team interaction, human-robot interaction and human-robot team interaction are given in Example 2.4.1.

Example 2.4.1. (Global and local behaviors.) *For robot teams, the typical examples of global behaviors are* rendezvous*,* foraging*,* cooperative manipulation*,* formation*,* coverage*, and* inter-robot avoidance*. Rendezvous describes a behavior in which the robots meet at a common point at a common time [Mur07]. Foraging refers to a behavior of collecting and delivering an object, cooperative manipulation to the joint handling of an object, formation to the maintenance of robot poses relative to each other or to a reference [DM06], [EX01], [LF01], and coverage refers to visiting areas of an environment for*

information acquisiton [CMKB04]. Coordination control of multi-agent systems *is a suitable control approach for accomplishing global behaviors by exchanging individual state information between agents (robots) through communication channels. In this context* consensus *is one of the canonical control problems [OM04]. For example, in order to accomplish a rendezvous behavior, the robots need to perform consensus on the position. The idea behind the consensus control is that each robot moves towards the weighted average of the states of its neighbors. There are multiple other control approaches that are used for cooperation of robot teams, e.g. artifical potential functions [LF01], Lyapunov analysis [OM04], sliding-mode control [Gaz05], behavioral control [AAC08], to name the few.*

Examples of local behaviors are obstacle avoidance *and* self-collision avoidance*. It should be noted that the classification of these behavior examples is not strict, but rather considers the "typical" case. If for example inter-robot avoidance is performed using only local sensors of the robots without information exchange, then this would be called a local behavior.*

A global behavior in human-robot interaction may be motion of a robot manipulator in its task space through a haptic device in teleoperation settings, while a local behavior may be self-collision avoidance, see e.g. [SAP+18]. In human-robot team interaction the human partner provides reference input to robot team global behaviors, see e.g. [LKL15].

2.4.2 Subtask-Based Control

In this thesis a shared-control framework that is suitable for all interaction paradigms, termed as *subtask-based control*, is introduced. It is a control approach that operates on *Subtask layer* of Figure 2.7.

Subtask-based control consists of three main components: (i) *decoupling control* that ensures behaviors do not interact or are appropriately prioritized, (ii) *passivity-based nominal control* that enables safe and stable interaction of the system with the human partner and the environment (iii) *game-theoretical controller that ensures a suitable contribution of the robot autonomy to the task execution.* Therefore, this framework resolves Challenge 2 through the decoupling control and Challenge 6 through the game-theoretical control (see Section 1.1 for more details on the thesis challenges). The subtask-based control architecture block diagrams for the direct manual, complementary and overlapping interaction paradigms are depicted in Figure 2.8a-c, respectively.

Command and feedback mappings: Subtask-based control increases flexibility of interface choice and enables a dimensionality reduction of command (and feedback) information. Knowing the level of autonomy implies which states of the robot system should be controllable by the human. In order to ensure controllability of those states, it is necessary to provide sufficient number of command channels. This number conditions the command interface suitable for the interaction. In terms of the appropriate feedback, the human operator should be informed about the states it controls. In that sense, the states which are controllable by the human should also be *observable.* In order to ensure observability of states it is necessary to provide sufficient number of feedback channels. This number conditions the feedback interface appropriate for the interaction.

The general feedback control inputs of the human and the robot partners, $\boldsymbol{u}_h$ and $\boldsymbol{u}_a$, are assumed to be state dependent and static, given as

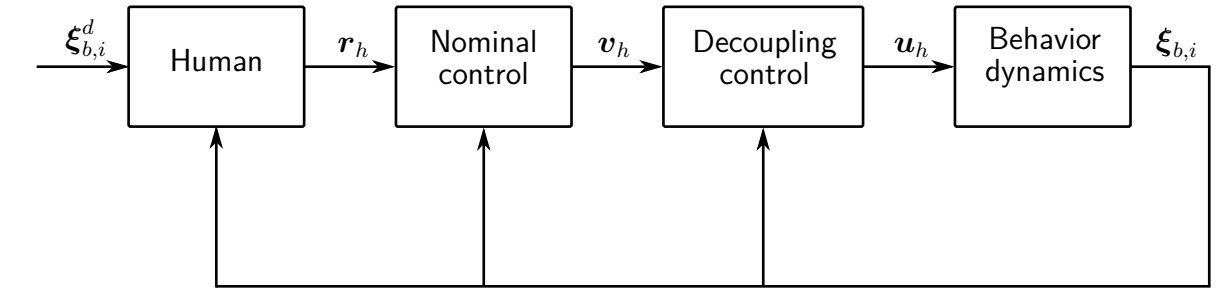

(a) Direct manual interaction paradigm.

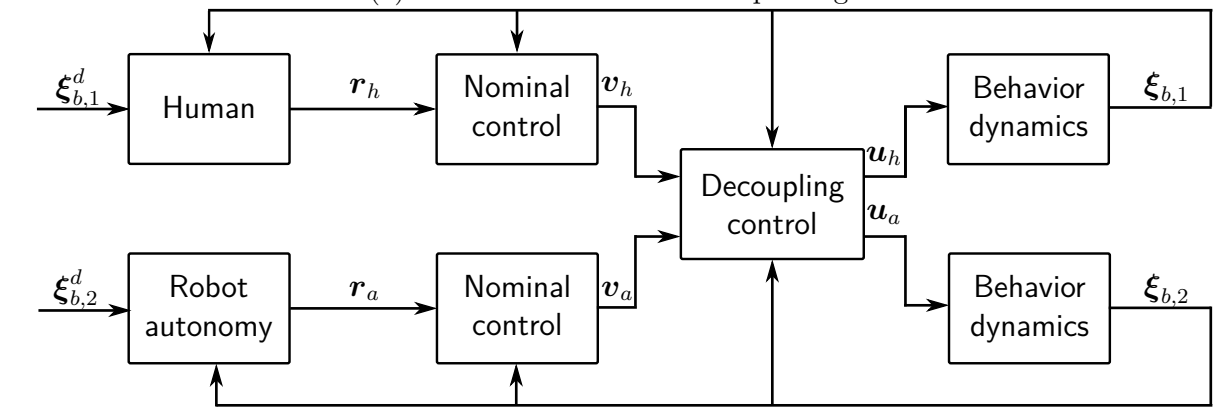

(b) Complementary interaction paradigm.

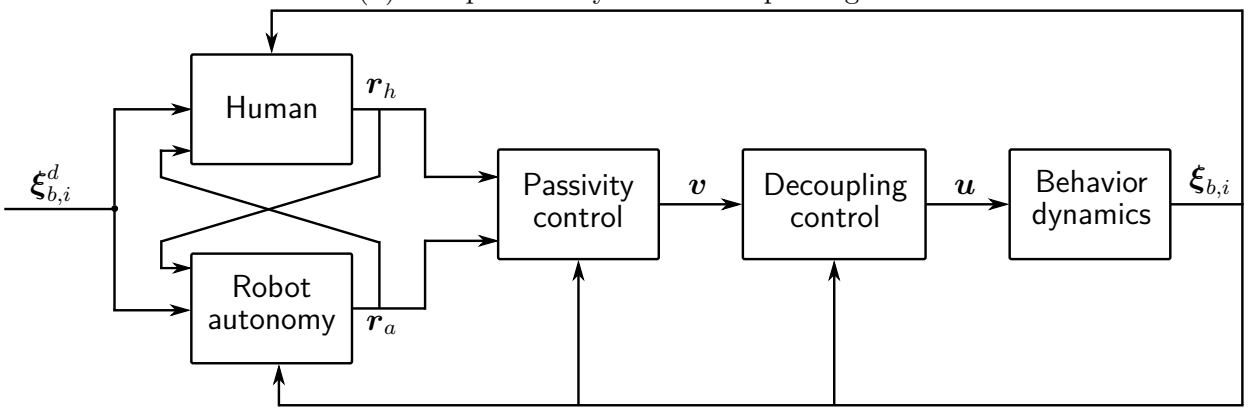

(c) Overlapping interaction paradigm.

Figure 2.8: Subtask-based control architecture for the interaction paradigms.

$$\begin{aligned} \boldsymbol{u}_h &= \boldsymbol{\alpha}_h(\boldsymbol{\xi}_b) + \boldsymbol{\Gamma}_h(\boldsymbol{\xi}_b)\boldsymbol{v}_h \\ \boldsymbol{u}_a &= \boldsymbol{\alpha}_a(\boldsymbol{\xi}_b) + \boldsymbol{\Gamma}_a(\boldsymbol{\xi}_b)\boldsymbol{v}_a, \end{aligned} \tag{2.32}$$

where matrices $\boldsymbol{\Gamma}_h(\boldsymbol{\xi}_b)$ and $\boldsymbol{\Gamma}_a(\boldsymbol{\xi}_b)$ are nonsingular in $\boldsymbol{\xi}_b$ and $\boldsymbol{v}_h$ and $\boldsymbol{v}_a$ are new reference inputs. Furthermore, it is necessary to ensure the reference inputs $\boldsymbol{v}_h$ and $\boldsymbol{v}_a$ *stabilize* the system (2.17). For that purpose, the property of *controlled invariance* needs to be imposed on the system (2.17), modified by (2.32). Let us consider only the i^{th} behavior under static control law (2.32)

$$\dot{\boldsymbol{\xi}}_{b,i} = \tilde{\boldsymbol{f}}_{b,i}(\boldsymbol{\xi}_b) + \tilde{\boldsymbol{G}}_{bh,i}(\boldsymbol{\xi}_b)\boldsymbol{v}_h + \tilde{\boldsymbol{G}}_{ba,i}(\boldsymbol{\xi}_b)\boldsymbol{v}_a, \tag{2.33}$$

where $\tilde{\boldsymbol{f}}_{b,i}(\boldsymbol{\xi}_b) = \boldsymbol{f}_{b,i}(\boldsymbol{\xi}_b) + \boldsymbol{G}_{b,i}(\boldsymbol{\xi}_b)\boldsymbol{\alpha}_h(\boldsymbol{\xi}_b) + \boldsymbol{G}_{b,i}(\boldsymbol{\xi}_b)\boldsymbol{\alpha}_a(\boldsymbol{\xi}_b)$, $\tilde{\boldsymbol{G}}_{bh,i}(\boldsymbol{\xi}_b) = \boldsymbol{G}_{b,i}(\boldsymbol{\xi}_b)\boldsymbol{\Gamma}_h(\boldsymbol{\xi}_b)$ and

$\tilde{\boldsymbol{G}}_{ba,i}(\boldsymbol{\xi}_b) = \boldsymbol{G}_{b,i}(\boldsymbol{\xi}_b)\boldsymbol{\Gamma}_a(\boldsymbol{\xi}_b)$. Proposition 2.4.1 introduces controlled invariance of the distribution $\Delta_h \in T\mathcal{M}_{bh}$ and $\Delta_a \in T\mathcal{M}_{ba}$. The proof can be found in [Isi13].

Proposition 2.4.1 ([Isi13])**.** *A distribution Δ_h is controlled invariant on $U_h \in \mathcal{M}_{bh}$ if there exists a feedback pair $(\boldsymbol{\alpha}_h, \boldsymbol{\Gamma}_h)$ defined on U_h such that Δ_h is invariant under the vector fields $\tilde{\boldsymbol{f}}_{b,i}, \tilde{\boldsymbol{g}}_{bh,i1}, ..., \tilde{\boldsymbol{g}}_{bh,il}$, i.e.*

$$[\tilde{\boldsymbol{f}}_{b,i}, \Delta_h] \subset \Delta_h, \quad [\tilde{\boldsymbol{g}}_{bh,ij}, \Delta_h] \subset \Delta_h \quad j = 1, ...l.$$

Local controlled invariance of the distribution Δ_h is guaranteed if and only if

$$\begin{aligned}&[\tilde{\boldsymbol{f}}_{b,i}, \Delta_h] \subset \Delta_h + \boldsymbol{G}_{b,i}\\ &[\tilde{\boldsymbol{g}}_{bh,ij}, \Delta_h] \subset \Delta_h + \boldsymbol{G}_{b,i} \quad j = 1, ...l.\end{aligned}$$

A distribution Δ_a is controlled invariant on $U_a \in \mathcal{M}_{ba}$ if there exists a feedback pair $(\boldsymbol{\alpha}_a, \boldsymbol{\Gamma}_a)$ defined on U_a such that Δ_a is invariant under the vector fields $\tilde{\boldsymbol{f}}_{b,i}, \tilde{\boldsymbol{g}}_{ba,i(l+1)}, ..., \tilde{\boldsymbol{g}}_{ba,im}$, i.e.

$$[\tilde{\boldsymbol{f}}_{b,i}, \Delta_a] \subset \Delta_a, \quad [\tilde{\boldsymbol{g}}_{ba,ij}, \Delta_a] \subset \Delta_a \quad j = l+1, ...m$$

Local controlled invariance of the distribution Δ_a is guaranteed if and only if

$$\begin{aligned}&[\tilde{\boldsymbol{f}}_{b,i}, \Delta_a] \subset \Delta_a + \boldsymbol{G}_{b,i}\\ &[\tilde{\boldsymbol{g}}_{ba,ij}, \Delta_a] \subset \Delta_a + \boldsymbol{G}_{b,i} \quad j = l+1, ...m.\end{aligned}$$

In the remainder the guidelines for subtask-based architecture design for complementary and overlapping interaction paradigms are introduced. They refer to the way the control law in (2.32) needs to be introduced for the decoupling, passivity and interaction control in Figure 2.8.

Decoupling and Passivity Control

Often the system (2.1) cannot be transformed into subsystems (2.25) with appropriate transformations, since the imposed assumptions are not satisfied. Then, these need to be met with appropriate control design (2.32). In this work complementary interaction paradigm is resolved through *noninteracting/decoupling control*. Such control ensures that the subtasks controlled by the robot autonomy are rendered uncontrollable by the human partner and vice versa, which results in the system dynamic representation as in (2.25). This is achieved for *Euler-Lagrangian* and *port-Hamiltonian* model representation of the system dynamics. Robot autonomy can be ensured with suitable high-level task-based optimal control. However, high-level control for complementary interaction paradigm is not the focus of this thesis.

Passivity is a requirement for the subtask-based control, since it implies safety and stability in the interaction with the human partner and the environment. Energetic passivity is enforced with *passivity-based control*. This is the topic of Chapter 3.

Human-Robot Control Input Blending

Total control input applied to a behavior in the overlapping interaction paradigm is a synthesis/blending of the human command input and the input from the robot autonomy. Their

blending is often considered in the linear form, given with (1.1). However, for a human-centric interaction a model of the human behavior is needed, since it is necessary to determine online the most appropriate robot control input based on the human action in order to accomplish a suitable assistance. Overlapping interaction paradigm can be achieved by imposing additional criteria, e.g. optimization of energy, effort and/or task error. This is the topic of Chapter 6. In this work the overlapping interaction paradigm is achieved by adding a high-level controller that considers interaction of the human and the robot autonomy in a game-theoretical sense.

Human Behavior Modeling

Modeling continuous interaction between a human and a robot (team) remains a largely open challenge. In classical teleoperation literature control design commonly relies on the assumption that the *trained* human behaves passive [Sir05]. The authors of [HCF15] use black-box methods to identify human decision-making behavior in the active role of commanding a robot swarm. The frequency analysis of the obtained linear time-invariant system, however, reveals that the human decision-making process violates the passivity condition in the high-frequency range. Accordingly, passivity-based models have their limitations and more research is needed in this area. In that sense, considering that the human operator is not passive is necessary and the control design needs to account for it accordingly. This has been considered in Chapter 5 through the design of an energy tank control that ensures passivity.

In the context of the hierarchical control architecture proposed with Figure 2.7, the human in the active role can provide control inputs to the subtask or the action layer. Therefore, the human partner in the active role can be included in the control architecture through the planning and the subtask layers as depicted in Figure 2.9. On the planning layer the human operator can select and allocate behaviors to the partners in the team and on the subtask layer the human operator can provide control input to the specific behaviors.

In this thesis the human operator/partner is considered in the subtask layer. The block structure of the general shared control architecture with the subtask-based controller and the additional requirements for a successful and intuitive task execution is depicted with Figure 5.2.

2.5 Discussion

Three interaction paradigms of human-robot team interaction are proposed: *direct*, *complementary* and *overlapping*. The paradigms are classified according to the *accessibility* and *controllability* property. The identified properties of the interaction paradigms ease the selection of the controller objectives and strategies. It can be concluded that tasks should be decomposed into multiple global and local subtasks. Furthermore, these subtasks should be prioritized according to the current state of the environment, decoupled to avoid interference, and preferably allocated dynamically to the human and/or the autonomous controller of the robot system. Other reviewed taxonomies do not provide guidelines on how to design controllers for human-robot interaction, unlike the taxonomy proposed in this chapter.

The novel concept of subtask-based control architecture is introduced as a suitable approach to achieve the proposed interaction paradigms irrespective of the type and complexity

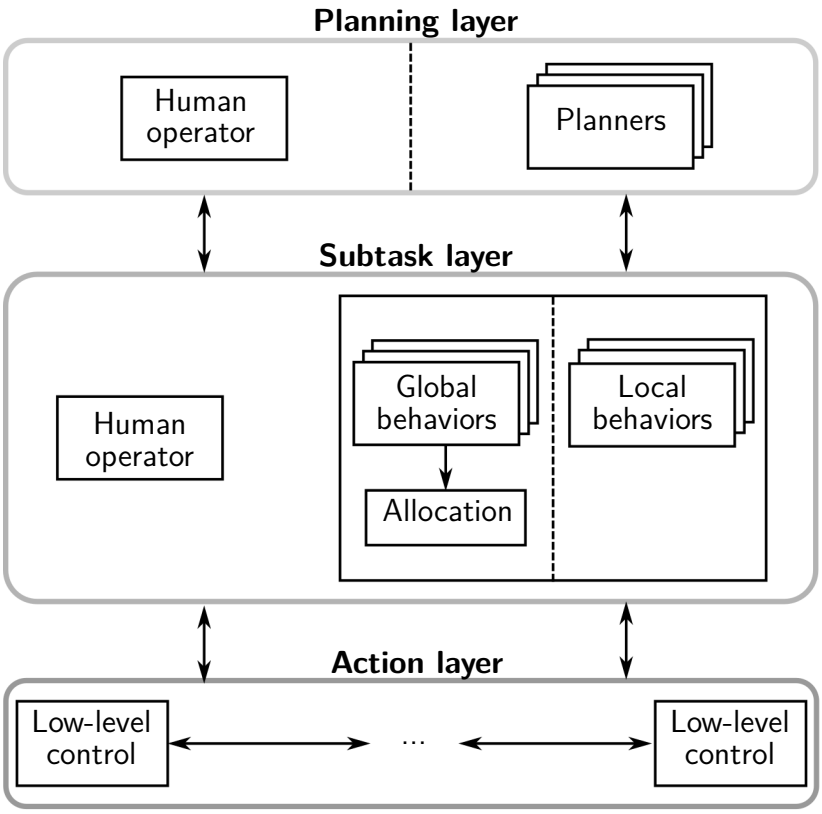

Figure 2.9: Human operator/partner in the active role can be included in the loop through the *planning layer* and the *subtask layer*.

of the robot system as well as the task. The interaction and control is, therefore, achieved on higher levels of abstraction that are independent of the configuration of the interactive system, which is novel compared to the existing literature. The proposed concept includes a requirement on the passivity of subtasks, i.e. a nominal passive controller is required to render the interaction on the level of subtasks safe and stable. Furthermore, the approach enables the use of high-level controllers, particularly suitable for the overlapping interaction paradigm that requires some form of human intention estimation or an appropriate decision-making model. The work presented in Section 2.2, Section 2.3 and Section 2.4 has been partially published in [MH18], [MH16] and [MH17], respectively.

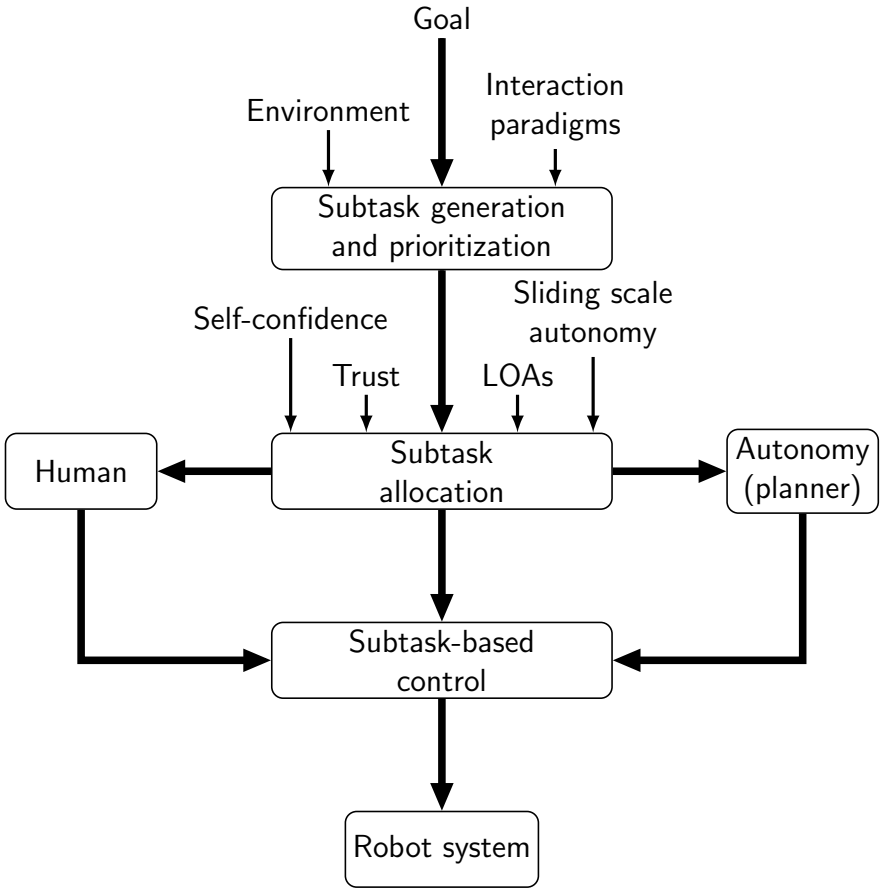

Figure 2.10: Block structure of the general hierarchical shared control architecture for human-robot team interaction. Based on a desired *goal* of the interaction and the *environment state* subtasks are generated and prioritized. Allocation of subtasks to the human and the robot team is dynamical and determined depending on the available *levels of autonomy*, current *self-confidence* of the human and its *trust in automation*. Low-level controllers receive desired control inputs either from the human or from the built-in robot team planners.

3

Complementary Shared Control

Control of complex dynamical systems with human in the loop and interaction with the physical environment is relevant in many application domains, e.g. process control, flight control, semi-autonomous driving and human-robot interaction [LSSS14]. Typically, multiple control objectives are defined for such systems in order to accomplish the overall task. Due to the complexity of the system, i.e. high number of degrees of freedom, the human operator cannot control all the system states toward accomplishing the task. Consequently, the human can only take over a limited number of system states to control, while the remaining states are controlled by the autonomous functions. Therefore, the *complementary interaction paradigm*, proposed in Chapter 2, is required. To resolve the aforementioned challenge, a novel, passive noninteracting (decoupling) shared-control approach for complementary interaction paradigm in human-robot team interaction is proposed in this chapter. It enables (i) control of the system on lower-dimensional subtask spaces, (ii) decoupling of subtasks that are simultaneously executed and (iii) safe and stable human-robot team interaction.

Related Work and Open Problems

Complementary interaction paradigm enables the achievement of multiple control goals, often simultaneously. This is accomplished by designing multiple, possibly noninteracting, control loops, so that the reference inputs of one control loop and its system states do not have undesired effects on the system states and outputs of the other control loops. *Noninteracting (decoupling) control* of general multi-input multi-output (MIMO) nonlinear, affine systems through state-feedback control is proposed in [Isi13]. This control approach decouples the system into multiple SISO subsystems. A more general case - the decoupling into multiple MIMO subsystems is a *block-partitioned noninteracting control* and is proposed in [Bat94]. However, explicit guidelines for the control design of noninteracting control for a class of Euler-Lagrangian systems are not proposed.

In robotics a hierarchical version of the decoupling control, termed as *redundancy resolution*, is used to control redundant robot systems. For example, it is applied on robot manipulators [HK87], humanoid robots [KSP08] and robot teams [AAC08]. In the case of robot teams, simplified models, e.g. single integrators, are often considered. Euler-Lagrangian robot team dynamics and decoupling control are considered in [DS05] but only for a specific task of cooperative manipulation. The noninteracting control is also applied in [BPB17] on a linearized model of dual manipulators, constrained by an object. For the shared-control teleoperation of robot teams, null-space based behavioral control is proposed in [Liu15],

a *passivity-based control* in [DS05, FSR+12] and an *impedance controller* for a robot hand teleoperation in [GPC05]. However, generalizing the approach to multiple and arbitrary tasks for Euler-Lagrangian dynamics is not considered so far.

Guaranteeing passivity of the closed-loop system implies safety of the interaction. Therefore, it is important for human-in-the-loop interaction, e.g. teleoperation through a haptic device [HB12], direct physical interaction [DSDB08], close-range teleoperation [AMH17] and interaction of the robot system with the environment [EH16]. Passivity also relates to the classical approaches of analyzing stability of dynamical systems, e.g. *Lyapunov theory* and $\mathcal{L}_2$ *stability* [KG02], and can, therefore, be used to analyze stability of human-robot control loops. Therefore, a noninteracting control approach with passivity guarantees is required. In summary, a shared-control approach that enables human and robot partners to control different aspects of the task without interference and with passivity guarantees is needed.

In this chapter an explicit, block-partitioned noninteracting control approach for Lagrangian systems is proposed to resolve the complementary interaction paradigm. It allows the decoupling of the system into multiple subsystems with each subsystem having a different control objective. Therefore, with this approach each subsystem models one subtask as proposed in Section 2.2. The contribution is the solution of the block-partitioned noninteracting control with passivity guarantees for Lagrangian systems, which is achieved by preserving Lagrangian dynamic properties after the system decoupling. This approach is applicable not only to robots in free motion but also to robots with physical coupling as it occurs, for example, in cooperative object manipulation. It ultimately allows safe control sharing in human-robot collaboration.

The chapter is organized as follows. The problem statement is given in Section 3.1, while the novel decoupling controller is proposed in Section 3.2. The simulation example and experimental results are given in Section 3.3. Discussion is given in Section 3.4.

3.1 Problem Statement

Let us assume the robot system dynamics is given by the Euler-Lagrange equation (2.6). For the sake of completeness of this chapter, the robot model dynamics in Lagrangian form is defined below as well

$$\boldsymbol{M}(\boldsymbol{\theta})\ddot{\boldsymbol{\theta}} + \boldsymbol{c}(\boldsymbol{\theta}, \dot{\boldsymbol{\theta}}) + \boldsymbol{\tau}_g(\boldsymbol{\theta}) = \boldsymbol{\tau}_c + \boldsymbol{\tau}_e, \tag{3.1}$$

where the vectors $\boldsymbol{\tau}_c$ and $\boldsymbol{\tau}_e$ are n-dimensional control, and external torque terms, respectively. Inertia matrix is positive-definite and symmetric, while $\dot{\boldsymbol{M}}(\boldsymbol{\theta}) - 2\boldsymbol{C}(\boldsymbol{\theta}, \dot{\boldsymbol{\theta}})$ is skew-symmetric. The system dynamics (3.1) can be represented in a nonlinear state-space affine form as

$$\begin{aligned}
&\dot{\boldsymbol{\xi}} = \boldsymbol{f}(\boldsymbol{\xi}) + \boldsymbol{G}(\boldsymbol{\xi})(\boldsymbol{\tau}_c + \boldsymbol{\tau}_e)\\
&\boldsymbol{y} = \boldsymbol{h}(\boldsymbol{\xi}),\\
&\boldsymbol{\xi} = [\boldsymbol{\theta}^\top, \dot{\boldsymbol{\theta}}^\top]^\top,\\
&\boldsymbol{f}(\boldsymbol{\xi}) = \begin{bmatrix}\boldsymbol{f}_1(\boldsymbol{\xi})\\ \boldsymbol{f}_2(\boldsymbol{\xi})\end{bmatrix} = \begin{bmatrix}\dot{\boldsymbol{\theta}}\\ -\boldsymbol{M}^{-1}(\boldsymbol{\theta})(\boldsymbol{C}(\boldsymbol{\theta}, \dot{\boldsymbol{\theta}})\dot{\boldsymbol{\theta}} + \boldsymbol{\tau}_g(\boldsymbol{\theta}))\end{bmatrix},\\
&\boldsymbol{G}(\boldsymbol{\xi}) = \begin{bmatrix}\boldsymbol{G}_1(\boldsymbol{\xi})\\ \boldsymbol{G}_2(\boldsymbol{\xi})\end{bmatrix} = \begin{bmatrix}\boldsymbol{0}\\ \boldsymbol{M}^{-1}(\boldsymbol{\theta})\end{bmatrix} = [\boldsymbol{g}_1, ..., \boldsymbol{g}_n].
\end{aligned} \tag{3.2}$$

The focus of this chapter are Lagrangian systems with certain structural properties, outlined with the following assumptions.

Assumption 3.1.1. *The system (3.2) has no zero dynamics.*

This assumption implies that there are no states the system in (3.2) can assume when the output is zero, i.e. $\boldsymbol{y} = \mathbf{0}$.

Remark 11. *From the robotics point of view the analysis is restricted to the systems with no external rigid constraints, redundancy with respect to the task or elastic structures as analyzed in [DL91].*

Redundancy with respect to the task, highlighted in Remark 11, sets a constraint on the dimensionality of the output function $\boldsymbol{y}$, given with Remark 12.

Remark 12. *The sum of the number of outputs $\boldsymbol{y}$ equals the total number of generalized coordinates, $\boldsymbol{\theta}$, i.e. $p = \sum_{i=1}^{k} k_i = n$. Inequality $p < n$ implies the system is redundant with respect to the task and that there are certain degrees of freedom of the system which could not be controlled with the input-output controller. If this is the case, the proposed control approach is not restrictive, but additional controller needs to be developed for the redundant degrees of freedom and the stability of the overall system needs to be guaranteed. The condition $p > n$ is not considered since in this case a prioritizing controller would be needed, which is not the focus of this thesis.*

Example 3.1.1. (Redundant robot system.) *A classical example of a redundant robot system is a redundant manipulator with 7 DoFs w.r.t the task in Cartesian space that requires 6 DoFs [NHY87]. The redundant degree of freedom is the elbow joint that, even if not necessary for the task, needs to be stabilized.*

The output vector is set as in (3.3), i.e. the outputs are equal to the behaviors necessary to achieve the task.

Assumption 3.1.2. *The outputs of the system (3.2) are behavior functions required to accomplish the task*

$$\boldsymbol{y} = \begin{bmatrix} \boldsymbol{x}_{b,1} \\ \vdots \\ \boldsymbol{x}_{b,k} \end{bmatrix} = \begin{bmatrix} \boldsymbol{\phi_1}(\boldsymbol{\xi}) \\ \vdots \\ \boldsymbol{\phi_k}(\boldsymbol{\xi}) \end{bmatrix}. \tag{3.3}$$

In order to represent (3.2) in the behavior dynamics form of (2.17), additional assumption needs to be imposed on the behavior Jacobian, $\boldsymbol{J}_b$, defined with (2.13).

Assumption 3.1.3. *The behavior Jacobian $\boldsymbol{J}_b$ in (2.13) has full rank.*

Remark 13. *Assumption 3.1.3 implies that singular cases and configurations of the robot system and/or the task are not considered, since in these cases the behavior Jacobian looses its rank. For example, for a robot manipulator a singular configuration is its fully extended kinematic structure.*

Finally, interaction with the human partner and the environment requires an additional assumption given below.

Assumption 3.1.4. *The human partner and the environment are passive.*

The following two problems are solved in the remainder of the chapter.

Problem 3. *Design a static control law*

$$\boldsymbol{\tau}_c = \boldsymbol{\alpha}(\boldsymbol{\xi}) + \boldsymbol{\Gamma}(\boldsymbol{\xi})\tilde{\boldsymbol{\tau}}_c, \tag{3.4}$$

with $\boldsymbol{\alpha}(\boldsymbol{\xi})$ *being an* n*-dimensional smooth vector field and* $\boldsymbol{\Gamma}(\boldsymbol{\xi})$ *being a nonsingular,* $n \times n$ *dimensional matrix, which decouples the system (3.2) into* k *subsystems, so that for each* $i = 1, ..., k$*, input block* $\tilde{\boldsymbol{\tau}}_{c,i}$ *affects* only *the output block* $\boldsymbol{y}_i$*. This means that for all* $i \neq j$ *the output* $\boldsymbol{y}_i$ *needs to be* invariant *under the input* $\tilde{\boldsymbol{\tau}}_{c,j}$*.*

Problem 4. *Design a control law* $\tilde{\boldsymbol{\tau}}_c$ *for the* k *subsystems, obtained by solving Problem 3, so that each subsystem is passive from the input* $\tilde{\boldsymbol{\tau}}_{e,i}$ *to the output* $\boldsymbol{y}_i$*.*

Remark 14. *In the context of human-robot interaction, each input block* $\tilde{\boldsymbol{\tau}}_{c,i}$ *represents input channels from the human operator or from the robot autonomous planner(s), see Example 3.2.3. The dimensionality and the type of the control inputs provided by the human depend on the interface through which the human interacts with the system, e.g. through a haptic device.*

3.2 Passive Noninteracting Control

In this section Problem 3 and Problem 4 are solved by proposing *passive noninteracting (decoupling) control* approach for Euler-Lagrangian systems. The design of the noninteracting controller is considered in two stages: (i) *input-output noninteracting control* with the design of the matrix $\boldsymbol{\Gamma}(\boldsymbol{\xi})$ in (3.4) and (ii) *state noninteracting control* is solved with the appropriate design of $\boldsymbol{\alpha}(\boldsymbol{\xi})$ in (3.4).

3.2.1 Input-Output Noninteracting Control

In order to ensure that the specific inputs affect only the specific outputs, it is necessary to render the input-output behavior of the robot dynamics, modeled by (3.2), *noninteractive*. For that purpose, (3.4) is inserted into (3.2) to obtain

$$\begin{aligned} \dot{\boldsymbol{\xi}} &= \tilde{\boldsymbol{f}}(\boldsymbol{\xi}) + \tilde{\boldsymbol{G}}(\boldsymbol{\xi})\tilde{\boldsymbol{\tau}}_c + \boldsymbol{G}(\boldsymbol{\xi})\boldsymbol{\tau}_e \\ \begin{bmatrix} \boldsymbol{y}_1 \\ \vdots \\ \boldsymbol{y}_k \end{bmatrix} &= \begin{bmatrix} \boldsymbol{h}_1(\boldsymbol{\xi}) \\ \vdots \\ \boldsymbol{h}_k(\boldsymbol{\xi}) \end{bmatrix}, \\ \tilde{\boldsymbol{f}} &= \begin{bmatrix} \boldsymbol{f}_1(\boldsymbol{\xi}) \\ \tilde{\boldsymbol{f}}_2(\boldsymbol{\xi}) \end{bmatrix}, \; \tilde{\boldsymbol{G}} = \begin{bmatrix} \boldsymbol{0} \\ \tilde{\boldsymbol{G}}_2(\boldsymbol{q}) \end{bmatrix}, \end{aligned} \tag{3.5}$$

where $\tilde{\boldsymbol{f}}_2(\boldsymbol{\xi}) = \boldsymbol{f}_2(\boldsymbol{\xi}) + \boldsymbol{G}_2(\boldsymbol{\xi})\boldsymbol{\alpha}(\boldsymbol{\xi})$ and $\tilde{\boldsymbol{G}}_2(\boldsymbol{\xi}) = \boldsymbol{G}_2(\boldsymbol{\xi})\boldsymbol{\Gamma}(\boldsymbol{\xi}) = [\tilde{\boldsymbol{g}}_1(\boldsymbol{\xi}), ..., \tilde{\boldsymbol{g}}_n(\boldsymbol{\xi})]$.

Without loss of generality, it is assumed that the i^{th} input block, $\tilde{\boldsymbol{\tau}}_{c,i}$ affects the i^{th} output block $\boldsymbol{y}_i$. A sufficient condition for achieving the input-output noninteraction is formulated with Proposition 3.2.1.

General Input-Output Noninteracting Solution

This section provides general conditions, constraints and requirements for the input-output noninteracting control solution of nonlinear affine system (2.1).

Proposition 3.2.1 ([NVdS90]). *Consider the system (3.5) and suppose that the output $\boldsymbol{y}_i$ is invariant under the input $\tilde{\boldsymbol{\tau}}_{c,j}$, where $i \neq j$. Then*

$$\begin{aligned} &\mathcal{L}_{\tilde{\boldsymbol{g}}_j} \boldsymbol{h}_i(\boldsymbol{\xi}) = \boldsymbol{0} \\ &\mathcal{L}_{\tilde{\boldsymbol{g}}_j} \mathcal{L}_{\boldsymbol{z}_1} ... \mathcal{L}_{\boldsymbol{z}_k} \boldsymbol{h}_i(\boldsymbol{\xi}) = \boldsymbol{0}, \end{aligned} \tag{3.6}$$

for all $\boldsymbol{\xi}$ and any combination of k vector fields $\boldsymbol{z}_i$ from the set $\{\tilde{\boldsymbol{f}}_2, \tilde{\boldsymbol{g}}_1, ..., \tilde{\boldsymbol{g}}_n\}$, where $k \leq n+1$.

According to Proposition 3.2.1, noninteracting control is achieved by ensuring that the inputs, which should not affect a particular output block, have a control effect in its *kernel*. Let us, therefore, define the following kernel distributions

$$\begin{aligned} &\Delta_i^K = \ker \mathrm{d}\boldsymbol{h}_i = \bigcap_{j=1}^{k_i} \ker \mathrm{d}h_{ij} \quad \forall i = 1, ..., k, \\ &\Delta^K = \bigcap_{i=1}^{k} \Delta_i^K, \end{aligned} \tag{3.7}$$

where Δ_i^K is the kernel distribution of the output block $\boldsymbol{y}_i$ and Δ^K is the intersection of all thus obtained kernel distributions. Furthermore, let us introduce the controllability distributions relevant for solving the input-output noninteracting problem

$$\begin{aligned} &\tilde{\Delta}_i = \langle \tilde{\boldsymbol{f}}_2, \tilde{\boldsymbol{g}}_1, ..., \tilde{\boldsymbol{g}}_n | \mathrm{span}\{\tilde{\boldsymbol{g}}_i\} \rangle, \quad \forall i = 1, ..., n, \\ &\tilde{\Delta}_i^\star = \langle \tilde{\boldsymbol{f}}_2, \tilde{\boldsymbol{g}}_1, ..., \tilde{\boldsymbol{g}}_n | \mathrm{span}\{\tilde{\boldsymbol{g}}_j : j \neq i\} \rangle, \quad \forall i = 1, ..., n, \\ &\tilde{\Delta}^\star = \bigcap_{i=1}^{n} \tilde{\Delta}_i^\star, \\ &\tilde{\Delta} = \langle \tilde{\boldsymbol{f}}_2, \tilde{\boldsymbol{g}}_1, ..., \tilde{\boldsymbol{g}}_n | \mathrm{span}\{\tilde{\boldsymbol{g}}_i : i = 1, ..., n\} \rangle, \end{aligned} \tag{3.8}$$

which are invariant under the vector fields $\{\tilde{\boldsymbol{f}}_2, \tilde{\boldsymbol{g}}_1, ..., \tilde{\boldsymbol{g}}_n\}$. The distribution $\tilde{\Delta}_i$ spans the block $\tilde{\boldsymbol{g}}_i$ of $\tilde{\boldsymbol{G}}_2$, while $\tilde{\Delta}_i^\star$ spans all the blocks $\tilde{\boldsymbol{g}}_j$ such that $j \neq i$. The distribution $\tilde{\Delta}^\star$ is the intersection of all $\tilde{\Delta}_i^\star$ distributions and $\tilde{\Delta}$ spans $\tilde{\boldsymbol{G}}_2$. Equivalent distributions to (3.8) for the open-loop system (3.2) are denoted as $\Delta_i, \Delta_i^\star, \Delta^\star$ and Δ, respectively.

Remark 15. *The following relationships between the distributions in (3.8) hold [NVdS90]*

$$\tilde{\Delta}_i^\star = \sum_{j \neq i} \tilde{\Delta}_j, \ \tilde{\Delta} = \sum_{i=1}^{n} \tilde{\Delta}_i \text{ and } \tilde{\Delta} = \tilde{\Delta}_i^\star + \bigcap_{j \neq i} \tilde{\Delta}_j^\star. \tag{3.9}$$

Remark 16. *Using the controllability distributions in (3.8) a sufficient condition for input-output noninteraction, given with Proposition 3.2.1, (3.6) can now be expressed as follows*

$$\tilde{\Delta}_j \subset \bigcap_{i \neq j} \Delta_i^K \text{ or } \tilde{\Delta}_i^\star \subset \Delta_i^K \text{ and } \tilde{\Delta}^\star \subset \Delta^K. \tag{3.10}$$

The first two equations imply that the controllability distribution that spans $\tilde{\boldsymbol{g}}_i$ lies in the intersection of the kernel distributions of all other $\tilde{\boldsymbol{g}}_j, j \neq i$, while the last one implies that the intersection of all controllability distributions $\tilde{\Delta}_i^\star, i = 1, ..., n$, has to lie in the intersection of all the kernel distribution $\Delta_i^K, i = 1, ..., k$.

According to constraints formulated with (3.10), solving Problem 1 implies finding maximal distributions $\tilde{\Delta}_i$ (or $\tilde{\Delta}_i^\star$) and $\tilde{\Delta}^\star$ that would satisfy constraints given with (3.10).

Input-Output Noninteracting Solution for Euler-Lagrangian Systems

In this section an explicit solution for the input-output noninteracting control of Euler-Lagrangian system (3.2) with outputs defined as in (3.3) is provided.

Since behaviors are smooth mappings (2.10) according to Definition 2.2.3, under Assumption 3.1.3 the codistributions defined by

$$\Omega_i = \sum_{j=1}^{k_i} \text{span}\{\text{d}h_{i,j}\} \quad \forall i = 1, ..., k, \tag{3.11}$$

are nonsingular with $\dim\{\Omega_i\} = k_i$. Now it is possible to find maximal controllability distributions $\tilde{\Delta}_i^\star$ which lie in Δ_i^K according to the *Controlled invariant distribution algorithm* in [Isi13]

$$\begin{aligned} \Omega_{i_0} &= \Omega_i \\ \Omega_{i_k} &= \Omega_{i_{k-1}} + \mathcal{L}_{\boldsymbol{f}_2}(\Omega_{i_{k-1}} \cap \Delta^{G\perp}) + \sum_{i=1}^{n} \mathcal{L}_{\boldsymbol{g}_i}(\Omega_{i_{k-1}} \cap \Delta^{G\perp}), \end{aligned} \tag{3.12}$$

where $\Delta^G = \text{span}\{\boldsymbol{G}_2\} = \text{span}\{\boldsymbol{g}_1, ..., \boldsymbol{g}_n\}$. If $\Omega_{i_{k+1}} = \Omega_{i_k}$ the solution is reached and $\tilde{\Delta}_i^\star = \Omega_{i_k}^\perp$.

Remark 17. *Note that the algorithm (3.12) is invariant under feedback transformation, since controllability distributions are controlled invariant by definition [Isi13]. Therefore, the algorithm (3.12) is equivalent to*

$$\begin{aligned} \Omega_{i_0} &= \Omega_i \\ \Omega_{i_k} &= \Omega_{i_{k-1}} + \mathcal{L}_{\tilde{\boldsymbol{f}}_2}(\Omega_{i_{k-1}} \cap \tilde{\Delta}^{G\perp}) + \sum_{i=1}^{n} \mathcal{L}_{\tilde{\boldsymbol{g}}_i}(\Omega_{i_{k-1}} \cap \tilde{\Delta}^{G\perp}), \end{aligned} \tag{3.13}$$

where $\tilde{\Delta}^G = span\{\tilde{\boldsymbol{G}}_2\} = span\{\tilde{\boldsymbol{g}}_1, ..., \tilde{\boldsymbol{g}}_n\}$.

Codistribution $(\Omega_{i_{k-1}} \cap \Delta^{G\perp})$ is trivial in the case of Lagrangian systems, since $\dim\{\Delta^{G\perp}\} = 0$ as the matrix $\boldsymbol{G}_2(\boldsymbol{\xi})$ is a full rank, square matrix. Therefore

$$\tilde{\Delta}_i^\star = \Omega_i^\perp. \tag{3.14}$$

The result given with (3.14) determines relevant properties of the controllability distributions in (3.8) for Euler-Lagrangian systems. They are summarized with Lemma 2.

Lemma 2. *Consider the dynamical system (3.2) under Assumptions 3.1.1-3.1.3. For such a system and taking into consideration the result in (3.14), the distributions $\tilde{\Delta}, \tilde{\Delta}^\star, \tilde{\Delta}_i, \tilde{\Delta}_i^\star, \forall i = 1, ..., n$, are nonsingular with $dim\{\tilde{\Delta}\} = n$, $dim\{\tilde{\Delta}^\star\} = 0$, $dim\{\tilde{\Delta}_i\} = k_i$, and $dim\{\tilde{\Delta}_i^\star\} = n - k_i$.*

Now it is possible to formulate the input-output decoupling control $\boldsymbol{\Gamma}(\boldsymbol{\xi})$.

Theorem 1. *Consider the dynamical system (3.2) under Assumptions 3.1.1-3.1.3. Provided that the conclusions of Lemma 2 for the controllability distributions $\tilde{\Delta}, \tilde{\Delta}^{\star}, \tilde{\Delta}_i, \tilde{\Delta}_i^{\star}, \forall i = 1, ..., n$, hold, the input-output noninteracting control problem is solvable with the invertible matrix $\boldsymbol{\Gamma}(\boldsymbol{\xi})$ being the solution of*

$$\tilde{\boldsymbol{J}}_b(\boldsymbol{\xi})\boldsymbol{G}_2(\boldsymbol{\xi})\boldsymbol{\Gamma}(\boldsymbol{\xi}) = \tilde{\boldsymbol{G}}_{b2}(\boldsymbol{\xi}), \tag{3.15}$$

where $\tilde{\boldsymbol{J}}_b(\boldsymbol{\xi})$ is an appropriate parametrization of the behavior Jacobian that serves as a coordinate transformation and

$$\tilde{\boldsymbol{G}}_{b2}(\boldsymbol{\xi}) = \begin{bmatrix} \boldsymbol{M}_{b,1}^{-1} & \dots & \boldsymbol{0} \\ \vdots & \vdots & \vdots \\ \boldsymbol{0} & \dots & \boldsymbol{M}_{b,k}^{-1} \end{bmatrix}, \tag{3.16}$$

is the input matrix of the system transformed to behavior coordinates, while $\boldsymbol{M}_{b,i}$ is a positive-definite matrix $\forall i = 1, ..., k$.

The Theorem 1 states that the resulting matrix $\tilde{\boldsymbol{G}}_{b2}$ needs to be block-diagonal after appropriate coordinate transformation $\tilde{\boldsymbol{J}}_b$, parametrized with the behavior Jacobian $\boldsymbol{J}_b$, in order for the system (3.2) to be input-output noninteracting from the input $\tilde{\boldsymbol{\tau}}_{c,i}$ to the output $\boldsymbol{y}_i$.

Remark 18. *It should be noted that the choice of the matrix $\boldsymbol{\Gamma}(\boldsymbol{\xi})$ is not unique. Furthermore, the block-diagonal matrices $\boldsymbol{M}_{b,i}^{-1}$ of $\tilde{\boldsymbol{G}}_{b2}$ can be interpreted as desired inverse inertial matrices of the behaviors. In that context, the input-output noninteracting control law $\boldsymbol{\Gamma}(\boldsymbol{\xi})$ is a form of an* inertia-shaping approach *[FH18], applied in this particular case on the abstract levels of behaviors.*

Example 3.2.1. (Input-output noninteracting for two behaviors.) *In the case of two behaviors*

$$\begin{bmatrix} \boldsymbol{y}_1 \\ \boldsymbol{y}_2 \end{bmatrix} = \begin{bmatrix} \boldsymbol{J}_{b,1}(\boldsymbol{\xi}) \\ \boldsymbol{J}_{b,2}(\boldsymbol{\xi}) \end{bmatrix} \dot{\boldsymbol{\theta}}, \tag{3.17}$$

the noninteraction control can be designed as

$$\boldsymbol{\Gamma}(\boldsymbol{\xi}) = \begin{bmatrix} \boldsymbol{K}_{b,2}(\boldsymbol{\xi})^{\top}\boldsymbol{J}_{b,1}(\boldsymbol{\xi})^{\top} \\ \boldsymbol{K}_{b,1}(\boldsymbol{\xi})^{\top}\boldsymbol{J}_{b,2}(\boldsymbol{\xi})^{\top} \end{bmatrix}, \tag{3.18}$$

where $\boldsymbol{K}_{b,i} = (\boldsymbol{I}_n - \boldsymbol{J}_{b,i}^{\#\boldsymbol{M}}\boldsymbol{J}_{b,i})$, $i = 1, 2$, is a kernel (null-space) matrix with

$$\boldsymbol{J}_{b,i}^{\#\boldsymbol{M}} = \boldsymbol{M}^{-1}\boldsymbol{J}_{b,i}^{\top}(\boldsymbol{J}_{b,i}\boldsymbol{M}^{-1}\boldsymbol{J}_{b,i}^{\top})^{-1}, \tag{3.19}$$

being the inertia-weighted pseudo-inverse matrix. Inserting (3.17) and (3.18) into (3.15) gives as a result a block-diagonal matrix of the form

$$\tilde{\boldsymbol{G}}_{b2} = \begin{bmatrix} \boldsymbol{J}_{b,1}\boldsymbol{M}^{-1}\boldsymbol{K}_{b,2}^{\top}\boldsymbol{J}_{b,1}^{\top} & \boldsymbol{0}_{k_1 \times k_2} \\ \boldsymbol{0}_{k_2 \times k_1} & \boldsymbol{J}_{b,2}\boldsymbol{M}^{-1}\boldsymbol{K}_{b,1}^{\top}\boldsymbol{J}_{b,2}^{\top} \end{bmatrix}.$$

Remark 19. *An approach that relies on inertia-weighted pseudo-inverse matrix is frequently used in robotics for* dynamically consistent redundancy resolution *of robot manipulators, see e.g. [KYC+96]. It is a part of the well-known* operational-space approach *[Kha87]. The difference of the decoupling approach, proposed with Theorem 1, and such redundancy resolution approaches is that the noninteracting input-output control does not assign priorities to the behaviors. In that sense, all the behaviors have the same priorities. However, while the redundancy resolution ensures that the highest priority behavior is executed while the lower priority behaviors may be executed if possible, the approach proposed with Theorem 1 is more restrictive, since it does not evolve at all on the behavior subspaces that intersect. Therefore, it is more suitable for robot systems with high number of degrees of freedom such as robot teams.*

An example given below refers to the classical *redundancy resolution* approach used in robotics and relates it to the introduced noninteracting control.

Example 3.2.2. (Redundancy resolution.) *Behaviors can be conducted according to a predefined priority. A common control strategy that ensures the prioritization is termed as* redundancy resolution *for single robots and* null-space based behavioral control *for robot teams [AAC08]. It is based on the projection of lower priority behaviors onto the null-space of the higher priority behavior. For example, in the case of two behaviors, the position of a robot manipulator in Cartesian space $\boldsymbol{x} \in \mathbb{R}^3$ would be*

$$\boldsymbol{x} = \boldsymbol{J}_{b,1}^{\dagger}\boldsymbol{x}_{b,1} + (\boldsymbol{I}_3 - \boldsymbol{J}_{b,1}^{\dagger}\boldsymbol{J}_{b,1})\boldsymbol{J}_{b,2}^{\dagger}\boldsymbol{x}_{b,2}, \tag{3.20}$$

where $\boldsymbol{J}_{b,1}^{\dagger}$ denotes the pseudo-inverse of the behavior Jacobian $\boldsymbol{J}_{b,1}$ and $\boldsymbol{N}_1 = (\boldsymbol{I} - \boldsymbol{J}_{b_1}^{\dagger}\boldsymbol{J}_{b_1})$ is the null-space projector (see Example 2.3.2 that provides a similar discussion). Note though, that the approach is kinematic*, which makes it unsuitable for the control of dynamic behaviors, e.g. when the inertia of the robots cannot be neglected. Additionally, the interaction with the environment, i.e. with objects or humans, cannot be handled appropriately. The dynamic decoupling control addresses these shortcomings. The allocation of responsibilities to the individual robots, according to the selected behaviors, and the role they have within the team is an important step and can be handled in various ways, see for example [GM04] and [ZXYW07].*

3.2.2 State Noninteracting Control

State noninteracting control enables representation of (3.2) in a fully decoupled form through the appropriate control design $\boldsymbol{\alpha}(\boldsymbol{\xi})$ in (3.4) and coordinate transformation to obtain

$$\begin{aligned}
\dot{\boldsymbol{x}}_b &= \dot{\boldsymbol{x}}_b \\
\ddot{\boldsymbol{x}}_{b,1} &= \tilde{\boldsymbol{f}}_{b,1}(\boldsymbol{x}_{b,1}, \dot{\boldsymbol{x}}_{b,1}) + \tilde{\boldsymbol{G}}_{b,1}(\boldsymbol{x}_b)(\tilde{\boldsymbol{\tau}}_{c,1} + \tilde{\boldsymbol{\tau}}_{e,1}) \\
&\vdots \\
\ddot{\boldsymbol{x}}_{b,k} &= \tilde{\boldsymbol{f}}_{b,k}(\boldsymbol{x}_{b,k}, \dot{\boldsymbol{x}}_{b,k}) + \tilde{\boldsymbol{G}}_{b,k}(\boldsymbol{x}_b)(\tilde{\boldsymbol{\tau}}_{c,k} + \tilde{\boldsymbol{\tau}}_{e,k}) \\
\boldsymbol{y}_1 &= \dot{\boldsymbol{x}}_{b,1} \\
&\vdots \\
\boldsymbol{y}_k &= \dot{\boldsymbol{x}}_{b,k}.
\end{aligned} \tag{3.21}$$

where $\boldsymbol{x}_b \in \mathcal{M}_b$ is the stacked vector of all behavior and $\tilde{\boldsymbol{\tau}}_{e,i}$ is the torque component that results from the interaction with the environment and contributes to the i^{th} behavior.

Remark 20. *Fully decoupled behavior dynamic representation (3.21) resembles the behavior dynamics introduced in Chapter 2 with (2.17). The difference is that while (2.17) is only transformed in new coordinates, i.e. to abstract (behavior) coordinates, (3.21) represents behavior dynamics in behavior coordinates which is additionally noninteracting.*

The coordinate transformation defines new states, termed in this thesis as *behavior states*. In Chapter 2 Proposition 2.2.1 defines the appropriate coordinate transformation through $\boldsymbol{\phi}(\boldsymbol{\xi})$ and the behavior Jacobian $\boldsymbol{J}_b$. Note that any basis of the codistribution Ω_i, defined with (3.11), is a valid coordinate transformation as long as the condition of Proposition 2.2.1 on its smoothness and nonsingularity of the corresponding Jacobian are satisfied.

Remark 21. *One of the valid coordinate transformations, which are parametrizations of the behavior Jacobian, $\boldsymbol{J}_b$, are those that satisfy the equality $\boldsymbol{J}_{b,i}\boldsymbol{J}_{b,j}^\top = \boldsymbol{0}$ for every $i \neq j$.*

In general, when an input-output noninteracting controller (3.15) is applied to (3.2), the state noninteraction is not immediately achieved due to the coupling effects in Coriolis and centrifugal terms [ODAS15]. More specifically, if $\ddot{\boldsymbol{\theta}} = \boldsymbol{J}_b^{-1}(\ddot{\boldsymbol{x}}_b - \dot{\boldsymbol{J}}_b\boldsymbol{J}_b^{-1}\dot{\boldsymbol{x}}_b)$ and $\dot{\boldsymbol{\theta}} = \boldsymbol{J}_b^{-1}\dot{\boldsymbol{x}}_b$ are inserted in (3.2), the representation of the dynamical system after the coordinate change is

$$\ddot{\boldsymbol{x}}_b = \underbrace{-\boldsymbol{J}_b\boldsymbol{M}^{-1}(\boldsymbol{C}\boldsymbol{J}_b^{-1}\dot{\boldsymbol{x}}_b + \boldsymbol{\tau}_g) + \dot{\boldsymbol{J}}_b\boldsymbol{J}_b^{-1}\dot{\boldsymbol{x}}_b}_{\tilde{\boldsymbol{f}}_b(\boldsymbol{x}_b,\dot{\boldsymbol{x}}_b)} + \boldsymbol{M}_b^{-1}\tilde{\boldsymbol{\tau}}_c + \boldsymbol{M}_b^{-1}\tilde{\boldsymbol{\tau}}_e,$$

where it is possible to write

$$\begin{aligned}\tilde{\boldsymbol{f}}_b(\boldsymbol{x}_b,\dot{\boldsymbol{x}}_b) &= -\boldsymbol{J}_b\boldsymbol{M}^{-1}\boldsymbol{C}\boldsymbol{J}_b^{-1}\dot{\boldsymbol{x}}_b + \dot{\boldsymbol{J}}_b\boldsymbol{J}_b^{-1}\dot{\boldsymbol{x}}_b - \boldsymbol{J}_b\boldsymbol{M}^{-1}\boldsymbol{\tau}_g \\ &= (-\underbrace{\boldsymbol{J}_b\boldsymbol{M}^{-1}\boldsymbol{\Gamma}}_{\boldsymbol{M}_b^{-1}}\boldsymbol{\Gamma}^{-1}\boldsymbol{C}\boldsymbol{J}_b^{-1} + \dot{\boldsymbol{J}}_b\boldsymbol{J}_b^{-1})\dot{\boldsymbol{x}}_b - \boldsymbol{J}_b\boldsymbol{M}^{-1}\boldsymbol{\tau}_g \\ &= -\boldsymbol{M}_b^{-1}(\boldsymbol{\Gamma}^{-1}\boldsymbol{C}\boldsymbol{J}_b^{-1} - \boldsymbol{M}_b\dot{\boldsymbol{J}}_b\boldsymbol{J}_b^{-1})\dot{\boldsymbol{x}}_b - \boldsymbol{J}_b\boldsymbol{M}^{-1}\boldsymbol{\tau}_g,\end{aligned} \tag{3.22}$$

and the Coriolis and centrifugal term after the change of coordinates is, therefore

$$\boldsymbol{C}_b = \boldsymbol{\Gamma}^{-1}\boldsymbol{C}\boldsymbol{J}_b^{-1}, \tag{3.23}$$

which, in general, has off-diagonal components. This means that $\tilde{\boldsymbol{f}}_{b,i}$ depends on $\dot{\boldsymbol{x}}_b$ instead of on the corresponding vector $\dot{\boldsymbol{x}}_{b,i}$ only, as envisioned with (3.21). Therefore, the state noninteraction needs to be achieved by compensating the coupling Coriolis and centrifugal terms with the control component $\boldsymbol{\alpha}(\boldsymbol{\xi})$ of (3.4). One approach could be to compensate for Coriolis, centrifugal and gravitational terms, i.e. to cancel out $\boldsymbol{f}_2(\boldsymbol{\xi})$ component in (3.5). This can be achieved locally with feedback input-output linearization. Instead, in this thesis, and similar to the control design for redundancy resolution in [ODAS15], $\boldsymbol{\alpha}(\boldsymbol{\xi})$ is designed to modify Coriolis and centrifugal matrix to a block-diagonal form $\tilde{\boldsymbol{C}}_b$ and to compensate gravity vector $\boldsymbol{\tau}_g$ as well as the component with the time derivative of the behavior Jacobian, $\dot{\boldsymbol{J}}_b$. As a consequence of such a control design, skew-symmetric property of $\dot{\boldsymbol{M}}_{b,i} - 2\tilde{\boldsymbol{C}}_{b,i}$, which is beneficial for passivity guarantees, is preserved in the new coordinates. Therefore, the following theorem proposes such a design of the vector $\boldsymbol{\alpha}(\boldsymbol{\xi})$.

Theorem 2. *Consider the dynamical system (3.2) under the Assumptions 3.1.1-3.1.3 and with the applied input-output noninteracting control law (3.15). For this system the state noninteraction problem with preserved Lagrangian dynamical structure and gravity compensation is solvable with*

$$\boldsymbol{\alpha}(\boldsymbol{\xi}) = \boldsymbol{M}\boldsymbol{J}_b^{-1}\boldsymbol{M}_b^{-1}\begin{bmatrix} \sum_{j=2}^{k} \boldsymbol{C}_{b,1j}\dot{\boldsymbol{x}}_{bj} \\ \vdots \\ \sum_{j=1}^{i-1} \boldsymbol{C}_{b,ij}\dot{\boldsymbol{x}}_{bj} + \sum_{j=i+1}^{k} \boldsymbol{C}_{b,ij}\dot{\boldsymbol{x}}_{bj} \\ \vdots \\ \sum_{j=1}^{k-1} \boldsymbol{C}_{b,pj}\dot{\boldsymbol{x}}_{bj} \end{bmatrix} - \dot{\boldsymbol{J}}_b\boldsymbol{J}_b^{-1}\dot{\boldsymbol{x}}_b + \boldsymbol{\tau}_g, \tag{3.24}$$

with $\boldsymbol{C}_{b,ij}$ being the off-diagonal matrix in the row block i and the column block j of $\boldsymbol{C}_b$.

From a practical point of view, allocating subtasks to the human operator or the robot autonomy means ensuring that the input provided from a particular source influences *only* the corresponding behavior, while *all* the remaining behaviors are not affected by this input. In the remainder of this section, an example of human-robot team interaction is given.

Example 3.2.3. (Object transportation task.) *If the task of* object transportation *is executed by a team of robot manipulators, possible subtasks may be:* grasping the object, nonviolation of constraints imposed by the object geometry (i.e. maintaining a desired formation), motion of the robot team in a formation towards the goal, inter-robot collision avoidance *and* obstacle avoidance. *Figure 3.1 depicts a teleoperation scenario where the human partner provides a desired trajectory command for the motion of the robot team in a formation towards the goal, while the robot team applies required grasping force on the object. These two subtasks need to be decoupled through the noninteracting control proposed with Theorem 1 and Theorem 2 in order to avoid interferences.*

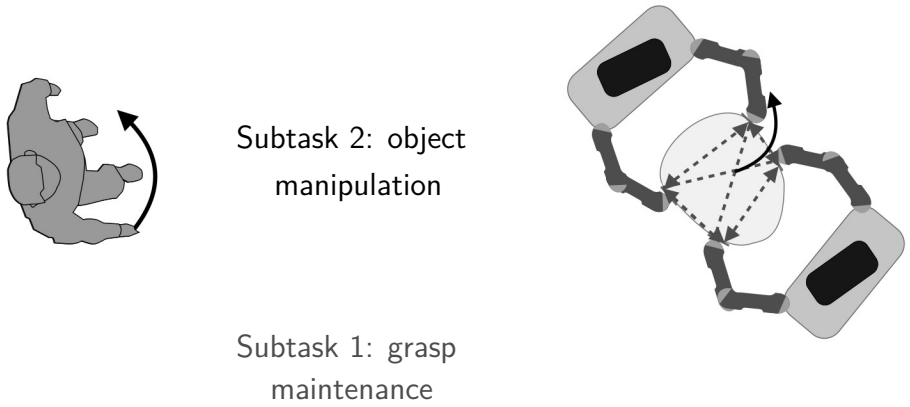

Figure 3.1: Subtask allocation to the human and the robot team partners in a cooperative manipulation task.

3.2.3 Passivity Guarantees

The objective of this section is to propose a nominal control approach $\tilde{\boldsymbol{\tau}}_{c,i}, i = 1, ..., k$, to solve Problem 4, i.e. to render the subsystems in (3.21) passive from the inputs $\tilde{\boldsymbol{\tau}}_{e,i}$ to the outputs $\dot{\boldsymbol{x}}_{b,i}$, $\forall i = 1, ..., k$.

The representation in (3.21) enables the assignement of different control goals to the behaviors. Therefore, the control design depends on the control goal for each behavior. Typical control goals in human-robot interaction are motion tracking or regulation if there is no interaction with the environment, and force tracking or regulation if there is contact with the environment. For example, motion of the human operator can be tracked via motion tracking system and used as a reference input in the task space of the robot. In combined motion and force tasks, the control goal is often to achieve a desired compliant interaction dynamics. Since such tasks are in the focus of this thesis, *impedance control* [VDS16] is chosen as an exemplary nominal controller to achieve subtasks and passivity guarantees. For that purpose, an additional coordinate change is introduced to (3.21)

$$\begin{aligned} \boldsymbol{e}_{b,i} &= \boldsymbol{x}_{b,i} - \boldsymbol{x}^d_{b,i} \\ \dot{\boldsymbol{e}}_{b,i} &= \dot{\boldsymbol{x}}_{b,i} - \dot{\boldsymbol{x}}^d_{b,i}, \quad \forall i = 1, ..., k \end{aligned}$$

where $\boldsymbol{x}^d_{b,i}$ is the desired setpoint or trajectory for the behavior state $\boldsymbol{x}_{b,i}$, while $\boldsymbol{e}_{b,i}$ and $\dot{\boldsymbol{e}}_{b,i}$ are subtask position and velocity tracking errors, respectively. The error dynamics of (3.21) in state-space form is

$$\begin{bmatrix} \dot{\boldsymbol{e}}_{b,i} \\ \ddot{\boldsymbol{e}}_{b,i} \end{bmatrix} = \begin{bmatrix} \dot{\boldsymbol{e}}_{b,i} \\ -\boldsymbol{M}^{-1}_{b,i}\boldsymbol{C}_{b,i}(\dot{\boldsymbol{e}}_{b,i} + \dot{\boldsymbol{x}}^d_{b,i}) \end{bmatrix} + \begin{bmatrix} \boldsymbol{0} \\ \boldsymbol{M}^{-1}_{b,i} \end{bmatrix} (\tilde{\boldsymbol{\tau}}_{c,i} + \tilde{\boldsymbol{\tau}}_{e,i}) - \ddot{\boldsymbol{x}}^d_{b,i}, \tag{3.25}$$

for each subtask, $i = 1, ..., k$. The desired error dynamics is defined as the impedance with the desired virtual damping and stiffness

$$\boldsymbol{M}_{b,i}\ddot{\boldsymbol{e}}_{b,i} + (\boldsymbol{C}_{b,i} + \boldsymbol{D}_i)\dot{\boldsymbol{e}}_{b,i} + \boldsymbol{w}_{\boldsymbol{K},i}(\boldsymbol{e}_{b,i}) = \tilde{\boldsymbol{\tau}}_{e,i}, \tag{3.26}$$

where $i = 1, ..., k$, $\boldsymbol{D}_i \in \mathbb{R}^{k_i \times k_i}$ is a positive-definite damping matrix, and $\boldsymbol{w}_{K,i} \in \mathbb{R}^{k_i}$ is a stiffness term which shapes the desired potential energy $V_K(\boldsymbol{e}_{b,i})$ to realize desired spring behavior.

Remark 22. *A typical way to realize desired spring behavior is to shape the potential energy V_K with virtual springs [CCMV08]*

$$V_K(\boldsymbol{e}_{b,i}) = \frac{1}{2}\boldsymbol{e}^\top_{b,i}\boldsymbol{K}_i\boldsymbol{e}_{b,i}, \tag{3.27}$$

where $\boldsymbol{K}_i \in \mathbb{R}^{k_i \times k_i}$ is a positive definite stiffness matrix. Then, the wrench resulting from the desired stiffness behavior, $\boldsymbol{w}_{K,i}$ is

$$\boldsymbol{w}_{K,i}(\boldsymbol{e}_{b,i}) = \left(\frac{\partial V_K(\boldsymbol{e}_{b,i})}{\partial \boldsymbol{e}_{b,i}}\right)^\top. \tag{3.28}$$

In order to achieve the desired error dynamics (3.26), it is sufficient to apply the following control law to (3.25)

$$\tilde{\boldsymbol{\tau}}_{c,i} = \boldsymbol{M}_{b,i}\ddot{\boldsymbol{x}}^d_{b,i} + \boldsymbol{C}_{b,i}\dot{\boldsymbol{x}}^d_{b,i} - \boldsymbol{D}_i\dot{\boldsymbol{e}}_{b,i} - \boldsymbol{w}_{\boldsymbol{K},i}. \tag{3.29}$$

Now it is possible to show that the subtask error dynamics (3.25), under the control law (3.29), is passive. Preserving passivity in the interaction is important because it guarantees a limited transfer of energy from the robot to the human operator or the environment. In that way, it is possible to maintain safe interactions. For that purpose, let us use the definition of passivity from [KG02].

Definition 3.2.1 ([KG02])**.** *The system is passive if there exists a positive semidefinite storage function $S_i(\boldsymbol{e}_{b,i}, \dot{\boldsymbol{e}}_{b,i})$ such that over a time period $[0, T]$*

$$\int_0^T \dot{\boldsymbol{e}}_{b,i}^\top \tilde{\boldsymbol{\tau}}_{e,i} \geq S(\boldsymbol{e}_{b,i}(T), \dot{\boldsymbol{e}}_{b,i}(T)) - S(\boldsymbol{e}_{b,i}(0), \dot{\boldsymbol{e}}_{b,i}(0)). \tag{3.30}$$

Let us show that the passivity of (3.25) is preserved with the control law (3.29).

Proposition 3.2.2. *Subtask error dynamics (3.25) is passive from the input $\tilde{\boldsymbol{\tau}}_{e,i}$ to the output $\dot{\boldsymbol{e}}_{b,i}$ with storage function*

$$S_i(\boldsymbol{e}_{b,i}, \dot{\boldsymbol{e}}_{b,i}) = \frac{1}{2} \dot{\boldsymbol{e}}_{b,i}^\top \boldsymbol{M}_{b,i} \dot{\boldsymbol{e}}_{b,i} + V_K(\boldsymbol{e}_{b,i}) \tag{3.31}$$

where $V_K(\boldsymbol{e}_{b,i})$ is defined in (3.27).

Fig. 3.2 depicts the block diagram of the overall interaction system with the proposed control architecture.

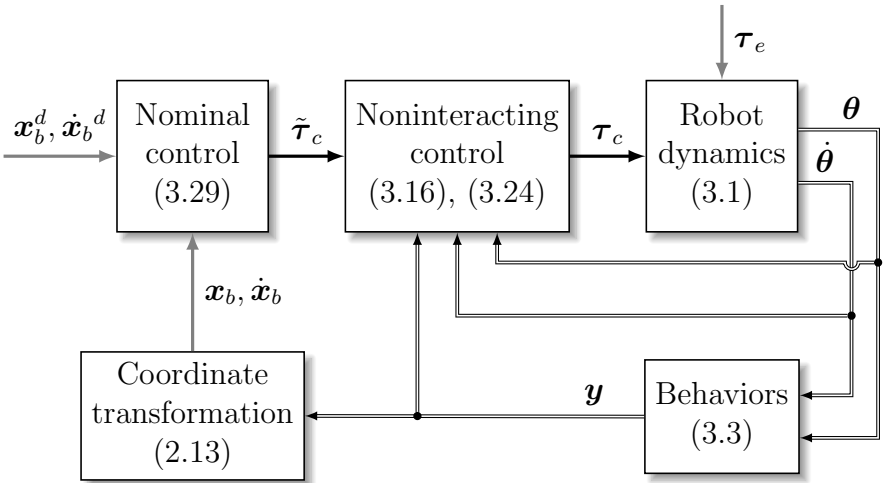

Figure 3.2: Block diagram of the proposed control approach.

3.3 Results

The proposed control approach is validated in a numerical simulation and an experiment with human in the loop and a haptic device.

3.3.1 Simulation Results

In this section simulation results of the Example 2.2.2 on *formation control* are presented. For that purpose, let us consider a robot team, consisting of two nonhomogeneous robots with second-order (point-mass) dynamics as in (2.4). The robots can move in $x-y$ plane and their generalized coordinates are

$$\boldsymbol{x}_i = [p_{x,i},\ p_{y,i}]^\top \in \mathbb{R}^2, \quad i = 1, 2.$$

The inertia matrix is defined as

$$\boldsymbol{M} = \begin{bmatrix} m_1 \boldsymbol{I}_2 & \boldsymbol{0}_{2\times 2} \\ \boldsymbol{0}_{2\times 2} & m_2 \boldsymbol{I}_2 \end{bmatrix},$$

where m_1 and m_2 are masses of the two robots. Coriolis, centrifugal and gravitational terms of the point-mass dynamics are $\boldsymbol{C} = \boldsymbol{0}_{4\times 4}$, and $\boldsymbol{\tau}_g = \boldsymbol{0}_{4\times 1}$. The robot team dynamics can be rewritten as in (3.2)

$$\begin{bmatrix} \dot{\boldsymbol{x}} \\ \ddot{\boldsymbol{x}} \end{bmatrix} = \begin{bmatrix} \dot{\boldsymbol{x}} \\ \boldsymbol{0} \end{bmatrix} + \begin{bmatrix} \boldsymbol{0} \\ \boldsymbol{M}^{-1} \end{bmatrix} (\boldsymbol{\tau}_c + \boldsymbol{\tau}_e). \tag{3.32}$$

According to the Example 2.2.2, the subtasks are: (i) the robots maintain a formation, i.e. fixed relative distance between each other and (ii) the robot team moves in $x-y$ plane as a single entity towards the goal position. These two subtasks need to be executed simultaneously. They can be suitable in e.g. object transportation tasks. The two following behaviors are defined as the outputs of (3.32)

$$\begin{aligned} \boldsymbol{y}_1 &= \underbrace{\frac{1}{2}[\boldsymbol{I}_2\ \boldsymbol{I}_2]}_{\boldsymbol{J}_{b,1}} \dot{\boldsymbol{x}} \\ \boldsymbol{y}_2 &= \underbrace{[\boldsymbol{I}_2\ -\boldsymbol{I}_2]}_{\boldsymbol{J}_{b,2}} \dot{\boldsymbol{x}}. \end{aligned} \tag{3.33}$$

Applying the noninteracting control proposed with Theorem 1 and Example 3.2.1 in the form of (3.18), as well as the coordinate transformation using the behavior Jacobian $\boldsymbol{J}_b$, generates the representation as in (3.21)

$$\begin{bmatrix} \dot{\boldsymbol{x}}_b \\ \ddot{\boldsymbol{x}}_b \end{bmatrix} = \begin{bmatrix} \boldsymbol{J}_b \dot{\boldsymbol{x}} \\ \boldsymbol{0} \end{bmatrix} + \begin{bmatrix} \boldsymbol{0}_{4\times 4} \\ \begin{bmatrix} \boldsymbol{M}_{b,1}^{-1} & \boldsymbol{0}_{2\times 2} \\ \boldsymbol{0}_{2\times 2} & \boldsymbol{M}_{b,2}^{-1} \end{bmatrix} \end{bmatrix} (\tilde{\boldsymbol{\tau}}_c + \tilde{\boldsymbol{\tau}}_e). \tag{3.34}$$

Now a control law $\tilde{\boldsymbol{\tau}}_c$ as in (3.29) can be applied to obtain desired error dynamics for both behaviors as in (3.26). Let the following control goals be imposed on the cooperative and relative behaviors

$$\begin{aligned} \boldsymbol{x}_{b,1}^d &= [2\sin(0.79\mathrm{t})\ 1]^\top \\ \boldsymbol{x}_{b,2}^d &= [1\ 1]^\top. \end{aligned}$$

The linear stiffness $\boldsymbol{w}_{\boldsymbol{K},i}(\boldsymbol{e}_{b,i}) = \boldsymbol{K}_i \boldsymbol{e}_{b,i}$ is used for both subtasks. The model and the control parameters are listed in Table 3.1.

t_s [ms]	m_1 [kg]	m_2 [kg]	$\boldsymbol{D}_1$ [Ns/m]	$\boldsymbol{D}_2$ [Ns/m]	$\boldsymbol{K}_1$ [N/m]	$\boldsymbol{K}_2[N/m]$
1	1	2	$53\boldsymbol{I}_2$	$25\boldsymbol{I}_2$	$25\boldsymbol{I}_2$	$50\boldsymbol{I}_2$

Table 3.1: Simulation parameters.

Desired and actual positions for the two behaviors defined with (3.33) are depicted in Figure 3.3 and Figure 3.4. Note that the y-coordinate for the behavior 2 is omitted in Figure 3.4 since its plot is similar to the x-coordinate. As can be observed, the simultaneous achievement of the subtasks is possible without interferences. More specifically, it is possible to control the robot team to move as an entity while simultaneously maintaining the desired distance between each other.

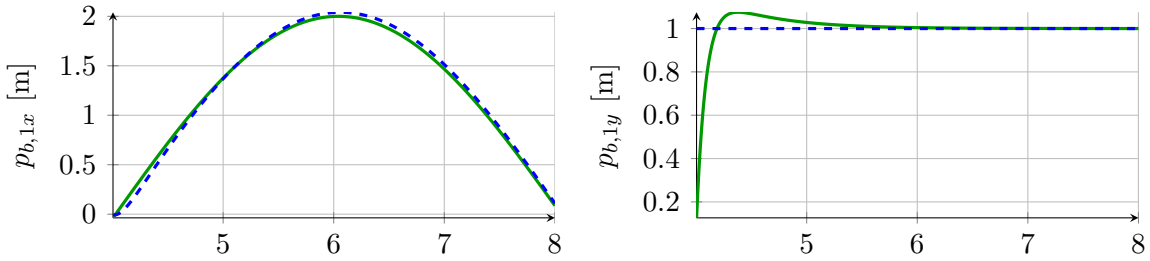

Figure 3.3: Desired - - - and actual — x-coordinate position (left) and y-coordinate position (right) of the robot team (behavior 1).

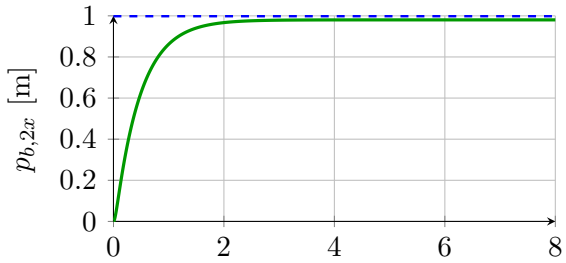

Figure 3.4: Desired - - - and actual — x-coordinate position between the robots (behavior 2).

The subtasks are passive according to (3.31). This can be observed from Figure 3.5 which depicts the storage functions for the two subtasks. It shows that the behavior subsystems (3.34) are passive, since the storage functions are positive semidefinite and their derivatives are negative semidefinite for all $t \geq 0$.

Let us now consider the coupling effects, i.e. if the noninteracting controller proposed with Theorem 1 is not applied. Instead, the behavior dynamics is obtained by applying coordinate transformation using the behavior Jacobian $\boldsymbol{J}_b$ to obtain the behavior dynamics as in (2.17). To emphasize the coupling effects let us consider two robots with higher inertia, $m_1 = 10$ [kg] and $m_2 = 15$ [kg]. Furthermore, let us consider the same desired trajectories and setpoints as in the previous example, but let behavior 1 be activated at $t = 4$ [s].

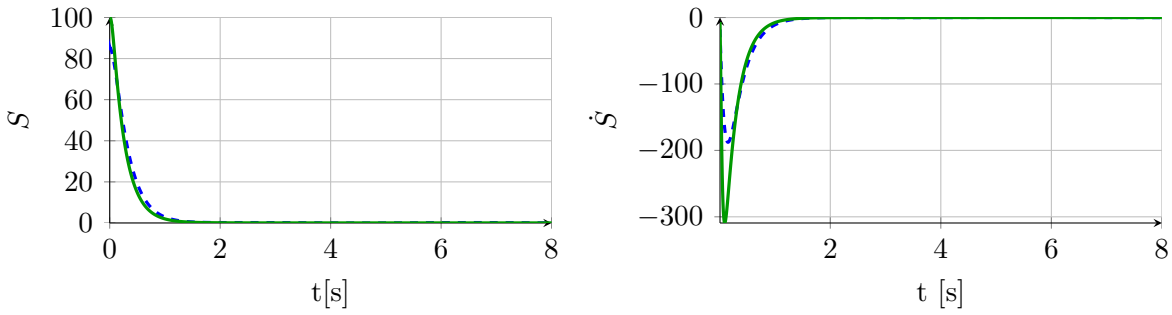

Figure 3.5: Storage functions for behavior 1 S_1 --- and behavior 2 S_2 — (left) and their derivatives $\dot{S}_1$ and $\dot{S}_2$ (right).

$$\boldsymbol{x}_{b,1}^d = [2\sin(0.79\mathrm{t})\ 1]^\top, \quad t \geq 4\,\mathrm{s}$$
$$\boldsymbol{x}_{b,2}^d = [1\ 1]^\top.$$

Desired and actual x positions for the two behaviors defined with (3.33) are depicted in Figure 3.6. As can be observed, the tracking of the desired behavior trajectories without the noninteracting control cannot be achieved simultaneously due to the coupling effects. Namely, the robot team "looses" the desired formation (behavior 2 tracking) once the behavior 1 is activated at $t = 4$ [s].

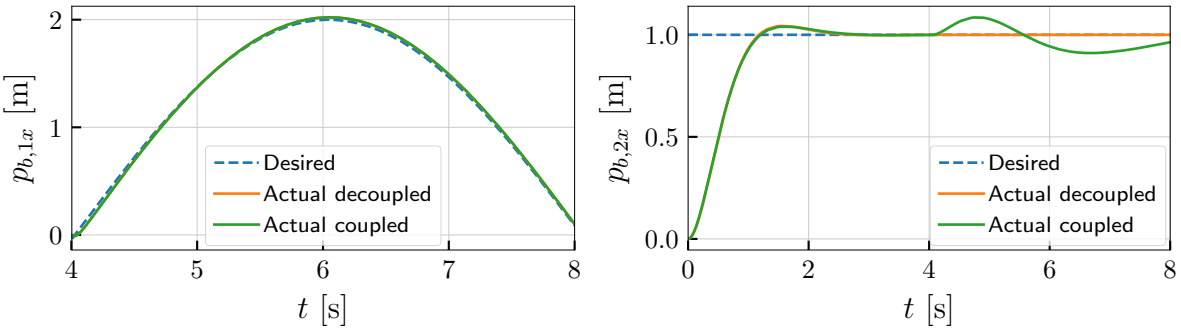

Figure 3.6: Desired and actual x-coordinate positions for the two robot team behaviors. Coupling effects that affect the tracking performance can be observed in the case when the noninteracting controller is not used.

In practice, the human operator can provide reference trajectory for the behavior 1 through a haptic device while the robot team performs the behavior 2 autonomously. In this case, coupling effects are highly undesirable, since they would affect the human through the haptic device feedback. This is shown experimentally in the following section.

3.3.2 Experimental Results

In this section experimental results of the proposed approach, suitable for haptic-enabled cooperative manipulation tasks, are provided. Let us consider two robot manipulators, modeled with Euler-Lagrangian dynamics as in (3.2) and the two subtasks, proposed in Example 3.2.3: (i) *object manipulation* and (ii) *grasp maintenance*. In order to achieve these

subtasks, *cooperative* and *relative* behaviors are proposed in this thesis. For the detailed definition of these behaviors, the reader is referred to Chapter 4, Section 4.2.

The desired cooperative behavior is achieved using the impedance control approach

$$\boldsymbol{w}_c = \boldsymbol{M}_c\dot{\boldsymbol{v}}_c + \boldsymbol{D}_c(\boldsymbol{v}_c - \boldsymbol{v}_c^d) + \boldsymbol{w}_{K,c}(\boldsymbol{x}_c, \boldsymbol{x}_c^d), \tag{3.35}$$

where $\boldsymbol{w}_c \in \mathbb{R}^6$ is cooperative control wrench in Cartesian space, $\boldsymbol{v}_c = [\dot{\boldsymbol{p}}_c^\top, \boldsymbol{\omega}_c^\top]^\top \in \mathbb{R}^6$ is cooperative velocity in Cartesian space, $\boldsymbol{x}_c = [\boldsymbol{p}_c^\top, \boldsymbol{q}_c^\top]^\top \in \mathrm{SE}(3)$ is cooperative pose, $\boldsymbol{D}_c = [d_c\boldsymbol{I}_3\,, \delta_c\boldsymbol{I}_3]^\top$ is damping and $\boldsymbol{w}_{K,c} = [k_c\boldsymbol{I}_3\,, \kappa_c\boldsymbol{I}_3]^\top[\boldsymbol{x}_c - \boldsymbol{x}_c^d\,, \Delta\boldsymbol{\epsilon}_c]$ is cooperative stiffness wrench. The vector $\Delta\boldsymbol{\epsilon}_c$ is the vector part of $\Delta\ \boldsymbol{q}_c = \boldsymbol{q}_c \star (\boldsymbol{q}_c^d)^{-1}$. The desired relative behavior is achieved with the force/impedance control. The impedance control is activated in the no-contact stage and during the transition from the no-contact to the contact stage

$$\boldsymbol{w}_r = \boldsymbol{D}_r(\boldsymbol{v}_r - \boldsymbol{v}_r^d) + \boldsymbol{w}_{K,r}(\boldsymbol{x}_r, \boldsymbol{x}_r^d), \tag{3.36}$$

where $\boldsymbol{w}_r \in \mathbb{R}^6$ is relative control wrench in Cartesian space, $\boldsymbol{v}_r = [\dot{\boldsymbol{p}}_r^\top, \boldsymbol{\omega}_r^\top]^\top \in \mathbb{R}^6$ is relative velocity in Cartesian space, $\boldsymbol{x}_r = [\boldsymbol{p}_r^\top, \boldsymbol{q}_r^\top]^\top \in SE(3)$ is relative pose, $\boldsymbol{D}_r = [d_r\boldsymbol{I}_3\,, \delta_r\boldsymbol{I}_3]^\top$ is damping and $\boldsymbol{w}_{K,r} = [k_r\boldsymbol{I}_3\,, \kappa_r\boldsymbol{I}_3]^\top[\boldsymbol{x}_r - \boldsymbol{x}_r^d\,, \Delta\boldsymbol{\epsilon}_r]$ is relative stiffness wrench. The force PI control is activated during the contact to maintain desired grasp maintenance forces

$$\boldsymbol{w}_r = \boldsymbol{K}_p(\boldsymbol{w}_{m,r} - \boldsymbol{w}_r^d) + \boldsymbol{K}_i \int (\boldsymbol{w}_{m,r} - \boldsymbol{w}_r^d)\mathrm{d}t, \tag{3.37}$$

where $\boldsymbol{w}_{m,r} \in \mathbb{R}^6$ is measured relative wrench, $\boldsymbol{w}_r^d \in \mathbb{R}^6$ is desired relative wrench, while $\boldsymbol{K}_p = k_p\boldsymbol{I}_3$ and $\boldsymbol{K}_i = k_i\boldsymbol{I}_3$ are control gains.

Experimental setup

The evaluation setup consists of two *KUKA iiwa* robot manipulators in a virtual reality and single *Omega7* haptic device. The manipulators interact with a 0.4 kg, box-shaped object. The human operator interacts with the system setup through the desktop haptic device, as depicted in Figure 3.7.

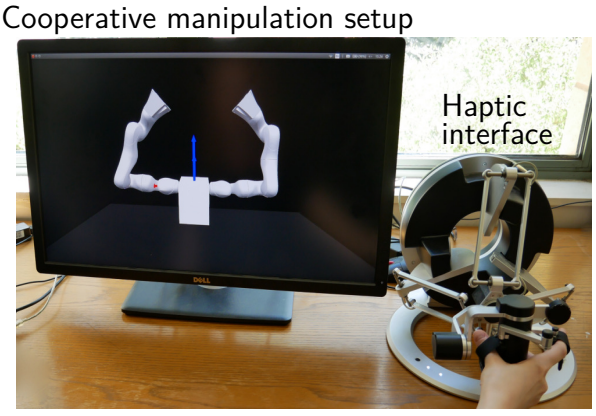

Figure 3.7: Experimental setup. The human operator interacts with the cooperative manipulation system in virtual reality through the Omega7 haptic device.

Omega7 has 7 degrees of freedom: 3 translational, 3 rotational, and 1 for grasping. The device has actuation capabilities for translations and grasping, and sensing capabilities for

orientation. The controller and the simulation environment are implemented using *SAI 2.0* framework [KBC+02], while the control of the haptic device is implemented using *chai3d* framework [CBB+03]. The sampling time of the controller and the haptic device is 1 kHz, and the simple time of the simulation is 3 kHz. The control parameters, used in the evaluation, are listed in Table 3.2.

Table 3.2: The control parameters.

Behaviors	$k_{c/r}$	$d_{c/r}$	$\kappa_{c/r}$	$\delta_{c/r}$	k_p	k_i
Cooperative	1400	560	312.5	100	/	/
Relative	900	420	225	25.5	1	1.5

First, the tracking performance of the controller with and without the decoupling is compared. The human operator is not included in the loop through the haptic interface. Instead, only the upward motion (z-coordinate) is commanded to the cooperative robot system. The recorded trajectories are shown in Figure 3.8 and the root mean squared error in Figure 3.9. As can be observed the tracking performance is better if the decoupling control is enabled.

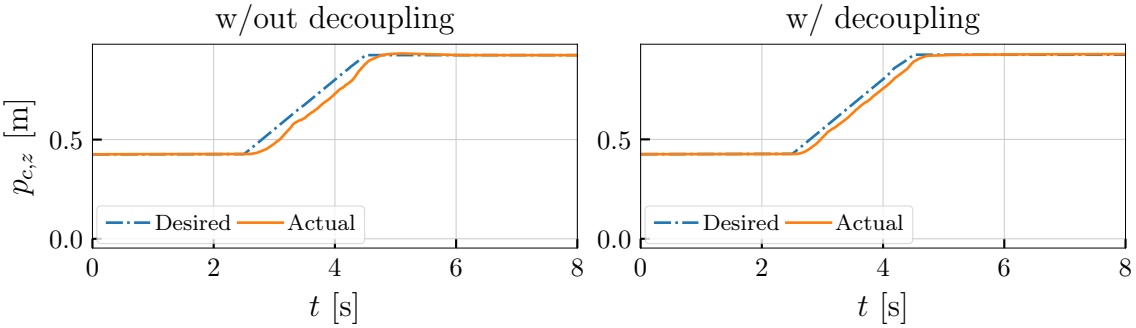

Figure 3.8: Simulation of upward motion of the cooperative system. Desired and actual z translation trajectories without (left) and with decoupling (right) are shown above.

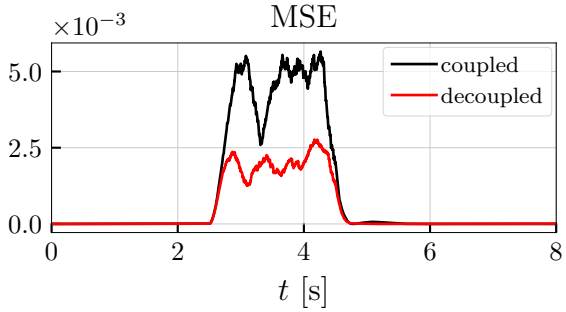

Figure 3.9: Root mean squared error of the trajectory tracking with coupling and without coupling effects.

In the second scenario the human operator is in the loop and controls the robot system through the haptic interface. First, the human operator controls both the cooperative and

the relative behaviors through the 7 degrees of freedom of the haptic device and the noninteracting control approach is used. The task is to lift the object along z-axis, transport the object along y-axis and rotate it around z-axis, while simultaneously maintaining the grasp over the object, by applying force along y-axis. The experimental results are depicted in Figure 3.10.

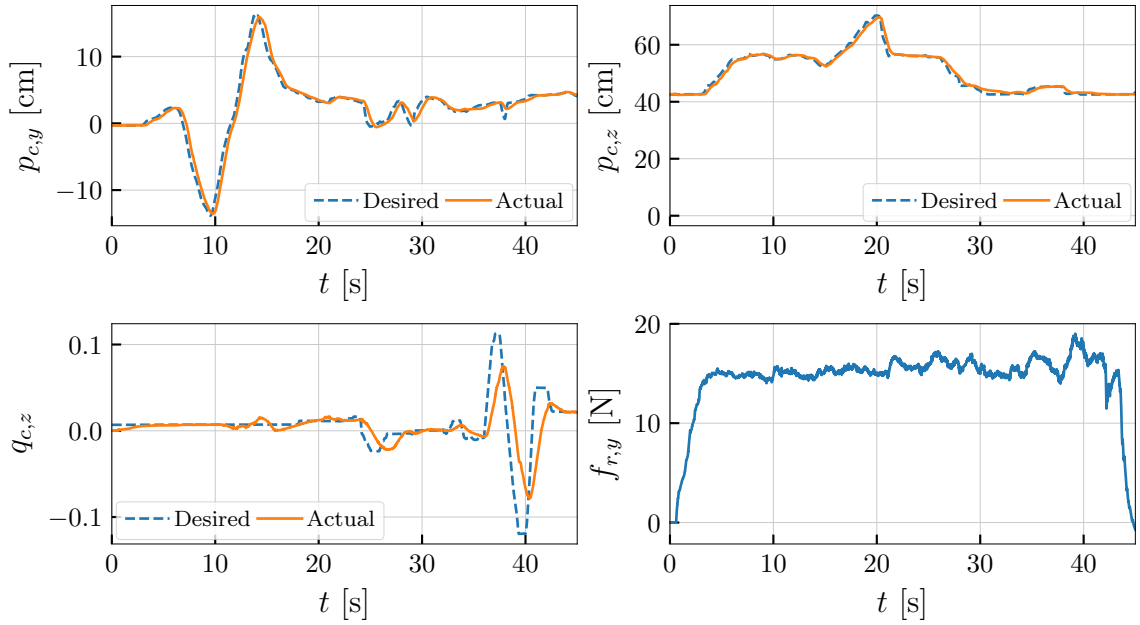

Figure 3.10: Experiment with the haptic interface and noninteracting control. The cooperative and relative behaviors are controlled by the human operator. The cooperative and relative forces are fed back to the human operator. Translation trajectories in y and z (above), rotation trajectory in z (below, left), and the relative force in y (below, right) are shown.

Figure 3.11 depicts the scenario without the noninteracting control, when the human operator controls both cooperative and relative behaviors through the haptic device. As can be observed, due to the coupling effects, the grasping (relative) force is very high. Its measured feedback reaches the force limits of the haptic device making it impossible to lift the object successfully and execute the task.

In the third scenario the relative behavior is controlled by the robot autonomy, while the human operator commands desired cooperative behavior trajectories through the haptic device. The translation trajectories in y and z directions, the rotation trajectory in z direction, and the relative force in y direction are depicted in Figure 3.12. A very good tracking of translation trajectories can be observed. Actual rotation trajectory follows closely the desired trajectory. The relative force which maintains the grasp is kept on a desired level. Its noise steams from the simulation of the rigid contacts.

3.4 Discussion

In this chapter a novel noninteracting control approach for Euler-Lagrangian systems with passivity guarantees is proposed. It is shown that it is possible to ensure that specific refer-

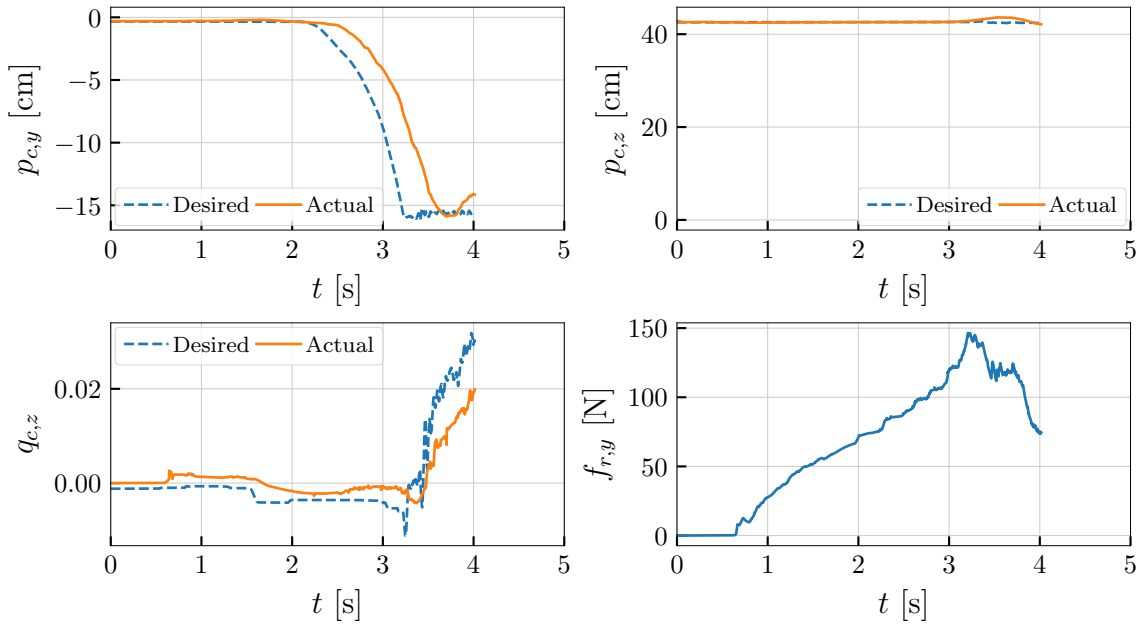

Figure 3.11: Experiment with the haptic interface, without the noninteracting control. The cooperative and relative behaviors are controlled by the human operator. The cooperative and relative forces are fed back to the human operator. Translation trajectories in y and z (above), rotation trajectory in z (below, left), and the relative force in y (below, right) are shown.

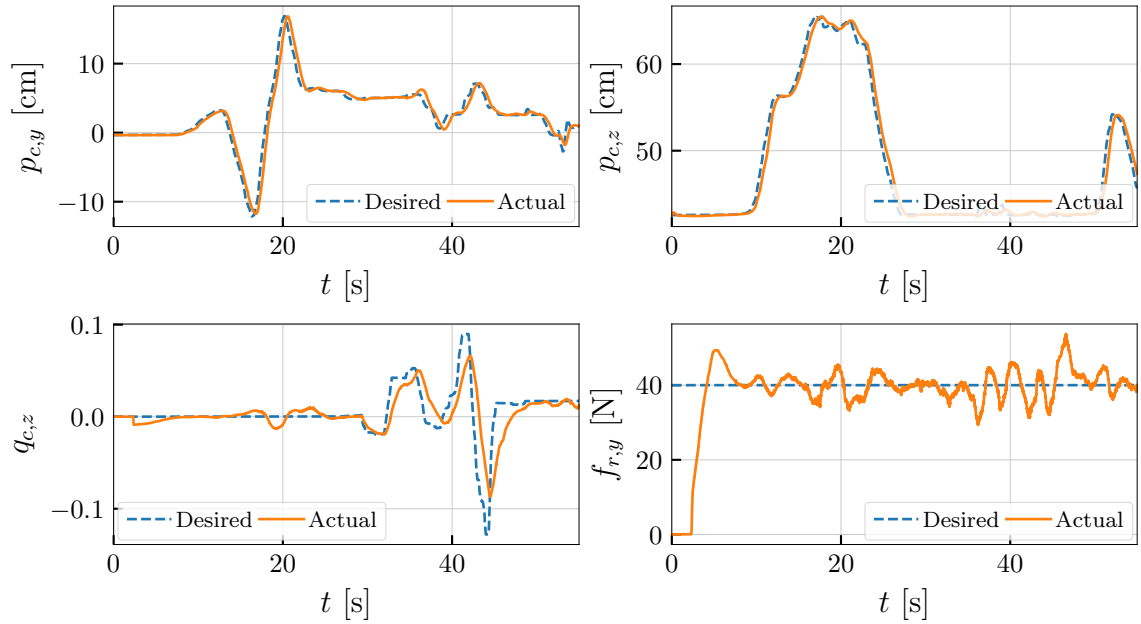

Figure 3.12: Experiment with the haptic interface. The relative behavior is controlled autonomously. The cooperative forces are fed back to the human operator. Translation trajectories in y and z (above), rotation trajectory in z (below, left), and the relative force in y (below, right) are shown.

ence inputs influence specific outputs/behaviors by applying the input-output noninteracting control. Furthermore, the system dynamics can be transformed into a set of subsystems through the state noninteracting control and appropriate coordinate transformation. By designing the noninteracting control law with the additional goal to preserve the Lagrangian properties of the obtained subsystems, the passivity property can be obtained. Then, each subsystem can have its own control goal. Through the simulation of a numerical example it is shown that it is possible to achieve control goals imposed on subtasks simultaneously and that without noninteracting control the coupling effects between the behaviors affect the trajectory tracking performance. The experimental results in a haptic cooperative manipulation scenario confirm these results. Furthermore, the experimental results show that this control architecture is suitable for complementary interaction paradigm in human robot-interaction, since it enables the human and the robot partner to perform different subtasks without interferences. The work presented in Section 3.1, Section 3.2 and Section 3.3.1 has been partially published in [MH18], and the work presented in Section 3.3.2 has been partially published in [MKH18] and in preparation for a a journal publication [MKH21].

4

Human-centric Shared Control for Cooperative Manipulation

Teleoperation of multi-robot systems, e.g. dual manipulators, in cooperative manipulation tasks requires haptic feedback of multi-contact interaction forces; for example, the manipulation of heavy and large objects in remote or dangerous environments. Here, the pure visual feedback is not sufficient. The challenge is to find alternative feedback channels, which provide sufficient information about the task while not limiting the human workspace. Another key challenge is to find an *intuitive* mapping from the low-dimensional human command signal to the control tasks of the robot team, which for the human enables an efficient learning on how to interact with the complex system. *Kinesthetic*, grounded haptic devices, typically used as interfaces in teleoperation, cannot provide multi-contact feedback signals and have limited workspace. A solution to these problems could be to use *cutaneous*, wearable haptic devices, since they introduce a simplification of the hardware and mobility of the human.

In this chapter the complementary interaction paradigm and the control approach, proposed in Chapter 3, are applied in human-robot team collaboration where a human operator teleoperates a robot team to perform a cooperative manipulation task. Furthermore, the suitability of wearable haptic devices in this scenario is evaluated through a user study. More specifically, the benefit of using wearable haptic fingertip devices to interact with a bimanual robot setup in a pick-and-place manipulation task is evaluated. It is shown that haptic feedback through wearable devices improves task performance compared to the base condition of no haptic feedback.

Related Work and Open Problems

In this section an overview of the existing control approaches for cooperative manipulation, task abstraction concepts and control architectures for teleoperation of robot teams are provided. Works on the existing command mappings and employed interaction interfaces in teleoperation of robot teams are also mentioned.

Control design for cooperative manipulation tasks typically includes two objectives: *tracking the desired trajectory* of the object and *zero internal loading* on the object. The object dynamics is either assumed to be known [EH16] or approximated with an impedance dynamics representation [SC92, CCMV08]. The problem of internal loading is solved through the control of *internal forces* which do not contribute to the object motion. The control approaches mainly differ in the way the internal forces are computed. For example, in [WK93]

a *virtual linkage* model is proposed to describe internal forces, in [CCMV08] and [BH96] a pseudo-inverse version of the grasp matrix null-space is used, while the authors of [EH16] use an inertia-weighted pseudo-inverse null-space of the grasp matrix. Majority of the approaches assume the object and the manipulators are rigidly coupled and can, therefore, be considered as one dynamic system. As a consequence, cooperative manipulation tasks further assume the object is already grasped (typically with a fixed grasp) and that the object dynamics is known. These assumptions are rather strong when operating in an unknown environment and the open problem is to consider the object manipulation task where the object has unknown dynamics.

The concept of *task abstraction* has been introduced in robotics to reduce the dimensionality of the problem and enable development of high-level controllers. For example, in [MK97] a set of manipulation task primitives for single manipulators is introduced. Their combinations enable the execution of different manipulation tasks. Similarly, task abstraction is employed on more complex robot systems, such as humanoid robots, through a combination of *behavior primitives* [SK05]. The task abstraction concept is also applied to multi-robot systems by defining their *global* and *local behaviors*. For example, in [BK04] *locked* and *shape behaviors* are introduced for multiple robots to describe their team motion and their formation shape, respectively. In [AAC08] a similar task-abstraction approach is used to control multi-robot system with *null-space based behavioral control*.

In the context of human-robot team interaction and task abstraction, the human operator typically provides desired input for global behaviors, e.g. guides collective motion of the robot team, while the robots within the team autonomously maintain desired local behaviors, e.g. relative coordination [DS05]. This corresponds to the concept of complementary shared control introduced in Chapter 2. This allocation of different responsabilities to the human partner and to the robot team means that local interactions within the team are often uncontrollable to human inputs, i.e. the human operator is unable to assist or intervene in cases of unexpected events or failures of the autonomy [SH19]. For teleoperation of robot teams the null-space based behavioral control is proposed in [Liu15] with cooperative manipulation as a motivational example. However, interaction with the environment is not considered. Teleoperation for a cooperative manipulation task is considered in [DS05] where a *passivity-based control* approach ensures desired performance of decoupled global and local behaviors. While global behavior is controlled by the human, local behavior is performed autonomously. However, a full-scale experiment is not conducted. Therefore, an experiment with human in the loop is needed.

Commands employed in human-robot interaction are typically obtained through mappings, e.g. task-based [SMG+17] and synergy-based [GFS+14], or gestures [WAV+13]. The approaches which use haptic interfaces resort to grounded, kinesthetic devices, e.g. master manipulators in teleoperation settings [DS05, Liu15]. However, these devices have relatively low number of degrees of freedom compared to robot teams causing *interaction asymmetry*. Furthermore, they cannot provide more than one interaction point which makes them unsuitable if the robot team interacts with environment through multiple contacts, e.g. in cooperative manipulation tasks. Additionally, they considerably limit the workspace of the human operator and can compromise stability in cases of time delays and/or hard contacts.

Wearable displays represent a promising solution since they are able to apply *cutaneous* feedback, e.g. on fingerpads, guaranteeing a high wearability and low encumbrance [PSS+17], while enabling the operator to command the robot system via free-hand motions, which ex-

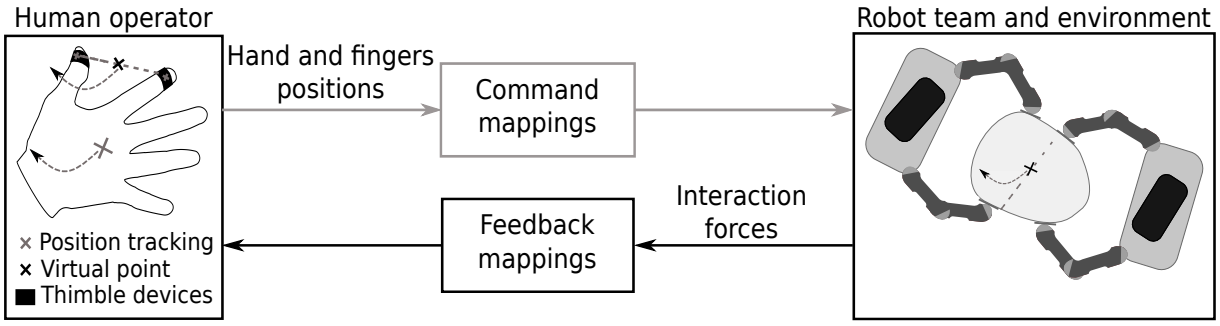

Figure 4.1: The overall human-robot team interaction system. The human operator through hand and fingers motions and command mappings guides the robot team to grasp and manipulate the object while maintaining the grasp over it. Sensed interaction forces between the robots and the object are fed back through feedback mappings to the wearable haptic fingertip devices, mounted on the human operator fingers.

tends the workspace of the operator. The suitability of wearable fingertip devices has been confirmed in a peg-in-hole task where the human teleoperates a robotic hand [PMC+15]. They have also been used to provide cues about shape geometry at the contact point [FSSB08]. The advantages of a wearable master system are twofold. Firstly, the master workspace is not limited by the workspace of the devices thanks to their wearability and portability. This furthermore enables the simultaneous stimulation of several interaction points on the human hand. Secondly, while with kinesthetic devices a stability of the overall system may be an issue in the case of communication delays and stiff contacts, cutaneous haptic devices are intrinsically stable [PMC+15]. However, even though cutaneous haptic devices are wearable, compact, light-weight, and have a relatively simple mechanical structure [PCPM13], they are not as precise as kinesthetic devices. The challenge is to effectively include wearable displays while guaranteeing good performance of the task execution. Therefore, developing a shared-control strategy for tasks with human in the loop and a multi-robot system through novel wearable haptic interfaces is an open problem.

This chapter is organized as follows. The overview of the control architecture is given in Section 4.1, while the model and control of the cooperative manipulation system are proposed in Section 4.2. The employed mapping strategies are described in Section 4.3. The experimental evaluation and the user study are given in Section 4.4.

4.1 Overview of the Human-Robot Team System

A teleoperation scenario where a human operator teleoperates a team of robot manipulators to grasp and manipulate an object is considered. Since the robot team can have a high number of *controllable* degrees of freedom compared to the human operator, a principal challenge is to resolve this *interaction asymmetry* through the appropriate *command mappings*. If the robot team interacts with the environment, e.g. an object, asymmetry may also arise if the used haptic devices provide insufficient number of feedback channels to the human operator, e.g. through contact points, impairing *observability* of the system. The overall human-robot team interaction system for a cooperative manipulation task is depicted in Figure 4.1.

The approach is based on the assumption that the robot team performs the overall task

through a set of *subtasks*, as proposed in Chapter 2. Subtasks may be conducted either sequentially or simultaneously. For example, in order to perform a cooperative manipulation task the robot team needs to *grasp*, *maintain the grasp* of the object and *manipulate* the object. The subtasks can be accomplished through modeling and controlling of the robot team restricted to task-related constraints, as introduced in Section 2.2. In this context, subtasks for a cooperative manipulation task can be achieved through *cooperative* and *relative* constraints. The cooperative constraint ensures that the robot team is able to move as an entity (global behavior) and is necessary for the object manipulation subtask. The relative constraint ensures that the robot team has a specific formation shape (local behavior) which is necessary to maintain the grasp of the object. The concept of subtasks resolves the challenge of interaction asymmetry because it describes the system on a higher abstraction level than the actuation level of the robot team.

The proposed approach is not limited to the considered scenario. It may also be applied to direct physical interaction, where the human interacts with the robot through a common, grasped object. Furthermore, the control approach proposed in this section and the mapping approach proposed in Section 4.3 may be applied to any other robot team system, e.g. team of UAVs, wheeled robots, or a heterogeneous robot team. The task does not necessarily need to be cooperative manipulation, but may be any task that requires the team to maintain a specific formation shape while moving in its environment.

Consequently, this control approach resolves the problem of asymmetry by enabling the human operator to interact with the robot team on a higher level of abstraction through transformation-based mappings. Second, the suitability of wearable haptic devices in this type of interaction and for cooperative manipulation tasks is investigated for the first time.

4.2 Control of Robot Team Behaviors

In this section robot team behaviors for cooperative manipulation task are formally defined and the shared-control strategy, suitable to achieve the overall task, is proposed.

4.2.1 Robot Team Model

Let us assume that N manipulators cooperatively grasp and manipulate an object, as shown in Figure 4.2. The pose of the i-th manipulator is defined by the position and orientation of its end-effector in Cartesian space, i.e. by the frame $\{c_i\}$ obtained w.r.t. the world frame $\{w\}$, described with the vector $\boldsymbol{x}_i = [\boldsymbol{p}_i^\top, \boldsymbol{q}_i^\top]^\top \in \mathrm{SE}(3)$, where $\boldsymbol{p}_i \in \mathbb{R}^3$ is a position vector and $\boldsymbol{q}_i = [\eta_i, \boldsymbol{\epsilon}_i^\top]^\top \in \mathrm{Spin}(3)$ is a unit quaternion.

The dynamics of the robot team is obtained by stacking N Euler-Lagrangian equations in Cartesian space to obtain

$$\boldsymbol{M}_x(\boldsymbol{\theta})\dot{\boldsymbol{v}} + \boldsymbol{c}_x(\boldsymbol{\theta}, \boldsymbol{v}) + \boldsymbol{w}_g(\boldsymbol{\theta}) = \boldsymbol{w} + \boldsymbol{w}_m, \tag{4.1}$$

where $\boldsymbol{M}_x(\boldsymbol{\theta}) = \mathrm{blockdiag}(\boldsymbol{M}_{x,1}(\boldsymbol{\theta}_1), ..., \boldsymbol{M}_{x,N}(\boldsymbol{\theta}_N))$ contains robots' inertial matrices, $\boldsymbol{c}_x = [\boldsymbol{c}_{x,1}^\top, ..., \boldsymbol{c}_{x,N}^\top]^\top$ stacks robots' Coriolis and centrifugal forces, and $\boldsymbol{w}_g = [\boldsymbol{w}_{g,1}^\top, ..., \boldsymbol{w}_{g,N}^\top]^\top$ stacks robots' gravitational forces. The control and measured wrenches for each robot are stacked in $\boldsymbol{w} = [\boldsymbol{w}_1^\top, ..., \boldsymbol{w}_N^\top]^\top$ and $\boldsymbol{w}_m = [\boldsymbol{w}_{m,1}^\top, ..., \boldsymbol{w}_{m,N}^\top]^\top$, respectively. The measured wrenches are obtained through torque sensing of the robots and known Jacobian transformation from the

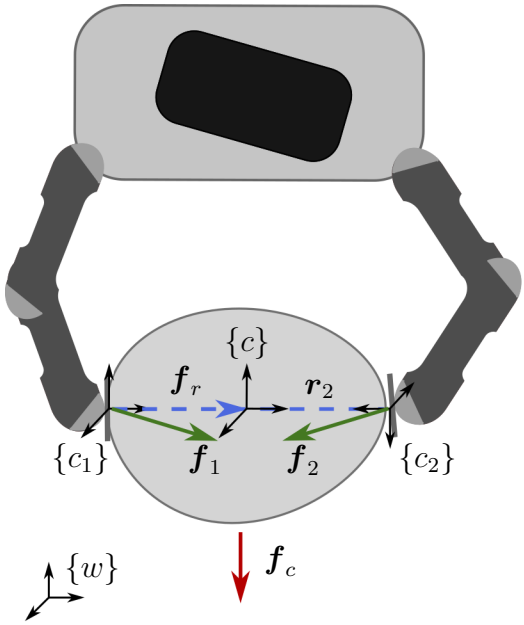

Figure 4.2: Dual-manipulator system grasps a common object. The end-effector coordinate frames are $\{c_1\}$ and $\{c_2\}$, while the cooperative frame is $\{c\}$. The world frame is denoted with $\{w\}$. Interaction forces, measured at the end-effectors, are denoted with $\boldsymbol{f}_1$ and $\boldsymbol{f}_2$. Their cooperative and relative force components are denoted with $\boldsymbol{f}_c$ and $\boldsymbol{f}_r$, respectively. Distances between $\{c_i\}$ and $\{c\}$ w.r.t. the world frame $\{w\}$ are $\boldsymbol{r}_i$, $i = 1, 2$.

robots' joint space to Cartesian space. The stacked vectors of pose, velocity and acceleration are $\boldsymbol{x}$, $\boldsymbol{v}$ and $\dot{\boldsymbol{v}}$, respectively. The velocity vector of the i^{th} robot is $\boldsymbol{v}_i = [\dot{\boldsymbol{p}}_i^\top, \boldsymbol{\omega}_i^\top]^\top \in \mathbb{R}^6$ with $\dot{\boldsymbol{p}}_i$ and $\boldsymbol{\omega}_i$ being translational and angular velocities of the end-effector, respectively. The joint angles of all the robots are stacked in the vector $\boldsymbol{\theta}$. The control wrench vector of the i^{th} robot is $\boldsymbol{w}_i = [\boldsymbol{f}_i^\top, \boldsymbol{m}_i^\top]^\top \in \mathbb{R}^6$, with $\boldsymbol{f}_i$ and $\boldsymbol{m}_i$ being force and torque vectors, respectively.

Remark 23. *The robot team of N manipulators has $n = 6N$ degrees of freedom in Cartesian space. Through haptic devices typically up to six degrees of freedom can be controlled which is not enough in case the interaction is established with individual robots within the team. This is the reason why we reduce the dimensionality of the system by abstracting its behaviors.*

In the robot task space the behaviors $\boldsymbol{x}_b$ of the robot team are defined as in (2.10) where $\boldsymbol{x}_{b,j} \in \mathcal{M}_{b,j}$ is the j^{th} behavior (a position and/or orientation equality constraint) out of k behaviors. Corresponding differential maps (velocities), according to (2.11) are

$$\boldsymbol{v}_{b,j} = \boldsymbol{J}_{b,j}(\boldsymbol{x})\boldsymbol{v}, \quad j = 1, ..., k \tag{4.2}$$

where $\boldsymbol{J}_{b,j}(\boldsymbol{x}) \in \mathbb{R}^{k_j \times n}$ is the j^{th} behavior Jacobian. The velocity $\boldsymbol{v}$ can be computed through

$$\boldsymbol{v} = \boldsymbol{P}_{b,1}(\boldsymbol{x})\boldsymbol{v}_{b,1} + \ldots + \boldsymbol{P}_{b,k}(\boldsymbol{x})\boldsymbol{v}_{b,k}, \tag{4.3}$$

where $\boldsymbol{P}_{b,j}(\boldsymbol{x})$, $j = 1, ..., k$, are properly parametrized behavior Jacobian inverse matrices. The behavior Jacobian $\boldsymbol{J}_b$ is used as a projection matrix to obtain a map of the robot team dynamics in lower dimensional spaces, as in Chapter 3.

Let us now formulate two behaviors required for the cooperative manipulaton task. In this work they are termed as *relative* and *cooperative* behaviors. The behaviors are defined for the team of two robots as depicted in Figure 4.2.

4.2.2 Relative Behavior

A suitable control of the robot team relative behavior enables the execution of the *grasping* and *grasp maintenance* subtasks. Therefore, it enables the robot team to establish a desired geometric formation shape in order to grasp and hold the object. This constraint defines the relative motion between the manipulators, necessary to grasp the object. Once the object is grasped, the relative motion between the manipulators generates an increase in the relative force which maintains the grasp. The corresponding relative force, $\boldsymbol{f}_r$, does not contribute to the motion of the object but only to the grasp maintenance, guaranteeing that the contact forces satisfy contact and friction constraints. Let us define the relative behavior as in (2.10) through the appropriate translation and orientation equality constraints.

Translation constraints

Distances between the robots are explicitly defined in order for the robot team to obtain a formation shape

$$\begin{aligned} \boldsymbol{p}_{r,1} &= \boldsymbol{R}_1 \, {}^1\boldsymbol{r}_{1,2} = \boldsymbol{p}_1 - \boldsymbol{p}_2 \\ &\vdots \\ \boldsymbol{p}_{r,N-1} &= \boldsymbol{R}_{N-1} \, {}^{N-1}\boldsymbol{r}_{N-1,N} = \boldsymbol{p}_{N-1} - \boldsymbol{p}_N, \end{aligned} \tag{4.4}$$

where $\boldsymbol{p}_{r,1}, ..., \boldsymbol{p}_{r,N-1}$ are relative positions between the robots within the team and $\boldsymbol{R}_i \in \mathrm{SO}(3)$ is a rotation matrix of the frame assigned to the i^{th} robot w.r.t. the world frame $\{w\}$.

Orientation constraints

Relative orientations between the robots need to be constrained to a constant value to avoid torsion and loss of contact

$$\begin{aligned} {}^2\boldsymbol{q}_1 &= \boldsymbol{q}_2^\star \, \boldsymbol{q}_1 = \textbf{const.} \\ &\vdots \\ {}^N\boldsymbol{q}_{N-1} &= \boldsymbol{q}_N^\star \, \boldsymbol{q}_{N-1} = \textbf{const.}, \end{aligned} \tag{4.5}$$

where $\boldsymbol{q}_i^\star$, $i = 1, ..., N$, is a quaternion conjugate. Velocities computed from (4.4) and (4.5) to obtain expression as in (4.2) for $i = 1, 2$ are

$$\boldsymbol{v}_r = \underbrace{\begin{bmatrix} \boldsymbol{I}_3 & \boldsymbol{S}(\boldsymbol{r}_{1,2}) & -\boldsymbol{I}_3 & \boldsymbol{0}_3 \\ \boldsymbol{0}_3 & \boldsymbol{I}_3 & \boldsymbol{0}_3 & -\boldsymbol{I}_3 \end{bmatrix}}_{\boldsymbol{J}_{b,r}} \boldsymbol{v}, \tag{4.6}$$

where $\boldsymbol{v}_r = [\dot{\boldsymbol{p}}_r^\top, \boldsymbol{\omega}_r^\top]^\top \in \mathbb{R}^6$ is the relative velocity vector, $\boldsymbol{S}(\cdot)$ is a skew-symmetric matrix, and $\boldsymbol{J}_{b,r}$ is the relative behavior Jacobian.

4.2.3 Cooperative Behavior

A suitable control of the robot team cooperative behavior enables the execution of the *object manipulation* subtask. The cooperative constraint defines the object motion, while the *cooperative force*, $\boldsymbol{f}_c$, accelerates the object and counterbalances the gravitational forces. Therefore, it enables the robot team to move as a single entity and is defined with the pose of the frame $\{c\}$, depicted in Figure 4.2, w.r.t. which all the robots within the team move cooperatively. Naturally, cooperative constraints can be satisfied only if the relative constraints are satisfied beforehand. Let us denote the pose of the frame $\{c\}$ w.r.t. $\{w\}$ with $\boldsymbol{x}_c = [\boldsymbol{p}_c^\top, \boldsymbol{q}_c^\top]^\top$. Let us further assume $\{c\}$ is located between the robots, with an arbitrary initial orientation. The cooperative constraint as in (2.10) is defined through the translation and orientation equality constraints.

Translation constraints

Based on the notations in Figure 4.2 the following equality constraints on translations are imposed between the robots and the cooperative frame $\{c\}$ in order for the robot team to move as an entity

$$\boldsymbol{p}_i = \boldsymbol{p}_c + \boldsymbol{r}_i = \boldsymbol{p}_c + \boldsymbol{R}_c \, {}^c\boldsymbol{r}_i, \quad i = 1, ..., N \tag{4.7}$$

where $\boldsymbol{R}_c \in \mathrm{SO}(3)$ is the rotational matrix of $\{c\}$ w.r.t. $\{w\}$.

Orientation constraints

In order for the robot team to rotate as an entity, relative orientation between the frames $\{c_i\}$, $i = 1, ..., N$, and $\{c\}$ needs to be constant during the manipulation

$${}^c\boldsymbol{q}_i = \boldsymbol{q}_c^\star \, \boldsymbol{q}_i = \textbf{const.}, \quad i = 1, ..., N. \tag{4.8}$$

Computing velocities from (4.7) and (4.8) to obtain expression as in (4.3), under the assumption the relative constraints are satisfied, we obtain for $i = 1, 2$

$$\boldsymbol{v} = \underbrace{\begin{bmatrix} \boldsymbol{I}_3 & \boldsymbol{S}^\top(\boldsymbol{r}_1) \\ \boldsymbol{0}_3 & \boldsymbol{I}_3 \\ \boldsymbol{I}_3 & \boldsymbol{S}^\top(\boldsymbol{r}_2) \\ \boldsymbol{0}_3 & \boldsymbol{I}_3 \end{bmatrix}}_{\boldsymbol{P}_{b,c}} \boldsymbol{v}_c, \tag{4.9}$$

where $\boldsymbol{v}_c = [\dot{\boldsymbol{p}}_c^\top, \boldsymbol{\omega}_c^\top]^\top \in \mathbb{R}^6$ is the cooperative velocity vector and $\boldsymbol{P}_{b,c}$ is the projection matrix from the cooperative tangent space to the tangent space of the robot team.

Remark 24. *The matrix $\boldsymbol{P}_{b,c}$ in (4.9) is equivalent to the grasp matrix if the actual object is tracked, as defined in [PJ08].*

Remark 25. *If the robot team has $n = 6N$ degrees of freedom, according to (4.9) six degrees of freedom are needed to define the cooperative subtask (through the pose of the frame $\{c\}$). In order to be able to achieve decoupling, the relative behavior needs to be defined through $n - 6$ degrees of freedom. We show that this is physically possible through the definition of relative constraints sequentially between all the robots yielding $n - 6$ equations of relative constraints.*

4.2.4 Noninteracting Control for Cooperative Manipulation

The algorithm for noninteracting control, presented in Chapter 3, is applied to compute the behavior dynamics as in (3.21). In this case, the behaviors are defined with the relative and cooperative constraints in Sections 4.2.2 and 4.2.2, respectively. Evaluating robot team dynamics along the constraints reduces system dimensionality and simplifies control design. Furthermore, this enables discrimination between the interaction wrenches caused by different behaviors. Cooperative and relative velocities can be computed according to (4.3)

$$\boldsymbol{v} = \underbrace{[\boldsymbol{P}_{b,c}(\boldsymbol{x}) \;\; \boldsymbol{P}_{b,r}(\boldsymbol{x})]}_{\boldsymbol{P}_b(\boldsymbol{x})} \underbrace{\begin{bmatrix}\boldsymbol{v}_c \\ \boldsymbol{v}_r\end{bmatrix}}_{\boldsymbol{v}_b}, \tag{4.10}$$

where

$$\boldsymbol{P}_{b,r}(\boldsymbol{x}) = \boldsymbol{M}^{-1}\boldsymbol{J}_{b,r}^{\top}(\boldsymbol{J}_{b,r}\boldsymbol{M}^{-1}\boldsymbol{J}_{b,r}^{\top})^{-1}, \tag{4.11}$$

is an inertia-weighted pseudoinverse of $\boldsymbol{J}_{b,r}$ as in (3.19). The acceleration is then obtained through

$$\dot{\boldsymbol{v}} = \boldsymbol{P}_b(\boldsymbol{x})\dot{\boldsymbol{v}}_b + \dot{\boldsymbol{P}}_b(\boldsymbol{x})\boldsymbol{v}_b. \tag{4.12}$$

Multiplying (4.1) with $\boldsymbol{P}_b^{\top}$ from the left generates an inertia-decoupled representation of the relative and the cooperative behavior dynamics

$$\begin{aligned}\boldsymbol{M}_r(\boldsymbol{\theta})\dot{\boldsymbol{v}}_r + \boldsymbol{c}_r(\boldsymbol{\theta},\boldsymbol{v}_b) + \boldsymbol{w}_{g,r}(\boldsymbol{\theta}) &= \boldsymbol{w}_r + \boldsymbol{w}_{m,r} \\ \boldsymbol{M}_c(\boldsymbol{\theta})\dot{\boldsymbol{v}}_c + \boldsymbol{c}_c(\boldsymbol{\theta},\boldsymbol{v}_b) + \boldsymbol{w}_{g,c}(\boldsymbol{\theta}) &= \boldsymbol{w}_c + \boldsymbol{w}_{m,c},\end{aligned} \tag{4.13}$$

where $\boldsymbol{w}_{m,r} = [\boldsymbol{f}_{m,r}^{\top}, \boldsymbol{m}_{m,r}^{\top}]^{\top}$ and $\boldsymbol{w}_{m,c} = [\boldsymbol{f}_{m,c}^{\top}, \boldsymbol{m}_{m,c}^{\top}]^{\top}$ represent contributions of the total wrenches to the grasp maintenance and accelerating the object together with counterbalancing the gravitational forces, respectively.

In order to achieve the desired performance of the defined behaviors, in this work a position-based impedance controller is used. It enables setting desired error dynamics of the relative and cooperative behaviors separately, in their corresponding manifolds as in (3.26). Therefore, the desired relative and cooperative error dynamics are set as

$$\boldsymbol{M}_r\dot{\boldsymbol{v}}_r + \boldsymbol{D}_r(\boldsymbol{v}_r^d - \boldsymbol{v}_r) + \boldsymbol{w}_{K,r}(\boldsymbol{x}_r^d, \boldsymbol{x}_r) = \boldsymbol{w}_{m,r}, \tag{4.14}$$

$$\boldsymbol{M}_c(\dot{\boldsymbol{v}}_c - \dot{\boldsymbol{v}}_c^d) + \boldsymbol{D}_c(\boldsymbol{v}_c^d - \boldsymbol{v}_c) + \boldsymbol{w}_{K,c}(\boldsymbol{x}_c^d, \boldsymbol{x}_c) = \boldsymbol{w}_{m,c}, \tag{4.15}$$

where $\boldsymbol{M_r}$ and $\boldsymbol{M_c}$ are the desired inertia matrices, $\boldsymbol{D}_r = \text{blockdiag}[d_r\boldsymbol{I}_3, \delta_r\boldsymbol{I}_3]$ and $\boldsymbol{D}_c = \text{blockdiag}[d_c\boldsymbol{I}_3, \delta_c\boldsymbol{I}_3]$ are the desired damping matrices, and the desired stiffnesses, $\boldsymbol{k}_c(\cdot)$ and $\boldsymbol{k}_r(\cdot)$, are defined as in [CCMV08]. In particular

$$\boldsymbol{w}_{K,r} = \begin{bmatrix} k_r\boldsymbol{I}_3(\boldsymbol{p}_r - \boldsymbol{p}_r^d) \\ \tilde{\boldsymbol{\kappa}}_r\Delta\boldsymbol{\epsilon}_r \end{bmatrix}, \quad \boldsymbol{w}_{K,c} = \begin{bmatrix} k_c\boldsymbol{I}_3(\boldsymbol{p}_c - \boldsymbol{p}_c^d) \\ \tilde{\boldsymbol{\kappa}}_c\Delta\boldsymbol{\epsilon}_c \end{bmatrix}, \tag{4.16}$$

where $\Delta\boldsymbol{\epsilon}_r$ and $\Delta\boldsymbol{\epsilon}_c$ are the vector parts of $\Delta\ \boldsymbol{q}_r = \boldsymbol{q}_r \star (\boldsymbol{q}_r^d)^{-1}$ and $\Delta\ \boldsymbol{q}_c = \boldsymbol{q}_c \star (\boldsymbol{q}_c^d)^{-1}$, respectively. Furthermore, $\tilde{\boldsymbol{\kappa}}_c = 2\boldsymbol{E}^{\top}(\Delta\boldsymbol{q}_c)\kappa_c$ and $\tilde{\boldsymbol{\kappa}}_r = 2\boldsymbol{E}^{\top}(\Delta\boldsymbol{q}_r)\kappa_r$, with $\boldsymbol{E}(\Delta\boldsymbol{q}_c) = \Delta\eta_c\boldsymbol{I} - \boldsymbol{S}(\Delta\boldsymbol{\epsilon}_c)$ and $\boldsymbol{E}(\Delta\boldsymbol{q}_r) = \Delta\eta_r\boldsymbol{I} - \boldsymbol{S}(\Delta\boldsymbol{\epsilon}_r)$, respectively.

Remark 26. *If the object motions are slow and $\dot{\boldsymbol{v}}$ can be neglected, the projection matrix $\boldsymbol{P}_{b,r}$ in (4.11) can be computed without the inertia weighting.*

Remark 27. *Note that the obtained relative and cooperative dynamics in (4.13) are decoupled in the input-output noninteracting sense, as proposed in Section 3.2.1.*

4.3 Mapping Strategy for Human-in-the-Loop Interaction with Wearable Haptics

In this section a mapping strategy that enables the human operator to *command* desired motions to the robot team and to receive *feedback* from the robot team via wearable fingertip devices is proposed.

Command and feedback mappings are defined with Definition 4.3.1 and Definition 4.3.2.

Definition 4.3.1. Command mapping *is a procedure necessary to provide desired control inputs to the robot system from the captured human operator motions.*

Definition 4.3.2. Feedback mapping *is a procedure necessary to map interaction forces sensed on the robot side to the haptic devices used at the master side.*

Remark 28. *The formulation of command and feedback mappings does not depend on the number of robots within the robot system.*

In the remainder of the section the solution to the command and feedback mappings is formulated.

4.3.1 Command Mapping

Let us assume the human operator is grasping a virtual object with M contact points, $\boldsymbol{p}_{f,i} \in \mathbb{R}^3$, $i = 1, ..., M$, as shown in Fig. 4.3. The virtual object is assumed to be a minimum volume sphere encircling all the contact points. Its pose is denoted as $\boldsymbol{x}_{vo} = [\boldsymbol{p}_{vo}^\top, \boldsymbol{q}_{vo}^\top]^\top$. Let us assume further that the pose of the human hand is known through the frame $\{h\}$ in $\{w\}$ and is denoted as $\boldsymbol{x}_h = [\boldsymbol{p}_h^\top, \boldsymbol{q}_h^\top]^\top$.

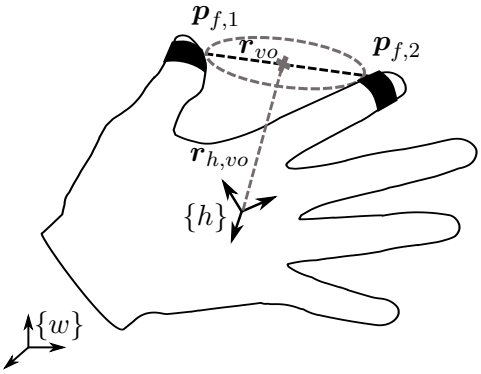

Figure 4.3: The human hand and finger motions are mapped to the inputs of the robot team behaviors. Frame $\{h\}$ is attached to the hand back. Positions of the tracked fingers are $\boldsymbol{p}_{f,i}$, $i = 1, ..., M$. The distance vector between the frame $\{h\}$ and the virtual object center is denoted as $\boldsymbol{r}_{h,vo}$, while the distance between the fingertips is $\boldsymbol{r}_{vo}$. Human fingertips are equipped with wearable haptic fingertip devices.

The pose of the virtual object can be computed from the hand pose

$$\begin{aligned} \boldsymbol{p}_{vo} &= \boldsymbol{p}_h + \boldsymbol{r}_{h,vo} = \boldsymbol{p}_h + \boldsymbol{R}_h \, {}^h\boldsymbol{r}_{h,vo} \\ {}^h\boldsymbol{q}_{vo} &= \textbf{const.}, \end{aligned} \tag{4.17}$$

where $\boldsymbol{R}_h$ is the rotational matrix of the frame $\{h\}$ w.r.t. the world frame $\{w\}$. From (4.17) the velocity of the virtual object, $\boldsymbol{v}_{vo}$, is

$$\boldsymbol{v}_{vo} = \begin{bmatrix} \boldsymbol{I}_3 & \boldsymbol{S}(\boldsymbol{r}_{h,vo}) \\ \boldsymbol{0}_3 & \boldsymbol{I}_3 \end{bmatrix} \boldsymbol{v}_h, \tag{4.18}$$

where $\boldsymbol{v}_h \in \mathbb{R}^6$ is the hand velocity. Desired cooperative velocity of the robot team is set with the velocity of the virtual object

$$\boldsymbol{v}_c^d = \boldsymbol{v}_{vo}. \tag{4.19}$$

The relative positions between the fingers are computed as in (4.4) with $\boldsymbol{p}_{fr,1}, ..., \boldsymbol{p}_{fr,M-1}$ and the corresponding velocities $\dot{\boldsymbol{p}}_{fr,1}, ..., \dot{\boldsymbol{p}}_{fr,M-1}$. It is assumed that the virtual object can be moved and deformed through the change of contact points' positions. The consequence of this assumption is the variability of the virtual object radius

$$\dot{r}_{vo} = \max\{||\dot{\boldsymbol{p}}_{fr,1}||, ..., ||\dot{\boldsymbol{p}}_{fr,(M-1)}||\}. \tag{4.20}$$

Assuming that the directions of the robots' normals to the actual object at the slave side are known, the relative behavior of the robot team can be obtained through the change of the virtual object radius at the master side as

$$\boldsymbol{v}_r^d = s_r \dot{r}_{vo} \boldsymbol{J}_{br,t} \hat{\boldsymbol{n}}, \tag{4.21}$$

where s_r is the scaling factor which takes into consideration different workspace dimensions of the robot team and the human hand and $\boldsymbol{J}_{br,t}$ is the translation part of $\boldsymbol{J}_{b,r}$. The stacked vector of directions of normals in $\{w\}$ to the object surface for all robots is $\hat{\boldsymbol{n}} = [\hat{\boldsymbol{n}}_1^\top, ..., \hat{\boldsymbol{n}}_N^\top]^\top$.

4.3.2 Feedback Mapping

Let us assume the human is equipped with M haptic devices as shown in Figure 4.3 in the case of wearable haptic devices. The computation of the feedback wrenches depends on the number of degrees of freedom of the used haptic devices and on the number of sensors available at the slave side. It is assumed that it is possible to compute the contact wrench of each robot. Generally, there could be a mismatch between the wrenches measured at the slave side and those that can be displayed on the master side. For instance, it could be possible to measure wrenches for four arms on the slave side and only have two wearable devices on the master side that can reproduce two force vectors. A possible solution in the case of dissimilar master and slave robots has been presented in [SMG+17].

The main idea of the proposed feedback mapping is to consider that the wrench applied to the grasped object at the slave side can be reproduced at the master side on the virtual object depicted in Figure 4.3, with a possible scaling factor $s_h = \dfrac{f_{\mathrm{h,max}}}{f_{\mathrm{m,max}}}$ determined by the ratio between the maximum force that can be rendered by the M haptic devices, $f_{\mathrm{h,max}}$, and the maximum force that is expected for the task, $f_{m,\mathrm{max}}$. Therefore, the total wrench to be rendered at the master side can be computed as

$$\boldsymbol{w}_h = s_h \boldsymbol{w}_m, \tag{4.22}$$

where $\boldsymbol{w}_m$ is the stacked vector of all the robot team measured wrenches. It is possible to consider two contributions to the feedback forces. One is related to the perception of the manipulated object weight and inertia and the other one is related to the perception of the tightness of the grasp. These two components are often referred to as *external*, $\boldsymbol{w}_{h,e}$, and *internal*, $\boldsymbol{w}_{h,in}$, forces. The external force contribution is computed using the measured cooperative wrenches of the robot team

$$\boldsymbol{w}_{h,e} = \boldsymbol{J}_{bh,c}^{\top} \boldsymbol{w}_{m,c}. \tag{4.23}$$

For the cooperative Jacobian on the master side following equality holds $\boldsymbol{J}_{bh,c}^{\top} = (\boldsymbol{P}_{bh,c}^{\top})^{\dagger}$ with

$$\boldsymbol{P}_{bh,c}^{\top} = \begin{bmatrix} \boldsymbol{I}_3 & \boldsymbol{0}_3 & \dots & \boldsymbol{I}_3 & \boldsymbol{0}_3 \\ \boldsymbol{S}(\boldsymbol{r}_{1,vo}) & \boldsymbol{I}_3 & \dots & \boldsymbol{S}(\boldsymbol{r}_{M,vo}) & \boldsymbol{I}_3 \end{bmatrix},$$

where $\boldsymbol{r}_{i,vo}$, $i = 1, ..., M$, is the vector between the contact point i and the virtual object center point. The internal force contribution depends on the homogeneous part of the solution of (4.23) that is not unique in general, see [SMG+17]. The solution of the homogeneous part is necessary to determine in which direction it is more convenient to render the forces related to grasp tightness. Among the possible solutions reported in [SMG+17], in this work the null-space projector $\boldsymbol{P}_{b,r}^{\top}(\boldsymbol{x})$, defined as in (4.11), has been selected to determine the directions for internal forces. Once the directions are determined the magnitude of the rendered internal forces is computed as

$$\boldsymbol{f}_{h,in} = \frac{1}{M} \underset{\boldsymbol{f}_{m,ri} \in \boldsymbol{f}_{m,r}}{\arg\max} \|\boldsymbol{f}_{m,ri}\|, \tag{4.24}$$

i.e., the relative force vector with the maximum norm is fed back to the human operator. With the proposed underactuated haptic thimble devices it is only possible to render forces, not torques, thus only this component of $\boldsymbol{w}_{m,r}$ has been considered. A block diagram of the control loop for human-robot team telemanipulation is depicted in Figure 4.4.

4.4 Experimental Evaluation

In this section the developed experimental setup of the robot team teleoperation for cooperative manipulation tasks is presented. The setup is used to conduct two experimental evaluations: (i) the performance of the proposed control architecture and (ii) the suitability of wearable haptic thimble devices for cooperative manipulation tasks. The evaluation of the haptic devices is performed through a user study by analyzing the effect of different types of feedback signals on various performance measures.

4.4.1 Experimental Setup

The experimental setup used for the evaluation is depicted in Figure 4.5. The teleoperated robot system consists of two 7 DoF KUKA LWR 4+ manipulators mounted on a common platform. The robot manipulators interact with a 1 kg box-shaped object. The interaction wrenches are estimated from the internal torque sensors' measurements and known manipulators Jacobian matrices. Local position controllers are used on the joint level.

The human operator is equipped with two wearable haptic thimble devices mounted on the thumb and index fingers of the right hand. The operator guides the cooperative manipulation

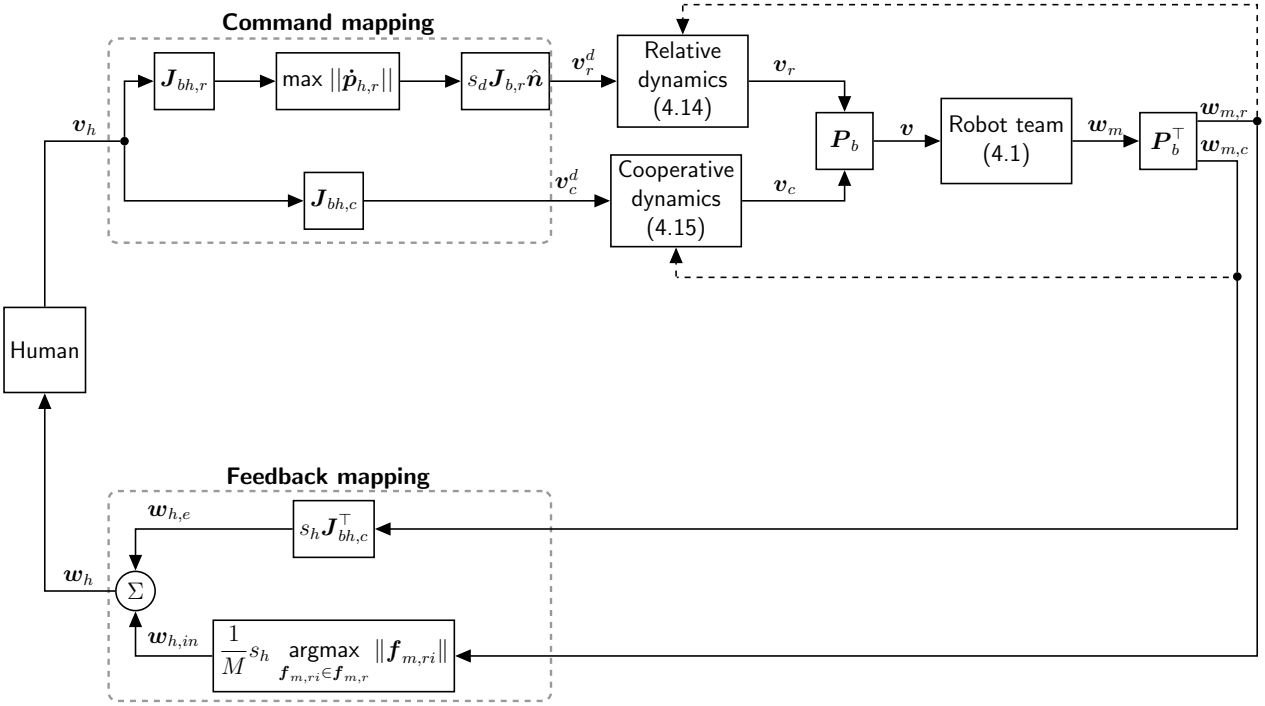

Figure 4.4: Block structure of the control loop for human-robot team interaction.

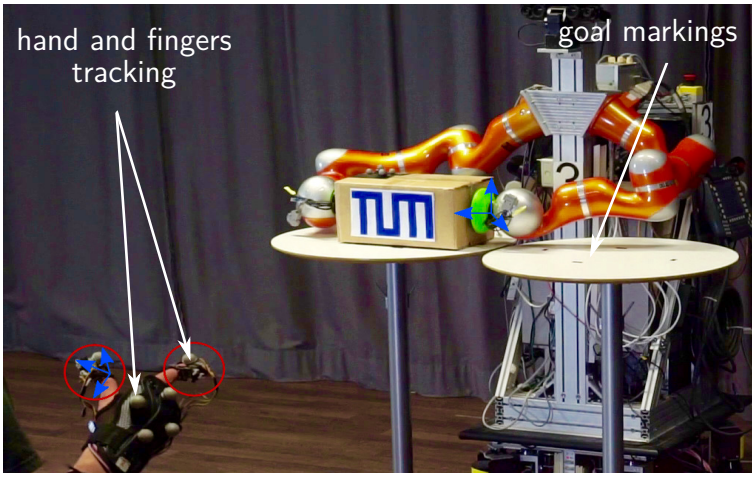

Figure 4.5: Experimental setup: two KUKA LWR 4+ robot manipulators are teleoperated by a human operator equipped with two wearable haptic thimble devices (marked with red circles). The coordinate frames of end-effectors and wearable fingertip devices are marked in blue. Goal locations of the pick-and-place task are marked on the table and are fully visible to the operator.

system to grasp and manipulate the object by motions transformed into desired reference trajectories using the command mappings proposed in Section 4.3. For that purpose the human operator is tracked with the marker-based motion tracking system, *Qualisys*. More specifically, four markers are mounted on the back of the right hand, and a marker is mounted on each thimble device. The number of markers is adequate for enabling the proposed interaction.

(a) (b)

Figure 4.6: The actuated fingertip device. (a) A rigid body, A, houses three servomotors, E, connected via three tensors, B, to the vertices of the slanting platform, G. The platform is located under the finger pulp of the user whose distal phalanx holds the fingertip in its position with a clamp, F. A force sensor, H, is located on the platform, under the finger pulp center. The initial position of the platform is held by three springs, D. (b) The hand setup with the fingertip devices and passive markers.

Mechanical structure of the fingertip device is depicted in Figure 4.6 and its components are denoted with capital letters. Three motors, E, control the length of the three tensors, B, which are connected to the vertices of the slanting platform, G. The tensors independently pull the three vertices of the platform resulting in its 3 DoFs: *roll*, α, *pitch*, β, and *displacement*, d. The device is equipped with FSR 400 force sensor, H, which measures the contact force between the platform and the human finger. More detailed operating principles of the fingertip device can be found in [PMC$^+$15, PCPM13, CMPP15]. The fingertip devices are connected to a *Raspberry Pi* which ensures wireless communication with the robot system. The controller presented in Section 4.2 operates on 1 kHz, while the Qualisys motion tracking system and the fingertip devices operate on 0.1 kHz. Due to the absence of the kinesthetic feedback the low sampling frequency of the wearable haptic fingertip devices does not cause instability [PMC$^+$15]. The control parameters are given in Table 4.1. General feedback forces $\boldsymbol{f}_h$, defined as a part of (4.22), are mapped to the 3 degrees of freedom of the fingertip device as follows

$$\alpha_j = \text{atan}\left(\frac{{}^{t_j}f_{h,ejx}}{{}^{t_j}f_{h,ejz}}\right),\ \beta_j = \text{atan}\left(\frac{{}^{t_j}f_{h,ejy}}{{}^{t_j}f_{h,ejz}}\right),\ d_j = s_h k_t \sqrt{\left({}^{t_j}\boldsymbol{f}_{h,in}\right)^\top {}^{t_j}\boldsymbol{f}_{h,in}}, \tag{4.25}$$

with the scaling factor $s_h = \frac{4.7}{30}$ and the fingertip compliance parameter $k_t = 2$ mm/N [PKH03]. The poses of the coordinate frames $t_j, j = 1, .., M$, which are located at point H in Figure 4.6 are assumed to be known in $\{w\}$. In the remainder, frame notation $\{t_j\}$ will be omitted, since all the forces displayed to the thimble device will be expressed w.r.t. its corresponding frame.

4.4.2 Evaluation of the Control Architecture Performance

The proposed control approach is evaluated on an example of a pick-and-place task with the control parameters listed in Table 4.1. Four experimental evaluations are performed:

(i) Tracking performance of the grasped object translation (cooperative behavior) without human in the loop by applying $\boldsymbol{v}_c^d = \boldsymbol{a}\sin(2\pi \boldsymbol{f} t)$ with $\boldsymbol{a} = [0\ 0.07\ 0.07]^\top$ m/s and

Table 4.1: The control parameters.

Control coefficients	Cooperative behavior	Relative behavior
d_c, d_r	200	300
δ_c, δ_r	5	5
k_c, k_r	500	500
κ_c, κ_r	15	15

$\boldsymbol{f} = [0\ 1/16\ 1/8]^\top$ Hz, resulting in a typical motion profile of a pick-and-place task in the $y-z$ plane of the defined $\{w\}$.

(ii) Tracking performance of the grasped object rotation (cooperative behavior), without human in the loop, by applying $\omega^d_{c,z} = a\sin(2\pi f t)$ with $a = -0.07$ rad/s and $f = 1/6$ Hz.

(iii) Tracking performance of the manipulators' relative behavior during object grasping (approaching) and manipulation (transportation) phases, without human in the loop, by applying $v^d_{r,y} = 0.05$ m/s during the grasping phase and $v^d_{r,y} = 0$ m/s during the transportation phase.

(iv) Tracking performance of a pick-and-place task with human in the loop commanding the desired relative and cooperative trajectories during the object grasping and transportation phases while receiving force feedback through the haptic devices.

Experiment (i): The desired and actual cooperative velocity profiles in y and z directions, as well as the corresponding tracking velocity errors, are depicted in Figure 4.7. Good tracking can be observed with a mean error of $[\Delta\bar{v}_{c,y}\ \Delta\bar{v}_{c,z}]^\top = [2.3\ 8.0]^\top \times 10^{-5}$ m/s.

Experiment (ii): The desired and actual angular cooperative velocity profiles in z direction, as well as the tracking velocity error, are depicted in Figure 4.8. Good tracking of angular velocity is achieved with a mean error of $\Delta\bar{\omega}_{c,z} = 1.8 \times 10^{-5}$ rad/s.

Experiment (iii): The desired and actual relative velocity profiles during the approaching and the manipulation phases are shown in Figure 4.9. After an initial overshoot producing an error of $\Delta v_{r,y} = 3.2 \times 10^{-2}$ m/s, the desired velocity is achieved until the impact with the object. The transition from *grasping (no contact)* to *grasp maintenance (contact)* stages is smooth due to the proposed control strategy. The error between the desired and the actual velocities in contact is a consequence of the hard object constraints. Therefore, the actual velocity drops to zero as manipulators are no longer able to move relative to each other. As a result, potential energy is stored in the virtual spring of the impedance controller which maintains the grasp. After $t = 8.5$ s and in the *manipulation phase* (right plot in Figure 4.9) the desired relative velocity is set to $v^d_{r,y} = 0$ m/s. During the manipulation phase the mean relative velocity error is very low $\Delta\bar{v}_{r,y} = 2.6 \times 10^{-3}$ m/s, confirming the noninteraction of the cooperative and relative behaviors.

Experiment (iv): The desired and actual cooperative velocity profiles, resulting from the motion commands of the human operator during a pick-and-place task are shown in Figure 4.10. With the mean tracking velocity errors of $[\Delta\bar{v}_{c,x}\ \Delta\bar{v}_{c,y}\ \Delta\bar{v}_{c,z}]^\top = [2.54\ 9.94\ 11]^\top \times 10^{-4}$ m/s it can be concluded that the desired velocities, provided by the human operator,

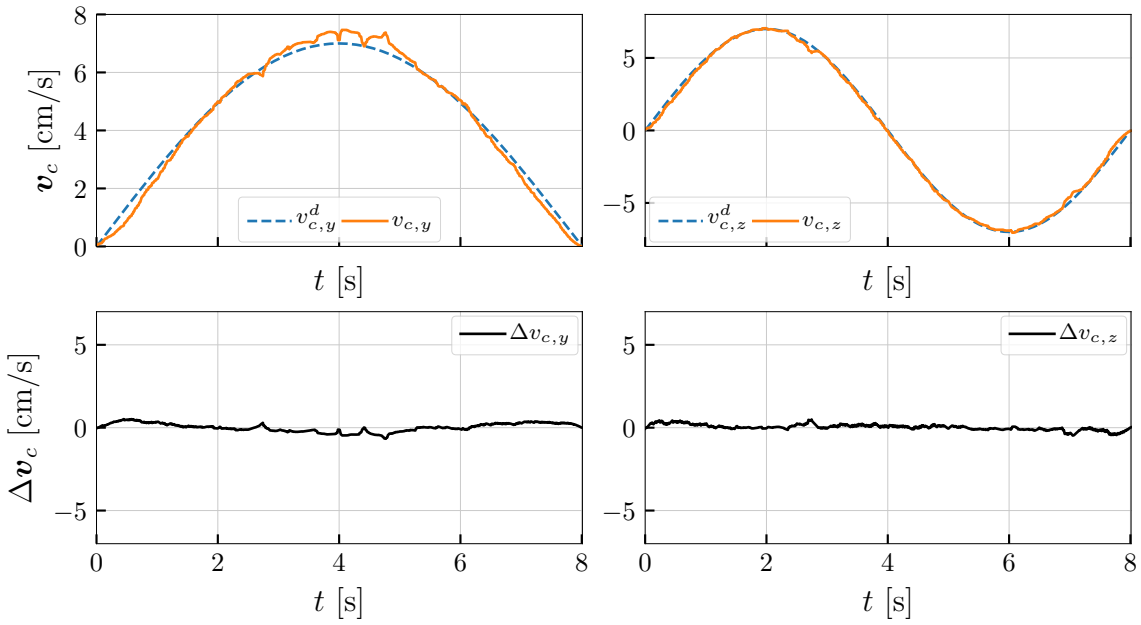

Figure 4.7: Desired (- - -) and actual (—) cooperative velocities (top), y (left) and z (right), and their corresponding tracking errors (bottom), without the human partner.

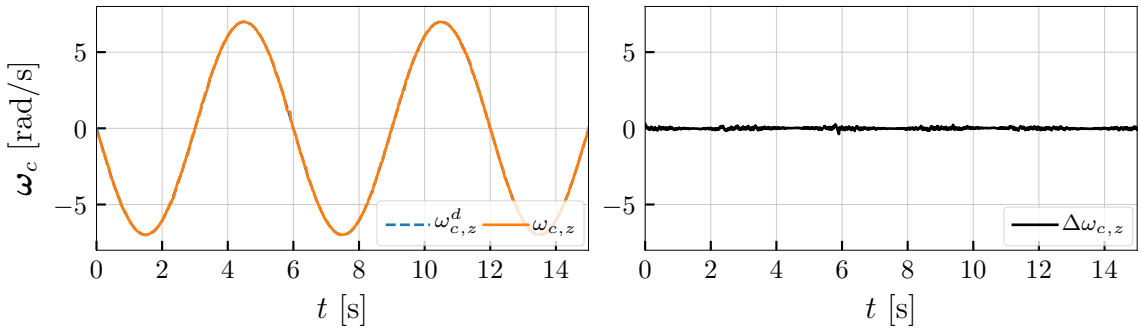

Figure 4.8: Desired (- - -) and actual (—) cooperative angular velocities (left), z component, and the corresponding tracking error (right), without the human partner.

are successfully tracked. Relative force profile, $f_{r,y}$, as well as the force in the local frame of the index fingertip device, $f_{h,2z}$, sensed by the human operator, are shown in Figure 4.11. It can be observed that the profile of $f_{h,2z}$ follows the profile of $f_{r,y}$, which indicates reasonable transparency of the system. However, possibly due to the curvature, the finger it is not perfectly centered on the force sensor. Therefore, low forces cannot be measured resulting in the dead zone of $f_{h,2z}$ until $t = 0.65$ s.

The performance of the proposed controller is satisfactory. Therefore, the human operator is able to command desired cooperative and relative velocities to accomplish the grasping subtask as well as the grasp maintenance and the object manipulation subtasks simultaneously. In the following subsection, results of a user study evaluating the suitability of the wearable haptic fingertip devices in the presented teleoperation system are presented.

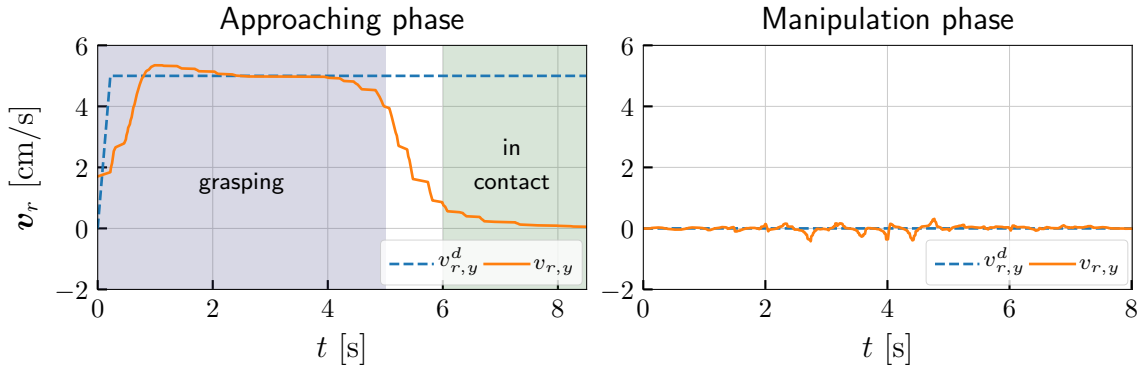

Figure 4.9: Desired (- - -) and actual (—) relative velocities, y component, during the approach to the object (left) and the manipulation of the object (right) phases, without the human partner.

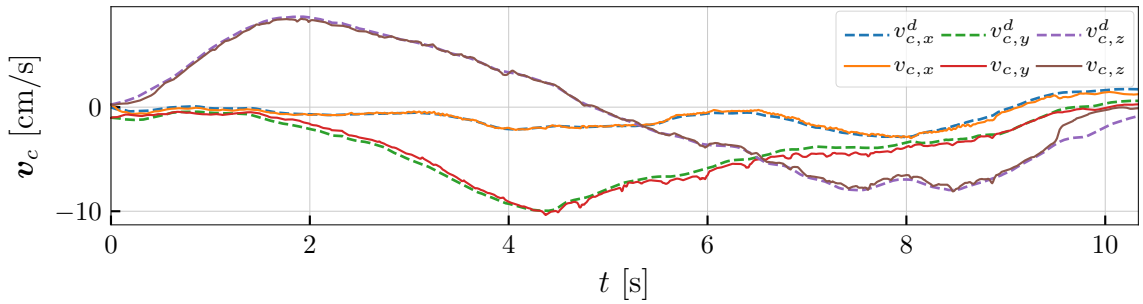

Figure 4.10: Desired and actual velocities, x, y, and z components, with desired velocities commanded by the human operator.

4.4.3 User Study Design

A user study to evaluate the performance of human partners in teleoperating a cooperative manipulation system using wearable thimble devices is conducted. Different types of feedback are compared to understand which feedback type results in the best task performance. For this purpose, two analysis are conducted: (i) a *within-subject analysis* and (ii) a *between-subject analysis*.

Experimental Task

The task is conducted on the experimental setup presented in Section 4.4.1 and depicted in Figure 4.5 with the control parameters reported in Table 4.1. The participants are asked to perform the pick-and-place task by: (i) commanding the grasping of the object to the robot manipulators, (ii) the desired trajectory of the object while maintaining the grasp and (iii) releasing the object once the desired goal is reached. In particular, it is required to guide the robots to grasp the object by commanding the relative motion. Afterwards, the operator needs to command the manipulators to apply sufficient amount of relative force to overcome gravitational forces during the object lifting. This is achieved through the continued relative motion between the thumb and index fingers. The object is assumed to be rigid, i.e. the commanded motion results in the relative force build-up between the manipulators. Desired

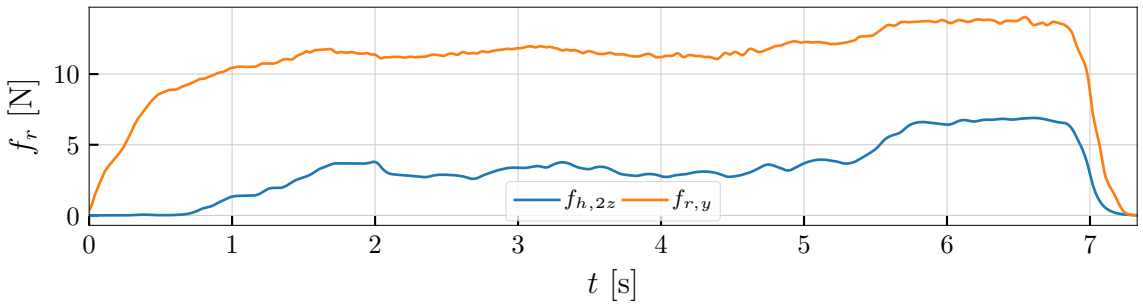

Figure 4.11: Relative force measured by the robot team along the $y-$axis and force sensed on the thimble device platform, mounted on the index finger.

object motion is commanded by the motion of the operator's hand. During the object transportation the operator needs to simultaneously control relative forces to avoid drops and slips.

Only translational degrees of freedom of the dual manipulator in the task space are activated, i.e. the rotations of the system cannot be controlled by the operator, but are controlled by the robot autonomy. The object is tracked by a motion capture system. The force at the end-effectors is estimated with the internal torque sensing of the manipulators and their known kinematic structure. The initial and final poses are marked on the table (see Figure 4.5). The human operator shares the workspace with the robots, i.e. they have the same reference frame $\{w\}$, and has direct visual feedback of the goal marks. The operator conducts the task while standing and can freely move in the workspace. Two fingertip devices are mounted on the human thumb and index fingers, as depicted in Figure 4.6b. Human hand, thumb, and index fingers are tracked with the motion tracking system. The setup with the human in the loop has wireless and fully wearable capabilities by establishing communication between the human and the robot system via Raspberry Pi. However, to avoid potential effects of delay and package losses on the user study results, the feedback is delivered through a local network.

Between-Subject Analysis

In the *between-subject (between-groups)* analysis different groups of people test different conditions (types of feedback to the wearable fingertip haptic devices).

Independent variables

Four types of feedback, mapped to the wearable fingertip devices, are tested:

1. *No feedback (NF):* Participants did not receive feedback through the fingertip devices. Instead, in order to conduct the task, they relied only on the visual feedback, i.e.

$$\boldsymbol{f}_{h,1} = \mathbf{0}_{3\times1} \text{ and } \boldsymbol{f}_{h,2} = \mathbf{0}_{3\times1}$$

for the fingertip devices mounted on the thumb and index fingers, respectively.

2. *Dynamic relative feedback (DF):* Participants received feedback through the fingertip devices that corresponds to the scaled version of the measured relative forces. In particular, the measured relative force component is equally distributed to the two fingertip devices as defined by (4.24). The mapping of the feedback forces to the degrees of freedom of the fingertip devices is achieved by d component defined in (4.25).

3. *Constant relative feedback (CF):* Participants received a scaled constant feedback through the fingertip devices, determined as follows

$$\boldsymbol{f}_{h,j} = \begin{cases} s_h 20 \text{ N}, & \text{if } \|\boldsymbol{f}_r\| \geq 20 \text{ N} \\ 0 \text{ N}, & \text{otherwise.} \end{cases} \quad j = 1, 2.$$

   The relative force of 20 N is sufficient to lift and move the object. Therefore, this feedback type informed the human operator if it is safe to transport the object to the goal without slips and drops.

4. *Binary feedback (BF):* Participants received constant feedback through the fingertip devices, determined as follows

$$\boldsymbol{f}_{h,j} = \begin{cases} s_h 7 \text{ N}, & \text{if } \|\boldsymbol{f}_r\| \geq 7 \text{ N} \\ 0 \text{ N}, & \text{otherwise,} \end{cases} \quad j = 1, 2.$$

   The relative force level of 7 N is not sufficient to move the object. Therefore, this type of feedback serves as a binary indicator for contact/no contact stages. As long as the contact is maintained, the feedback does not change. If the object drops, or is released, the feedback is 0 N.

Subjects

Participants signed a written informed consent, approved by the ethics committee of the medical faculty of the Technical University of Munich. Forty eight healthy subjects (12 females and 36 males) participated in the user study. The participants were assigned to one of the four groups which correspond to the types of feedback. Twelve subjects were in every group. Each participant performed the experiment ten times.

Performance measures

The effect of different types of feedback is evaluated by the following performance measures: (i) *mean of the measured relative force*, (ii) *maximum measured relative force*, (iii) *power-based effort* and (iv) *work* applied during the task execution.

Mean and maximum relative force: Mean relative force measured by the robot manipulators during the interaction with the object is computed as follows

$$\bar{f}_{r,y} = \frac{\sum_{i=1}^{K} f_{r,y_i}}{K}, \tag{4.26}$$

where K is the number of samples in the sequence. The maximum relative force applied during the lifting stage of the object is denoted as $f_{r,y}^{\max} = \max(f_{r,y})$.

Power-based effort and work: The effort measure is calculated as power

$$P = \bar{\dot{p}}\bar{f}_m, \tag{4.27}$$

where $\bar{\dot{p}}$ is the average translation velocity with $\dot{p}_i = ||\dot{\boldsymbol{p}}_i||$ being the velocity norm of sample i and $\bar{f}_m$ is the average measured force with $f_{m,i} = ||\boldsymbol{f}_{m,i}||, i = 1, ..., K$.

The work done during the object manipulation stage is computed as follows

$$W = \int_0^T P \, \mathrm{d}t, \tag{4.28}$$

where T is the duration of the object manipulation stage.

Statistical tests and hypotheses

The mean across all subjects and all trials is computed for each performance measure to test the effects of different types of feedback. *One-way analysis of variance (ANOVA)* is performed and significant differences are accepted at $p < 0.05$. A post-hoc test is carried out by *Tukey-Kramer multiple comparison method*. A posttest effect sizes are calculated to evaluate the practical significance of effects using *Cohen's d effect size measure* [LL16]. Three hypotheses are tested:

1. H1: *Relative force feedback* conditions, i.e. DF and CF, improve task performance compared to the *no haptic feedback* condition, NF.

2. H2: *Relative force feedback* conditions, i.e. DF and CF, improve task performance compared to the *binary feedback* condition, BF.

3. H3: *Dynamic relative feedback* condition, DF, improves task performance compared to the *constant relative feedback* condition, CF.

Data analysis

The recorded measurements are filtered with a second order Butterworth digital low-pass filter at a cut-off frequency of $f_c = 6$ Hz. There were 13 error measurements. The *slip force* is detected from the recorded relative force at the point of a drop [HKK+15] and is estimated to approximately $||\boldsymbol{f}_r||_{\text{slip}} = 9$ N. Measurements in which the system was uncontrollable by subjects were removed. More specifically, the trials in which subjects were unable to control the relative subtask because their thumb and index fingers were too close (connected) before the lifting stage of the object, are excluded from the analysis, as well as the trials in which the tracking of the passive markers on the human fingers is briefly lost. In total, there are 51 excluded measurements, which constitutes approximately 10% of the collected measurements.

Results of the user study

Bar plots for all the performance measures are shown in Fig 4.12. It can be observed in Figure 4.12a that the mean relative force measured by the robot system is the lowest for the dynamic and constant relative feedback types. The difference between the dynamic feedback

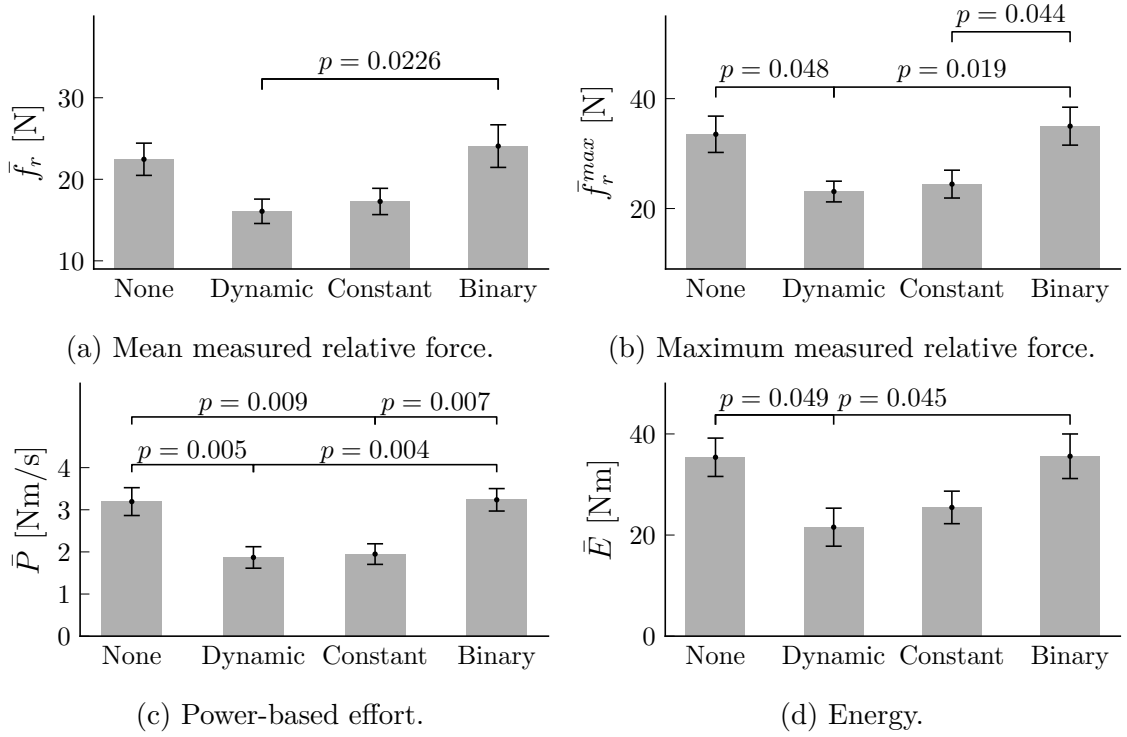

(a) Mean measured relative force.

(b) Maximum measured relative force.

(c) Power-based effort.

(d) Energy.

Figure 4.12: Bar plots showing the average values of relevant performance measures across 10 trials. The vertical bars in the plots are standard errors (SEs).

and the binary feedback types is significant with very large effect ($F_{3,44} = 4.2416, p = 0.0102, d = 1.22$). The post-hoc test revealed no significant differences between the dynamic and the constant relative feedback types. Additionally, no significant differences are revealed between the no feedback type and the relative feedback types.

Maximum relative force, obtained during the lifting stage of the object, is the lowest for the dynamic and the constant feedback types, see Figure 4.12b. These differences are significantly different compared to the no feedback and the binary feedback types with very large effect ($F_{3,44} = 4.9603, p = 0.0047, d = 1.252$). The maximum relative forces during the lifting stage of the object across 10 trials are shown in Figure 4.13a. It can be observed that the relative force levels out after trial no. 4 for the dynamic and the constant feedback types at approximately 24.2 N and 27.3 N, respectively. For the no feedback and the binary feedback types the maximum relative force increases across trials which is not optimal. Additionally, safety margin is larger for the no feedback and the binary feedback types compared to the dynamic and the constant feedback types.

The power-based effort and the total energy used to perform the task are the lowest for the dynamic and the constant feedback types. ANOVA revealed significant difference for the power-based effort and the energy as well, ($F_{3,44} = 8.1643, p = 0.0002, d = 1.494$) with very large effect and ($F_{3,44} = 3.7666, p = 0.0172, d = 1.108$) with large effect, respectively. Significant differences obtained from the multiple comparison post-hoc test are denoted in Figure 4.12c and 4.12d. Figure 4.13b depicts the power-based effort measure across 10 trials. It can be observed that the effort for relative feedback types is lower than for no feedback and binary feedback types. Additionally, effort for the relative feedback types is very similar which is also true for the no feedback and the binary feedback types. Therefore, the binary feedback type has a very similar effect on the overall performance as the no feedback type.

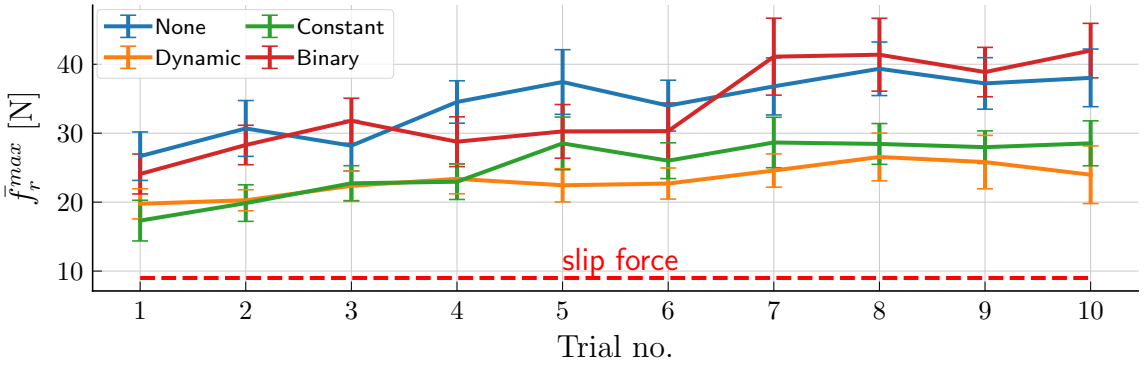

(a) Maximum relative force during the object lifting stage.

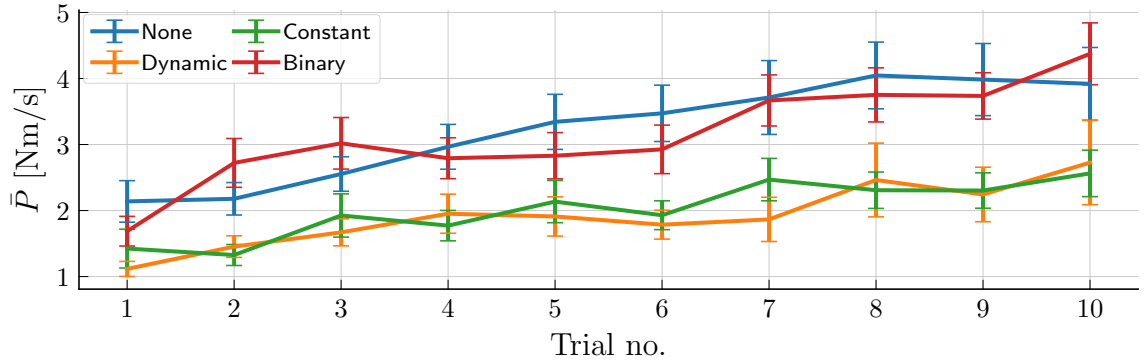

(b) Power-based effort.

Figure 4.13: Performance measures across 10 trials.

Discussion of the Results

H1. and H2. Relative force feedback conditions improve task performance compared to the no feedback and the binary feedback conditions.

The dynamic and constant relative feedback force types improve task performance compared to the no feedback and the binary feedback types. The mean relative force is not significantly lower in the case of the relative feedback types, compared to the no feedback type, but the maximum relative force during the lifting of the object is significantly different. The effort representing the combined effect of the mean relative force and the mean velocity of the manipulators is also significantly lower for the relative feedback types. The energy representing the effect of the effort and duration of the task is also the lowest for the relative force feedback types, with the dynamic feedback type being significantly lower. For the dynamic feedback type we can conclude that H1 is confirmed in terms of the maximum relative force, the effort, and the energy measures, while H2 is strongly confirmed. For the constant feedback type, H1 can be confirmed in terms of the total effort measure, while H2 can be confirmed in terms of the maximum relative force and the effort measures.

H3. Dynamic relative feedback improves task performance compared to the constant relative force feedback.

No significant differences were observed between the dynamic and the constant relative feedback types in all the performance measures. Furthermore, the performance for both feedback types was very similar. A possible reason may be that the dynamic feedback does not convey the information about the weight of the object and, therefore, may be as good as the constant feedback type for relatively small object weights as in this particular case. The constant feedback is parametrized to be approximately twice the amount of slip force, i.e. sufficient to manipulate the object. Therefore, it indirectly conveys the information of the weight of the object. The result also indicates the potential benefit of providing assistance through haptics, especially if the device is underactuated and cannot provide all task-relevant information. Namely, the constant feedback type informed the subjects that it is safe to lift and manipulate the object with the applied amount of force. This means that providing relevant assistance through haptics may improve the task performance. Therefore, H3 is not confirmed but implies that assisting the human operator by providing relevant information through haptics may be beneficial.

4.4.4 Within-Subject Analysis

In the *within-subject (repeated-measured)* analysis the same person, in the role of the human partner, tests all the conditions (types of feedback to the wearable fingertip haptic devices).

Independent variables

In this analysis, three independent conditions are the types of force feedback received through the haptic devices similar to the between-subjects analysis:

1. *No feedback (NF)*: No force feedback is displayed on the haptic devices.

2. *Dynamic relative feedback (DF)*: The operator receives direct visual feedback and feedback of the relative force applied by the manipulators to the object. The rotational degrees of freedom of the haptic devices are not activated. Therefore, the displacement degree of freedom of the devices exerts normal forces on the operator fingers. In particular

$$f_{h,1} = f_{h,2} = s_h \frac{f_r}{2},$$

   where $s_h = \frac{4.7}{30}$ is a scaling factor. The resulting displacements are

$$d_1 = k_t f_{h,1} \quad \text{and} \quad d_2 = k_t f_{h,2}, \tag{4.29}$$

   with the constant fingertip compliance parameter $k_t = 2$ mm/N [PKH03].

3. *Total measured interaction force (MF)*: The operator receives direct visual feedback and feedback about both the total measured interaction forces. The rotational degrees of freedom of the devices are activated. Three DoFs of the thumb device display forces

measured at the end-effector 1, while the index device displays forces measured at the end-effector 2

$$\alpha_j = \text{atan}\left(\frac{f_{m,jx}}{f_{m,jz}}\right),\ \beta_j = \text{atan}\left(\frac{f_{m,jy}}{f_{m,jz}}\right),\quad d_j = k_t s_h \sqrt{\left(\boldsymbol{f}_{m,j}\right)^\top \boldsymbol{f}_{m,j}},\quad j = 1,2 \quad (4.30)$$

where α and β provide shear forces at the contact points, while d displays the total force intensity.

Hypothesis and data analysis

H: The force feedback conditions, DF and MF, outperform the visual feedback condition, NF.

Error measurements caused by the loss of hand tracking were excluded. There were 11% of such measurements that were linearly interpolated. The dependent variables are computed from the obtained data, filtered with a low-pass frequency filter with $f_c = 6$ Hz cut-off frequency. Statistical analysis is conducted using a *repeated-measures analysis of variance (rANOVA)*. A post-hoc multicomparison analysis is conducted using *Tukey-Kramer* method. *Mauchly's test of sphericity* revealed that all dependent variables violate the sphericity condition. Therefore, modification to the degrees of freedom is performed using *Greenhouse-Geiger* correction.

Dependent variables

In order to evaluate the performance of the three feedback conditions the four dependent variables proposed for the between-subject analysis in Section 4.4.4 are considered in this within-subject analysis as well. Additional considered variable is *number of drops and slips*.

Subjects

Sixteen healthy subjects participated in the user study. Each condition is performed 10 times. In order to avoid bias towards certain independent conditions, the order in which the conditions are performed is random for each subject.

Results

Figure 4.14 shows the mean and the standard deviation for the relative and cooperative forces for all the feedback conditions, normalized to $t = 1$ s. It can be observed that the lowest measured relative force is achieved with DF condition. The cooperative force is similar for all conditions. Figure 4.15 shows that the ratio of the relative and cooperative forces is consistently the lowest for DF condition. The ratio for MF condition is lower than NF condition during the lifting stage. However, during the transportation stage the ratios for NF and MF conditions are very similar. This indicates that the MF condition is not a very beneficial form of haptic feedback during the object motion. The reason may be that the displacement degree of freedom of the haptic device is overloaded with both the relative and cooperative forces, which may generate difficulties in discriminating the type of force sensed at the fingertips.

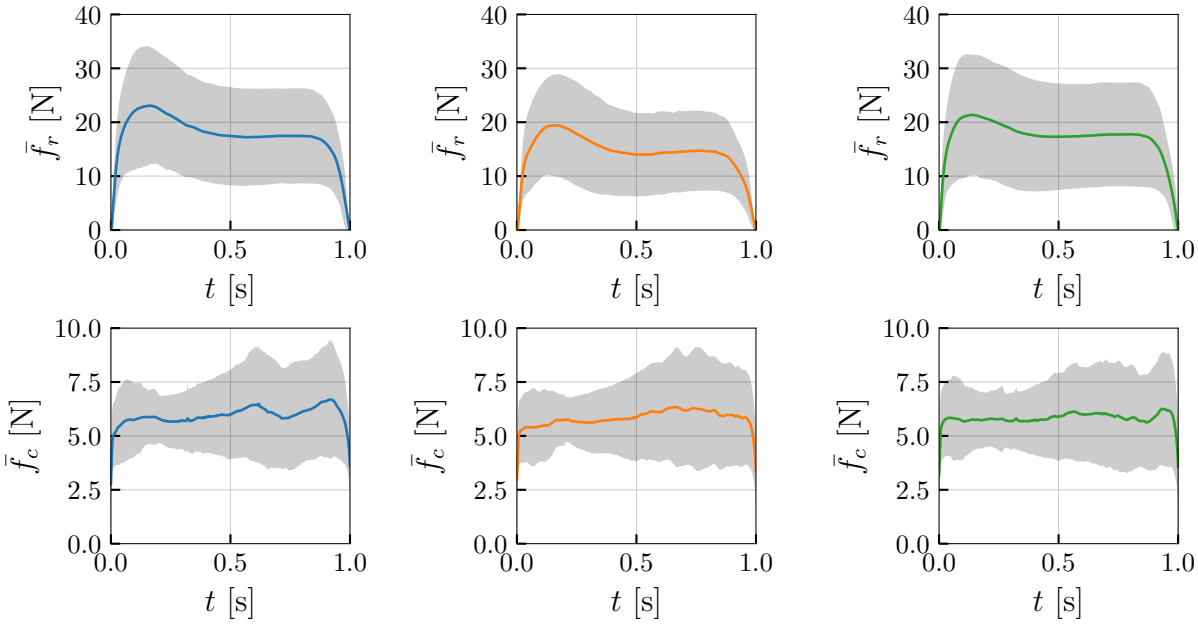

(a) NF (b) DF (c) MF

Figure 4.14: Relative and cooperative force mean and standard deviation for the three considered feedback conditions in the within-subject analysis. With DF feedback condition the lowest relative force is applied on the object.

In the remainder of this subsection the results of the statistical analysis are presented. The significant differences between the conditions are denoted with $\star$ if $p < .05$, $\star\star$ if $p < .01$, $\star\star\star$ if $p < .001$, and $\star\star\star\star$ if $p < .0001$. Exact pairwise comparison p values are listed in Table 4.2.

Mean relative force and maximum lift relative force

The bar plots of the five last trials for the mean relative force and maximum relative force during the lifting stage are depicted in Figure 4.12a and Figure 4.12b, respectively. Drops were excluded from the analysis to avoid their effect on reducing the overall mean. No outliers were detected for the mean relative force measure, while 1% of the total measurements were outliers in the maximum relative force measure. The statistical test did not reveal

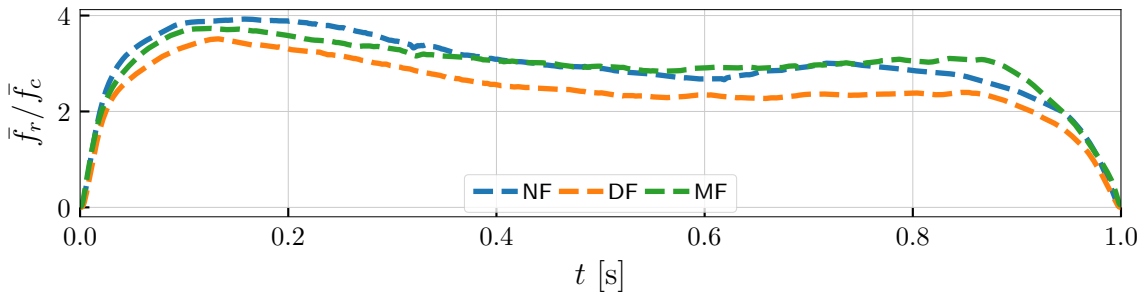

Figure 4.15: Ratio between the relative and cooperative force.

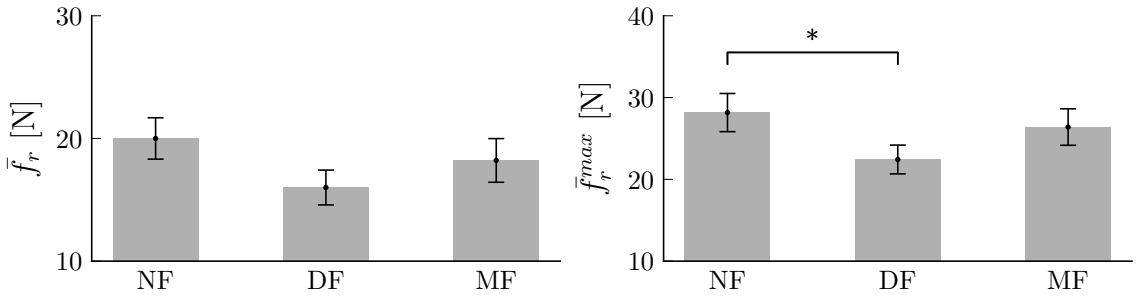

(a) Mean measured relative force. (b) Maximum measured lift relative force.

Figure 4.16: Bar plots of the average values of relevant performance measures across last five trials and all subjects. The vertical bars in the plots are standard errors (SEs).

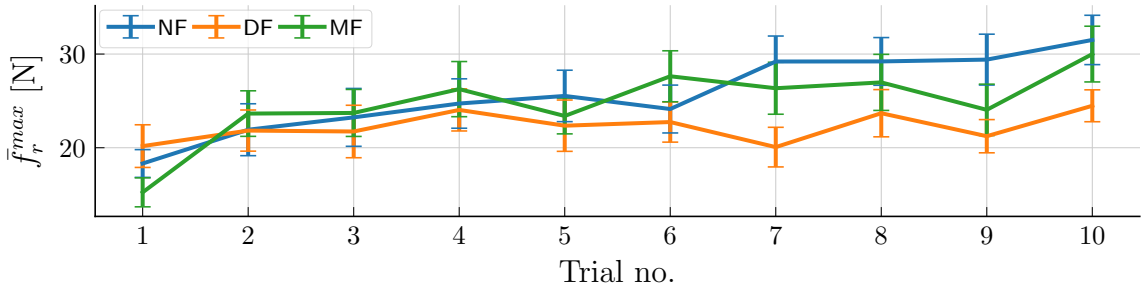

Figure 4.17: Maximum measured relative force per 10 trials and across all subjects.

significant difference between the feedback conditions for the mean relative force measure ($F(2, 30) = 2.9964, p = 0.068$). However, a significant difference was revealed for the maximum relative force measure ($F(2, 30) = 3.4413, p = 0.47$). In both cases the measured force is the lowest for the DF condition. Multiple comparison test revealed significant difference between NF and DF conditions for the maximum lift relative force measure. Figure 4.17 depicts maximum relative force across 10 trials for all feedback conditions. The relative force is consistently the lowest and kept constant for the DF feedback condition.

Total effort and energy

The bar plots for the total effort and energy are depicted in Figure 4.12c and Figure 4.12d, respectively. In the case of the effort dependent measure, 4% of the data were detected as outliers. Statistical analysis revealed significant differences between the feedback conditions ($F(2, 30) = 11.832, p = 0.00017$) for the effort measure but revealed no significant differences between conditions for the total energy measure ($F(2, 30) = 2.3744, p = 0.11$). Both the effort and the energy are the lowest for the DF condition. Furthermore, the effort for the DF condition is significantly different compared to the NF condition. This indicates the importance of force feedback in reducing the effort of task execution.

Figure 4.19 shows that for the DF condition the energy is the lowest and that it is approximately constant across all trials. For the NF condition the total energy increases with the number of trials indicating fatigue of participants.

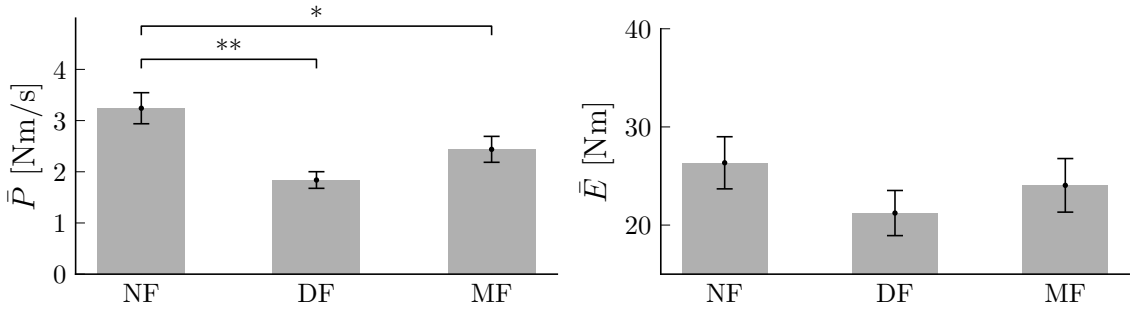

(a) Total effort. (b) Total energy.

Figure 4.18: Bar plots of the average values of relevant performance measures across last five trials and all subjects. The vertical bars in the plots are standard errors (SEs).

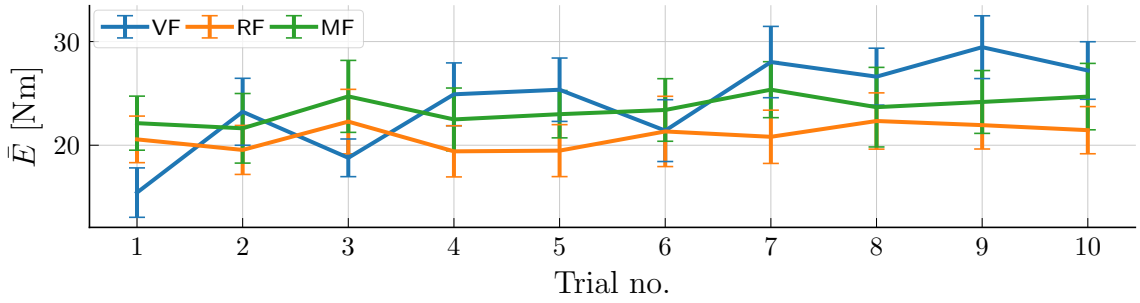

Figure 4.19: Mean energy per 10 trials and across all subjects. The energy needed to conduct the task is consistently the lowest for DF.

Table 4.2: Multiple comparison p values obtained with Bonferroni method.

Dependent variables	NF vs. DF	NF vs. MF	DF vs. MF
Mean rel. force, $\bar{f}_r$	0.07	0.44	0.44
Max. rel. force, $\bar{f}_r^{max}$	**0.04**	0.6	0.2
Effort, $\bar{P}$	**0.0007**	**0.03**	0.13
Energy, $\bar{E}$	0.1	0.59	0.5

Drops and slips

Figure 4.20 shows a cumulative bar plot with the total number of drops and slips across the trials for each condition. The highest number of drops is detected for NF condition, while the lowest (only one drop) for the MF condition, indicating that the rotational degrees of freedom of the used haptic device are beneficial in reducing drops and slips. The statistical analysis did not reveal significant differences between the conditions. However, based on the occurrence of drops and slips per trials, it can be concluded that for the NF condition the drops and slips are the most frequent in earlier trials (1-4), but their frequency reduces in later trials as the applied relative force increases. Drops are more frequent in the later trials in the DF condition which may be an indication of fatigue.

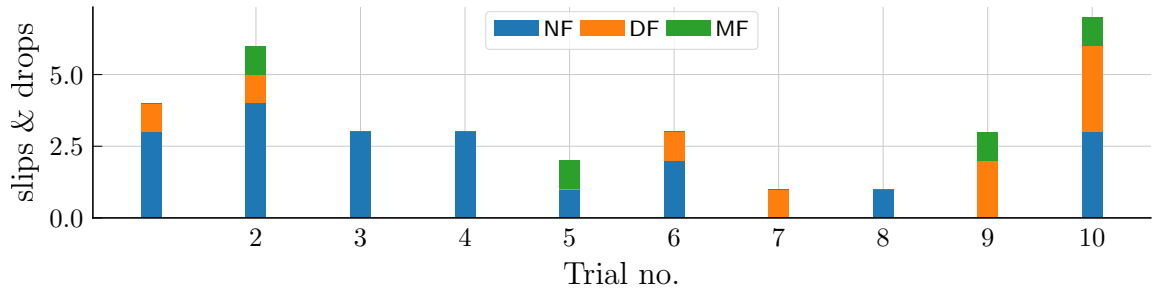

Figure 4.20: Cumulative bar plot of the total number of drops and slips per 10 trials. The highest number of drops and slips is detected for NF condition. The lowest number of drops and slips is detected for MF condition.

Discussion of the Results

The presented results show that the haptic feedback indeed improves the task performance. In particular, the devices are suitable to convey information about relative force, DF. The feedback about the measured forces, MF, at the contact points did not convey equally good results, even though its difference from the purely visual feedback, NF, is significant in terms of total effort needed to conduct the task. The number of drops and slips is by far the lowest for the MF type of feedback, indicating that it is possible to perceive slips through the rotational degrees of freedom conveying shear forces. However, the results for this type of feedback are still not conclusive and a simplified feedback of relative forces through the use of the displacement degree of freedom conveyed the best results. Therefore, the hypothesis H is only partially confirmed.

4.5 Discussion

A control architecture for human-robot team interaction in cooperative manipulation tasks is proposed in this chapter. The control approach is based on the concept of *subtasks*, which represent task-based constraints, see Chapter 2 for more details, and an input-output noninteracting shared controller, proposed in Chapter 3. It is shown that grasping, grasp maintenance, and object manipulation subtasks can be performed along the introduced *co-operative* and *relative* constraints in order to successfully achieve the overall task. Furthermore, through the appropriate command and feedback mappings the control approach enables interaction between a human operator and the system on a higher level of abstraction. Wearable fingertip devices are used as haptic interfaces to enable teleoperation in a multi-contact setting which increases flexibility of interaction and workspace of the human operator. User performance with different types of feedback is evaluated and the results show that the feedback of grasping forces improves task performance compared to no haptic feedback.

The work presented in Sections 4.1-4.4.2 as well as the between-subject user study analysis in Section 4.4.3 has been published in [MSgD+19]. The work in Section 4.4.4, related to the within-subject user study analysis has been published in [MPH19].

5

Port-Hamiltonian Cooperative Manipulation

Cooperative manipulation task is challenging in terms of the system complexity and the control synthesis. Since *port-Hamiltonian (pH) framework* is suitable for modeling interconnected systems, it can be used for modeling and control of cooperative manipulation tasks.

Human-robot team interaction for teleoperation of a cooperative manipulation task is modeled and controlled using the port-Hamiltonian framework. The robot team, grasping the object, is considered as a physically constrained system. The results of this chapter show that the considered subtask-based controller is consistent with modeling and controlling physically constrained systems in the port-Hamiltonian framework as well. An energy tank is introduced to guarantee passivity of the system commanded by the human and safety of human-robot team interaction in the robot environment. The proposed approach is validated with simulation and experiments.

Related Work and Open Problems

The port-Hamiltonian framework is a powerful method for modelling complex and interconnected systems [vdS06]. It is based on the interconnection of *atomic structure elements*, e.g. inertias, springs and dampers for mechanical systems, and on the known *energy function* of the system, the *Hamiltonian*. It is possible to model and control teleoperation of coordinated robot teams, as well as physical human-robot team interaction within the port-Hamiltonian framework [FSM+11, GSDP16]. However, modeling a robot team as a constrained port-Hamiltonian system has not been done so far.

Control schemes for cooperative manipulation tasks are typically object-centered and are based on *impedance control* and *grasp theory*, as reviewed in Chapter 4. Making impedance control physically interpretable motivated the development of the *intrinsically passive control (IPC)* approach within the *port-Hamiltonian framework* [SMv98]. It is designed as an interconnection of virtual atomic structure elements to achieve a desired behavior in grasping. These virtual structures are also used in *formation control* to establish a desired geometric shape of robotic agents [VSvdSP14]. Therefore, designing a control strategy for robot formations and for cooperative manipulation tasks within the port-Hamiltonian framework is intuitive.

Actively stabilizing a port-Hamiltonian system at a certain energy level is termed as *energy shaping control* [OvME99]. If it is represented within the port-Hamiltonian framework, *control by interconnection* of the port-Hamiltonian system [OvCA08] is obtained. Control by

interconnection of constrained port-Hamiltonian systems is not analyzed in literature. Another important control approach in the port-Hamiltonian framework is *energy transfer control*, with *energy tank* as its most widely used concept [VSvdSP14]. Energy tanks allow to bound the energy supply to the system. Appropriately limiting energy in the system enhances safety of intefraction with the environment and/or with humans on-site and is, therefore, a suitable control methodology for human-in-the loop settings.

A teleoperation scenario for cooperative manipulation tasks has not been considered within the port-Hamiltonian framework. The cooperative robot system, constrained by a rigid object, is modeled in Section 5.1 in the sense of subtask-based control proposed in Chapter 2. A control approach for human-robot team interaction with passivity and safety guarantees is proposed in Section 5.2. The approach is validated in simulation and experiment, with the results reported in Section 5.3, while Section 5.4 provides concluding remarks.

5.1 Port-Hamiltonian Modeling of Robot Teams

In this section a port-Hamiltonian model of a cooperative manipulation system is proposed. The cooperative robot team with a grasped, rigid object is represented as a constrained system in an implicit and explicit input-state-output forms. Let us assume a setting depicted in Figure 5.1 where N manipulators are rigidly connected to the object. The world (inertial) frame is denoted as $\{w\}$, the object frame as $\{o\}$ and the end-effector frames as $\{i\}$ where $i = 1, ..., N$. The object and the end-effectors are represented as inertial elements (see Appendix 9 for a more detailed introduction to the port-Hamiltonian framework), where the momentum of the object is ${}^{o}\tilde{\boldsymbol{p}}_o$ and the momenta of the robots are ${}^{i}\tilde{\boldsymbol{p}}_i$, $i = 1, ..., N$. The potential energy of the complete system is represented with a single spring, connecting the object and the ground, with the displacement denoted with transformation matrix as

$$\boldsymbol{H}_o = \begin{bmatrix} \boldsymbol{R}_o & \boldsymbol{p}_o \\ \boldsymbol{0}_{1\times 3} & 1 \end{bmatrix}. \tag{5.1}$$

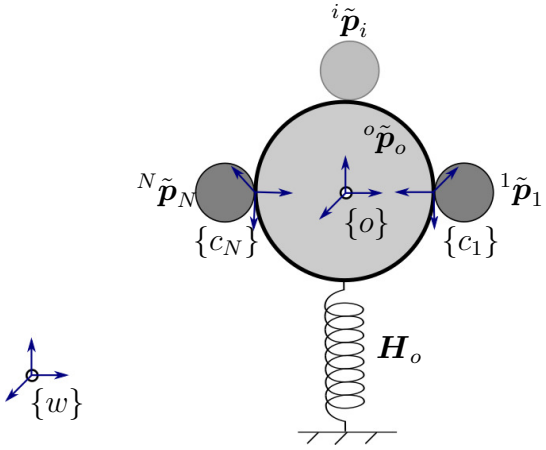

Figure 5.1: Cooperative manipulation system model represented as a set of interconnected energy storing elements, inertias and a spring.

The explicit port-Hamiltonian model form is

$$\begin{aligned}\dot{\boldsymbol{\xi}} &= [\boldsymbol{J}(\boldsymbol{\xi}) - \boldsymbol{D}(\boldsymbol{\xi})]\frac{\partial \mathcal{H}}{\partial \boldsymbol{\xi}}(\boldsymbol{\xi}) + \boldsymbol{G}(\boldsymbol{\xi})\boldsymbol{u} \\ \boldsymbol{y} &= \boldsymbol{G}^\top(\boldsymbol{\xi})\frac{\partial \mathcal{H}_s}{\partial \boldsymbol{\xi}}(\boldsymbol{\xi}),\end{aligned} \tag{5.2}$$

where $\boldsymbol{\xi} \in \mathcal{M}$ stacks configuration variables of the gravity spring and the momenta of the object and the N manipulators, $\boldsymbol{\xi} = [\boldsymbol{H}_o^\top, {}^o\tilde{\boldsymbol{p}}_o^\top, {}^1\tilde{\boldsymbol{p}}_1^\top, ..., {}^N\tilde{\boldsymbol{p}}_N^\top]^\top$, $\boldsymbol{J}(\boldsymbol{\xi})$ is a skew-symmetric structure matrix and $\boldsymbol{D}$ is a positive semi-definite damping matrix. The matrix $\boldsymbol{G}$ is the input mapping matrix, $\boldsymbol{u} \in \mathcal{K}$ an m-dimensional input vector, $\boldsymbol{y} \in \mathcal{V}^*$ an m-dimensional output vector and $\mathcal{H}_s$ is a Hamiltonian, a non-negative function $\mathcal{H}_s \geq 0$, which represents the total energy stored in the system. The rate of the energy change of (5.2) is

$$\dot{\mathcal{H}}_s = \boldsymbol{y}^\top \boldsymbol{u} - \frac{\partial^\top \mathcal{H}_s}{\partial \boldsymbol{\xi}}\boldsymbol{D}(\boldsymbol{\xi})\frac{\partial \mathcal{H}_s}{\partial \boldsymbol{\xi}}. \tag{5.3}$$

Remark 29. *According to (5.3) every port-Hamiltonian system described in the form of (5.2) is passive from input $\boldsymbol{u}$ to output $\boldsymbol{y}$.*

The constrained system depicted in Figure 5.1 can be represented in an implicit port-Hamiltoninan form as follows

$$\begin{aligned}\dot{\boldsymbol{\xi}} &= \boldsymbol{J}(\boldsymbol{\xi})\frac{\partial \mathcal{H}_s}{\partial \boldsymbol{\xi}}(\boldsymbol{\xi}) + \boldsymbol{A}(\boldsymbol{\xi})\boldsymbol{\lambda} + \boldsymbol{G}(\boldsymbol{\xi})\boldsymbol{u} \\ \boldsymbol{0} &= \boldsymbol{A}^\top(\boldsymbol{\xi})\frac{\partial \mathcal{H}_s}{\partial \boldsymbol{\xi}}(\boldsymbol{\xi}) \\ \boldsymbol{y} &= \boldsymbol{G}^\top(\boldsymbol{\xi})\frac{\partial \mathcal{H}_s}{\partial \boldsymbol{\xi}}(\boldsymbol{\xi}),\end{aligned} \tag{5.4}$$

where $\boldsymbol{A}(\boldsymbol{\xi})$ is a constraint matrix with $\boldsymbol{\lambda} \in \mathbb{R}^l$ being the constraining wrenches. The structure and the mapping matrices are

$$\begin{aligned}\boldsymbol{J}(\boldsymbol{\xi}) &= \begin{bmatrix} \boldsymbol{0} & \boldsymbol{H}_o & \boldsymbol{0} & \cdots & \boldsymbol{0} \\ -\boldsymbol{H}_o^\top & \boldsymbol{C}_o & \boldsymbol{0} & \cdots & \boldsymbol{0} \\ \boldsymbol{0} & \boldsymbol{0} & \boldsymbol{C}_1 & \cdots & \boldsymbol{0} \\ \vdots & \vdots & \vdots & \ddots & \vdots \\ \boldsymbol{0} & \boldsymbol{0} & \boldsymbol{0} & \cdots & \boldsymbol{C}_N \end{bmatrix} \\ \boldsymbol{G}(\boldsymbol{\xi}) &= \begin{bmatrix} \boldsymbol{0} & \boldsymbol{0} & \cdots & \boldsymbol{0} \\ \boldsymbol{Ad}_{{}^o\boldsymbol{H}_w} & \boldsymbol{0} & \cdots & \boldsymbol{0} \\ \boldsymbol{0} & \boldsymbol{Ad}_{{}^1\boldsymbol{H}_w} & \cdots & \boldsymbol{0} \\ \vdots & \vdots & \ddots & \vdots \\ \boldsymbol{0} & \boldsymbol{0} & \cdots & \boldsymbol{Ad}_{{}^N\boldsymbol{H}_w} \end{bmatrix},\end{aligned} \tag{5.5}$$

where $\boldsymbol{C}_*$ accounts for the Coriolis and centrifugal terms. The stacked input vector consists of the external wrenches acting on the inertias $\boldsymbol{u} = [\boldsymbol{w}_o, \boldsymbol{w}_1, ..., \boldsymbol{w}_i, ..., \boldsymbol{w}_N]$. The outputs are the twists of the inertias $\boldsymbol{y} = [\boldsymbol{t}_o^\top, \boldsymbol{t}_1^\top, ..., \boldsymbol{t}_i^\top, ..., \boldsymbol{t}_N^\top]^\top$. The Hamiltonian energy $\mathcal{H}_s$ is the sum of the energies of all the elements

$$\mathcal{H}_s(\boldsymbol{\xi}) = \mathcal{H}_P(\boldsymbol{H}_o) + \mathcal{H}_K({}^o\tilde{\boldsymbol{p}}_o) + \sum_{i=1}^{N} \mathcal{H}_K({}^i\tilde{\boldsymbol{p}}_i). \tag{5.6}$$

The interaction of the manipulators with the rigid object imposes *kinematic constraints* on the complete system. This implies that there is no relative motion between the object and the end-effectors which can be denoted as

$$\boldsymbol{t}_o = \boldsymbol{t}_i, \ \forall i = 1..N, \tag{5.7}$$

where $\boldsymbol{t}_o$ denotes the twist of the object and $\boldsymbol{t}_i$ stands for the twist of the i^{th} manipulator. With a change of coordinates ${}^{o,w}\boldsymbol{t}_o = \boldsymbol{Ad}_{{}^o\boldsymbol{H}_i}\, {}^{i,w}\boldsymbol{t}_i$ the constraint equation is

$$\boldsymbol{0} = \underbrace{\begin{bmatrix} \boldsymbol{0} & \boldsymbol{I}_6 & -\boldsymbol{Ad}_{{}^o\boldsymbol{H}_1} & \cdots & \boldsymbol{0} \\ \vdots & \vdots & \vdots & \ddots & \vdots \\ \boldsymbol{0} & \boldsymbol{I}_6 & \boldsymbol{0} & \cdots & -\boldsymbol{Ad}_{{}^o\boldsymbol{H}_N} \end{bmatrix}}_{\boldsymbol{A}^\top(\boldsymbol{\xi})} \frac{\partial \mathcal{H}_s}{\partial \boldsymbol{\xi}}(\boldsymbol{\xi}), \tag{5.8}$$

where $\boldsymbol{A}(\boldsymbol{\xi}) \in \mathbb{R}^{n \times l}$ is the *constraint* matrix with l being the number of independent kinematic constraints. The violation of constraints generates internal stress on the object [EH16]. The constraining forces are considered using *Lagrangian multipliers*, $\boldsymbol{\lambda}$. Therefore, the port-Hamiltonian formulation of the constrained model is a set of differential and algebraic equations. To restore the explicit input-state-output form, given with (5.2), the implicit model needs to be restricted to the constraint manifold $\mathcal{M}_c$, which can be achieved by eliminating the Lagrangian multipliers from (5.4).

5.1.1 Elimination of Constraints

The differential-algebraic equation (5.4) can be reduced to a set of ordinary differential equations (5.2) by multiplying it with a full-rank left annihilator of the constraint matrix, $\boldsymbol{A}^\perp(\boldsymbol{\xi})$, such that $\boldsymbol{A}^\perp(\boldsymbol{\xi})\boldsymbol{A}(\boldsymbol{\xi})\boldsymbol{\lambda} = \boldsymbol{0}$. The annihilator can be calculated as the kernel of $\boldsymbol{A}(\boldsymbol{\xi})$. The left annihilator is used in the following form

$$\boldsymbol{A}^\perp(\boldsymbol{\xi}) = \begin{bmatrix} \boldsymbol{I}_6 & \boldsymbol{0}_6 & \boldsymbol{0}_6 & \cdots & \boldsymbol{0}_6 \\ \boldsymbol{0}_6 & \underbrace{\begin{matrix} \boldsymbol{I}_3 & \boldsymbol{S}(\tilde{\boldsymbol{p}}_o) \\ \boldsymbol{0}_3 & \boldsymbol{I}_3 \end{matrix}}_{\boldsymbol{P}_o} & \underbrace{\begin{matrix} \boldsymbol{I}_3 & \boldsymbol{S}(\tilde{\boldsymbol{p}}_1) \\ \boldsymbol{0}_3 & \boldsymbol{I}_3 \end{matrix}}_{\boldsymbol{P}_1} & \cdots & \underbrace{\begin{matrix} \boldsymbol{I}_3 & \boldsymbol{S}(\tilde{\boldsymbol{p}}_N) \\ \boldsymbol{0}_3 & \boldsymbol{I}_3 \end{matrix}}_{\boldsymbol{P}_N} \end{bmatrix} \tag{5.9}$$

where the combined matrix $\boldsymbol{P} = [\boldsymbol{P}_o, \boldsymbol{P}_1, ..., \boldsymbol{P}_N] \in \mathbb{R}^{6\times 6(N+1)}$ is the *grasp matrix*. Multiplying (5.4) with the annihilator (5.9) the following is obtained

$$\boldsymbol{A}^\perp \dot{\boldsymbol{\xi}} = \boldsymbol{A}^\perp \boldsymbol{J}(\boldsymbol{\xi}) \frac{\partial \mathcal{H}_s}{\partial \boldsymbol{\xi}}(\boldsymbol{\xi}) + \boldsymbol{A}^\perp \boldsymbol{G}(\boldsymbol{\xi})\boldsymbol{u}. \tag{5.10}$$

Remark 30. *Effectively, $\boldsymbol{A}^\perp\dot{\boldsymbol{\xi}}$ is a coordinate transformation [vdS13], resulting from the* physically imposed *equality constraints. Therefore, this approach is physically consistent with the* subtask-based control *concept, proposed in Chapter 2. With the proposed annihilator of the constraint matrix, $\boldsymbol{A}^\perp$, the configuration $\boldsymbol{H}_o$ is unaffected by the transformation.*

Let us denote a new $(n-6N)$-dimensional state as $\tilde{\boldsymbol{\xi}}$. The resulting state evolves on a constrained manifold

$$\mathcal{M}_c = \{\boldsymbol{\xi} \in \mathcal{M} | \boldsymbol{A}^\top(\boldsymbol{\xi}) \frac{\partial \mathcal{H}_s}{\partial \boldsymbol{\xi}} = \boldsymbol{0}\}. \tag{5.11}$$

Now it is possible to obtain the model in an explicit input-state-output form as in (5.2)

$$\begin{aligned} \dot{\tilde{\boldsymbol{\xi}}} &= \tilde{\boldsymbol{J}}(\boldsymbol{\xi}) \frac{\partial \tilde{\mathcal{H}}_s}{\partial \tilde{\boldsymbol{\xi}}} + \tilde{\boldsymbol{G}}(\boldsymbol{\xi}) \boldsymbol{u} \\ \boldsymbol{y} &= \tilde{\boldsymbol{G}}^\top(\boldsymbol{\xi}) \frac{\partial \tilde{\mathcal{H}}_s}{\partial \tilde{\boldsymbol{\xi}}}, \end{aligned} \tag{5.12}$$

where $\tilde{\mathcal{H}}_s$ is the Hamiltonian function evolving on the constrained manifold (5.11). The reduced structure matrix $\tilde{\boldsymbol{J}}(\boldsymbol{\xi}) = \boldsymbol{A}^\perp \boldsymbol{J}(\boldsymbol{\xi})(\boldsymbol{A}^\perp)^\top$ is again skew-symmetric, i.e. the explicit input-state-output port-Hamiltonian representation of the constrained system is obtained. The new mapping matrix $\tilde{\boldsymbol{G}}(\boldsymbol{x}) = [\tilde{\boldsymbol{G}}_o \; \tilde{\boldsymbol{G}}_\mathrm{m}]$ decomposes into two parts: $\tilde{\boldsymbol{G}}_o \in \mathbb{R}^{12\times 6}$ represents the interaction of the object with the environment, while $\tilde{\boldsymbol{G}}_m \in \mathbb{R}^{12\times 6N}$ represents the interaction with the controller. The energy balance of (5.12) is $\dot{\tilde{\mathcal{H}}}_s = \boldsymbol{y}^T \boldsymbol{u}$, i.e. the system is power-conservative.

5.2 Control for Human-Robot Team Interaction

In this section a *passivity-based control* methodology within the port-Hamiltonian framework for human-robot team interaction is proposed. The approach is a cascade of *energy shaping control strategy* with the *damping injection* and the *energy transfer control*. Energy shaping is achieved by exploiting the available information on the energetic state obtained from the controller and the modeled system. A maximum level of the energy to be stored in the controller and the system limits both the velocity and the forces. The energy bound of the controller-system interconnection is ensured by sourcing it from an energy tank. The block structure of the complete system is depicted in Figure 5.2.

5.2.1 Energy Shaping and Damping Injection

The proposed controller has a physical interpretation since it is based on the virtual mechanical structures assumed to interconnect the robots and the human with the object. Therefore, the controller can be represented in the port-Hamiltonian framework. There are two alternatives to establish a desired formation of the robots around the grasped object: (i) the use of non-zero rest-length springs connecting the robots pairwise or (ii) the introduction of a *virtual object* as a hinge point [SMA99]. In this work the virtual object concept is used. The virtual object is connected by a virtual spring and a virtual damper to the human hand. The end-effectors are coupled to the surface of the virtual object with constant virtual springs and virtual dampers. The proposed virtual structure is depicted in Figure 5.3.

In the remainder, only an interconnection of the i-th manipulator is given in the equations. The state vector $\boldsymbol{\xi}_c$ is a stacked vector of:

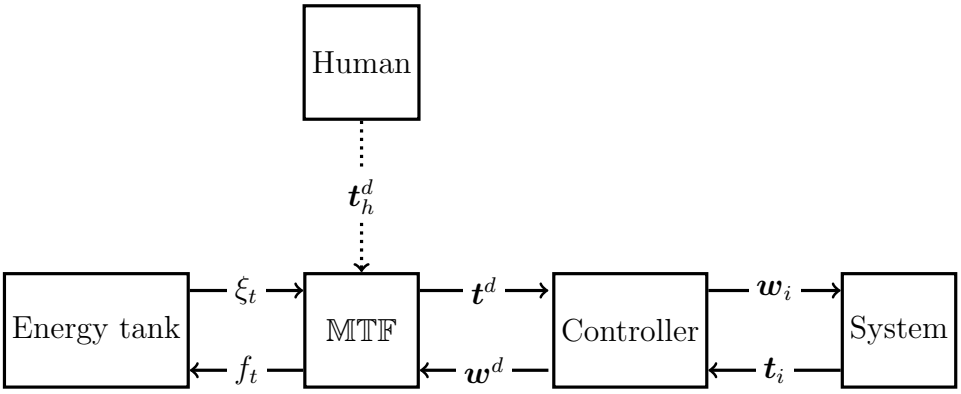

Figure 5.2: Block structure of the human-robot system: The *energy tank* supplies energy to the *controller*, while the *human* is energetically decoupled (indicated by dotted lines). The energy flow depends on the human input and is controlled via the *modulated transformer* ($\mathbb{MTF}$). The output of the transformer is the (modified) reference trajectory $\boldsymbol{t}^d$. The wrench applied by the end-effectors is $\boldsymbol{w}_i$ and the twists of the end-effectors are $\boldsymbol{t}_i$.

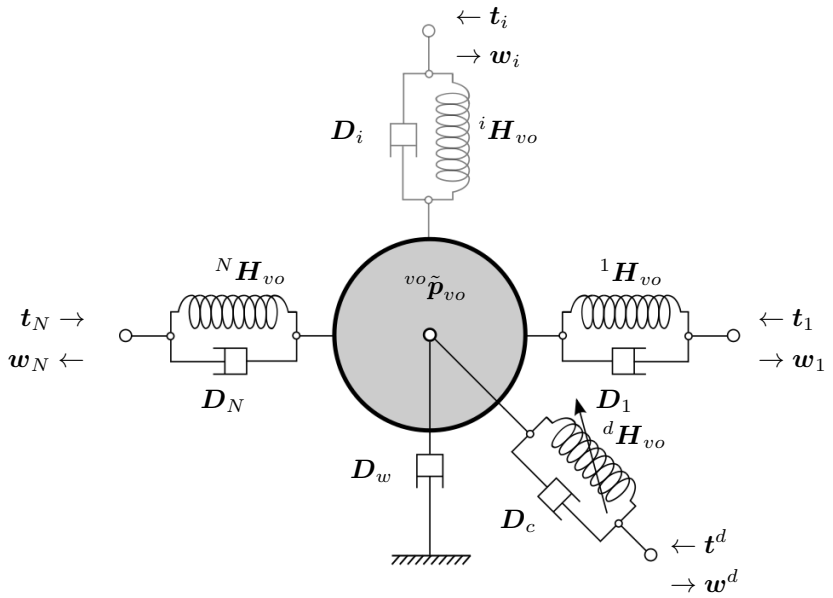

Figure 5.3: Interaction controller represented as a virtual structure of inertia, (variable) springs and (variable) dampers.

- the variable virtual spring, ${}^d\boldsymbol{H}_{vo}$, connecting the human hand and the virtual object,
- the virtual object momenta, ${}^{vo}\tilde{\boldsymbol{p}}_{vo}$ and
- the virtual spring, ${}^i\boldsymbol{H}_{vo}$, connecting the virtual object and the i-th end-effector.

The extension to N interconnections is straightforward. The controller in the port-Hamiltonian framework is represented as

$$\begin{aligned}\dot{\boldsymbol{\xi}}_c &= [\boldsymbol{J}_c(\boldsymbol{\xi}_c) - \boldsymbol{D}_c(\boldsymbol{\xi}_c)]\frac{\partial \mathcal{H}_c}{\partial \boldsymbol{\xi}_c}(\boldsymbol{\xi}_c) + \boldsymbol{G}_c(\boldsymbol{\xi}_c)\boldsymbol{u}_c \\ \boldsymbol{y}_c &= \boldsymbol{G}_c^\top(\boldsymbol{\xi}_c)\frac{\partial \mathcal{H}_c}{\partial \boldsymbol{\xi}_c}(\boldsymbol{\xi}_c),\end{aligned} \tag{5.13}$$

with the components

$$\begin{aligned}\dot{\boldsymbol{\xi}}_c &= \begin{bmatrix} {}^d\boldsymbol{t}_{vo} \\ {}^{vo}\dot{\tilde{\boldsymbol{p}}}_{vo} \\ {}^i\boldsymbol{t}_{vo}\end{bmatrix}, \boldsymbol{u}_c = \begin{bmatrix}\boldsymbol{t}^d \\ \boldsymbol{t}_i\end{bmatrix}, \boldsymbol{y}_c = \begin{bmatrix}\boldsymbol{w}^d \\ \boldsymbol{w}_i\end{bmatrix} \\ \boldsymbol{J}_c &= \begin{bmatrix} \boldsymbol{0} & {}^d\boldsymbol{H}_{vo} & \boldsymbol{0} \\ -{}^d\boldsymbol{H}_{vo}^\top & \boldsymbol{C}_{vo} & -{}^i\boldsymbol{H}_{vo}^\top \\ \boldsymbol{0} & {}^i\boldsymbol{H}_{vo} & \boldsymbol{0}\end{bmatrix}, \\ \boldsymbol{D}_c &= \begin{bmatrix}\boldsymbol{0} & \boldsymbol{0} & \boldsymbol{0} \\ \boldsymbol{0} & \boldsymbol{D}_{vo} + \boldsymbol{D}_i + \boldsymbol{D}_w & \boldsymbol{0} \\ \boldsymbol{0} & \boldsymbol{0} & \boldsymbol{0}\end{bmatrix}, \\ \boldsymbol{G}_c &= \begin{bmatrix}\boldsymbol{G}_{c_1} & \boldsymbol{G}_{c_2}\end{bmatrix} = \begin{bmatrix} -{}^d\boldsymbol{H}_{vo}\boldsymbol{Ad}_{{}^{vo}\boldsymbol{H}_w} & \boldsymbol{0} \\ \boldsymbol{D}_{vo}\boldsymbol{Ad}_{{}^{vo}\boldsymbol{H}_w} & \boldsymbol{D}_i\boldsymbol{Ad}_{{}^{vo}\boldsymbol{H}_w} \\ \boldsymbol{0} & -{}^i\boldsymbol{H}_{vo}\boldsymbol{Ad}_{{}^{vo}\boldsymbol{H}_w}\end{bmatrix}.\end{aligned} \tag{5.14}$$

The Hamiltonian energy of the controller is the sum of energies stored in all its atomic elements

$$\mathcal{H}_c(\boldsymbol{\xi}_c) = \mathcal{H}_P({}^d\boldsymbol{H}_{vo}) + \sum_{i=1}^{N}\mathcal{H}_P({}^i\boldsymbol{H}_{vo}) + \mathcal{H}_K({}^{v\tilde{o}}\boldsymbol{p}_{vo}). \tag{5.15}$$

The controller is energy-conservative and due to the assigned damping it is also passive. It is suitable for achieving both the desired velocity set-point and formation preservation of the robots. The formation preservation ensures that the constraints are not violated. In the next subsection the interconnection of the model and the controller is studied.

Connection of the Controller and the Model

The output of the controller, $\boldsymbol{w}_i$, is the input for the model and the output of the model, $\boldsymbol{t}_i$, is the input for the controller. Therefore, the interconnected system is

$$\begin{aligned}\underbrace{\begin{bmatrix}\dot{\tilde{\boldsymbol{\xi}}} \\ \dot{\boldsymbol{\xi}}_c\end{bmatrix}}_{\dot{\boldsymbol{\xi}}_{cs}} &= \underbrace{\begin{bmatrix}\tilde{\boldsymbol{J}} & \tilde{\boldsymbol{G}}_m\boldsymbol{G}_{c_2}^\top \\ -\boldsymbol{G}_{c_2}\tilde{\boldsymbol{G}}_m^\top & \boldsymbol{J}_c - \boldsymbol{D}_c\end{bmatrix}}_{\boldsymbol{J}_{cs}} \underbrace{\begin{bmatrix}\frac{\partial \mathcal{H}_{cs}}{\partial \tilde{\boldsymbol{\xi}}} \\ \frac{\partial \mathcal{H}_{cs}}{\partial \boldsymbol{\xi}_c}\end{bmatrix}}_{\partial \mathcal{H}_{cs}/\partial \boldsymbol{\xi}_{cs}} + \underbrace{\begin{bmatrix}\tilde{\boldsymbol{G}}_o & \boldsymbol{G}_{c_1}\end{bmatrix}}_{\boldsymbol{G}_{cs}}\begin{bmatrix}\boldsymbol{w}_o \\ \boldsymbol{t}^d\end{bmatrix} \\ \begin{bmatrix}\boldsymbol{t}_o \\ \boldsymbol{w}^d\end{bmatrix} &= \begin{bmatrix}\tilde{\boldsymbol{G}}_o^\top & \boldsymbol{G}_{c_1}^\top\end{bmatrix}\begin{bmatrix}\frac{\partial \mathcal{H}_{cs}}{\partial \tilde{\boldsymbol{\xi}}} \\ \frac{\partial \mathcal{H}_{cs}}{\partial \boldsymbol{\xi}_c}\end{bmatrix}.\end{aligned} \tag{5.16}$$

The external ports of the controller-model interconnection are for the interaction with the human via the port $(\boldsymbol{t}^d, \boldsymbol{w}^d)$ and for the interaction with the environment via the port $(\boldsymbol{w}_o, \boldsymbol{t}_o)$,

i.e. via the object. The interconnection given with (5.16) is passive as the interconnected subsystems are passive. In the next section the human guiding the cooperative system is energetically decoupled to ensure passivity of the complete system and safety for humans on-site.

5.2.2 Energy Transfer Control

As the human and the system are not physically coupled, but the human commands the system with hand gestures, they can be interconnected with virtual structures. In order to guarantee both stability and safety, an energy transfer control in the form of an energy tank that supplies the controller and the system is proposed. The energy tank maintains a safe energy level in the system and can be integrated into the port-Hamiltonian representation of the complete system.

For human-robot interaction various safety metrics exist, see [Had13] for an overview. In this work the focus is limited on the energy-based injury criteria. Experimental studies indicate minimal amounts of energy that cause a cranial bone failure [Woo71] and a fracture of neck bones [YPM+96]. Based on these results, a maximum amount of energy that can be stored in the system is defined. It represents the maximum level of the energy that can be stored in the tank

$$\mathcal{H}_t^{max} = \begin{cases} 517 \text{ J} & \text{adult cranium bone failure,} \\ 30 \text{ J} & \text{neck fracture.} \end{cases} \tag{5.17}$$

The combination of the energy tank and the controlled system, given with (5.16), is formally analyzed in the remainder. The energy tank sources the controller and the controller resupplies its virtually dissipated energy to the energy tank. The energy tank is a virtual storage element defined with the Hamiltonian, $\mathcal{H}_t$. Let $\xi_t \in \mathbb{R}$ denote the (scalar) energy state of the tank and let $\mathcal{H}_t(\xi_t) = \frac{1}{2}\xi_t^2$. The input-state-output, port-Hamiltonian representation of the energy tank is

$$\begin{aligned} \dot{\xi}_t &= f_t \\ \xi_t &= \frac{\partial \mathcal{H}_t(\xi_t)}{\partial \xi_t}, \end{aligned} \tag{5.18}$$

where (f_t, ξ_t) is the flow-effort pair. The re-routing of the virtually dissipated energy into the tank is accomplished by choosing the tank input as

$$f_t = \frac{1}{\xi_t} \frac{\partial^\top \mathcal{H}_{cs}}{\partial \boldsymbol{\xi}_{cs}} \boldsymbol{D}_c \frac{\partial \mathcal{H}_{cs}}{\partial \boldsymbol{\xi}_{cs}} + \tilde{f}_t, \tag{5.19}$$

where the first term of (5.19) represents the dissipated power. In order to have an open port to connect the tank to the controller, a new input $\tilde{f}_t$ to the energy tank is introduced. The energy balance of the tank is

$$\dot{\mathcal{H}}_t(\xi_t) = \xi_t f_t = \frac{\partial^\top \mathcal{H}_{cs}}{\partial \boldsymbol{\xi}_{cs}} \boldsymbol{D}_c \frac{\partial \mathcal{H}_{cs}}{\partial \boldsymbol{\xi}_{cs}} + \xi_t \tilde{f}_t. \tag{5.20}$$

In this work the tank and the controller are connected by a modulated transformer $\mathbb{MTF}$ [SMC10] as depicted in Figure 5.2. The block $\mathbb{MTF}$ is a lossless element that dynamically shapes the energy transfer with its variable transformer ratio $\boldsymbol{r}$. The transformer

ratio determines the energy flow and is set by the human to specify the desired velocity $\boldsymbol{t}_h^d$. The $\mathbb{MTF}$ representation in the port-Hamiltonian framework is

$$\begin{aligned} \boldsymbol{t}^d &= \boldsymbol{r}\xi_t \\ \tilde{f}_t &= -\boldsymbol{r}^\top \boldsymbol{w}^d, \end{aligned} \tag{5.21}$$

where $\boldsymbol{r}$ is dynamically adapted to replicate the human command

$$\boldsymbol{n} = \frac{\boldsymbol{t}_h^d}{\xi_t}. \tag{5.22}$$

The representation (5.21) is power-conservative, since

$$\boldsymbol{t}^{d\top} \boldsymbol{w}_{vo} = \xi_t \boldsymbol{r}^\top \boldsymbol{w}_{vo} = -\xi_t \tilde{f}_t, \tag{5.23}$$

i.e. the transformer is lossless for any $\boldsymbol{r}$. A combined port-Hamiltonian representation of the controlled system and the tank is

$$\begin{bmatrix} \dot{\boldsymbol{\xi}}_{cs} \\ \dot{\xi}_t \end{bmatrix} = \begin{bmatrix} \boldsymbol{J}_{cs} & \frac{\boldsymbol{t}^d}{\xi_t} \\ -\frac{\boldsymbol{t}^{d\top}}{\xi_t} + \frac{1}{\xi_t}\frac{\partial^\top \tilde{\mathcal{H}}}{\partial \boldsymbol{\xi}_{cs}}\boldsymbol{D}_c & \boldsymbol{0} \end{bmatrix} \begin{bmatrix} \frac{\partial \tilde{\mathcal{H}}}{\partial \boldsymbol{\xi}_{cs}} \\ \frac{\partial \mathcal{H}}{\partial \xi_t} \end{bmatrix}. \tag{5.24}$$

The combined system is *lossless* for free object motion, i.e. for $\boldsymbol{w}_o = \boldsymbol{0}$,

$$\frac{d}{dt}\tilde{\mathcal{H}}(\boldsymbol{\xi}_{cs}, \xi_t) = \begin{bmatrix} \frac{\partial^\top \tilde{\mathcal{H}}}{\partial \boldsymbol{\xi}_{cs}} & \frac{\partial^\top \tilde{\mathcal{H}}}{\partial \xi_t} \end{bmatrix} \begin{bmatrix} \dot{\boldsymbol{\xi}}_{cs} \\ \dot{\xi}_t \end{bmatrix} = \boldsymbol{0}, \tag{5.25}$$

where the Hamiltonian $\tilde{\mathcal{H}}(\boldsymbol{\xi}_{cs}, \xi_t)$ is the total energy of the energy tank, the controller and the system.

5.2.3 Energy Shaped Stiffness and Damping

When $\xi_t = 0$ the energy tank is depleted and unable to passively perform the action commanded by the human, $\boldsymbol{t}_h^d$. A total depletion is avoided by suspending the input, i.e. $\boldsymbol{t}_h^d = \boldsymbol{0}$ if $\xi_t < \epsilon$, where $\epsilon > 0$ is a small number [SMC10]. To avoid depletion of the energy tank without modifying the human input, the coupling of the set-point and the virtual object velocity is rendered variable. By adapting the coupling stiffness and the damping as a function of the available energy, the flow of energy between the tank and the controller is shaped. Stiffness and damping are constant if the energy in the tank is sufficient for executing the velocity command. If the tank level falls below a certain threshold, the coupling is relaxed to limit the power flow. If the tank level is close to zero, $\mathcal{H}_t < \epsilon$, the energy transfer is completely disabled by setting the stiffness and the damping to zero.

A change of stiffness affects the energy stored in the spring. Relaxing the stiffness sets energy free, while increasing the stiffness requires the supply of energy. Let us assume a stiffness-dependent Hamiltonian for the spring

$$\mathcal{H}_P : \mathrm{SE}(3) \times \mathcal{K} \to \mathbb{R}^+; ({}^{vo}\boldsymbol{H}_o, \boldsymbol{K}) \mapsto \mathcal{H}_P({}^{vo}\boldsymbol{H}_o, \boldsymbol{K}) \tag{5.26}$$

where $\boldsymbol{K}$ is the variable stiffness defined as follows

$$\boldsymbol{K} = \begin{cases} \boldsymbol{K}_{dv} & \text{if } \mathcal{H}_t(\xi_t) \geq \mathcal{H}_t^{th} \\ \boldsymbol{K}_{dv} \dfrac{\mathcal{H}_t(\xi_t) - \epsilon}{\mathcal{H}_t^{th}} & \text{if } \epsilon \leq \mathcal{H}_t(\xi_t) < \mathcal{H}_t^{th}, \\ \boldsymbol{0} & \text{if } \mathcal{H}_t(\xi_t) < \epsilon \end{cases} \tag{5.27}$$

where $\boldsymbol{K}_{dv} \in \mathbb{R}^{6\times 6}$ is a stiffness matrix and $\mathcal{H}_t$ is a function of the tank level. Above a certain threshold of $\mathcal{H}_t^{th}$ the stiffness is constant. When the tank is close to depletion the stiffness is reduced. The rate of energy change w.r.t. a variable stiffness $\boldsymbol{K}$ is

$$\dot{\mathcal{H}}_{\boldsymbol{K}} = \frac{\partial \mathcal{H}_{\boldsymbol{K}}}{\partial \boldsymbol{K}} \frac{d\boldsymbol{K}}{dt} = \xi_K^\top f_K, \tag{5.28}$$

which corresponds to the product of the effort ($\frac{\partial \mathcal{H}_P}{\partial \boldsymbol{K}}$) and the flow ($\dot{\boldsymbol{K}}$) and forms a power port (f_K, ξ_K). The port-Hamiltonian representation of the variable stiffness is given by

$$\begin{aligned} \begin{bmatrix} {}^d\dot{\boldsymbol{H}}_{vo} \\ \dot{\boldsymbol{K}} \end{bmatrix} &= \begin{bmatrix} {}^d\boldsymbol{H}_{vo} \boldsymbol{Ad}_{{}^{vo}\boldsymbol{H}_w} & \boldsymbol{0} \\ \boldsymbol{0} & \boldsymbol{I} \end{bmatrix} \begin{bmatrix} \boldsymbol{t}_{vo} - \boldsymbol{t}^d \\ f_K \end{bmatrix} \\ \begin{bmatrix} {}^w\boldsymbol{w}_{vo} \\ \xi_K \end{bmatrix} &= \begin{bmatrix} \boldsymbol{Ad}^\top_{{}^{vo}\boldsymbol{H}_w} {}^d\boldsymbol{H}_{vo}{}^\top & \boldsymbol{0} \\ \boldsymbol{0} & \boldsymbol{I} \end{bmatrix} \begin{bmatrix} \dfrac{\partial \mathcal{H}_K}{\partial {}^d\boldsymbol{H}_{vo}} \\ \dfrac{\partial \mathcal{H}_K}{\partial \boldsymbol{K}} \end{bmatrix}. \end{aligned} \tag{5.29}$$

One can express $\boldsymbol{K}$ as a function of the tank level using (5.20)

$$\dot{\boldsymbol{K}} = \begin{cases} \boldsymbol{0} & \text{if } \mathcal{H}_t(\xi_t) \geq \mathcal{H}_t^{th} \\ \dfrac{\boldsymbol{K}_{dv}}{\mathcal{H}_t^{th}} \dot{\mathcal{H}}_t(\xi_t) = \dfrac{\boldsymbol{K}_{dv}}{\mathcal{H}_t^{th}} \dot{\xi}_t \dfrac{\partial \bar{\mathcal{H}}}{\partial \xi_t} & \text{if } \mathcal{H}_t(\xi_t) < \mathcal{H}_t^{th}. \end{cases} \tag{5.30}$$

The power exchanged between the variable spring and the tank due to variability of the stiffness is

$$\dot{\tilde{\mathcal{H}}} = \frac{\partial \tilde{\mathcal{H}}}{\partial \boldsymbol{K}} \dot{\boldsymbol{K}} = \begin{cases} 0 & \text{if } \mathcal{H}_t(\xi_t) \geq \mathcal{H}_t^{th} \\ \dfrac{\partial \tilde{\mathcal{H}}}{\partial \boldsymbol{K}} \dfrac{\boldsymbol{K}_{dv}}{\mathcal{H}_t^{th}} \dot{\xi}_t \dfrac{\partial \tilde{\mathcal{H}}}{\partial \xi_t} & \text{if } \mathcal{H}_t(\xi_t) < \mathcal{H}_t^{th}. \end{cases} \tag{5.31}$$

The power exchanged by the energy tank is of the form $\dot{\mathcal{H}}_t(\xi_t) = \frac{\tilde{\mathcal{H}}}{\partial \xi_t} f_t$, therefore $\frac{\partial \tilde{\mathcal{H}}}{\partial \boldsymbol{K}} \frac{\boldsymbol{K}_{dv}}{\mathcal{H}_t^{th}} \dot{\xi}_t$ is an input for the energy tank. One can now obtain the port-Hamiltonian representation of the variable stiffness spring and the energy tank

$$\begin{bmatrix} \dot{\boldsymbol{\xi}}_{cs} \\ \dot{\xi}_t \\ \dot{\boldsymbol{K}} \end{bmatrix} = \left[\begin{bmatrix} \boldsymbol{J}_{cs} & \frac{\boldsymbol{t}^d}{\xi_t} & \boldsymbol{0} \\ -\frac{\boldsymbol{t}^{d\top}}{\xi_t} & 0 & -\frac{\boldsymbol{K}_{dv}}{\mathcal{H}_t^{\text{th}}} \dot{\xi}_t \\ \boldsymbol{0} & \frac{\boldsymbol{K}_{dv}}{\mathcal{H}_{\text{th}}} \dot{\xi}_t & \boldsymbol{0} \end{bmatrix} - \begin{bmatrix} \boldsymbol{0} & \boldsymbol{0} & \boldsymbol{0} \\ -\frac{1}{\xi_t} \frac{\partial \tilde{\mathcal{H}}^\top}{\partial \boldsymbol{\xi}_{cs}} \boldsymbol{D}_c & \boldsymbol{0} & \boldsymbol{0} \\ \boldsymbol{0} & \boldsymbol{0} & \boldsymbol{0} \end{bmatrix} \right] \begin{bmatrix} \dfrac{\partial \tilde{\mathcal{H}}}{\partial \boldsymbol{\xi}_{cs}} \\ \dfrac{\partial \mathcal{H}}{\partial \xi_t} \\ \dfrac{\partial \mathcal{H}}{\partial \boldsymbol{K}} \end{bmatrix}. \tag{5.32}$$

The combination of such a system with the variable stiffness spring and the tank is lossless

$$\frac{d}{dt} \tilde{\mathcal{H}}(\boldsymbol{\xi}_{cs}, \xi_t, \boldsymbol{K}) = 0. \tag{5.33}$$

The mapping matrix $\boldsymbol{G}_c$ in (5.16) shows that the damping directly influences the energy exchange. In this work the damping is reduced in the same manner as for the stiffness. With a depletion of the energy tank the damping $\boldsymbol{D}_{dv} \in \mathbb{R}^{6\times6}$, parallel to the variable spring, is reduced. The coupling between the human and the virtual object is relaxed

$$\boldsymbol{D} = \begin{cases} \boldsymbol{D}_{dv} & \text{if } \mathcal{H}_t(\xi_t) \geq \mathcal{H}_t^{th} \\ \boldsymbol{D}_{dv}\dfrac{\mathcal{H}_t(\xi_t)}{\mathcal{H}_t^{th}} & \text{if } \epsilon \leq \mathcal{H}_t(\xi_t) < \mathcal{H}_t^{th}. \\ \boldsymbol{0} & \text{if } \mathcal{H}_t(\xi_t) < \epsilon \end{cases} \tag{5.34}$$

5.3 Results

The proposed model and control strategies are implemented in *MATLAB/Simulink*. The cooperative system of two robots with the masses $\mathrm{M}_{1,2} = 10\mathrm{kg} \cdot \boldsymbol{I}_3$ and the moments of inertia $\mathrm{J}_{1,2} = 0.5\mathrm{kgm}^2 \cdot \boldsymbol{I}_3$ manipulates an object with the mass $\mathrm{M}_o = 1.4\mathrm{kg} \cdot \boldsymbol{I}_3$ and the moment of inertia $\mathrm{J}_o = 0.5\mathrm{kgm}^2 \cdot \boldsymbol{I}_3$. The solver uses the Euler's method (*ode1*) and the sample time is 1 ms. The parameters of the controller are summarized in Table 5.1.

Table 5.1: Controller parameters.

	linear	angular
Virtual inertia	$1.4\mathrm{kg} \cdot \boldsymbol{I}_3$	$0.5\mathrm{kgm}^2 \cdot \boldsymbol{I}_3$
Damping	$250\mathrm{kg/s} \cdot \boldsymbol{I}_3$	$30\mathrm{kgm}^2/\mathrm{s} \cdot \boldsymbol{I}_3$
Stiffness	$125\mathrm{N/m} \cdot \boldsymbol{I}_3$	$15\mathrm{Nm} \cdot \boldsymbol{I}_3$

Simulation results are shown in Figure 5.4. The available energy budget, $\mathcal{H}_t^{max} = 25$ J, complies with the safety limits from (5.17). At $t = 1$ s the commanded velocity is too high w.r.t. the available energy budget, i.e. the energy at disposal is not sufficient to reach it. Therefore, the tank level is depleted. Trajectories exceeding the energetic limit are adapted with the variable stiffness and the damping in order to guarantee safety. The reduction of the stiffness and the damping starts as soon as the energy level falls under a threshold, $\mathcal{H}_t^{th} = 5$ J. As a consequence, the velocity is kept constant at the energetically feasible maximum until $t = 2$ s when the tank is refilled again and the commanded velocity is feasible. Limiting velocity and forces, the interaction safety of the system is enhanced. Additionally, the internal wrenches applied on the object are zero.

The experiment is conducted with a robotic system of two KUKA LWR manipulators, mounted on a movable platform and depicted in the Figure 5.5. The sampling time is 1 ms. The obtained results are shown in Figure 5.6 and Figure 5.7. In Figure 5.6 the tank energy level is depleted and the velocity is limited close to the maximum commanded velocity of 0.11 m/s.

In Figure 5.7 the tank energy budget is enough to supply the system when the commanded velocity changes from $0.1 - 0.3$ m/s. The energy level does not reach the energetic threshold for the commanded velocity and is sufficient for reaching the desired velocity. This approach is also suitable for a physical interaction between the human and the robots. For example, an interaction for a cooperative manipulation task where the human is physically coupled to

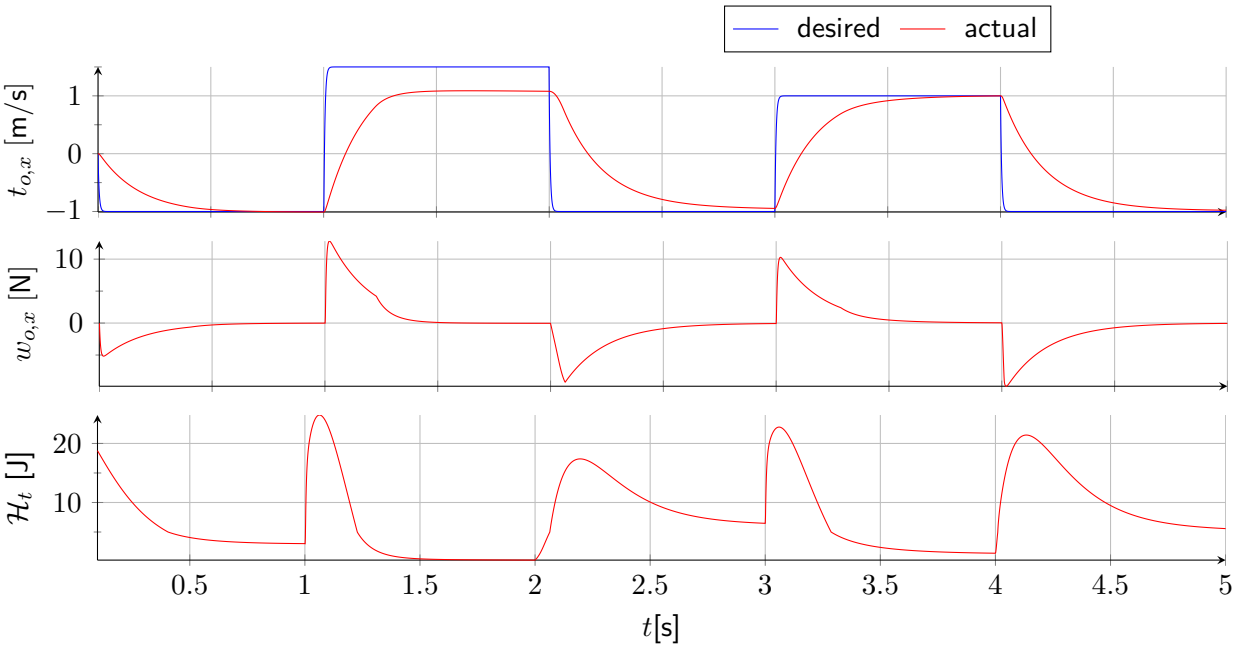

Figure 5.4: Simulation results. Top: commanded and actual object velocity. Middle: force applied on the object. Bottom: energy level of the tank with $\mathcal{H}_t^{max} = 25$ J and $\mathcal{H}_t^{th} = 5$ J.

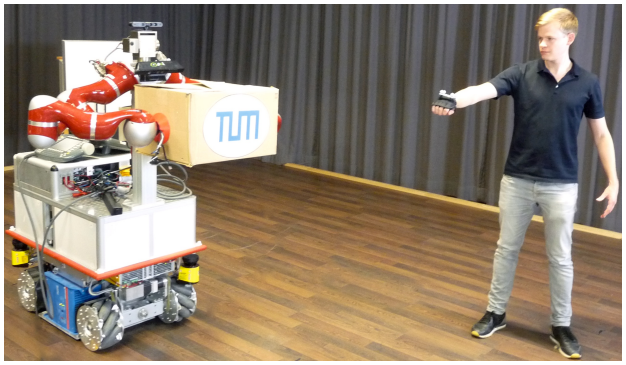

Figure 5.5: Experimental setup. The human and the robotic system share the workspace. The human teleoperates the robotic system by the hand motion.

the object can be safely established with the proposed approach. However, the experiments in this direction are left for future work.

5.4 Discussion

A control scheme for human-robot team interaction in a teleoperation setting for a cooperative manipulation task is developed using the port-Hamiltonian framework to model the constrained robotic system. It has been shown that the representation of the system on the constrained manifold is again a port-Hamiltonian system. The proposed control approach maintains the desired formation between the robots and the desired behavior of the overall

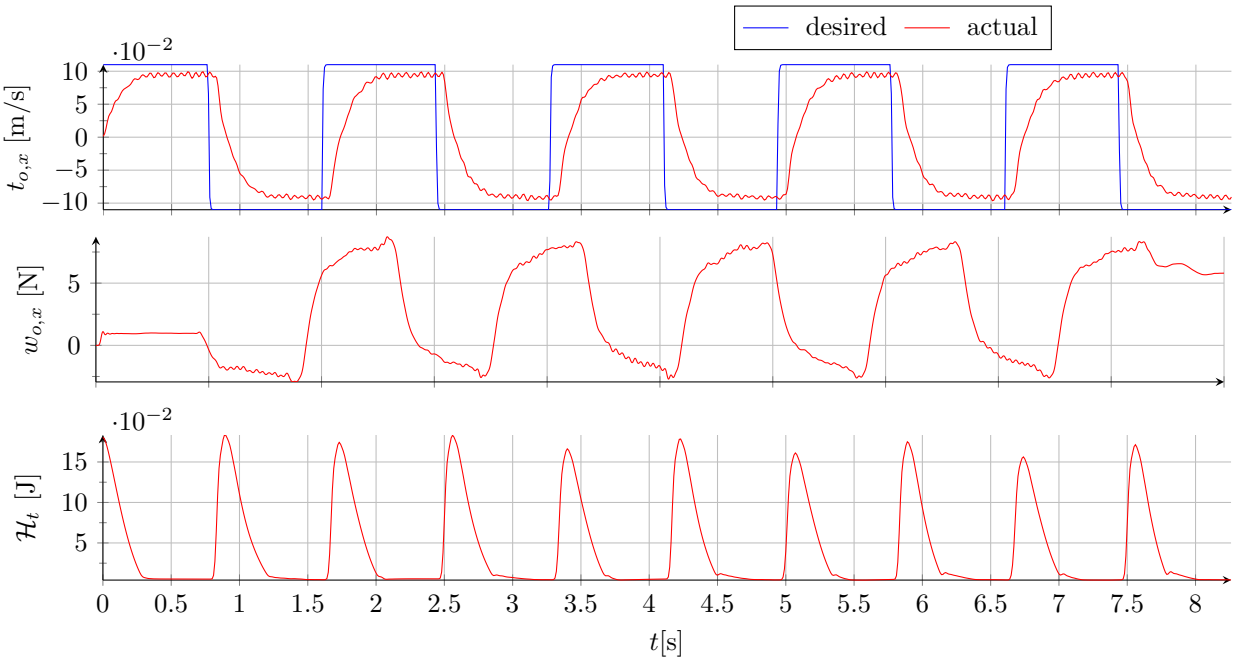

Figure 5.6: Experimental results. Top: commanded and actual object velocity. Middle: force applied on the object. Bottom: energy level of the tank with $\mathcal{H}_t^{max} = 0.2$ J and $\mathcal{H}_t^{th} = 0.01$ J.

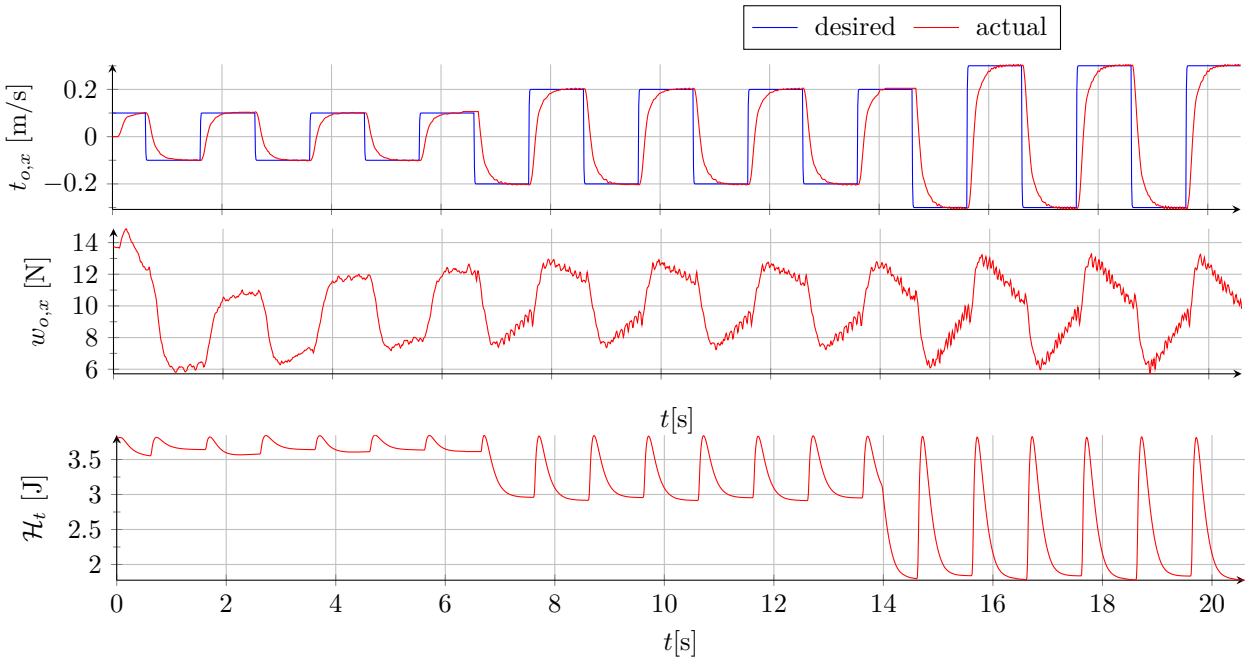

Figure 5.7: Experimental results. Top: commanded and actual object velocity. Middle: force applied on the object. Bottom: energy level of the tank with $\mathcal{H}_t^{max} = 3.8$ J and $\mathcal{H}_t^{th} = 1$ J.

system, commanded by the human. It is shown that the interconnection of the proposed controller and the model is a port-Hamiltonian system. The complete system is passive and allows for a safe interaction with the human. Furthermore, it is consistent with the proposed concept of *subtask-based control* for complementary interaction paradigm. The control approach is successfully validated in the simulation and the experiments. The work presented in this chapter has been partially published in [AMH17].

6

Overlapping Shared Control

Human-robot interaction that enables the human and the robot partners to jointly perform a common task may be beneficial in many application examples, e.g. rehabilitation, telesurgery, elder care, exploration of inaccessible or dangerous environments and collaborative manufacturing. Such interaction paradigms are classified *overlapping interaction paradigms* in this thesis. There are two general requirements of shared-control strategies for the overlapping interaction paradigms: (i) *efficiency* in terms of task performance and (ii) *intuitiveness* of the interaction so that the human can interpret decisions of the robot system and vice versa. While many existing shared-control approaches are efficient, intuitiveness is more difficult to achieve and requires an understanding of human decision making in control-sharing settings. In overlapping interaction paradigms the modeling of the human is important, since it is necessary to determine the most appropriate robot control input based on the human behavior, in order to accomplish a satisfactory task execution and/or assistance.

In this chapter a shared control approach for overlapping interaction paradigms, where both partners (human and robot) know the task goal and jointly work to achieve it, is proposed.

Related Work and Open Problems

Research shows that *optimal control* can be used to describe behavior of *trained* humans, since humans act in agreement with the *principle of rationality* when carrying out a familiar sensorimotor task [MW19]. This principle states that a trained agent will act in the most appropriate manner, according to his own objectives and the situational logic imposed by the environment. This implies that the human aims to act in an optimal way with respect to an unknown internal metric in tasks that he/she was trained for. It stands to reason that this internal metric is an unknown cost function that maps possible actions to their respective cost. According to [JF18], optimal control can support both cognition (top-down) and information processing (bottom-up) components of human behavior. Therefore, it has the potential to unify *high-level human decision making* and *low-level human motor control*. For example, humans minimize jerk in reaching tasks [FH85] and energy in locomotion tasks [AP01]. Human decision-making and motor behaviors are unified in [TJ02b] with *stochastic optimal feedback control*. Analogously to optimal control, it is shown that motor interaction between two humans can be modeled within the *game-theoretical framework* [DABW09].

Designing an optimal control strategy of the robot autonomy for human-robot interaction that fits the definition of overlapping interaction paradigm has already been done, see

e.g. [MLH15] and [RBCC15]. However, it is shown experimentally that the cost function of the human changes in control-sharing tasks compared to the fully manual tasks [IEFH18]. Therefore, it is important to consider couplings between the partners and their effects on the human decision making which is possible with the *game-theoretical framework*.

The game-theoretical concept has already been considered in human-robot collaboration scenarios as well. A classification of interaction paradigms for two-agent haptic tasks that are possible within the game-theoretical framework and for human-robot collaboration is proposed in [JCB12]. However, a consideration of multiple agents is still not considered. The framework has predominantly been used in semi-autonomous driving use cases for assistance in wheel steering [NC15, FOSH14]. However, only exemplary simulation results are provided. A stochastic game-theoretical approach that mitigates conflicts in driver-machine interactions when the human and the autonomy perform different tasks - driving and obstacle avoidance, is proposed in [JYN+19]. A Nash equilibria solution for reaching tasks in human-robot cooperation is proposed in [LCG+19]. The obtained results show the performance improvement compared to the fully manual task execution. However, no consideration of human-robot collaboration in trajectory tracking tasks and within the game-theoretical framework has been done. Therefore, a shared-control approach that considers couplings between the human and the robot partners and its effect on human decision making, while enabling multi-agent interaction for trajectory tracking tasks, needs to be developed.

In this chapter, a shared-approach for overlapping interaction paradigm is proposed. For this purpose, a game-theoretical framework is used to describe a general haptic collaboration task. Optimal control of the semi-autonomous partner is computed to obtain Nash equilibrium. The problem is posed in Section 6.1. The shared control approach is proposed in Section 6.2. In Section 6.3 experimental results are given. Concluding remarks are in Section 6.4.

6.1 Problem Statement

In this section the problem of designing a shared control strategy for overlapping interaction paradigms and within the game-theoretical framework is posed.

Let us assume a single subtask of *trajectory tracking* in task space needs to be performed by the human and the robot partners jointly. Let us further assume that the task is defined as a second-order linear time-invariant dynamical system as in (3.21) and that it is already controlled on the lower level with an impedance controller as in (3.29) to guarantee passivity and obtain its desired impedance behavior

$$\begin{bmatrix} \dot{\boldsymbol{x}} \\ \ddot{\boldsymbol{x}} \end{bmatrix} = \underbrace{\begin{bmatrix} \boldsymbol{0} & \boldsymbol{I} \\ \boldsymbol{0} & -\boldsymbol{M}^{-1}\boldsymbol{D} \end{bmatrix}}_{\boldsymbol{A}} \underbrace{\begin{bmatrix} \boldsymbol{x} \\ \dot{\boldsymbol{x}} \end{bmatrix}}_{\boldsymbol{\xi}} + \underbrace{\begin{bmatrix} \boldsymbol{0} \\ \boldsymbol{M}^{-1} \end{bmatrix}}_{\boldsymbol{B}} (\boldsymbol{u}_h + \boldsymbol{u}_a), \tag{6.1}$$

where $\boldsymbol{x}, \dot{\boldsymbol{x}}, \ddot{\boldsymbol{x}} \in \mathbb{R}^n$ are the n-dimensional position, velocity, and acceleration vectors in the subtask space, $\boldsymbol{M}, \boldsymbol{D} \in \mathbb{R}^{n \times n}$ are the positive-definite inertia and damping matrices, respectively, and $\boldsymbol{u}_h, \boldsymbol{u}_a \in \mathbb{R}^n$ are the human and the robot control inputs, respectively. Let us assume the desired trajectory and its first derivative are bounded, available online and given with the vectors $\boldsymbol{\xi}^d = [\boldsymbol{x}^{d\top}, \dot{\boldsymbol{x}}^{d\top}]^\top$ and $\dot{\boldsymbol{\xi}}^d = [\dot{\boldsymbol{x}}^{d\top}, \ddot{\boldsymbol{x}}^{d\top}]^\top \in \mathbb{R}^{2\times n}$, respectively. The

state $\boldsymbol{\xi}$ in (6.1) can be changed to the tracking error state $\boldsymbol{\xi}_e = \boldsymbol{\xi} - \boldsymbol{\xi}^d$ to obtain the tracking error dynamics

$$\dot{\boldsymbol{\xi}}_e = \boldsymbol{A}\boldsymbol{\xi}_e + \boldsymbol{B}(\boldsymbol{u}_h + \boldsymbol{u}_a) + \underbrace{\boldsymbol{A}\boldsymbol{\xi}^d - \dot{\boldsymbol{x}}^d}_{\boldsymbol{c}}, \tag{6.2}$$

where $\boldsymbol{c}$ is an offset that depends on the desired trajectory.

Let $\Gamma_i \in \mathbb{R}^n$ be a class of permissible strategies, $\boldsymbol{\gamma}_i$, such that $\boldsymbol{u}_i = \boldsymbol{\gamma}_i(\boldsymbol{\xi}_e)$, $i = \{h, a\}$. In order for the problem to be a well-defined differential game, uniqueness of the solution to (6.2) needs to be guaranteed. For that purpose, Assumption 6.1.1 and Lemma 3 are introduced.

Assumption 6.1.1. *The dynamics (6.2) and permissible strategies $\boldsymbol{\gamma}_i \in \Gamma_i$, $i = \{h, a\}$, are uniformly Lipschitz in $\boldsymbol{\xi}_e$, $\boldsymbol{u}_h$ and $\boldsymbol{u}_a$.*

Lemma 3 ([BO98])**.** *If Assumption 6.1.1 is satisfied, (6.2) has a unique solution for every $\boldsymbol{\gamma}_i$ so that $\boldsymbol{u}_i = \boldsymbol{\gamma}_i(\boldsymbol{\xi}_e)$, $i = \{h, a\}$, and this solution is continuous.*

Assumption 6.1.1 does not impose restrictions on the considered problem since the task is continuous and the human input is smooth. In order for the human and the robot partners to be players of the game defined with (6.2), they need to optimize their own cost functionals

$$J_i(\boldsymbol{\xi}_e, \boldsymbol{u}_h, \boldsymbol{u}_a) = \int_0^T g_i(\boldsymbol{\xi}_e, \boldsymbol{u}_h, \boldsymbol{u}_a)\mathrm{d}t, \quad i = \{h, a\}. \tag{6.3}$$

Furthermore, it is assumed that the human partner behaves according to the *principle of rationality* and, consequently, in the optimal sense.

Assumption 6.1.2. *The human partner has executed the task (6.2) multiple times and can predict the outcomes of his actions. Therefore, the human partner is modeled as an optimal controller that acts according to an internal cost metric to optimally track a desired trajectory $\boldsymbol{\xi}^d$. The basic structure of the metric is known, but not its parameter values.*

In this thesis, a quadratic cost function structure is used in order to penalize the input magnitude, i.e. the *effort*, and the deviation from the desired trajectory, i.e. the *task goal*. These two aspects are important for every biophysical movement [MW19]. Therefore, the following cost function is assumed for the human partner

$$g_h(\boldsymbol{\xi}_e, \boldsymbol{u}_h) = \frac{1}{2}(\boldsymbol{\xi}_e^\top \boldsymbol{Q}_h \boldsymbol{\xi}_e + \boldsymbol{u}_h^\top \boldsymbol{u}_h), \tag{6.4}$$

where $\boldsymbol{Q}_h \in \mathbb{R}^{n\times n}$ is a positive semi-definite matrix. The cost function of the robot partner is defined as

$$g_a(\boldsymbol{\xi}_e, \boldsymbol{u}_h, \boldsymbol{u}_a) = \frac{1}{2}(\boldsymbol{\xi}_e^\top \boldsymbol{Q}_a \boldsymbol{\xi}_e + \boldsymbol{u}_a^\top \boldsymbol{u}_a + \boldsymbol{u}_h^\top \boldsymbol{u}_h), \tag{6.5}$$

where $\boldsymbol{Q}_a \in \mathbb{R}^{n\times n}$ is a positive semi-definite matrix.

Remark 31. *According to the cost functional (6.4), the human partner is expected to minimize the task error and the exerted effort. According to the cost functional (6.5), the robot partner simultaneously minimizes the task error as well, rendering the interaction* cooperative*. Additionally, the robot partner seeks to minimize its own effort as well as the effort of the human partner. The latter renders the posed interaction* assistive *to the human partner.*

In this work it is assumed that full state information is available to both partners at every point in time, which is stated with Assumption 6.1.3.

Assumption 6.1.3. *The task state $\boldsymbol{\xi}_e$ is measurable to both the human and the robot.*

In this thesis a differential game in which both the human and the robot partners have a *closed-loop perfect state information pattern (CLPS)* is considered. Let $\boldsymbol{\eta}^i(t)$ determine the state information gathered by the partner i at time t. Then, a CLPS information pattern implies $\boldsymbol{\eta}^i(t) = \{\boldsymbol{\xi}_e(s), 0 \leq s \leq t\}$, $t \in [0, \infty)$, $i = \{h, a\}$ ([BO98]). This information pattern assumes that the control input of each player depends causally on the system state at some point in time $s \in [0, t]$ and, consequently, the control input of the other player ([BO98]). The consideration of the CLPS information pattern in this case is reasonable because: (i) the state is measurable and (ii) the interaction is continuous and achieved via the haptic channel, so that both players receive information about the control input of another player online.

Now the human and the robot partners are two *players* of the game (6.2) with their own cost functions. The problem to be solved in the remainder of the paper is introduced below.

Problem 5. *Design a shared control approach so that the robot control input $\boldsymbol{u}_a$ and the human control input $\boldsymbol{u}_h$ achieve a* Nash equilibrium solution.

Remark 32. *In the considered setting the control input of the human, $\boldsymbol{u}_h$, is not measured directly. Instead, its online estimator, $\hat{\boldsymbol{u}}_h$, is used.*

6.2 Game-Theoretical Shared-Control Approach

In this section a game-theoretical shared-control approach for overlapping interaction paradigm is proposed.

6.2.1 Shared Control with the Nash Equilibrium Solution

A Nash equilibrium is defined as follows

$$\begin{aligned} &J_h(\boldsymbol{\xi}_e, \boldsymbol{u}_h^\star) \leq J_h(\boldsymbol{\xi}_e, \boldsymbol{u}_h) \\ &J_r(\boldsymbol{\xi}_e, \boldsymbol{u}_h^\star, \boldsymbol{u}_a^\star) \leq J_a(\boldsymbol{\xi}_e, \boldsymbol{u}_h^\star, \boldsymbol{u}_a), \end{aligned} \tag{6.6}$$

where $\boldsymbol{u}_h^\star, \boldsymbol{u}_a^\star$ are the optimal control inputs in the sense of the Nash equilibrium (NE). Equation (6.6) implies that in Nash equilibrium neither of the partners benefit if they change their control strategy. The following lemma provides a general Nash equilibrium solution for the game-theoretical problem with CLPS information pattern, posed with (6.2)-(6.5).

Lemma 4 ([BO98])**.** *For a 2-person differential game, strategies $\boldsymbol{\gamma}_h^\star \in \Gamma_h$ and $\boldsymbol{\gamma}_a^\star \in \Gamma_a$ provide a CLPS Nash equilibrium solution if there exist functions $V_i : \mathbb{R}^{2\times n} \to \mathbb{R}, i = \{h, a\}$, satisfying*

$$\begin{aligned} -\frac{dV_h(\boldsymbol{\xi}_e)}{dt} &= \min_{\boldsymbol{u}_h} \left[\frac{\partial V_h(\boldsymbol{\xi}_e)}{\partial \boldsymbol{\xi}_e} \boldsymbol{f}(\boldsymbol{\xi}_e, \boldsymbol{u}_h, \boldsymbol{\gamma}_a^\star) + \boldsymbol{g}_h(\boldsymbol{\xi}_e, \boldsymbol{u}_h, \boldsymbol{\gamma}_a^\star) \right], \\ -\frac{dV_a(\boldsymbol{\xi}_e)}{dt} &= \min_{\boldsymbol{u}_a} \left[\frac{\partial V_a(\boldsymbol{\xi}_e)}{\partial \boldsymbol{\xi}_e} \boldsymbol{f}(\boldsymbol{\xi}_e, \boldsymbol{\gamma}_h^\star, \boldsymbol{u}_a) + \boldsymbol{g}_a(\boldsymbol{\xi}_e, \boldsymbol{\gamma}_h^\star, \boldsymbol{u}_a) \right]. \end{aligned} \tag{6.7}$$

Lemma 4 determines the Nash equilibrium solution with optimal control inputs $\boldsymbol{u}_h^\star = \boldsymbol{\gamma}_h^\star(\boldsymbol{\xi}_e)$ and $\boldsymbol{u}_a^\star = \boldsymbol{\gamma}_a^\star(\boldsymbol{\xi}_e)$. For the problem posed with (6.2)-(6.5) it is possible to obtain an explicit solution to (6.7) with the following theorem.

Theorem 3. *For a dynamic game defined by (6.2)-(6.5) let there exist matrices $\boldsymbol{Z}_h$ and $\boldsymbol{Z}_a$ that satisfy*

$$\begin{aligned} &\dot{\boldsymbol{Z}}_h + \tilde{\boldsymbol{F}}^\top \boldsymbol{Z}_h + \boldsymbol{Z}_h \tilde{\boldsymbol{F}} + \boldsymbol{Q}_h + \boldsymbol{Z}_h \boldsymbol{B}\boldsymbol{B}^\top \boldsymbol{Z}_h = \boldsymbol{0} \\ &\dot{\boldsymbol{Z}}_a + \tilde{\boldsymbol{F}}^\top \boldsymbol{Z}_a + \boldsymbol{Z}_a \tilde{\boldsymbol{F}} + \boldsymbol{Q}_a + \boldsymbol{Z}_a \boldsymbol{B}\boldsymbol{B}^\top \boldsymbol{Z}_a + \boldsymbol{Z}_h \boldsymbol{B}\boldsymbol{B}^T \boldsymbol{Z}_h = \boldsymbol{0}, \end{aligned} \tag{6.8}$$

and vectors $\boldsymbol{k}_h$ and $\boldsymbol{k}_a$ such that

$$\begin{aligned} &\dot{\boldsymbol{k}}_h + \tilde{\boldsymbol{F}}^\top \boldsymbol{k}_h + \boldsymbol{Z}_h \boldsymbol{B}\boldsymbol{B}^\top \boldsymbol{k}_h + \boldsymbol{Z}_h \boldsymbol{h} = \boldsymbol{0} \\ &\dot{\boldsymbol{k}}_a + \tilde{\boldsymbol{F}}^\top \boldsymbol{k}_a + \boldsymbol{Z}_h \boldsymbol{B}\boldsymbol{B}^\top \boldsymbol{k}_h + \boldsymbol{Z}_a \boldsymbol{B}\boldsymbol{B}^\top \boldsymbol{k}_a + \boldsymbol{Z}_a \boldsymbol{h} = \boldsymbol{0}, \end{aligned} \tag{6.9}$$

where

$$\begin{aligned} \tilde{\boldsymbol{F}} &= \boldsymbol{A} - \boldsymbol{B}\boldsymbol{B}^\top (\boldsymbol{Z}_h + \boldsymbol{Z}_a), \\ \boldsymbol{h} &= \boldsymbol{c} - \boldsymbol{B}\boldsymbol{B}^\top (\boldsymbol{k}_h + \boldsymbol{k}_a). \end{aligned} \tag{6.10}$$

Then the differential game admits a closed-loop Nash equilibrium solution with the strategy of the human partner

$$\boldsymbol{\gamma}_h^\star = -\boldsymbol{B}^\top (\boldsymbol{Z}_h \boldsymbol{\xi}_e + \boldsymbol{k}_h), \tag{6.11}$$

and the strategy of the robot partner

$$\boldsymbol{\gamma}_a^\star = -\boldsymbol{B}^\top (\boldsymbol{Z}_a \boldsymbol{\xi}_e + \boldsymbol{k}_a). \tag{6.12}$$

According to Theorem 3, in trajectory tracking tasks the human and the robot partners behave as controllers with feedback and feedforward terms. The proof of Theorem 3 can be found in Appendix 8.

6.2.2 Estimation of the Human Control Input

Since in the considered problem the human control input, $\boldsymbol{u}_h$, cannot be measured directly, it is necessary to estimate it online. It is assumed that the human control input is given with (6.11). In order to obtain the estimate $\hat{\boldsymbol{Z}}_h$ of the human feedback control gain $\boldsymbol{Z}_h$ and the estimate $\hat{\boldsymbol{k}}_h$ of the human feedforward term $\boldsymbol{k}_h$, an *adaptive input observer* is applied [IF06].

Remark 33. *With the proposed input observer the gain and the feedforward term, $\boldsymbol{Z}_h$ and $\boldsymbol{k}_h$, are estimated. This is a particularity of the proposed approach, since standard adaptive input observers update the control input estimator, $\hat{\boldsymbol{u}}_h$, directly [NA12].*

First, the estimate of the task dynamics (6.2) under the human control input estimator $\hat{\boldsymbol{u}}_h$ is formulated as in [LCG+19]

$$\dot{\hat{\boldsymbol{\xi}}}_e = \boldsymbol{A}\hat{\boldsymbol{\xi}}_e + \boldsymbol{B}\hat{\boldsymbol{u}}_h + \boldsymbol{B}\boldsymbol{u}_a + \boldsymbol{c} - \boldsymbol{\Lambda}\tilde{\boldsymbol{\xi}}_e, \tag{6.13}$$

where $\hat{\boldsymbol{\xi}}_e$ is the state estimate, $\tilde{\boldsymbol{\xi}}_e = \hat{\boldsymbol{\xi}}_e - \boldsymbol{\xi}_e$ is the state estimation error and $\boldsymbol{\Lambda}$ is a block-diagonal matrix. It is assumed that the feedforward term in (6.11) depends on the first

derivative of the desired trajectory, $\dot{\boldsymbol{\xi}}^d$, and can be written as $\boldsymbol{k}_h = -\boldsymbol{K}_h\dot{\boldsymbol{\xi}}^d$. Therefore, in accordance to (6.11), $\hat{\boldsymbol{u}}_h$ is

$$\hat{\boldsymbol{u}}_h = -\boldsymbol{B}^\top(\hat{\boldsymbol{Z}}_h\boldsymbol{\xi}_e - \hat{\boldsymbol{K}}_h\dot{\boldsymbol{\xi}}^d). \tag{6.14}$$

Let the gain estimation errors be denoted as $\tilde{\boldsymbol{Z}}_h = \hat{\boldsymbol{Z}}_h - \boldsymbol{Z}_h$ and $\tilde{\boldsymbol{K}}_h = \hat{\boldsymbol{K}}_h - \boldsymbol{K}_h$. By subtracting (6.2) from (6.13) the estimation error dynamics is

$$\dot{\tilde{\boldsymbol{\xi}}}_e = \boldsymbol{A}\tilde{\boldsymbol{\xi}}_e - \boldsymbol{B}\boldsymbol{B}^\top(\tilde{\boldsymbol{Z}}_h\boldsymbol{\xi}_e - \tilde{\boldsymbol{K}}_h\dot{\boldsymbol{\xi}}^d) - \boldsymbol{\Gamma}\tilde{\boldsymbol{\xi}}_e. \tag{6.15}$$

In order to obtain the adaptation laws, the following Lyapunov function candidate is proposed

$$V(\tilde{\boldsymbol{\xi}}_e, \tilde{\boldsymbol{Z}}_h, \tilde{\boldsymbol{K}}_h) = \frac{1}{2}\tilde{\boldsymbol{\xi}}_e^\top\tilde{\boldsymbol{\xi}}_e^\top + \frac{1}{2\alpha}\mathrm{tr}(\tilde{\boldsymbol{Z}}_h^\top\tilde{\boldsymbol{Z}}_h + \tilde{\boldsymbol{K}}_h^\top\tilde{\boldsymbol{K}}_h), \tag{6.16}$$

where α is a constant and $\mathrm{tr}(\cdot)$ is a matrix trace. The formulation of the adaptive input observer is given with Proposition 6.2.1.

Proposition 6.2.1. *If $\boldsymbol{\Lambda}$ is chosen so that $(\boldsymbol{\Lambda}-\boldsymbol{A})$ is a positive-definite matrix and the rates of the gain estimation errors, $\tilde{\boldsymbol{Z}}_h$ and $\tilde{\boldsymbol{K}}_h$, are updated according to the following adaptive laws*

$$\begin{aligned}\dot{\tilde{\boldsymbol{Z}}}_h &= \frac{\alpha}{2}\boldsymbol{B}\boldsymbol{B}^\top\tilde{\boldsymbol{\xi}}_e\boldsymbol{\xi}_e^\top \\ \dot{\tilde{\boldsymbol{K}}}_h &= -\frac{\alpha}{2}\boldsymbol{B}\boldsymbol{B}^\top\tilde{\boldsymbol{\xi}}_e\dot{\boldsymbol{\xi}}^{d\top},\end{aligned} \tag{6.17}$$

then $\dot{V} \leq 0$, $\hat{\boldsymbol{Z}}_h, \hat{\boldsymbol{K}}_h$ and $\tilde{\boldsymbol{\xi}}_e$ are bounded, and $\lim_{t\to\infty}\tilde{\boldsymbol{\xi}}_e \to 0$.

Remark 34. *It is assumed that $\lim_{t\to\infty}\dot{\boldsymbol{Z}}_h \to 0$, $\lim_{t\to\infty}\dot{\boldsymbol{Z}}_a \to 0$ in (6.8) and $\lim_{t\to\infty}\dot{\boldsymbol{K}}_h \to 0$. Therefore, $\lim_{t\to\infty}\dot{\tilde{\boldsymbol{Z}}}_h \to \dot{\hat{\boldsymbol{Z}}}_h$ and $\lim_{t\to\infty}\dot{\tilde{\boldsymbol{K}}}_h \to \dot{\hat{\boldsymbol{K}}}_h$ which means that the proposed adaptation laws (6.17) can be used to compute $\hat{\boldsymbol{Z}}_h$ and $\hat{\boldsymbol{K}}_h$. The convergence of $\hat{\boldsymbol{Z}}_h$ and $\hat{\boldsymbol{K}}_h$ to their actual values, $\boldsymbol{Z}_h$ and $\boldsymbol{K}_h$, respectively, can be achieved if $\boldsymbol{\xi}_e$ and $\boldsymbol{\xi}^d$ are persistently exciting signals [NA12].*

The block structure of the proposed control scheme is depicted in Figure 6.1. The human and the robot are coupled and communicate their control inputs, $\boldsymbol{u}_h$ and $\boldsymbol{u}_a$, via haptic channels. The state of the task, $\boldsymbol{\xi}_e$, is measurable to both partners, as well as the desired trajectory and its derivative, $\boldsymbol{\xi}^d$ and $\dot{\boldsymbol{\xi}}^d$, respectively.

6.3 Results

In this section the proposed overlapping shared control is implemented and evaluated with a numerical simulation and a direct physical human-robot interaction scenario with a haptic device.

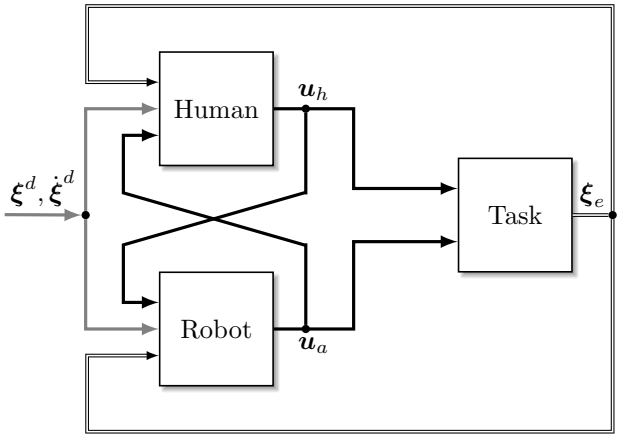

Figure 6.1: Block structure.

6.3.1 Simulation Results

In this section simulation results for a one-dimensional trajectory tracking task are presented. The results provide a comparison of two cases: (i) *manual* - the system is controlled only by the human, $u = u_h$ and (ii) *shared* - the system is controlled by the human and the robot, $u = u_h + u_a$. The gains of the human control input, $\boldsymbol{Z}_h$ and $\boldsymbol{K}_h$, are chosen so that in the case (i) the trajectory tracking could be improved through a shared-control approach. The desired trajectory is the sum of sine waves where the number of frequencies is twice as large as the number of unknown parameters, which guarantees convergence of the adaptive laws (6.17) [Ast87]

$$x^d = \sin(0.1t) + \sin(0.5t) + \sin(0.7t) + \sum_{i=1}^{4} \frac{1}{\omega_i} \sin(\omega_i t),$$

where $\omega_i = 0.5(1 + i)$. The relevant parameters are listed in Table 1.

Table 1. Simulation parameters.

t_s [ms]	m [kg]	d [Ns/m]	$Z_h(2,1)$	$Z_h(2,2)$	$K_h(2,2)$	$\boldsymbol{Q}_a$	$\boldsymbol{\Lambda}$	α
1	1	20	10	5	1	500 $\boldsymbol{I}_2$	800 $\boldsymbol{I}_2$	10^4

The value of the constant α is relatively high in order to achieve convergence of the unknown parameters faster. Since noise is not simulated, α can be arbitrarily large. The goal is to apply the proposed shared-control approach while estimating $\hat{\boldsymbol{Z}}_h$ and $\hat{\boldsymbol{K}}_h$ online. Note that the relevant gains that need to be estimated are $Z_h(2,1) = P_{h,1}^{fd} = 10$, $Z_h(2,2) = P_{h,2}^{fd} = 5$, as well as $K_h(2,2) = P_{h,2}^{ff} = 1$.

Figure 6.2 shows the tracking performance when the task is controlled only by the human partner (manual) and when the task is controlled by both the human and the robot partners (shared), where the shared scenario is achieved with the proposed shared-control scheme. It can be observed that the shared-control approach improves trajectory tracking performance. The simulated human control input, u_h and its estimator, $\hat{u}_h$, are depicted in Figure 6.3. It can be observed that the convergence of the human control input estimator to the simulated human control input, by applying the adaptation law (6.17), is achieved. Therefore, the

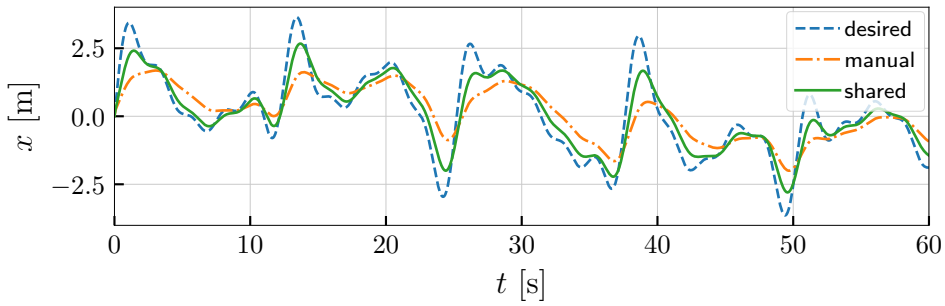

(a) Position trajectories.

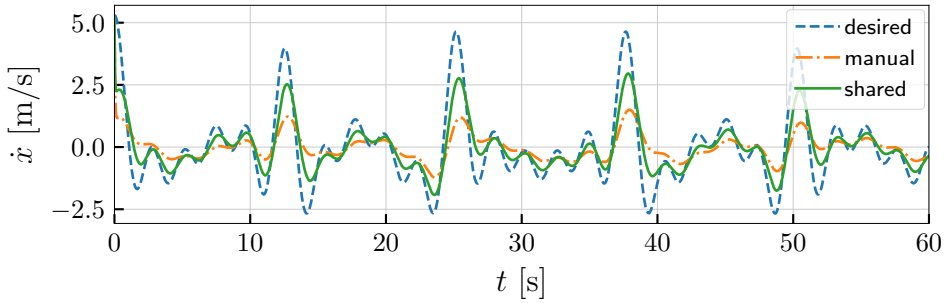

(b) Velocity trajectories.

Figure 6.2: Simulation results. Tracking performance for the manual and the shared cases.

approach enables an online estimation of the human input. Figure 6.3 also depicts the total control input, applied by the human and the robot partners, u. It can be observed that the robot control input amplifies the human control input in order to reach the task goal in the optimal sense.

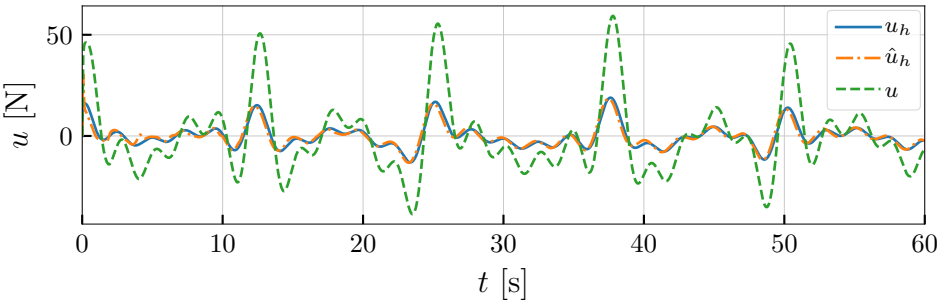

Figure 6.3: Simulation results. Simulated human control input is denoted with u_h, its estimator with $\hat{u}_h$ and the total control input with u. All trajectories are recorded for the shared case.

The top row of Figure 6.4 depicts a successful convergence of the relevant human control gain parameters to the desired values using the adaptation law (6.17). The bottom row of Figure 6.4 depicts relevant autonomous control gains, $Z_a(2,1) = P_{a,1}^{fd}$, $Z_a(2,2) = P_{a,2}^{fd}$, as well as the feedforward term $k_a(2)$. It can be observed that the gains and the feedforward term of the autonomy converge to the expected values that ensure Nash equilibrium. Therefore, the solutions of (6.8) and (6.9) converge even if the control gains of the partner are initially

unknown and estimated online, as long as $\boldsymbol{\xi}_e$ and $\dot{\boldsymbol{\xi}}^d$ are sufficiently exciting trajectories.

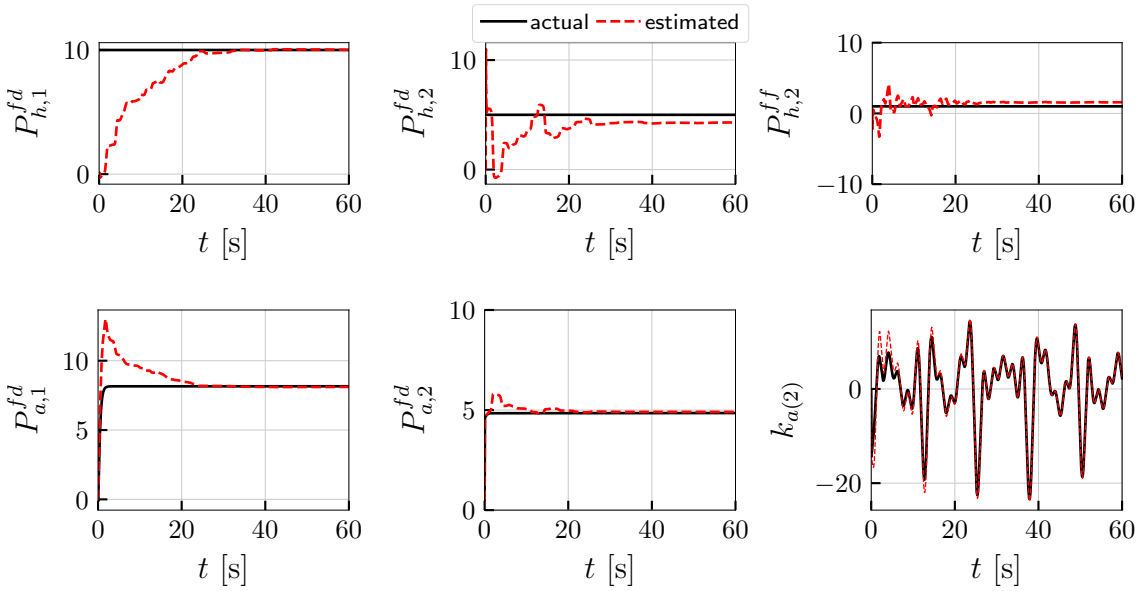

Figure 6.4: Simulation results. Unknown parameters of the human input u_h converge to their true values (upper row). Consequently, the parameters of the autonomous input converge to their expected values to ensure Nash equilibrium (bottom row).

6.3.2 Experiment Results

The tracking performance of the proposed shared control approach is evaluated experimentally. The convergence of the control gains of the robot partner to constant values is evaluated as well. The results for the manual and the shared cases from Subsection 6.3.1 are shown.

Figure 6.5a depicts the experimental setup. The human partner interacts with the *sigma.7* haptic device (robot partner) from Force Dimension to collaboratively track the desired trajectory in the virtual environment (Figure 6.5b) which is implemented using *chai3d* framework [CBB+03]. The task dynamics (6.2) is assigned to the end-effector of the haptic device. The human and the robot partners jointly track a one-dimensional trajectory along y-direction. The desired trajectory is the sum of eight sine waves

$$x^d = 0.01(\sin(0.5t) + \sin(0.7t) + \sin(t)) + 0.02 \sum_{i=1}^{5} \frac{1}{\omega_i} \sin(\omega_i t),$$

where $\omega_i \in \{1.2, 1.5, 1.7, 2, 2.5\}$. The sampling time of the haptic device is $t_{s,h} = 0.5$ ms, while the controller sampling time is $t_{s,c} = 1$ ms. The parameters are listed in Table 6.1. Parameter α is considerably reduced compared to the simulation and in the case (ii) due to its noise sensitivity.

Figure 6.6 depicts desired and actual trajectories along y axis, y^d and y_h, as well as the corresponding velocities $\dot{y}^d$ and $\dot{y}_h$ for the manual case. Even though the task can be accomplished, it can be observed that the human operator cannot track the trajectory well in the fully manual case and that a lag is observed in the human behavior.

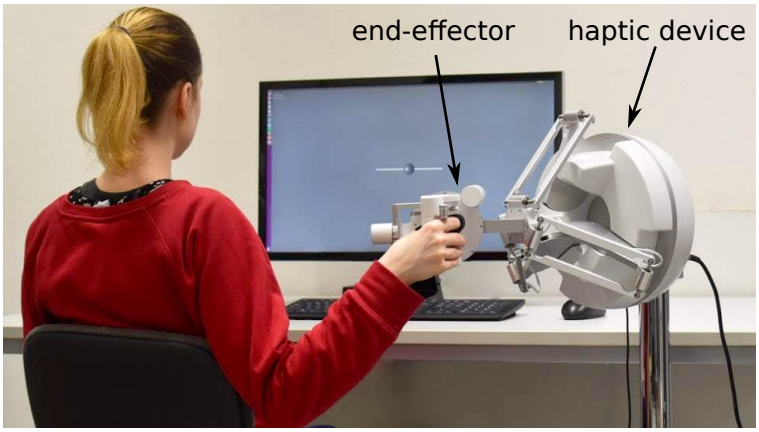

(a) The experimental setup.

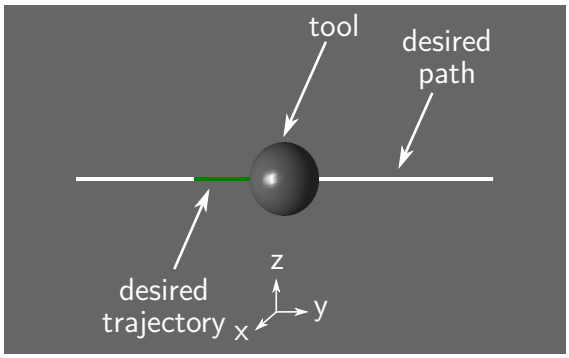

(b) The virtual environment.

Figure 6.5: The experimental setup. The human and the robot partner (the haptic device) collaborate to accomplish the task, (a). In (b) the desired path is a line, marked with white. The desired trajectory is marked with green. The goal is to track the desired trajectory as precisely as possible with the tool (the sphere).

Figure 6.7 shows the estimated human control input $\hat{u}_h$. The human control input gains are depicted in Figure 6.8. It can be observed that the convergence of the gains is achieved in ∼20 s.

Figure 6.9 shows the tracking performance when the proposed shared control scheme is applied. It can be seen that the tracking is improved compared to Figure 6.6. The robot control input force assists the human operator to track the desired trajectory. The total control input from the human and the robot is depicted in Figure 6.10. Figure 6.11 depicts the gains of the robot control input and its feedforward term.

The errors in position and velocity tracking for the manual and the shared scenarios are depicted in Figure 6.12. Evidently, the shared control approach improves the task performance in terms of tracking.

m [kg]	d [Ns/m]	$\boldsymbol{Q}_a$	$\boldsymbol{\Lambda}$	α
0.2	10	150 $\boldsymbol{I}_2$	500 $\boldsymbol{I}_2$	(i) 1000, (ii) 10

Table 6.1: Experiment parameters.

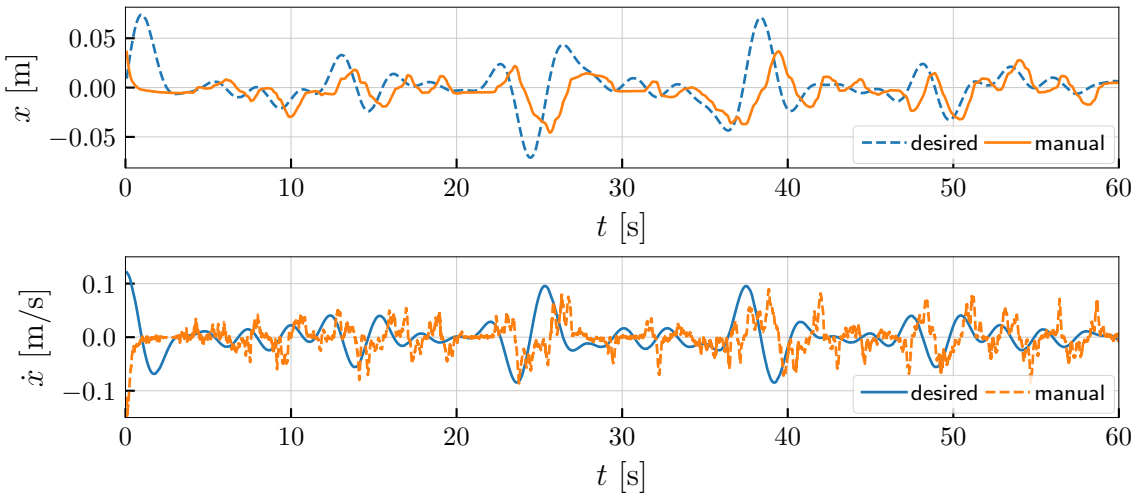

Figure 6.6: Experimental results for the manual scenario. The desired and the actual position and velocity trajectories. The tracking task is controlled by the human operator through the haptic device.

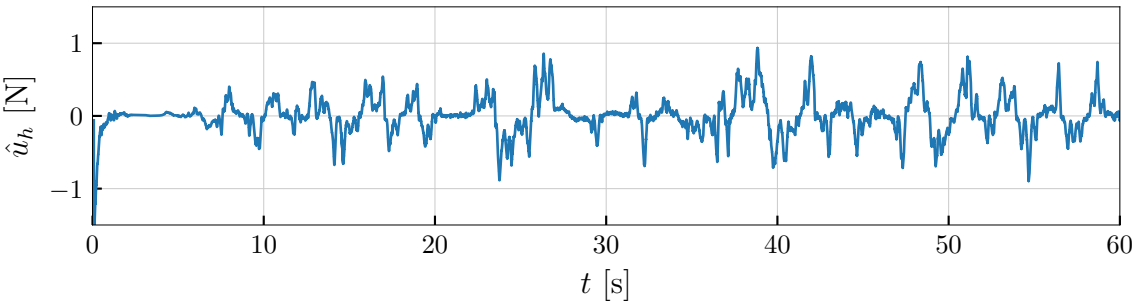

Figure 6.7: Experimental results for the manual scenario. The estimated human control input, $\hat{u}_h$.

6.4 Discussion

In this chapter an overlapping shared-control approach for tracking tasks, based on the differential game-theoretical framework, is proposed. It is assumed that the human partner admits an optimal control strategy and the control strategy of the robot is chosen so that the Nash equilibrium can be achieved during haptic collaboration. The tracking performance of the proposed controller and the convergence of the control gains to constant values is evaluated experimentally. The experimental results show that the proposed control approach outperforms the manual case (the task performed only by the human operator). The work presented in this chapter has been partially published in [MH20].

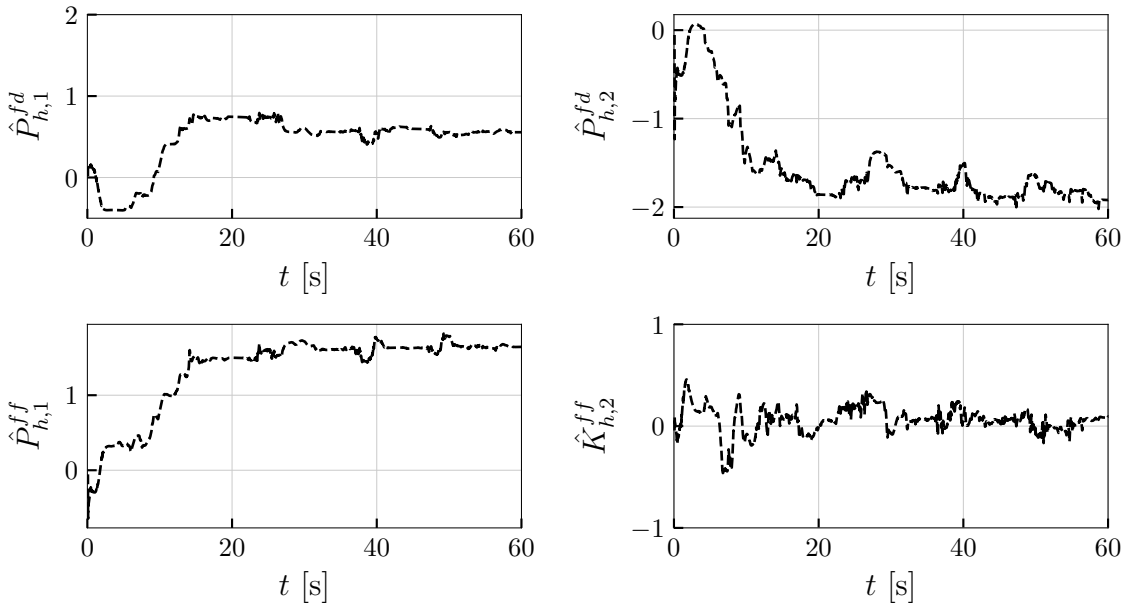

Figure 6.8: Experimental results for the manual scenario. The estimated parameters of the human input, obtained with the adaptive input observer.

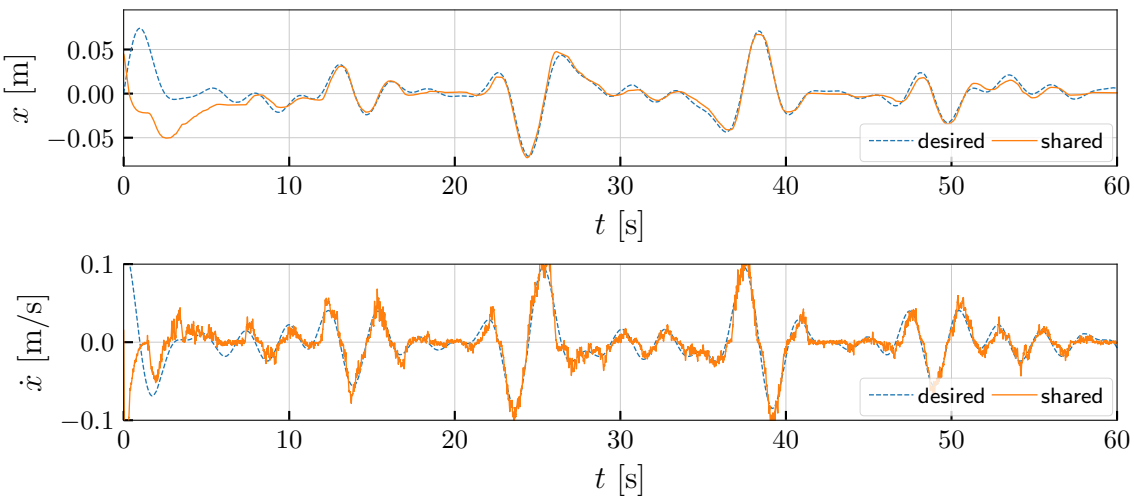

Figure 6.9: Experimental results for the shared scenario. The tracking performance. The tracking task is controlled by the human and the robot partners.

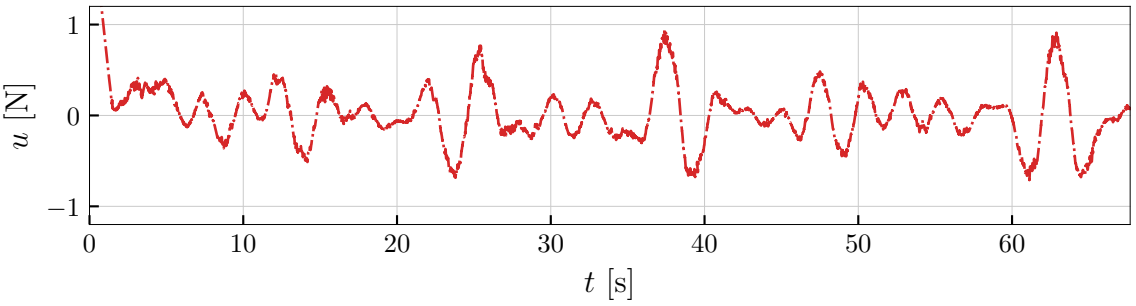

Figure 6.10: Experimental results for the shared scenario. The total control input as the sum of the human and the robot inputs.

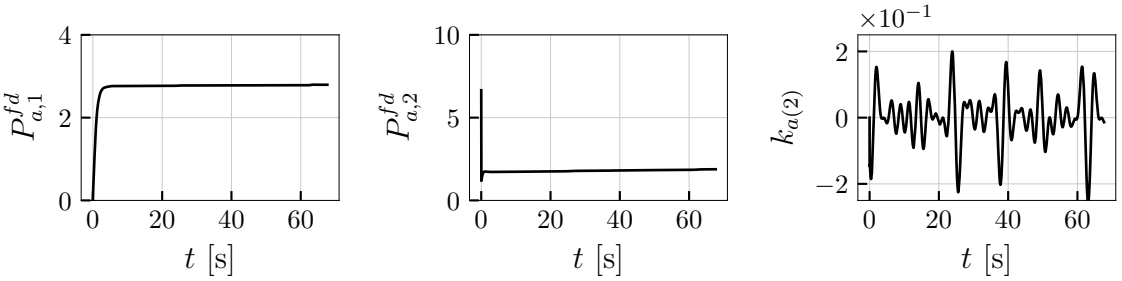

Figure 6.11: Experimental results for the shared scenario. The parameters of the robot control input gains.

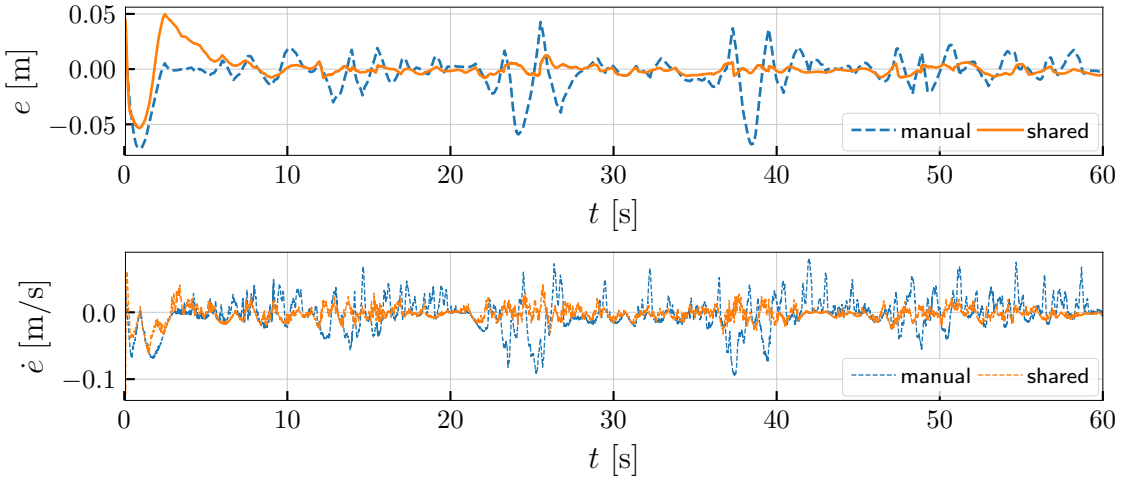

Figure 6.12: Experimental results. The position and velocity tracking errors for the manual and the shared scenarios.

7

Conclusion and Future Directions

Summary of Contributions

This thesis aims at developing a control framework for human-robot shared-control in haptic interaction tasks by addressing the six challenges outlined in Section 1.1. In that sense, the main contributions of this thesis are:

- a novel taxonomy and classification of human-robot interaction paradigms for continuous, haptic human-robot interaction (Challenge 1),
- a *subtask-based control* that enables simultaneous execution of multiple task-based control objectives by the human and the robot partners, while guaranteeing passivity of the human-robot interaction and the interaction with the environment (Challenge 2),
- defining command and feedback mappings on a reduced space of task-based behaviors and employing wearable interface solutions to reduce the design space in human-robot interaction scenarios while increasing its flexibility (Challenge 3-4),
- a *game-theoretical feedback controller* for haptic interaction tasks that considers the human behavior in continuous, trajectory tracking haptic tasks in the optimal control sense (Challenge 5-6).

Outlook

In addition to the challenges solved in this thesis, several open research problems remain to be studied in future works.

Modeling of human behavior

With the increase of autonomous capabilities of robots, the role of the human in the interaction is not reduced. Humans gain more high-level responsibilities, which increases the complexity of the human-robot interaction. Therefore, it is important to consider the human behavior in the control loop as a decision-making dynamical system. Therefore, decision-making dynamical models, developed within the field of cognitive psychology, might provide a useful construct.

Varying levels of autonomy

Developing a control architecture which tunes the autonomous functions of the robot system depending on the monitored human workload and situational awareness can enable humans and robots to function as a team and further improve their collaborative performance. Therefore, mixed-initiative control sharing is a promising concept for further research. Another important aspect is how to effectively and appropriately choose suitable level of autonomy. A lot of potential lies in the approaches that optimize the level of autonomy with respect to the human confidence in performing a task, i.e. by modeling trust in automation and human self-confidence. The problem of optimally assigning levels of autonomy during the task execution has not been treated so far.

Multitasking control

A major challenge is to design and execute multiple subtasks. This largely depends on the state of the environment and the available levels of autonomy. If multiple subtasks are considered, the control loop needs to handle multitasking situations. Incorporating multitasking human decision-making models into the control loop would be a challenging research goal. Multitasking control should also be considered in more complex application scenarios, e.g. scenarios that require a transition from teleoperation to direct physical interaction, or scenarios that consider recovery in the case of failures during task execution, e.g. re-grasp in the case of object slip or drop in object manipulation tasks.

Subtask allocation

In many applications, especially in time-critical tasks, it is necessary to prioritize and allocate subtasks according to the availability of resources of the human and the robot. However, the priority between subtasks is, so far, determined in advance and cannot dynamically change during the task execution. It is also constant during the task execution and the level of the robot autonomy is fixed. This is problematic as it reduces the flexibility of the interaction. Furthermore, if multiple subtasks need to be executed, their prioritization is of fixed order. It would be beneficial to be able to dynamically change the priorities of the subtasks according to the stage of the task execution and to allocate the responsibilities of the subtasks online.

Multimodal interfaces

Due to the complexity of human-robot interaction it is beneficial to provide feedback about the system states as well as feedback about the activity of the robot, e.g. in the form of warnings in the case of change of the autonomy level and sensitivity to future activities [WTFR04]. Gestures and speech form a natural and intuitive way of human-robot interaction. So far, this type of communication has been mostly employed in interactions where the human operator performs high-level planning and decision making and commands goals to the robotic system. However, this type of natural interaction may be suitable in continuous interaction where the human partner is in the active role.

Game-theoretical stochastic approach

Game-theoretical framework provides a promising basis for understanding human behavior in interaction scenarios and it enables design of robot control that is intuitive to the human partner. However, research shows that human behavior depends not only on the task goal and the behavior of their partner, but on the risk component as well. Therefore, humans are not risk-neutral in general. Research into stochastic, possibly risk-sensitive game-theoretical approaches can be an interesting future work.

Overall, sophisticated shared-control strategies that rely on a deeper understanding of human behavior, mixed-initiative interaction, multitasking capabilities, dynamical prioritization and allocation of subtasks will bring us closer to *intuitive and efficient* human-robot team interaction.

8

Formal Proofs

Proofs from Chapter 2

Proof of Proposition 2.2.1. *Since* $\sum_{i=1}^{k} k_i = n$, $\boldsymbol{\phi}(\boldsymbol{\xi})$ *is an* n*-dimensional vector and the behavior Jacobian* $\boldsymbol{J}_b(\boldsymbol{\xi})$ *is a square,* $n \times n$ *matrix. Since* $\boldsymbol{J}_b(\boldsymbol{\xi})$ *is nonsingular at point* $\boldsymbol{\xi} = \boldsymbol{\xi}_0$*, the behavior Jacobian has a full rank at this point,* $rank(\boldsymbol{J}_b(\boldsymbol{\xi})) = n$*. This implies that the behavior vector* $\boldsymbol{\phi}(\boldsymbol{\xi})$ *is a local diffeomorphism, i.e. it is a valid coordinate transformation in the neighborhood of* $\boldsymbol{\xi} = \boldsymbol{\xi}_0$ *[Isi13].* □

Proof of Proposition 2.3.1. *Provided Assumption 2.3.1 is valid, the imposed equality* $\sum_{i=1}^{k} dim\{\Delta^c_{bh,i}\} = n$ *implies that a concatenated* n*-dimensional behavior state* $\boldsymbol{\xi}_b$ *is accessible to* $\boldsymbol{u}_h$ *because the distributions* $\Delta^G_{bh,i}, i = 1, ..., k$*, are nonsingular which is already imposed by Proposition 2.2.1. The condition* $\sum_{i=1}^{k} dim\{\Delta^c_{ba,i}\} = 0$ *is a direct consequence of Assumption 2.3.2.* □

Proof of Lemma 1. *Since vector fields* $\boldsymbol{f}_{b,i}, \boldsymbol{g}_{bh,i1}, ..., \boldsymbol{g}_{bh,il}$ *in (2.17) are in* $T\mathcal{M}_{b,i}$ *for* $i = 1, ..., d$ *and according to Assumption 2.3.3, by transforming them to the new coordinates with* $\boldsymbol{\phi}_{bh}(\boldsymbol{\xi}_b)$

$$\boldsymbol{f}_{bh}(\boldsymbol{\xi}_{bh}, \boldsymbol{\xi}_{ba}) = [\frac{\partial \boldsymbol{\phi}_{bh}}{\partial \boldsymbol{\xi}_b} \boldsymbol{f}_b(\boldsymbol{\xi}_b)]_{\boldsymbol{\xi}_b = \boldsymbol{\phi}_{bh}^{-1}(\boldsymbol{\xi}_{bh}, \boldsymbol{\xi}_{ba})}$$

$$\boldsymbol{G}_{bh}(\boldsymbol{\xi}_{bh}, \boldsymbol{\xi}_{ba}) = [\frac{\partial \boldsymbol{\phi}_{bh}}{\partial \boldsymbol{\xi}_b} \boldsymbol{G}_b(\boldsymbol{\xi}_b)]_{\boldsymbol{\xi}_b = \boldsymbol{\phi}_{bh}^{-1}(\boldsymbol{\xi}_{bh}, \boldsymbol{\xi}_{ba})},$$

the last $k - d$ *elements of* $\boldsymbol{f}_b$ *and* $\boldsymbol{G}_b$ *vanish, yielding*

$$\boldsymbol{f}_{bh}(\boldsymbol{\xi}_{bh}, \boldsymbol{\xi}_{ba}) = col(\boldsymbol{f}_{bh,1}(\boldsymbol{\xi}_{bh}, \boldsymbol{\xi}_{ba}), ..., \boldsymbol{f}_{bh,d}(\boldsymbol{\xi}_{bh}, \boldsymbol{\xi}_{ba}), \boldsymbol{0}_{k-d})$$

$$\boldsymbol{G}_{bh}(\boldsymbol{\xi}_{bh}, \boldsymbol{\xi}_{ba}) = \begin{bmatrix} \boldsymbol{G}_{bh,1} \\ \vdots \\ \boldsymbol{G}_{bh,d} \\ \boldsymbol{0}_{(k-d)\times m}. \end{bmatrix}$$

Analogously, by transforming vector fields $\boldsymbol{f}_{b,i}, \boldsymbol{g}_{ba,i(l+1)}, ..., \boldsymbol{g}_{ba,im}$ *in (2.17) for* $i = d + 1, ..., k$ *to the new coordinates with* $\boldsymbol{\phi}_{b,a}(\boldsymbol{\xi}_b)$

$$\boldsymbol{f}_{ba}(\boldsymbol{\xi}_{bh}, \boldsymbol{\xi}_{ba}) = [\frac{\partial \boldsymbol{\phi}_{ba}}{\partial \boldsymbol{\xi}_b} \boldsymbol{f}_b(\boldsymbol{\xi}_b)]_{\boldsymbol{\xi}_b = \boldsymbol{\phi}_{ba}^{-1}(\boldsymbol{\xi}_{bh}, \boldsymbol{\xi}_{ba})}$$

$$\boldsymbol{G}_{ba}(\boldsymbol{\xi}_{bh}, \boldsymbol{\xi}_{ba}) = [\frac{\partial \boldsymbol{\phi}_{ba}}{\partial \boldsymbol{\xi}_b} \boldsymbol{G}_b(\boldsymbol{\xi}_b)]_{\boldsymbol{\xi}_b = \boldsymbol{\phi}_{ba}^{-1}(\boldsymbol{\xi}_{bh}, \boldsymbol{\xi}_{ba})},$$

the first d elements of $\boldsymbol{f}_b$ and $\boldsymbol{G}_b$ vanish, yielding

$$\boldsymbol{f}_{ba}(\boldsymbol{\xi}_{bh}, \boldsymbol{\xi}_{ba}) = col(\mathbf{0}_d, \boldsymbol{f}_{ba,d+1}(\boldsymbol{\xi}_{bh}, \boldsymbol{\xi}_{ba}), ..., \boldsymbol{f}_{ba,k}(\boldsymbol{\xi}_{bh}, \boldsymbol{\xi}_{ba}))$$
$$\boldsymbol{G}_{ba}(\boldsymbol{\xi}_{bh}, \boldsymbol{\xi}_{ba}) = \begin{bmatrix} \mathbf{0}_{d\times m} \\ \boldsymbol{G}_{bh,d+1} \\ \vdots \\ \boldsymbol{G}_{bh,k} \end{bmatrix}.$$

This generates a transformed system of the form (2.25) and completes the proof. □

Proof of Proposition 2.3.2. *Provided Assumption 2.3.3 is valid and the behavior subsystems are represented as in (2.25), according to Lemma 1 the imposed equality $dim\{\Delta^c_{bh}\} = \sum_{i=1}^{d} k_i$ implies that a concatenated behavior state $\boldsymbol{\xi}_{bh}$ is accessible to $\boldsymbol{u}_h$ because the distributions $\Delta^G_{bh,i}, i = 1, ..., d$ are nonsingular and their dimension is $\sum_{i=1}^{d} k_i$ which is already imposed by Proposition 2.2.1 and Lemma 1. The imposed equality $dim\{\Delta^c_{ba}\} = \sum_{i=d+1}^{k} k_i$ implies that a concatenated behavior state $\boldsymbol{\xi}_{ba}$ is accessible to $\boldsymbol{u}_h$ because the distributions $\Delta^G_{ba,i}, i = d+1, ..., k$ are nonsingular and their dimension is $\sum_{i=d+1}^{k} k_i$ which is already imposed by Proposition 2.2.1 and Lemma 1.* □

Proof of Proposition 2.3.3. *The imposed equalities $dim\{\Delta^c_{bh,i}\} = k_i$ and $dim\{\Delta^c_{ba,i}\} = k_i$ implies that a behavior state $\boldsymbol{\xi}_{b,i}$ is accessible to $\boldsymbol{u}_h$ and $\boldsymbol{u}_a$ because the distribution $\Delta^G_{bh,i}$ and $\Delta^G_{ba,i}$ are nonsingular and their dimension is k_i which is already imposed by Proposition 2.2.1.* □

Proofs from Chapter 3

Proof of Lemma 2. *Since the inertial matrix $\boldsymbol{M}(\boldsymbol{\xi})$ is full-rank, the system satisfies the strong accessibility rank condition at each point $\boldsymbol{\xi}_0 \in \mathcal{M}$. Therefore, $dim\{\Delta\} = n$ as it spans $\boldsymbol{G}$. Under the static control law (3.4) the accessibility of the closed-loop system does not change [NVdS90], which means that $dim\{\tilde{\Delta}\} = dim\{\Delta\} = n$. Considering the equality for $\tilde{\Delta}^\star$ in (3.8) and the result given with (3.14) by duality the following holds for $(\tilde{\Delta}^\star)^\perp$*

$$(\tilde{\Delta}^\star)^\perp = \sum_{i=1}^{k} \sum_{j=1}^{k_i} dh_{i,j},$$

and $dim\{(\tilde{\Delta}^\star)^\perp\} = n$ due to the discussion in Remark 12. Therefore, $dim\{\tilde{\Delta}^\star\} = 0$. Since $dim\{\Delta^K_i\} = k_i$ and (3.14) holds, it follows that $dim\{\tilde{\Delta}^\star_i\} = n - k_i$. Lastly, since $\tilde{\Delta}^\star_i + \tilde{\Delta}_i = \tilde{\Delta}$, it follows that $dim\{\tilde{\Delta}_i\} = k_i$, which completes the proof. □

Proof of Theorem 1. *Multiplying the matrices on the left side of (3.15) and assigning $\tilde{\boldsymbol{G}}_2$ a block-diagonal form proposed with (3.16) results in the following equality*

$$\begin{bmatrix} \boldsymbol{J}_{b,1}\boldsymbol{G}_2\boldsymbol{\Gamma}_1 & \dots & \boldsymbol{J}_{b,1}\boldsymbol{G}_2\boldsymbol{\Gamma}_k \\ \vdots & \vdots & \vdots \\ \boldsymbol{J}_{b,k}\boldsymbol{G}_2\boldsymbol{\Gamma}_1 & \dots & \boldsymbol{J}_{b,k}\boldsymbol{G}_2\boldsymbol{\Gamma}_k \end{bmatrix} = \begin{bmatrix} \boldsymbol{M}^{-1}_{b,1} & \dots & \mathbf{0} \\ \vdots & \vdots & \vdots \\ \mathbf{0} & \dots & \boldsymbol{M}^{-1}_{b,k} \end{bmatrix}, \tag{8.1}$$

where a generated block-diagonal matrix consists of k blocks and each block i, according to Lemma 2, has a full rank k_i, $i = 1, ..., k$. Each off-diagonal term of the matrix on the left side of (8.1) is equal to zero

$$\boldsymbol{J}_{b,i}\boldsymbol{G}_2\boldsymbol{\Gamma}_j = \boldsymbol{J}_{b,i}\tilde{\boldsymbol{G}}_2 = \mathbf{0}, \quad \forall i \neq j. \tag{8.2}$$

Since $\tilde{\boldsymbol{G}}_2 = \boldsymbol{G}_2\boldsymbol{\Gamma}$ *and (3.14) holds, then* $\tilde{\Delta}_j^G \subset \Omega_i^{\perp}$ *holds for each* $i \neq j$*, since* $\tilde{\Delta}_j^G \subset \mathcal{D}_i^{\star}$*. Then, since (3.11) holds,* $\boldsymbol{J}_{b,i}\tilde{\boldsymbol{g}}_j = \boldsymbol{0}$ *for each* $i \neq j$*. Furthermore, as* $\boldsymbol{G}_2\boldsymbol{\Gamma}_j = \tilde{\boldsymbol{g}}_j$*, (8.2) can be rewritten as*

$$\mathcal{L}_{\tilde{\boldsymbol{g}}_j}\boldsymbol{h}_i(\boldsymbol{\xi}) = \boldsymbol{0},$$

which corresponds to the first equality of (3.6) in Proposition 3.2.1 and represents a sufficient condition for the input-output noninteraction. Therefore, this proves the theorem. □

Proof of Theorem 2. *After applying the coordinate transformation (2.10) and full non-interacting control law, given by (3.4), (3.15) and (3.24), the following set of dynamical systems is obtained*

$$\begin{aligned}
\dot{\boldsymbol{x}}_b &= \boldsymbol{J}_b\dot{\boldsymbol{\theta}} \\
\ddot{\boldsymbol{x}}_{b,1} &= -\boldsymbol{M}_{b,1}^{-1}\tilde{\boldsymbol{C}}_{b,1}\dot{\boldsymbol{x}}_{b,1} + \boldsymbol{M}_{b,1}^{-1}(\tilde{\boldsymbol{\tau}}_{c,1} + \tilde{\boldsymbol{\tau}}_{e,1}) \\
&\vdots \\
\ddot{\boldsymbol{x}}_{b,k} &= -\boldsymbol{M}_{b,k}^{-1}\tilde{\boldsymbol{C}}_{b,k}\dot{\boldsymbol{x}}_{b,k} + \boldsymbol{M}_{b,k}^{-1}(\tilde{\boldsymbol{\tau}}_{c,k} + \tilde{\boldsymbol{\tau}}_{e,k}) \\
\boldsymbol{y}_1 &= \dot{\boldsymbol{x}}_{b,1} \\
&\vdots \\
\boldsymbol{y}_k &= \dot{\boldsymbol{x}}_{b,k},
\end{aligned} \tag{8.3}$$

with $\tilde{\boldsymbol{\tau}}_e = \boldsymbol{\Gamma}^{-1}\boldsymbol{\tau}_e$*. It can be observed that (8.3) corresponds to (3.21) which completes the proof.* □

Proof of Proposition 3.2.2. *Storage function (3.31) is an energy function and is positive semidefinite. Its derivative is*

$$\begin{aligned}
\dot{S}_i &= \dot{\boldsymbol{e}}_i^{\top}\boldsymbol{M}_{b,i}\ddot{\boldsymbol{e}}_i + \frac{1}{2}\dot{\boldsymbol{e}}_i^{\top}\dot{\boldsymbol{M}}_{b,i}\dot{\boldsymbol{e}}_i + \boldsymbol{w}_{K,i}\dot{\boldsymbol{e}}_i \\
&= \dot{\boldsymbol{e}}_i^{\top}\tilde{\boldsymbol{\tau}}_{e,i} - \dot{\boldsymbol{e}}_i^{\top}\boldsymbol{D}_i\dot{\boldsymbol{e}}_i + \frac{1}{2}\underbrace{\dot{\boldsymbol{e}}_i^{\top}[\dot{\boldsymbol{M}}_{b,i} - 2\tilde{\boldsymbol{C}}_{b,i}]\dot{\boldsymbol{e}}_i}_{=\boldsymbol{0}} < \dot{\boldsymbol{e}}_i^{\top}\tilde{\boldsymbol{\tau}}_{e,i}.
\end{aligned} \tag{8.4}$$

According to (3.30) it can be concluded that the system is strictly passive. □

Proofs from Chapter 6

Proof of Theorem 3. *Let us assume* $V_i(\boldsymbol{\xi}_e)$ *for* $i = h, a$ *to be*

$$V_i(\boldsymbol{\xi}_e) = \frac{1}{2}\boldsymbol{\xi}_e^{\top}\boldsymbol{Z}_i\boldsymbol{\xi}_e + \boldsymbol{\xi}_e^{\top}\boldsymbol{k}_i + \boldsymbol{n}_i \tag{8.5}$$

where

$$\dot{\boldsymbol{n}}_i + \boldsymbol{h}^{\top}\boldsymbol{k}_i + \frac{1}{2}\boldsymbol{k}_i\boldsymbol{B}\boldsymbol{B}^{\top}\boldsymbol{k}_i = \boldsymbol{0}$$

If (8.5) is inserted in (6.7), equations (6.8), (6.9), (6.10), (6.11) and (6.12) are readily obtained. □

Proof of Proposition 6.2.1. *The time derivative of (6.16) is*

$$\begin{aligned}\dot{V} = &-\tilde{\boldsymbol{\xi}}_e^\top(\boldsymbol{\Lambda}-\boldsymbol{A})\tilde{\boldsymbol{\xi}}_e - \frac{1}{2}\tilde{\boldsymbol{\xi}}_e^\top \boldsymbol{B}\boldsymbol{B}^\top \tilde{\boldsymbol{Z}}_h \boldsymbol{\xi}_e + \frac{1}{2}\tilde{\boldsymbol{\xi}}_e^\top \boldsymbol{B}\boldsymbol{B}^\top \tilde{\boldsymbol{K}}_h \dot{\boldsymbol{\xi}}^d \\ &+ \frac{1}{\alpha} tr(\tilde{\boldsymbol{Z}}_h^\top \dot{\tilde{\boldsymbol{Z}}}_h + \tilde{\boldsymbol{K}}_h^\top \dot{\tilde{\boldsymbol{K}}}_h).\end{aligned} \tag{8.6}$$

Since

$$\begin{aligned}\tilde{\boldsymbol{\xi}}_e^\top \boldsymbol{B}\boldsymbol{B}^\top \tilde{\boldsymbol{Z}}_h \boldsymbol{\xi}_e &= tr(\boldsymbol{\xi}_e^\top \tilde{\boldsymbol{Z}}_h^\top \boldsymbol{B}\boldsymbol{B}^\top \tilde{\boldsymbol{\xi}}_e) = tr(\tilde{\boldsymbol{Z}}_h^\top \boldsymbol{B}\boldsymbol{B}^\top \tilde{\boldsymbol{\xi}}_e \boldsymbol{\xi}_e^\top), \\ \tilde{\boldsymbol{\xi}}_e^\top \boldsymbol{B}\boldsymbol{B}^\top \tilde{\boldsymbol{K}}_h \dot{\boldsymbol{\xi}}^d &= tr(\dot{\boldsymbol{\xi}}^{d\top} \tilde{\boldsymbol{K}}_h^\top \boldsymbol{B}\boldsymbol{B}^\top \tilde{\boldsymbol{\xi}}_e) = tr(\tilde{\boldsymbol{K}}_h^\top \boldsymbol{B}\boldsymbol{B}^\top \tilde{\boldsymbol{\xi}}_e \dot{\boldsymbol{\xi}}^{d\top}),\end{aligned}$$

the last three terms in (8.6) can be canceled by imposing (6.17). Then (8.6) can be simplified to

$$\dot{V} = -\tilde{\boldsymbol{\xi}}_e^\top(\boldsymbol{\Lambda}-\boldsymbol{A})\tilde{\boldsymbol{\xi}}_e. \tag{8.7}$$

□

9

Port-Hamiltonian Framework

The port-Hamiltonian framework is based on a known energy function, the *Hamiltonian*, $\mathcal{H}$, and provides the energy-consistent description of a physical system. As the power conservative interconnection of port-Hamiltonian systems is again a port-Hamiltonian system, this framework is suitable for modeling complex and interconnected systems. Modeling of mechanical systems in the port-Hamiltonian framework can be achieved by interconnecting elementary/atomic structure elements: *inertias, dampers and springs*. Every atomic element is defined by its own Hamiltonian energy function and interacts with the other elements by exchanging energy through a *port*. The port is described by a pair of variables, *efforts*, $\boldsymbol{y}$ and *flows*, $\boldsymbol{u}$. Their dual product is *power*.

An input-state-output form of a port-Hamiltonian system is:

$$\begin{aligned} \dot{\boldsymbol{\xi}} &= [\boldsymbol{J}(\boldsymbol{\xi}) - \boldsymbol{D}(\boldsymbol{\xi})]\frac{\partial \mathcal{H}}{\partial \boldsymbol{\xi}}(\boldsymbol{\xi}) + \boldsymbol{G}(\boldsymbol{\xi})\boldsymbol{u} \\ \boldsymbol{y} &= \boldsymbol{G}^{\top}(\boldsymbol{\xi})\frac{\partial \mathcal{H}}{\partial \boldsymbol{\xi}}(\boldsymbol{\xi}). \end{aligned} \tag{9.1}$$

Twists and wrenches

In order to introduce twists and wrenches within the port-Hamiltonian framework, let us assume the frame $\{w\}$ is the reference frame, while the frame $\{i\}$ is assigned to a body. Then a transformation from $\{w\}$ to $\{i\}$ is given by a *homogeneous matrix*

$$^{i}\boldsymbol{H}_{w} = \begin{bmatrix} ^{i}\boldsymbol{R}_{w} & ^{i}\boldsymbol{p}_{w} \\ \boldsymbol{0}_{1\times 3} & 1 \end{bmatrix} \in \mathrm{SE}(3), \tag{9.2}$$

which consists of a translation vector $^{i}\boldsymbol{p}_{w} \in \mathbb{R}^3$ and a rotation matrix $^{i}\boldsymbol{R}_{w} \in \mathrm{SO}(3)$. The rigid body motion in the port-Hamiltonian framework is described with *twist*, see e.g. [Str01]. The twist associated with the frame $\{i\}$, relative to the frame of another body, denoted as $\{j\}$, and expressed in the reference frame $\{w\}$ is

$$^{w,j}\boldsymbol{t}_{i} = \begin{bmatrix} (^{w,j}\boldsymbol{\omega}_{i})^{\top} & (^{w,j}\boldsymbol{v}_{i})^{\top} \end{bmatrix}^{\top}, \tag{9.3}$$

and consists of angular velocity $^{w,j}\boldsymbol{\omega}_{i} \in \mathbb{R}^3$ around a screw axis and a translation velocity $^{w,j}\boldsymbol{v}_{i} \in \mathbb{R}^3$ along the same axis. A coordinate transformation of twist $^{w,j}\boldsymbol{t}_{i}$ from $\{w\}$ to $\{j\}$ is given by

$$ {}^{j,j}\boldsymbol{t}_i = {}^{j}\boldsymbol{t}_i = \underbrace{\begin{bmatrix} {}^{j}\boldsymbol{R}_w & \boldsymbol{0}_3 \\ \boldsymbol{S}({}^{j}\boldsymbol{p}_w){}^{j}\boldsymbol{R}_w & {}^{j}\boldsymbol{R}_w \end{bmatrix}}_{\boldsymbol{Ad}_{j\boldsymbol{H}_w}} {}^{w,j}\boldsymbol{t}_i. \tag{9.4} $$

The dual quantity of twist is *wrench*. The wrench $\boldsymbol{w}_i$ which acts on a body associated with the frame $\{i\}$, expressed in the reference frame $\{w\}$ is

$$ \boldsymbol{w}_i = \begin{bmatrix} (\boldsymbol{m}_i)^\top & (\boldsymbol{f})^\top \end{bmatrix}^\top, \tag{9.5} $$

where $\boldsymbol{m}_i \in \mathbb{R}^3$ are moments and $\boldsymbol{f}_i \in \mathbb{R}^3$ are forces. A coordinate transformation of the wrench $\boldsymbol{w}_i$ from $\{w\}$ to $\{j\}$ is given by

$$ {}^{j}\boldsymbol{w}_i = \boldsymbol{Ad}^\top_{\boldsymbol{H}_j} \boldsymbol{w}_i. \tag{9.6} $$

Atomic elements

In this section, the atomic mechanical elements (inertias, dampers and springs) are defined in the port-Hamiltonian form.

Inertias

The kinetic energy stored in a body is a function of its relative motion with respect to the body frame $\{i\}$

$$ \mathcal{H}_\mathrm{K}({}^{i}\tilde{\boldsymbol{p}}_i) = \frac{1}{2}({}^{i}\tilde{\boldsymbol{p}}_i)^\top \boldsymbol{M}^{-1}{}^{i}\tilde{\boldsymbol{p}}_i, \tag{9.7} $$

where ${}^{i}\tilde{\boldsymbol{p}}_i$ is the momentum of the body and $\boldsymbol{M}$ is the inertial matrix of the body.

The input-state-output form of the body is defined by the momentum ${}^{i}\tilde{\boldsymbol{p}}_i$ (state), the twist ${}^{i,w}\boldsymbol{t}_i$ (output) and the wrench ${}^{i}\boldsymbol{w}_i$ (input)

$$ \begin{aligned} {}^{i}\dot{\tilde{\boldsymbol{p}}}_i &= \boldsymbol{C}_i \frac{\partial \mathcal{H}_\mathrm{K}({}^{i}\tilde{\boldsymbol{p}}_i)}{\partial {}^{i}\tilde{\boldsymbol{p}}_i} + \boldsymbol{I}_6^i \boldsymbol{w}_i \\ {}^{i,w}\boldsymbol{t}_i &= \boldsymbol{I}_6 \frac{\partial \mathcal{H}_\mathrm{K}({}^{i}\tilde{\boldsymbol{p}}_i)}{\partial {}^{i}\tilde{\boldsymbol{p}}_i}, \end{aligned} \tag{9.8} $$

where $\boldsymbol{C}_i$ represents Coriolis and centrifugal forces.

Dampers

Energy dissipation is represented as an input-output mapping between wrenches and twists

$$ {}^{i}\boldsymbol{w}_i = F({}^{i,w}\boldsymbol{t}_i). \tag{9.9} $$

For linear dampers with constant $\boldsymbol{D}$ the wrench is directly proportional to the twist

$$ {}^{i}\boldsymbol{w}_i = \boldsymbol{D}^{i,w}\boldsymbol{t}_i. \tag{9.10} $$

The dissipated (co-)energy in this case is:

$$\mathcal{H}_{\mathrm{D}}^{*} = \frac{1}{2}{}^{i,w}\boldsymbol{t}_i^{\top}\boldsymbol{D}^{i,w}\boldsymbol{t}_i. \tag{9.11}$$

Springs

A spring is defined between two bodies, i and j. The potential energy stored in the spring is a positive definite function of the displacement ${}^{j}\boldsymbol{H}_i$

$$\mathcal{H}_{\mathrm{P}} : \mathrm{SE}(3) \to \mathbb{R}^{+};\ {}^{j}\boldsymbol{H}_i \mapsto \mathcal{H}_{\mathrm{P}}({}^{j}\boldsymbol{H}_i). \tag{9.12}$$

Energy functions of different types of springs are summarized in [Str01]. The input-state-output form of the spring is defined by the displacement ${}^{j}\boldsymbol{H}_i$ (state), the wrench ${}^{i}\boldsymbol{w}_i$ (output) and the twist ${}^{i,j}\boldsymbol{t}_i$ (input)

$$\begin{aligned} {}^{j}\dot{\boldsymbol{H}}_i &=^{j} \boldsymbol{H}_i^{i,j}\boldsymbol{t}_i \\ {}^{i}\boldsymbol{w}_i &=^{j} \boldsymbol{H}_i^{\top}\frac{\partial \mathcal{H}_{\mathrm{P}}({}^{j}\boldsymbol{H}_i)}{\partial {}^{j}\boldsymbol{H}_i}. \end{aligned} \tag{9.13}$$

10

Mathematical Concepts

Definition 10.0.1. (Surjective mapping.) *A mapping*

$$T\boldsymbol{\phi}_i : T\mathcal{M} \to T\mathcal{M}_{b,i},$$

is a surjection, *if for every element* $\boldsymbol{x}$ *in* $\mathcal{M}$, *there is at least one element* $\boldsymbol{x}_{b,i}$ *in* $\mathcal{M}_{b,i}$.

Definition 10.0.2. (Submersion.) *A differentiable map*

$$\boldsymbol{\phi}_i : \mathcal{M} \to \mathcal{M}_{b,i}, \quad \boldsymbol{x}_{b,i} = \boldsymbol{\phi}_i(\boldsymbol{x}),$$

is submersion *if its differential is everywhere surjective.*

Definition 10.0.3 ([NVdS90])**.** (Distribution.) *A* distribution Δ *is a map which assigns to each* $\boldsymbol{\xi} \in \mathcal{M}$ *a linear subspace* $\Delta(\boldsymbol{\xi})$ *of the tangent space* $T_{\boldsymbol{\xi}}\mathcal{M}$. *Distribution* Δ *is smooth if around any point* $\boldsymbol{\xi} \in \mathcal{M}$ *these subspaces* $\Delta(\boldsymbol{\xi})$ *are spanned by smooth vector fields* $\boldsymbol{f}_i, i = 1, ..., d$

$$\Delta(\boldsymbol{\xi}) = span\{\boldsymbol{f}_1(\boldsymbol{\xi}), ..., \boldsymbol{f}_d(\boldsymbol{\xi})\}.$$

Definition 10.0.4 ([Isi13])**.** (Controllability distribution.) *A distribution* Δ *is a* controllability distribution *on* $\mathcal{U} \in \mathcal{M}$ *if it is involutive and there exist a feedback pair* $(\boldsymbol{\alpha}, \boldsymbol{\Gamma})$ *on* $\mathcal{U}$ *such that* $\Delta \cap \tilde{\boldsymbol{G}} = span\{\tilde{\boldsymbol{g}}_i : i \in I\}$, *where* $I \subseteq \{1, ..., m\}$, *and* Δ *is the smallest distribution invariant under* $\tilde{\boldsymbol{f}}, \tilde{\boldsymbol{g}}_1, ..., \tilde{\boldsymbol{g}}_m$ *and contains* $\tilde{\boldsymbol{g}}_i, \forall i \in I$, *which is denoted as*

$$\Delta = \langle \tilde{\boldsymbol{f}}, \tilde{\boldsymbol{g}}_1, ..., \tilde{\boldsymbol{g}}_m | span\{\tilde{\boldsymbol{g}}_i, \forall i \in I\} \rangle.$$

Definition 10.0.5 ([NVdS90])**.** (Codistribution.) *The dual object of a distribution is a* codistribution. *A codistribution* Ω *on* $\mathcal{M}$ *is a map which assigns to any* $\boldsymbol{\xi} \in \mathcal{M}$ *a linear subspace* $\Omega(\boldsymbol{\xi})$ *of the cotangent space* $T^\star\boldsymbol{\xi}\mathcal{M}$. *Codistribution* Ω *is smooth if around any point* $\boldsymbol{\xi} \in \mathcal{M}$ *these subspaces* $\Omega(\boldsymbol{\xi})$ *are spanned by smooth covector fields* $\omega_i, i = 1, ..., d$

$$\Omega(\boldsymbol{\xi}) = span\{\boldsymbol{\omega}_1(\boldsymbol{\xi}), ..., \boldsymbol{\omega}_d(\boldsymbol{\xi})\}.$$

List of Figures

List of Tables

Bibliography

[AAC08] G. Antonelli, F. Arrichiello, and S. Chiaverini. The null-space-based behavioral control for autonomous robotic systems. *Intelligent Service Robotics*, 1(1):27–39, 2008.

[AAC09] G. Antonelli, F. Arrichiello, and S. Chiaverini. Experiments of Formation Control With Multirobot Systems Using the Null-Space-Based Behavioral Control. *IEEE Transactions on Control Systems Technology*, 17(5):1173–1182, 2009.

[AEK05] D. Aarno, S. Ekvall, and D. Kragic. Adaptive Virtual Fixtures for Machine-Assisted Teleoperation Tasks. In *Proceedings of the IEEE International Conference on Robotics and Automation*, pages 1139–1144, 2005.

[AMCG15] C. K. Alder, S. J. McDonald, M. B. Colton, and M. A. Goodrich. Toward haptic-based management of small swarms in cordon and patrol. In *2015 Swarm/Human Blended Intelligence Workshop (SHBI)*, pages 1–8, 2015.

[AMH17] M. Angerer, S. Musić, and S. Hirche. Port-Hamiltonian based control for human-robot team interaction. In *2017 IEEE International Conference on Robotics and Automation (ICRA)*, pages 2292–2299, 2017.

[AMLL+15] J. Alonso-Mora, S. Haegeli Lohaus, P. Leemann, R. Siegwart, and P. Beardsley. Gesture based human - Multi-robot swarm interaction and its application to an interactive display. In *2015 IEEE International Conference on Robotics and Automation (ICRA)*, pages 5948–5953, May 2015.

[AP01] F.C. Anderson and M.G. Pandy. Dynamic Optimization of Human Walking. *Journal of Biomechanical Engineering*, 123(5):381–390, 05 2001.

[Ast87] Karl Johan Astrom. Adaptive feedback control. *Proceedings of the IEEE*, 75(2):185–217, 1987.

[BAH+13] H. Boessenkool, D. A. Abbink, C. J. M. Heemskerk, F. C. T. van der Helm, and J. G. W. Wildenbeest. A Task-Specific Analysis of the Benefit of Haptic Shared Control During Telemanipulation. *IEEE Transactions on Haptics*, 6(1):2–12, 2013.

[Bat94] Stefano Battilotti. *Noninteracting control with stability for nonlinear systems*. Springer-Verlag London, 1994.

[BBE+07] C. Belta, A. Bicchi, M. Egerstedt, E. Frazzoli, E. Klavins, and G. J. Pappas. Symbolic planning and control of robot motion [Grand Challenges of Robotics]. *IEEE Robotics Automation Magazine*, 14(1):61–70, March 2007.

[BFB+05] D. J. Bruemmer, D. A. Few, R. L. Boring, J. L. Marble, M. C. Walton, and C. W. Nielsen. Shared understanding for collaborative control. *IEEE Transactions on Systems, Man, and Cybernetics - Part A: Systems and Humans*, 35(4):494–504, 2005.

[BH96] R. C. Bonitz and T. C. Hsia. Internal force-based impedance control for cooperating manipulators. *IEEE Transactions on Robotics and Automation*, 12(1):78–89, 1996.

[BJG14] D. S. Brown, S. Y. Jung, and M. A. Goodrich. Balancing human and inter-agent influences for shared control of bio-inspired collectives. In *2014 IEEE International Conference on Systems, Man, and Cybernetics (SMC)*, pages 4123–4128, Oct 2014.

[BK04] C. Belta and V. Kumar. Abstraction and control for groups of robots. *IEEE Transactions on Robotics*, 20(5):865–875, Oct 2004.

[BK18] Gerald Brantner and Oussama Khatib. Controlling Ocean One. In Marco Hutter and Roland Siegwart, editors, *Field and Service Robotics*, pages 3–17, Cham, 2018. Springer International Publishing.

[BKG14] Daniel S. Brown, Sean C. Kerman, and Michael A. Goodrich. Human-Swarm Interactions Based on Managing Attractors. In *Proceedings of the 2014 ACM/IEEE International Conference on Human-Robot Interaction*, HRI '14, page 90–97, New York, NY, USA, 2014. Association for Computing Machinery.

[BO98] T. Başar and G. Olsder. *Dynamic Noncooperative Game Theory, 2nd Edition.* Society for Industrial and Applied Mathematics, 1998.

[BPB17] M. Bonilla, L. Pallottino, and A. Bicchi. Noninteracting constrained motion planning and control for robot manipulators. In *2017 IEEE International Conference on Robotics and Automation (ICRA)*, pages 4038–4043, May 2017.

[BSS04] J. Brookshire, S. Singh, and R. Simmons. Preliminary results in sliding autonomy for assembly by coordinated teams. In *2004 IEEE/RSJ International Conference on Intelligent Robots and Systems (IROS) (IEEE Cat. No.04CH37566)*, volume 1, pages 706–711 vol.1, 2004.

[BY04] M. Baker and H. A. Yanco. Autonomy mode suggestions for improving human-robot interaction. In *2004 IEEE International Conference on Systems, Man and Cybernetics (IEEE Cat. No.04CH37583)*, volume 3, pages 2948–2953 vol.3, 2004.

[CB14] J. Y. C. Chen and M. J. Barnes. Human Agent Teaming for Multirobot Control: A Review of Human Factors Issues. *IEEE Transactions on Human-Machine Systems*, 44(1):13–29, Feb 2014.

[CBB+03] F. Conti, F. Barbagli, R. Balaniuk, M. Halg, C. Lu, D. Morris, L. Sentis, J. Warren, O. Khatib, and K. Salisbury. The CHAI libraries. In *Proceedings of Eurohaptics 2003*, pages 496–500, Dublin, Ireland, 2003.

[CBH11] J. Y. C. Chen, M. J. Barnes, and M. Harper-Sciarini. Supervisory Control of Multiple Robots: Human-Performance Issues and User-Interface Design. *IEEE Transactions on Systems, Man, and Cybernetics, Part C (Applications and Reviews)*, 41(4):435–454, 2011.

[CCDd11] J. W. Crandall, M. L. Cummings, M. Della Penna, and P. M. A. de Jong. Computing the Effects of Operator Attention Allocation in Human Control of Multiple Robots. *IEEE Transactions on Systems, Man, and Cybernetics - Part A: Systems and Humans*, 41(3):385–397, 2011.

[CCMV08] F. Caccavale, P. Chiacchio, A. Marino, and L. Villani. Six-DOF Impedance Control of Dual-Arm Cooperative Manipulators. *IEEE/ASME Transactions on Mechatronics*, 13(5):576–586, 2008.

[CDE13] R. Chipalkatty, G. Droge, and M. B. Egerstedt. Less Is More: Mixed-Initiative Model-Predictive Control With Human Inputs. *IEEE Transactions on Robotics*, 29(3):695–703, 2013.

[CGON05] J. W. Crandall, M. A. Goodrich, D. R. Olsen, and C. W. Nielsen. Validating human-robot interaction schemes in multitasking environments. *IEEE Transactions on Systems, Man, and Cybernetics - Part A: Systems and Humans*, 35(4):438–449, July 2005.

[CHWT12] M. L. Cummings, J. P. How, A. Whitten, and O. Toupet. The Impact of Human–Automation Collaboration in Decentralized Multiple Unmanned Vehicle Control. *Proceedings of the IEEE*, 100(3):660–671, 2012.

[CL12] G. Coppin and F. Legras. Autonomy Spectrum and Performance Perception Issues in Swarm Supervisory Control. *Proceedings of the IEEE*, 100(3):590–603, 2012.

[CMKB04] J. Cortes, S. Martinez, T. Karatas, and F. Bullo. Coverage control for mobile sensing networks. *IEEE Transactions on Robotics and Automation*, 20(2):243–255, 2004.

[CMPP15] F. Chinello, M. Malvezzi, C. Pacchierotti, and D. Prattichizzo. Design and development of a 3RRS wearable fingertip cutaneous device. In *2015 IEEE International Conference on Advanced Intelligent Mechatronics (AIM)*, pages 293–298, July 2015.

[CSB+16] M. Chiou, R. Stolkin, G. Bieksaite, N. Hawes, K. L. Shapiro, and T. S. Harrison. Experimental analysis of a variable autonomy framework for controlling a remotely operating mobile robot. In *2016 IEEE/RSJ International Conference on Intelligent Robots and Systems (IROS)*, pages 3581–3588, 2016.

[CSL08] M. Cao, A. Stewart, and N. E. Leonard. Integrating human and robot decision-making dynamics with feedback: Models and convergence analysis. In *2008 47th IEEE Conference on Decision and Control*, pages 1127–1132, 2008.

[CSP17] J. Corredor, J. Sofrony, and A. Peer. Decision-Making Model for Adaptive Impedance Control of Teleoperation Systems. *IEEE Transactions on Haptics*, 10(1):5–16, Jan 2017.

[CZMC08] C. Cipriani, F. Zaccone, S. Micera, and M. C. Carrozza. On the Shared Control of an EMG-Controlled Prosthetic Hand: Analysis of User–Prosthesis Interaction. *IEEE Transactions on Robotics*, 24(1):170–184, 2008.

[DABW09] P. A. Ortega D. A. Braun and D. M. Wolpert. Nash Equilibria in Multi-Agent Motor Interactions. *PLOS Computational Biology*, 5(8):1–8, 08 2009.

[dav13] 2013. https://www.heise.de/tp/features/Unter-dem-Messer-des-Operationsroboters-3400512.html.

[DCG09] Birsen Donmez, M.L. Cummings, and Hudson D. Graham. Auditory Decision Aiding in Supervisory Control of Multiple Unmanned Aerial Vehicles. *Human Factors*, 51(5):718–729, 2009. PMID: 20196296.

[DdlCE13] M. Diana, J. P. de la Croix, and M. Egerstedt. Deformable-medium affordances for interacting with multi-robot systems. In *2013 IEEE/RSJ International Conference on Intelligent Robots and Systems*, pages 5252–5257, Nov 2013.

[DL91] Alessandro De Luca. Zero dynamics in robotic systems. In *Nonlinear Synthesis*, pages 68–87. Springer, 1991.

[DM06] William B. Dunbar and Richard M. Murray. Distributed receding horizon control for multi-vehicle formation stabilization. *Automatica*, 42(4):549 – 558, 2006.

[DS05] Dongjun Lee and M. W. Spong. Bilateral Teleoperation of Multiple Cooperative Robots over Delayed Communication Networks: Theory. In *Proceedings of the 2005 IEEE International Conference on Robotics and Automation*, pages 360–365, 2005.

[DS13] Anca D Dragan and Siddhartha S Srinivasa. A policy-blending formalism for shared control. *The International Journal of Robotics Research*, 32(7):790–805, 2013.

[DSDB08] Agostino De Santis, Bruno Siciliano, Alessandro De Luca, and Antonio Bicchi. An atlas of physical human–robot interaction. *Mechanism and Machine Theory*, 43(3):253 – 270, 2008.

[DY05] M. Desai and H. A. Yanco. Blending human and robot inputs for sliding scale autonomy. In *ROMAN 2005. IEEE International Workshop on Robot and Human Interactive Communication, 2005.*, pages 537–542, 2005.

[EBS+07] Jeremy L Emken, Raul Benitez, Athanasios Sideris, James E Bobrow, and David J Reinkensmeyer. Motor adaptation as a greedy optimization of error and effort. *Journal of neurophysiology*, 97(6):3997–4006, 2007.

[EH16] S. Erhart and S. Hirche. Model and analysis of the interaction dynamics in cooperative manipulation tasks. *IEEE Transactions on Robotics*, 32(3):672–683, 2016.

[End95] Mica R. Endsley. Toward a Theory of Situation Awareness in Dynamic Systems. *Human Factors*, 37(1):32–64, 1995.

[EX01] M. Egerstedt and Xiaoming Hu. Formation constrained multi-agent control. *IEEE Transactions on Robotics and Automation*, 17(6):947–951, 2001.

[FH85] T Flash and N Hogan. The coordination of arm movements: an experimentally confirmed mathematical model. *Journal of Neuroscience*, 5(7):1688–1703, 1985.

[FH18] Shamel Fahmi and Thomas Hulin. Inertial Properties in Haptic Devices: Non-Linear Inertia Shaping vs. Force Feedforward. *IFAC-PapersOnLine*, 51(22):79 – 84, 2018. 12th IFAC Symposium on Robot Control SYROCO 2018.

[FOSH14] M. Flad, J. Otten, S. Schwab, and S. Hohmann. Steering driver assistance system: A systematic cooperative shared control design approach. In *2014 IEEE International Conference on Systems, Man, and Cybernetics (SMC)*, pages 3585–3592, 2014.

[FRS+11] A. Franchi, P. Robuffo Giordano, C. Secchi, H. I. Son, and H. H. Bülthoff. A passivity-based decentralized approach for the bilateral teleoperation of a group of UAVs with switching topology. In *2011 IEEE International Conference on Robotics and Automation*, pages 898–905, 2011.

[FSM+11] M. Franken, S. Stramigioli, S. Misra, C. Secchi, and A. Macchelli. Bilateral Telemanipulation With Time Delays: A Two-Layer Approach Combining Passivity and Transparency. *IEEE Transactions on Robotics*, 27(4):741–756, 2011.

[FSR+12] A. Franchi, C. Secchi, M. Ryll, H. H. Bulthoff, and P. R. Giordano. Shared Control : Balancing Autonomy and Human Assistance with a Group of Quadrotor UAVs. *IEEE Robotics Automation Magazine*, 19(3):57–68, 2012.

[FSSB08] A. Frisoli, M. Solazzi, F. Salsedo, and M. Bergamasco. A Fingertip Haptic Display for Improving Curvature Discrimination. *Presence: Teleoperators and Virtual Environments*, 17(6):550–561, 2008.

[FTG+09] Daniela Feth, Binh An Tran, Raphaela Groten, Angelika Peer, and Martin Buss. *Shared-Control Paradigms in Multi-Operator-Single-Robot Teleoperation*, pages 53–62. Springer Berlin Heidelberg, Berlin, Heidelberg, 2009.

[Gaz05] V. Gazi. Swarm aggregations using artificial potentials and sliding-mode control. *IEEE Transactions on Robotics*, 21(6):1208–1214, 2005.

[GFS+14] G. Gioioso, A. Franchi, G. Salvietti, S. Scheggi, and D. Prattichizzo. The Flying Hand: a Formation of UAVs for Cooperative Tele-Manipulation. In *IEEE International Conference on Robotics and Automation (ICRA)*, 2014.

[GM04] Brian P. Gerkey and Maja J. Matarić. A Formal Analysis and Taxonomy of Task Allocation in Multi-Robot Systems. *The International Journal of Robotics Research*, 23(9):939–954, 2004.

[GMA+07] M. A. Goodrich, T. W. McLain, J. D. Anderson, J. Sun, and J. W. Crandall. Managing autonomy in robot teams: Observations from four experiments. In *2007 2nd ACM/IEEE International Conference on Human-Robot Interaction (HRI)*, pages 25–32, 2007.

[GPC05] Weston B. Griffin, William R. Provancher, and Mark R. Cutkosky. Feedback Strategies for Telemanipulation with Shared Control of Object Handling Forces. *Presence: Teleoperators and Virtual Environments*, 14(6):720–731, 2005.

[GQC05] Michael A. Goodrich, Morgan Quigley, and Keryl Cosenzo. Task Switching and Multi-Robot Teams. In Lynne E. Parker, Frank E. Schneider, and Alan C. Schultz, editors, *Multi-Robot Systems. From Swarms to Intelligent Automata Volume III*, pages 185–195, Dordrecht, 2005. Springer Netherlands.

[GSDP16] M. Geravand, E. Shahriari, A. De Luca, and A. Peer. Port-based modeling of human-robot collaboration towards safety-enhancing energy shaping control. In *2016 IEEE International Conference on Robotics and Automation (ICRA)*, pages 3075–3082, 2016.

[GSMP13] G. Gioioso, G. Salvietti, M. Malvezzi, and D. Prattichizzo. Mapping Synergies From Human to Robotic Hands With Dissimilar Kinematics: An Approach in the Object Domain. *IEEE Transactions on Robotics*, 29(4):825–837, 2013.

[GWHP16] M. Geravand, C. Werner, K. Hauer, and A. Peer. An Integrated Decision Making Approach for Adaptive Shared Control of Mobility Assistance Robots. *International Journal of Social Robotics*, (8):631–648, 2016.

[Had13] Sami Haddadin. *Towards safe robots: approaching Asimov's 1st law*, volume 90. Springer, 2013.

[HB12] S. Hirche and M. Buss. Human-Oriented Control for Haptic Teleoperation. *Proceedings of the IEEE*, 100(3):623–647, 2012.

[HCF15] T. Hatanaka, N. Chopra, and M. Fujita. Passivity-based bilateral human-swarm-interactions for cooperative robotic networks and human passivity analysis. In *2015 54th IEEE Conference on Decision and Control (CDC)*, pages 1033–1039, Dec 2015.

[HG09] Benjamin Hardin and Michael A. Goodrich. On Using Mixed-initiative Control: A Perspective for Managing Large-scale Robotic Teams. In *Proceedings of the 4th ACM/IEEE International Conference on Human Robot Interaction*, pages 165–172, 2009.

[Hir14] S. Hirche. Control Challenges in Physical Human-Robot Interaction. In *2014 European Control Conference*, pages 4685–4691, Hamburg, Germany, 2014.

[HK87] J. Hollerbach and Ki Suh. Redundancy resolution of manipulators through torque optimization. *IEEE Journal on Robotics and Automation*, 3(4):308–316, 1987.

[HKK+15] Yuichi Hiramatsu, Daisuke Kimura, Koji Kadota, Taro Ito, and Hiroshi Kinoshita. Control of Precision Grip Force in Lifting and Holding of Low-Mass Objects. *PLOS ONE*, 10(9):1–19, 2015.

[IEFH18] J. Inga, M. Eitel, M. Flad, and S. Hohmann. Evaluating Human Behavior in Manual and Shared Control via Inverse Optimization. In *2018 IEEE International Conference on Systems, Man, and Cybernetics (SMC)*, pages 2699–2704, 2018.

[IF06] Petros Ioannou and Bariş Fidan. *Adaptive control tutorial*. SIAM, 2006.

[Isi13] Alberto Isidori. *Nonlinear control systems*. Springer Science & Business Media, 2013.

[JBBJ10] G. Jones, N. Berthouze, R. Bielski, and S. Julier. Towards a situated, multimodal interface for multiple UAV control. In *2010 IEEE International Conference on Robotics and Automation*, pages 1739–1744, 2010.

[JBR14] A. D. Fisk J.M. Beer and W. A. Rogers. Toward a Framework for Levels of Robot Autonomy in Human-Robot Interaction. *Journal of Human-Robot Interaction*, 3(2):74–99, July 2014.

[JCB12] Nathanaël Jarrassé, Themistoklis Charalambous, and Etienne Burdet. A Framework to Describe, Analyze and Generate Interactive Motor Behaviors. *PLOS ONE*, 7(11):1–13, 11 2012.

[JF18] Richard J Jagacinski and John M Flach. *Control theory for humans: Quantitative approaches to modeling performance*. CRC Press, 2018.

[JL06] Ji Gao and J. D. Lee. Extending the decision field theory to model operators' reliance on automation in supervisory control situations. *IEEE Transactions on Systems, Man, and Cybernetics - Part A: Systems and Humans*, 36(5):943–959, 2006.

[JYN+19] X. Ji, K. Yang, X. Na, C. Lv, and Y. Liu. Shared Steering Torque Control for Lane Change Assistance: A Stochastic Game-Theoretic Approach. *IEEE Transactions on Industrial Electronics*, 66(4):3093–3105, 2019.

[KBC+02] Oussama Khatib, Oliver Brock, Kyong-Sok Chang, Francois Conti, Diego Ruspini, and Luis Sentis. Robotics and Interactive Simulation. *Commun. ACM*, 45(3):46–51, March 2002.

[KG02] Hassan K Khalil and Jessy W Grizzle. *Nonlinear systems*, volume 3. Prentice hall Upper Saddle River, NJ, 2002.

[Kha87] Oussama Khatib. A unified approach for motion and force control of robot manipulators: The operational space formulation. *IEEE Journal on Robotics and Automation*, 3(1):43–53, 1987.

[KSP08] Oussama Khatib, Luis Sentis, and Jae-Heung Park. *A Unified Framework for Whole-Body Humanoid Robot Control with Multiple Constraints and Contacts*, pages 303–312. Springer Berlin Heidelberg, Berlin, Heidelberg, 2008.

[KTC97] A. Kheddar, C. Tzafestas, and P. Coiffet. The hidden robot concept-high level abstraction teleoperation. In *Proceedings of the 1997 IEEE/RSJ International Conference on Intelligent Robot and Systems. Innovative Robotics for Real-World Applications.*, volume 3, pages 1818–1825, 1997.

[KWC+16] A. Kolling, P. Walker, N. Chakraborty, K. Sycara, and M. Lewis. Human Interaction With Robot Swarms: A Survey. *IEEE Transactions on Human-Machine Systems*, 46(1):9–26, 2016.

[KYC+96] Oussama Khatib, Kazu Yokoi, K Chang, Diego Ruspini, Robert Holmberg, and Arancha Casal. Vehicle/arm coordination and multiple mobile manipulator decentralized cooperation. In *Intelligent Robots and Systems' 96, IROS 96, Proceedings of the 1996 IEEE/RSJ International Conference on*, volume 2, pages 546–553. IEEE, 1996.

[LCG+19] Y Li, G Carboni, F Gonzalez, D Campolo, and E Burdet. Differential game theory for versatile physical human–robot interaction. *Nature Machine Intelligence*, 1(1):36–43, 2019.

[Lee08] Dongjun Lee. Semi-Autonomous Teleoperation of Multiple Wheeled Mobile Robots Over the Internet. In *ASME 2008 Dynamic Systems and Control Conference, Parts A and B*, pages 147–154, 2008.

[LF01] N. E. Leonard and E. Fiorelli. Virtual leaders, artificial potentials and coordinated control of groups. In *Proceedings of the 40th IEEE Conference on Decision and Control (Cat. No.01CH37228)*, volume 3, pages 2968–2973 vol.3, 2001.

[LFS+13] D. Lee, A. Franchi, H. I. Son, C. Ha, H. H. Bülthoff, and P. R. Giordano. Semi-autonomous Haptic Teleoperation Control Architecture of Multiple Unmanned Aerial Vehicles. *IEEE/ASME Transactions on Mechatronics*, 18(4):1334–1345, 2013.

[LH10] D. Lee and K. Huang. Passive-Set-Position-Modulation Framework for Interactive Robotic Systems. *IEEE Transaction on Robotics*, 26(2):354–369, 2010.

[Liu15] Yen-Chen Liu. Task-space coordination control of bilateral human–swarm systems. *Journal of the Franklin Institute*, 352(1):311 – 331, 2015.

[LK07] S. G. Loizou and V. Kumar. Mixed Initiative Control of Autonomous Vehicles. In *Proceedings 2007 IEEE International Conference on Robotics and Automation*, pages 1431–1436, 2007.

[LKL15] C. W. Lin, M. H. Khong, and Y. C. Liu. Experiments on Human-in-the-Loop Coordination for Multirobot System With Task Abstraction. *IEEE Transactions on Automation Science and Engineering*, 12(3):981–989, July 2015.

[LL16] W. Lenhard and A. Lenhard. Calculation of effect sizes. Dettelbach (Germany): Psychometrica, 2016.

[LOZ+18] N. Li, D. W. Oyler, M. Zhang, Y. Yildiz, I. Kolmanovsky, and A. R. Girard. Game Theoretic Modeling of Driver and Vehicle Interactions for Verification and Validation of Autonomous Vehicle Control Systems. *IEEE Transactions on Control Systems Technology*, 26(5):1782–1797, 2018.

[LS04] John D. Lee and Katrina A. See. Trust in Automation: Designing for Appropriate Reliance. *Human Factors*, 46(1):50–80, 2004. PMID: 15151155.

[LSSS14] Wenchao Li, Dorsa Sadigh, S. Shankar Sastry, and Sanjit A. Seshia. Synthesis for Human-in-the-Loop Control Systems. In Erika Ábrahám and Klaus Havelund, editors, *Tools and Algorithms for the Construction and Analysis of Systems*, pages 470–484, Berlin, Heidelberg, 2014. Springer Berlin Heidelberg.

[LTC+15] Y. Li, K. P. Tee, W. L. Chan, R. Yan, Y. Chua, and D. K. Limbu. Role adaptation of human and robot in collaborative tasks. In *2015 IEEE International Conference on Robotics and Automation (ICRA)*, pages 5602–5607, 2015.

[LTT+01] C. Laschi, G. Teti, G. Tamburrini, E. Datteri, and P. Dario. Adaptable semi-autonomy in personal robots. In *Proceedings of the 10th IEEE International Workshop on Robot and Human Interactive Communication*, pages 152–157, 2001.

[MBF03] J. L. Marble, D. J. Bruemmer, and D. A. Few. Lessons learned from usability tests with a collaborative cognitive workspace for human-robot teams. In *SMC'03 Conference Proceedings. 2003 IEEE International Conference on Systems, Man and Cybernetics. Conference Theme - System Security and Assurance (Cat. No.03CH37483)*, volume 1, pages 448–453 vol.1, 2003.

[MD07] S. Mau and J. Dolan. Scheduling for humans in multirobot supervisory control. In *2007 IEEE/RSJ International Conference on Intelligent Robots and Systems*, pages 1637–1643, Oct 2007.

[MFG+05] Christopher A Miller, Harry Funk, Robert Goldman, John Meisner, and Peggy Wu. Implications of adaptive vs. adaptable UIs on decision making: Why automated adaptiveness is not always the right answer. In *Proceedings of the 1st international conference on augmented cognition*, pages 22–27, 2005.

[MH16] Selma Musić and Sandra Hirche. Classification of human-robot team interaction paradigms. *IFAC-PapersOnLine*, 49(32):42 – 47, 2016. Cyber-Physical & Human-Systems CPHS 2016.

[MH17] Selma Musić and Sandra Hirche. Control sharing in human-robot team interaction. *Annual Reviews in Control*, 44:342 – 354, 2017.

[MH18] S. Musić and S. Hirche. Passive noninteracting control for human-robot team interaction. In *2018 IEEE Conference on Decision and Control (CDC)*, pages 421–427, 2018.

[MH20] Selma Musić and Sandra Hirche. Haptic Shared Control for Human-Robot Collaboration: A Game-Theoretical Approach. In *Proceedings of the 21st IFAC World Congress*, 2020.

[MK97] J. D. Morrow and P. K. Khosla. Manipulation task primitives for composing robot skills. In *Proceedings of International Conference on Robotics and Automation*, volume 4, pages 3354–3359, April 1997.

[MKH18] S. Musić, O. Khatib, and S. Hirche. Shared control for robot-team teleoperation. In *2018 IEEE/RSJ International Conference on Intelligent Robots and Systems, Workshop on "Haptic-enabled shared control of robotic systems: a compromise between teleoperation and autonomy"*, Madrid, Spain, 2018.

[MKH21] S. Musić, O. Khatib, and S. Hirche. Haptic Shared Control for Cooperative Manipulation Tasks. *Frontiers in Robotics and AI*, 2021. in preparation.

[MLH15] J. R. Medina, T. Lorenz, and S. Hirche. Synthesizing Anticipatory Haptic Assistance Considering Human Behavior Uncertainty. *IEEE Transactions on Robotics*, 31(1):180–190, Feb 2015.

[MLK+12] Alexander Mörtl, Martin Lawitzky, Ayse Kucukyilmaz, Metin Sezgin, Cagatay Basdogan, and Sandra Hirche. The role of roles: Physical cooperation between humans and robots. *The International Journal of Robotics Research*, 31(13):1656–1674, 2012.

[MPH19] S. Musić, D. Prattichizzo, and S. Hirche. Human-Robot Interaction Through Fingertip Haptic Devices for Cooperative Manipulation Tasks. In *2019 28th IEEE International Conference on Robot and Human Interactive Communication (RO-MAN)*, pages 1–7, 2019.

[MS11] Pawel Malysz and Shahin Sirouspour. Trilateral teleoperation control of kinematically redundant robotic manipulators. *The International Journal of Robotics Research*, 30(13):1643–1664, 2011.

[MSB+17] S. Musić, G. Salvietti, P. Budde gen. Dohmann, F. Chinello, D. Prattichizzo, and S. Hirche. Robot team teleoperation for cooperative manipulation using wearable haptics. In *2017 IEEE/RSJ International Conference on Intelligent Robots and Systems (IROS)*, pages 2556–2563, 2017.

[MSgD+19] S. Musić, G. Salvietti, P. B. g. Dohmann, F. Chinello, D. Prattichizzo, and S. Hirche. Human–Robot Team Interaction Through Wearable Haptics for Cooperative Manipulation. *IEEE Transactions on Haptics*, 12(3):350–362, 2019.

[Mur07] Richard M. Murray. Recent Research in Cooperative Control of Multivehicle Systems. *Journal of Dynamic Systems, Measurement, and Control*, 129(5):571–583, 05 2007.

[MW19] Daniel McNamee and Daniel M. Wolpert. Internal Models in Biological Control. *Annual Review of Control, Robotics, and Autonomous Systems*, 2(1):339–364, 2019.

[NA12] Kumpati S Narendra and Anuradha M Annaswamy. *Stable adaptive systems*. Courier Corporation, 2012.

[NC15] X. Na and D. J. Cole. Game-Theoretic Modeling of the Steering Interaction Between a Human Driver and a Vehicle Collision Avoidance Controller. *IEEE Transactions on Human-Machine Systems*, 45(1):25–38, 2015.

[NHY87] Yoshihiko Nakamura, Hideo Hanafusa, and Tsuneo Yoshikawa. Task-Priority Based Redundancy Control of Robot Manipulators. *The International Journal of Robotics Research*, 6(2):3–15, 1987.

[NSR+08] Y. Nevatia, T. Stoyanov, R. Rathnam, M. Pfingsthorn, S. Markov, R. Ambrus, and A. Birk. Augmented autonomy: Improving human-robot team performance in urban search and rescue. In *2008 IEEE/RSJ International Conference on Intelligent Robots and Systems*, pages 2103–2108, Sept 2008.

[NVdS90] Henk Nijmeijer and Arjan Van der Schaft. *Nonlinear dynamical control systems*, volume 175. Springer, 1990.

[NWL+13] Steven Nunnally, Phillip Walker, Mike Lewis, Nilanjan Chakraborty, and Katia Sycara. Using Haptic Feedback in Human Robotic Swarms Interaction. *Proceedings of the Human Factors and Ergonomics Society Annual Meeting*, 57(1):1047–1051, 2013.

[ODAS15] Christian Ott, Alexander Dietrich, and Alin Albu-Schäffer. Prioritized multi-task compliance control of redundant manipulators. *Automatica*, 53:416–423, 2015.

[OM04] R. Olfati-Saber and R. M. Murray. Consensus problems in networks of agents with switching topology and time-delays. *IEEE Transactions on Automatic Control*, 49(9):1520–1533, 2004.

[OvCA08] R. Ortega, A. van der Schaft, F. Castanos, and A. Astolfi. Control by Interconnection and Standard Passivity-Based Control of Port-Hamiltonian Systems. *IEEE Transactions on Automatic Control*, 53(11):2527–2542, 2008.

[OvME99] R. Ortega, A. van der Schaft, B. Maschke, and G. Escobar. Energy-shaping of port-controlled Hamiltonian systems by interconnection. In *Proceedings of the 38th IEEE Conference on Decision and Control (Cat. No.99CH36304)*, volume 2, pages 1646–1651 vol.2, 1999.

[OWLM14] Linda Onnasch, Christopher D. Wickens, Huiyang Li, and Dietrich Manzey. Human Performance Consequences of Stages and Levels of Automation: An Integrated Meta-Analysis. *Human Factors*, 56(3):476–488, 2014. PMID: 24930170.

[PBCM07] Raja Parasuraman, Michael Barnes, Keryl Cosenzo, and Sandeep Mulgund. Adaptive Automation for Human-Robot Teaming in Future Command and Control Systems. Technical report, DTIC Document, 2007.

[PCPM13] D. Prattichizzo, F. Chinello, C. Pacchierotti, and M. Malvezzi. Towards Wearability in Fingertip Haptics: A 3-DoF Wearable Device for Cutaneous Force Feedback. *IEEE Transactions on Haptics*, 6(4):506–516, Oct 2013.

[PJ08] D. Prattichizzo and Trinkle J. Grasping. In Bruno Siciliano and Oussama Khatib, editors, *Springer Handbook of Robotics*, chapter 28, pages 671–700. Springer, 2008.

[PK06] Jaeheung Park and Oussama Khatib. A Haptic Teleoperation Approach Based on Contact Force Control. *The International Journal of Robotics Research*, 25(5-6):575–591, 2006.

[PKH03] Kwi-Ho Park, Byoung-Ho Kim, and Shinichi Hirai. Development of a soft-fingertip and its modeling based on force distribution. In *IEEE International Conference on Robotics and Automation*, volume 3, pages 3169–3174, 2003.

[PMC+15] C. Pacchierotti, L. Meli, F. Chinello, M. Malvezzi, and D. Prattichizzo. Cutaneous haptic feedback to ensure the stability of robotic teleoperation systems. *International Journal of Robotics Research*, 34(14):1773–1787, 2015.

[PR97] Raja Parasuraman and Victor Riley. Humans and Automation: Use, Misuse, Disuse, Abuse. *Human Factors*, 39(2):230–253, 1997.

[PSS+17] C. Pacchierotti, S. Sinclair, M. Solazzi, A. Frisoli, V. Hayward, and D. Prattichizzo. Wearable Haptic Systems for the Fingertip and the Hand: Taxonomy, Review, and Perspectives. *IEEE Transactions on Haptics*, 10(4):580–600, Oct 2017.

[PST+15] J. R. Peters, V. Srivastava, G. S. Taylor, A. Surana, M. P. Eckstein, and F. Bullo. Human Supervisory Control of Robotic Teams: Integrating Cognitive Modeling with Engineering Design. *IEEE Control Systems Magazine*, 35(6):57–80, 2015.

[PSW00] R. Parasuraman, T. B. Sheridan, and C. D. Wickens. A model for types and levels of human interaction with automation. *IEEE Transactions on Systems, Man, and Cybernetics - Part A: Systems and Humans*, 30(3):286–297, May 2000.

[RBCC15] L. Rozo, D. Bruno, S. Calinon, and D. G. Caldwell. Learning optimal controllers in human-robot cooperative transportation tasks with position and force constraints. In *2015 IEEE/RSJ International Conference on Intelligent Robots and Systems (IROS)*, pages 1024–1030, 2015.

[RHH+04] Emilie M. Roth, Mark L. Hanson, Chris Hopkins, Vince Mancuso, and Greg L. Zacharias. Human in the Loop Evaluation of a Mixed-Initiative System for Planning and Control of Multiple UAV Teams. *Proceedings of the Human Factors and Ergonomics Society Annual Meeting*, 48(3):280–284, 2004.

[RND02] Heath A. Ruff, S. Narayanan, and Mark H. Draper. Human Interaction with Levels of Automation and Decision-Aid Fidelity in the Supervisory Control of Multiple Simulated Unmanned Air Vehicles. *Presence: Teleoperators and Virtual Environments*, 11(4):335–351, 2002.

[RTE+10] E. J. Rodríguez-Seda, J. J. Troy, C. A. Erignac, P. Murray, D. M. Stipanovic, and M. W. Spong. Bilateral Teleoperation of Multiple Mobile Agents: Coordinated Motion and Collision Avoidance. *IEEE Transactions on Control Systems Technology*, 18(4):984–992, 2010.

[SAP+18] M. Selvaggio, F. Abi-Farraj, C. Pacchierotti, P. R. Giordano, and B. Siciliano. Haptic-Based Shared-Control Methods for a Dual-Arm System. *IEEE Robotics and Automation Letters*, 3(4):4249–4256, 2018.

[SC92] S. A. Schneider and R. H. Cannon. Object impedance control for cooperative manipulation: theory and experimental results. *IEEE Transactions on Robotics and Automation*, 8(3):383–394, 1992.

[SCN+12] A. Stewart, M. Cao, A. Nedic, D. Tomlin, and N. Leonard. Towards Human–Robot Teams: Model-Based Analysis of Human Decision Making in Two-Alternative Choice Tasks With Social Feedback. *Proceedings of the IEEE*, 100(3):751–775, 2012.

[SFC+13] H. I. Son, A. Franchi, L. L. Chuang, J. Kim, H. H. Bulthoff, and P. Robuffo Giordano. Human-Centered Design and Evaluation of Haptic Cueing for Teleoperation of Multiple Mobile Robots. *IEEE Transactions on Cybernetics*, 43(2):597–609, 2013.

[SH19] D. Sieber and S. Hirche. Human-guided multirobot cooperative manipulation. *IEEE Transactions on Control Systems Technology*, 27(4):1492–1509, 2019.

[She11] T. B. Sheridan. Adaptive Automation, Level of Automation, Allocation Authority, Supervisory Control, and Adaptive Control: Distinctions and Modes of Adaptation. *IEEE Transactions on Systems, Man, and Cybernetics - Part A: Systems and Humans*, 41(4):662–667, 2011.

[Sir05] S. Sirouspour. Modeling and control of cooperative teleoperation systems. *IEEE Transactions on Robotics*, 21(6):1220–1225, 2005.

[SK05] Luis Sentis and Oussama Khatib. Synthesis of whole-body behaviors through hierarchical control of behavioral primitives. *International Journal of Humanoid Robotics*, 2(04):505–518, 2005.

[SKE15] T. Setter, H. Kawashima, and M. Egerstedt. Team-level properties for haptic human-swarm interactions. In *2015 American Control Conference (ACC)*, pages 453–458, July 2015.

[SLP+15] K Sycara, C Lebiere, Y Pei, D Morrison, Y Tang, and M Lewis. Abstraction of analytical models from cognitive models of human control of robotic swarms. In *Proceedings of ICCM 2015 - 13th International Conference on Cognitive Modeling*, pages 13 – 18, January 2015.

[SMA99] S. Stramigioli, C. Melchiorri, and S. Andreotti. A passivity-based control scheme for robotic grasping and manipulation. In *Proceedings of the 38th IEEE Conference on Decision and Control (Cat. No.99CH36304)*, volume 3, pages 2951–2956 vol.3, 1999.

[SMC10] S. Stramigioli, R. Mahony, and P. Corke. A novel approach to haptic teleoperation of aerial robot vehicles. In *2010 IEEE International Conference on Robotics and Automation*, pages 5302–5308, 2010.

[SMG+17] G. Salvietti, L. Meli, G. Gioioso, M. Malvezzi, and D. Prattichizzo. Multicontact Bilateral Telemanipulation With Kinematic Asymmetries. *IEEE/ASME Transactions on Mechatronics*, 22(1):445–456, Feb 2017.

[SMH15] D. Sieber, S. Musić, and S. Hirche. Multi-robot manipulation controlled by a human with haptic feedback. In *2015 IEEE/RSJ International Conference on Intelligent Robots and Systems (IROS)*, pages 2440–2446, 2015.

[SMS+16] H. Saeidi, F. McLane, B. Sadrfaidpour, E. Sand, S. Fu, J. Rodriguez, J. R. Wagner, and Y. Wang. Trust-based mixed-initiative teleoperation of mobile robots. In *2016 American Control Conference (ACC)*, pages 6177–6182, July 2016.

[SMv98] Stefano Stramigioli, Bernhard Maschke, and Arjan van der Schaft. Passive Output Feedback and Port Interconnection. *IFAC Proceedings Volumes*, 31(17):591 – 596, 1998. 4th IFAC Symposium on Nonlinear Control Systems Design 1998 (NOLCOS'98), Enschede, The Netherlands, 1-3 July.

[SOJ+11] David Schuster, Scott Ososky, Florian Jentsch, Elizabeth Phillips, Christian Lebiere, and William A. Evans. A Research Approach to Shared Mental Models and Situation Assessment in Future Robot Teams. *Proceedings of the Human Factors and Ergonomics Society Annual Meeting*, 55(1):456–460, 2011.

[SS79] T. B. Sheridan and H. G. Stassen. *Definitions, Models and Measures of Human Workload*, pages 219–233. Springer US, Boston, MA, 1979.

[STP06] Peter Squire, Greg Trafton, and Raja Parasuraman. Human Control of Multiple Unmanned Vehicles: Effects of Interface Type on Execution and Task Switching Times. In *Proceedings of the 1st ACM SIGCHI/SIGART Conference on Human-Robot Interaction*, HRI '06, page 26–32, New York, NY, USA, 2006. Association for Computing Machinery.

[Str01] Stefano Stramigioli. *Modeling and IPC Control of Interactive Mechanical Systems: A Coordinate-Free Approach*, volume 266 of *LNCIS*. Springer, 2001.

[SV78] Thomas B Sheridan and William L Verplank. Human and Computer Control of Undersea Teleoperators. Technical report, DTIC Document, 1978.

[TGS11] A. Thobbi, Y. Gu, and W. Sheng. Using human motion estimation for human-robot cooperative manipulation. In *2011 IEEE/RSJ International Conference on Intelligent Robots and Systems*, pages 2873–2878, Sep. 2011.

[TJ02a] Emanuel Todorov and Michael I. Jordan. A Minimal Intervention Principle for Coordinated Movement. In *Proceedings of the 15th International Conference on Neural Information Processing Systems*, NIPS'02, page 27–34, Cambridge, MA, USA, 2002. MIT Press.

[TJ02b] Emanuel Todorov and Michael I Jordan. Optimal feedback control as a theory of motor coordination. *Nature neuroscience*, 5(11):1226, 2002.

[TLT+10] L. Tonin, R. Leeb, M. Tavella, S. Perdikis, and J. d. R. Millán. The role of shared-control in BCI-based telepresence. In *2010 IEEE International Conference on Systems, Man and Cybernetics*, pages 1462–1466, 2010.

[Tra15] P. Trautman. Assistive Planning in Complex, Dynamic Environments: A Probabilistic Approach. In *2015 IEEE International Conference on Systems, Man, and Cybernetics*, pages 3072–3078, 2015.

[vdS06] Arjan J. van der Schaft. Port-Hamiltonian systems: an introductory survey. In *Proc. Int. Congress of Mathematicians*, pages 1339–1365, 2006.

[vdS13] A. J. van der Schaft. *Port-Hamiltonian Differential-Algebraic Systems*, pages 173–226. Springer Berlin Heidelberg, Berlin, Heidelberg, 2013.

[VDS16] Luigi Villani and Joris De Schutter. Force control. In *Springer Handbook of Robotics*, pages 195–220. Springer, 2016.

[VSvdSP14] Ewoud Vos, Jacquelien M.A. Scherpen, Arjan J. van der Schaft, and Ate Postma. Formation Control of Wheeled Robots in the Port-Hamiltonian Framework. *IFAC Proceedings Volumes*, 47(3):6662 – 6667, 2014. 19th IFAC World Congress.

[VZ13] Paul Varnell and Fumin Zhang. Dissipativity-Based Teleoperation with Time-Varying Communication Delays. *IFAC Proceedings Volumes*, 46(27):369 – 376, 2013. 4th IFAC Workshop on Distributed Estimation and Control in Networked Systems (2013).

[WAV+13] M. T. Wolf, C. Assad, M. T. Vernacchia, J. Fromm, and H. L. Jethani. Gesture-based robot control with variable autonomy from the JPL BioSleeve. In *IEEE International Conference on Robotics and Automation*, pages 1160–1165, 2013.

[WK93] D. Williams and O. Khatib. The virtual linkage: a model for internal forces in multi-grasp manipulation. In *[1993] Proceedings IEEE International Conference on Robotics and Automation*, pages 1025–1030 vol.1, 1993.

[WL07] J. Wang and M. Lewis. Human control for cooperating robot teams. In *2007 2nd ACM/IEEE International Conference on Human-Robot Interaction (HRI)*, pages 9–16, March 2007.

[WNL+13] Phillip Walker, Steven Nunnally, Michael Lewis, Nilanjan Chakraborty, and Katia Sycara. Levels of Automation for Human Influence of Robot Swarms. *Proceedings of the Human Factors and Ergonomics Society Annual Meeting*, 57(1):429–433, 2013.

[Woo71] Jack L. Wood. Dynamic response of human cranial bone. *Journal of Biomechanics*, 4(1):1 – 12, 1971.

[WTFR04] D. D. Woods, J. Tittle, M. Feil, and A. Roesler. Envisioning human-robot coordination in future operations. *IEEE Transactions on Systems, Man, and Cybernetics, Part C (Applications and Reviews)*, 34(2):210–218, 2004.

[YD04] H. A. Yanco and J. Drury. Classifying human-robot interaction: an updated taxonomy. In *2004 IEEE International Conference on Systems, Man and Cybernetics (IEEE Cat. No.04CH37583)*, volume 3, pages 2841–2846 vol.3, 2004.

[YPM+96] N. Yoganandan, F.A. Pintar, D.J. Maiman, J.F. Cusick, A. Sances, and P.R. Walsh. Human head-neck biomechanics under axial tension. *Medical Engineering and Physics*, 18(4):289 – 294, June 1996.

[YSD03] Haoyong Yu, Matthew Spenko, and Steven Dubowsky. An Adaptive Shared Control System for an Intelligent Mobility Aid for the Elderly. *Autonomous Robots*, 15(1):53–66, Jul 2003.

[Zil15] Shlomo Zilberstein. Building strong semi-autonomous systems. In *Twenty-Ninth AAAI Conference on Artificial Intelligence*, 2015.

[ZXYW07] Dandan Zhang, Guangming Xie, Junzhi Yu, and Long Wang. Adaptive task assignment for multiple mobile robots via swarm intelligence approach. *Robotics and Autonomous Systems*, 55(7):572–588, 2007.